DISSERTATION


BIOFILM DYNAMICS AND THE RESPONSE TO N-OXIDES IN *Burkholderia pseudomallei*



Submitted by:

Mihnea R. Mangalea

Department of Microbiology, Immunology and Pathology



In partial fulfillment of the requirements

For the Degree of Doctor of Philosophy

Colorado State University

Fort Collins, Colorado

Summer 2019



Doctoral Committee:

      Advisor: Bradley R. Borlee

      Richard A. Slayden
      Richard A. Bowen
      Mark D. Stenglein
      Amy O. Charkowski

ABSTRACT


BIOFILM DYNAMICS AND THE RESPONSE TO N-OXIDES IN *Burkholderia pseudomallei*

      *Burkholderia pseudomallei* is a saprophytic bacterium inhabiting wet soils in tropical regions and is the causative agent of melioidosis, an emerging infectious disease of high mortality. Although the incidence of melioidosis is more prevalent in the monsoonal wet season in Southeast Asia and Northern Australia, gardens and farms also serve as a reservoir for *B. pseudomallei* infection in the dry season, due to anthropogenic disturbances including irrigation and application of nitrogen (N)-based fertilizer use. Melioidosis is historically associated with rice farming in rural regions of the tropics where rain-fed lowland environments predominate and planting fields are often managed by the addition of N-based fertilizers to keep up with the demand for global rice consumption. In these oxygen-limiting environments, *B. pseudomallei* is a facultative anaerobic organism capable of growth in anoxic conditions by substituting nitrate ($NO_3^-$) as a terminal electron acceptor. *B. pseudomallei* is capable of complete denitrification, a step-wise enzymatic reaction that is carried out by four individual enzyme complexes or reductases, that reduce $NO_3^-$ to $N_2$. Denitrification among proteobacteria is regulated by sensing systems that depend on both the presence of substrate and hypoxic conditions, however little is known about this ecological and physiological phenomenon in *B. pseudomallei*. In hosts infected with *B. pseudomallei*, similar oxygen tensions are experienced by the organisms in abscesses, lesions, and during intracellular growth; however, little is known regarding the extent of anaerobic metabolism and defense from host-associated reactive nitrogen intermediates in *B. pseudomallei*. This study examines the predicted nitrate sensing and metabolism genes in a clinical isolate, *B. pseudomallei* 1026b, and specifically their role in regulating biofilm dynamics. We hypothesized that nitrate sensing and metabolism negatively regulate biofilm formation and aimed to describe the genetic and metabolic determinants of this phenotype in *B. pseudomallei*.

      In Aim I of this study, we characterized a dose-dependent biofilm inhibition model that responds to increasing concentrations of sodium nitrate and sodium nitrite, donors of the inorganic anions $NO_3^-$ and $NO_2^-$, respectively. Based on *in silico* analyses of predicted nitrate sensing and metabolism loci, we screened transposon insertional mutants to identify candidates involved in the biofilm inhibitory response. We identified five mutants that no longer respond to nitrate-mediated biofilm inhibition in genes predicted to comprise key components of the denitrification pathway: the alpha and beta subunits of the dissimilatory nitrate reductase *narGHJI-1*, the *narX-narL* two-component regulatory system, and the nitrate/nitrite extrusion gene *narK-1*. Using LC-MS/MS, we quantified the intracellular concentration of the secondary metabolite cyclic-di-GMP, and observed a significant decrease of this key biofilm-associated molecule in response to sodium nitrate treatment. Furthermore, we evaluated the expression of cyclic-di-GMP regulatory enzymes to propose a mechanism for the nitrate-dependent biofilm inhibition phenotype in *B. pseudomallei*.

      In Aim II, we examined the functions of NarX and NarL in response to exogenous sodium nitrate and sodium nitrite and the biofilm inhibition model using separate in-frame deletion mutants. We characterized a disparity in biofilm inhibition that is dependent on nitrate but not nitrite in this two-component sensing system, before analyzing the global transcriptome of these mutants relative to the wild type in growth conditions supplemented with either N-oxide. Differential expression analysis of RNA sequencing reads revealed significant transcriptomic shifts in several gene clusters associated with biofilm formation, nitrate metabolism, general metabolism, antibiotic resistance, virulence, and secondary metabolite biosynthesis that responded similarly to both $NO_3^-$ and $NO_2^-$ supplementation. Additionally, we demonstrated that *narX* and *narL* mutants are deficient in intracellular survival in murine macrophages, providing a link between nitrate sensing and metabolism and *B. pseudomallei* host-pathogen interactions. These data suggest that denitrification is an important mechanism for biofilm dynamics and is also relevant to survival and pathogenicity in animal hosts during *B. pseudomallei* infection.

iv

DEDICATION

*To my mother, Smaranda, who sacrificed much to offer me the opportunities and educational experiences that shaped me into the scientist that I am today: without your guidance, I could not have succeeded as a graduate student. You were my first mentor and I owe my success to you.*

TABLE OF CONTENTS

# LIST OF FIGURES

# CHAPTER 1: *Burkholderia pseudomallei* in the environment[1]

The genus *Burkholderia* consists of a diverse group of related organisms that occupy equally diverse ecological niches across the planet (1, 2). *Burkholderia* species are abundant in tropical environments (3), where they make up an important part of soil microbial communities, plant and animal surfaces, water, and the rhizosphere (4-6). Members of the genus *Burkholderia* range from beneficial plant-growth-promoting bacteria that are rarely pathogenic (7-9), or opportunistic pathogens that can be acquired directly from the environment to cause difficult-to-treat diseases in humans, animals, and plants (1). As such, an ambiguous overlap exists among clinical pathogens and environmental symbionts (10, 11). Within the identified *Burkholderia* species that are opportunistic pathogens, two distinct groups of organisms have been classified belonging to the *Burkholderia cepacia* complex (Bcc) or the *Burkholderia pseudomallei* complex (Bpc). To date, over 20 Bcc species have been characterized and placed into nine taxonomic genomovars (12). Of those species, *B. cenocepacia* (genomovar III) is a major pathogen for immunocompromised individuals with cystic fibrosis, accounting for 70% of all Bcc infections (13). The ecological distribution of the Bcc overlaps with that of the Bpc, as several Bcc isolates were identified during recent surveillance for *B. pseudomallei*, the etiological agent of melioidosis in Northern Australia (14). The Bpc consists of the well-characterized human and animal pathogens, *B. pseudomallei* and *B. mallei,* and closely related non-pathogenic soil saprophytes. This introductory chapter will discuss the global distribution of *B. pseudomallei*, the physicochemical factors influencing its environmental survival, occupational and recreational risks for acquiring melioidosis, and address key aspects of melioidosis epidemiology.

---

[1] This chapter contains minimal segments of writing that will appear in a book chapter titled "Cyclic-di-GMP in *Burkholderia* spp." by Borlee, G.I., **Mangalea, M.R.**, and Borlee, B.R. 2019.

## 1.1 *B. pseudomallei*

The first record of *Burkholderia pseudomallei* in the scientific literature was described by Whitmore and Karishnaswami from the Pathological Laboratory of Rangoon General Hospital in Rangoon, Burma (Myanmar) in 1912 (15). Whitmore and Karishnaswami could readily distinguish this bacterium from the more well-known causative agent of glanders (formerly *Bacillus mallei*) and noted the prevalence of this novel bacterium among the "ill-nourished, neglected, wastrels of the town" (15). Whitmore further characterized the "glanders-like disease" among a cluster of patients with morphine addictions, noted the bacterium's infectivity in guinea pigs, and proposed the name *Bacillus pseudomallei* (16). Over the past century, the etiological agent of melioidosis has had several names including Whitmore's Bacillus and *Pseudomonas pseudomallei* (17), before its incorporation into the *Burkholderia* genus in 1992 (2). The genus *Burkholderia* was proposed in honor of American bacteriologist, W. M. Burkholder, for his identification of the etiological agent of soft rot in onions, *Burkholderia cepacia*, in 1949 (2).

A majority of *B. pseudomallei* research has been published within the last 20 years despite numerous anecdotal and historical reports of the disease and the accepted worldwide distribution of this bacterium across six continents by the 1990s (18). Indeed, the distribution of *B. pseudomallei* is evidently pandemic between the latitudes 20°N and 20°S (19). The history of published and accessible research regarding *B. pseudomallei* is also undoubtedly influenced and skewed by its secretive development as an offensive biological weapon by the Soviet Union biological warfare program (20). Additionally, *B. pseudomallei* research in the United States is restricted due to its classification as a Tier 1 select agent under the Federal Select Agent Program since 2012 (21). As such, *B. pseudomallei* research is regulated by the Centers for Disease Control and Prevention as well as the U.S. Department of Agriculture Animal and Plant Health Inspection Service and must be handled in a biosafety level 3 (BSL-3) laboratory (22). Specifically, Tier 1 select agent status exists for *B. pseudomallei* due to the severe risk and

threat to public and animal health, difficult treatment regimen with limited options, ease of aerosolization, and complicated diagnosis.

*Burkholderia pseudomallei* is the causative agent of melioidosis, a complex infectious disease with no pathognomic clinical syndrome. The name melioidosis was coined in 1921 by Stanton and Fletcher, who characterized a similar disease to Whitmore's and Karishnaswami's accounts and proposed "Melis" as a Greek root for a variety of conditions resembling glanders (23). Accurate clinical diagnosis of melioidosis is difficult due to the large variability in presenting symptoms, thus having earned it the name "the great mimicker" (24). Melioidosis results in acute infection characterized by localized abscesses and sepsis with or without pneumonia in 85% of cases, chronic infections in 10% of cases, and reactivation from latency in roughly 5% of cases (25). The presentation of disease does not depend on route of infection which can occur through inhalation, cutaneous inoculation, or ingestion of bacteria, and importantly, in 78% or more melioidosis cases, the cause of infection is undetermined (26). However, the rate and severity of *B. pseudomallei* infection is contingent on the route of infection, as shown in mice (27) and hamster models (28). Nonetheless, it is evident that infection with *B. pseudomallei* results from exposure to soil and water in the environments where this bacterium is endemic.

*B. pseudomallei* is an environmental saprophyte and sapronotic disease agent that transitions directly from the environment to cause disease in susceptible humans and animals (29). The saprophytic lifestyle is shared among the other organisms in the Bpc phylogenetic group (30), apart from *B. mallei,* which is a host-adapted pathogen (31). The additional members of the Bpc include *B. thailandensis*, *B. oklahomensis*, and *B. humptydooensis*, and are generally non-pathogenic although opportunistic infections have been documented (32). The Bpc clade is comprised of organisms that share high sequence similarity and group together in a monophyletic nature despite complex genomic plasticity (30, 33); however, large differences in the pathogenicity and niche adaptation exist among members of this group. Notably, *B. pseudomallei*, *B. thailandensis*, and *B. mallei* share high nucleotide sequence

3

identity and genomic synteny (34), yet one is a sapronotic disease agent, another is a non-pathogenic saprophyte, and the other is a host-adapted pathogen that does not survive in the environment.

### 1.1.2 Evolution of *B. mallei*

The closest phylogenetic relative to *B. pseudomallei*, *B. mallei*, the etiological agent of glanders, has adapted to an obligate intracellular lifestyle in animals (horses, donkeys, mules, camels, humans, and nonhuman primates among others (35)) and has deleted or mutated over 1000 genes during this evolution (36). *B. mallei* has retained a smaller core-genome with high sequence homology to *B. pseudomallei*, while maintaining a larger variable gene set amid genome rearrangement events that ultimately shaped *B. mallei* speciation (37). Based on multilocus sequence typing (MLST) analysis, *B. mallei* distinctly represents a clone of *B. pseudomallei* that has been elevated to species status based on correlation with the glanders disease and genomic reduction (38). Interestingly, the evolution of *B. pseudomallei* and *B. mallei* as pathogens has been proposed to hinge on the loss of the arabinose assimilation pathway (39), which has been characterized as an anti-virulence marker in non-pathogenic bacteria (40). The classical example of this disparity exists in the Bpc, where arabinose metabolic function differentiates non-pathogenic *B. thailandensis* from *B. pseudomallei* (41). Thus, in addition to the large genomic reduction experienced in *B. mallei* evolution, loss of arabinose assimilation also occurred during its adaptation to an obligate intracellular pathogen that cannot survive in the environment (39).

The genome of *B. mallei* is 1.5 Mb smaller than that of *B. pseudomallei* (7.3 Mb) with missing or mutated genes, 627 on chromosome I and 819 genes on chromosome II, resulting in 5535 open reading frames (ORFs) (42). Additionally, the *B. mallei* genome contains over 12,000 simple sequence repeats in two thirds of the coding sequences, which can disrupt functionality of genes and lead to phase variation and immune evasion during chronic infection (42). Despite

the large genomic reduction, *B. mallei* has retained several virulence-associated gene clusters (43, 44), antibiotic resistance mechanisms (45, 46), and secondary metabolite biosynthesis genes (47, 48), resulting in a successful host-restricted pathogen. Importantly, the genomic erosion of *B. mallei* is ongoing during its intracellular evolution leading to potential virulence reduction in the future (49). The reductive evolution in *B. mallei* is also mirrored by *B. pseudomallei* during chronic infection where positive selection for host adaptation and commensalism drives genome-wide mutations (50). However, adaptive changes in *B. pseudomallei* during persistent infections are associated with increased bacterial tolerance and relapse scenarios (51, 52).

### 1.1.3 Nonvirulent *B. thailandensis* as a model organism

*B. thailandensis* is the next closest genetic relative to *B. pseudomallei* in the Bpc (30), with high genomic conservation in both accessory and core metabolic functions, physiology, and virulence-associated genes (53). However, *B. thailandensis* is considered a nonvirulent relative of *B. pseudomallei* and considered a model surrogate organism for studying *B. pseudomallei* pathogenicity in a select agent exempt setting (54). Although *B. thailandensis* rarely causes disease (55), it is considered to have a low pathogenic potential (56) and requires a much higher infectious dose (57). As noted previously, one explanation for the evident avirulence in *B. thailandensis* lies in its ability to assimilate arabinose from the environment while *B. pseudomallei* cannot (58). Regulation of arabinose metabolic activity has been linked to transcriptional control of bacterial secretion systems and carbon metabolism, which provides a mechanistic link for attenuation of virulence in *B. thailandensis (59)*. This metabolic distinction is also exemplified geographically. Soil sampling in Thailand revealed majority arabinose-negative isolates in northeast Thailand (where *B. pseudomallei* clinical disease is prevalent) and arabinose-positive isolates of *B. thailandensis* in central Thailand where clinical infection is rare

(60). Indeed, *B. thailandensis* and *B. pseudomallei* are rarely found together in soil samples from the same location (61).

Experimental competition between the closely related soil saprophytes suggest that *B. pseudomallei* inhibits *B. thailandensis* growth and dissemination through a variety of mechanisms including contact-dependent inhibition (CDI) systems and flagellar inhibition (62). Despite its competitive disadvantages, *B. thailandensis* is widely used as a model organism for studying quorum sensing (63), biofilm formation (64), CDI systems (65, 66), and secondary metabolism (67, 68). One of the major antigenic differences between *B. pseudomallei* and *B. thailandensis* is that the latter lacks capsule I (CPSI), an important virulence determinant (69) (see **Fig A3.7**), which can obfuscate infection and biofilm assays using *B. thailandensis*. In summary, research using *B. thailandensis* offers several benefits as a model organism for the closely related human pathogens *B. pseudomallei* and *B. mallei* due to its ecological and genetic similarities as well as the relative ease of genetic manipulation (70). For these reasons, *B. thailandensis* E264 was used in the pilot study exploring an *in planta* model of *Burkholderia* colonization and dissemination among rice plants in the TerraForma 2.0 box (**Appendix 1**).

## 1.2 Global distribution of *B. pseudomallei*

*B. pseudomallei* has long been considered a leading cause of bacterial pneumonia in Thailand and sepsis in northern Australia and (71), regions that are considered classical hotspots for this organism. However, a comprehensive understanding of the global distribution of *B. pseudomallei* has been lacking. Since the characterization of melioidosis over 100 years ago, one of the most challenging facets of understanding the disease has been related to the unknown and incomplete distribution of *B. pseudomallei* on a global scale. This is a multifaceted problem that is based on a lack of adequate facilities for diagnosis, lack of awareness in endemic areas, and lack of reliable detection methods for soil surveillance (72).

An important first step to understanding melioidosis is characterizing the global burden of the disease based on evidence of *B. pseudomallei* isolated from humans, animals, and the environment worldwide. In 2016, Limmathurotsakul and colleagues published a landmark study presenting a comprehensive database of over 20,000 geo-tagged records of *B. pseudomallei* isolated between 1910 and 2014 (73). According to this most recent global consensus, zones of greatest risk for melioidosis comprise Southeast Asia including the Indian subcontinent, Northern Australia, the Middle East, sub-Saharan Africa, South and Central America (73) (**Figure 1.1**). *B. pseudomallei* distribution is ubiquitous in the tropical and subtropical regions of the world, causing an estimated 165,000 human infections resulting in approximately 89,000 deaths per year in these areas, which is higher than the global mortality of dengue and leptospirosis combined (73).
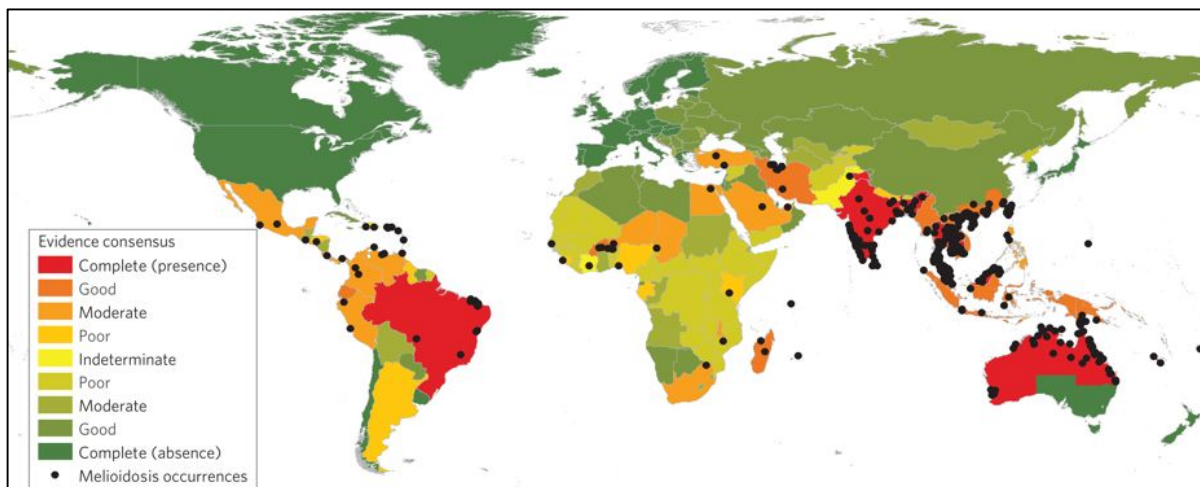


**Figure 1.1 Global distribution of *B. pseudomallei* based on evidence consensus of geo-tagged records of melioidosis occurrences in humans/animals or environmental isolation of *B. pseudomallei*.** Taken from Limmathurotsakul et al. (73), this global consensus is based on over 100 years of data from records spanning 1910 to 2014. Political boundaries are represented in a green-red color gradient where green indicates complete absence of *B. pseudomallei* records and red indicates complete presence of *B. pseudomallei*. Black dots represent individual records of melioidosis or *B. pseudomallei*. The map is likely incomplete due to frequent misdiagnosis, non-standardized soil surveillance methods, political misinformation, and general lack of awareness of melioidosis among healthcare workers and lay persons alike.

The global distribution of soil saprophytes such as *B. pseudomallei* depends on environmental disruption in endemic areas and movement of people, animals, and goods contaminated with bacteria. A recent phylogenetic study on the pan-genome of *B. pseudomallei* points to Australia as the origin and early reservoir for the species, leading to a single transmission event from the Australian continent to Southeast Asia (74). According to this recent phylogenetic dissemination analysis, transmission of *B. pseudomallei* flowed over land to West Africa where South and Central American isolates most likely originated from the trans-Atlantic slave trade between 1650 – 1850 (74). In addition to the phylogenetic analysis based on core genome mapping of 469 sequenced *B. pseudomallei* isolates across each continent (**Figure 1.2**), Chewapreecha and colleagues analyzed kmer enrichment (sequence reads of length k that can be used to separate species) and clusters of orthologous groups (COGs) in a genome-wide association study (GWAS) to identify region-specific virulence-associated loci (74). One of the most striking results of this study was the correlation between the frequency of encephalomyelitis in Australia with region-specific chemotaxis clusters and the intracellular motility gene, *bimA* (74). The value of large-scale genomic characterization on a truly global scale is useful not only for providing tangible numbers for melioidosis incidence (73) but also for refining region-specific clinical outcomes for this global organism.

Mapping the global distribution of *B. pseudomallei* is a challenging task not only because of difficulties in isolation and identification, but because boundaries shown in maps are political and are not representative of bacterial dissemination across regions (18). After the presentation of the global burden of melioidosis in 2016, which included a model prediction of the environmental suitability for *B. pseudomallei* (**Figure 1.3**) (73), many reports have emerged from endemic areas to take stock of melioidosis status and the biogeographic distribution of *B. pseudomallei*. In Australia, the proposed origin of the *B. pseudomallei* species (75), a recent analysis of the genotype distribution of the "Top End" shows extensive diversity among the ancestral population yet restricted geographic dispersal of specific sequence types (ST) (76).
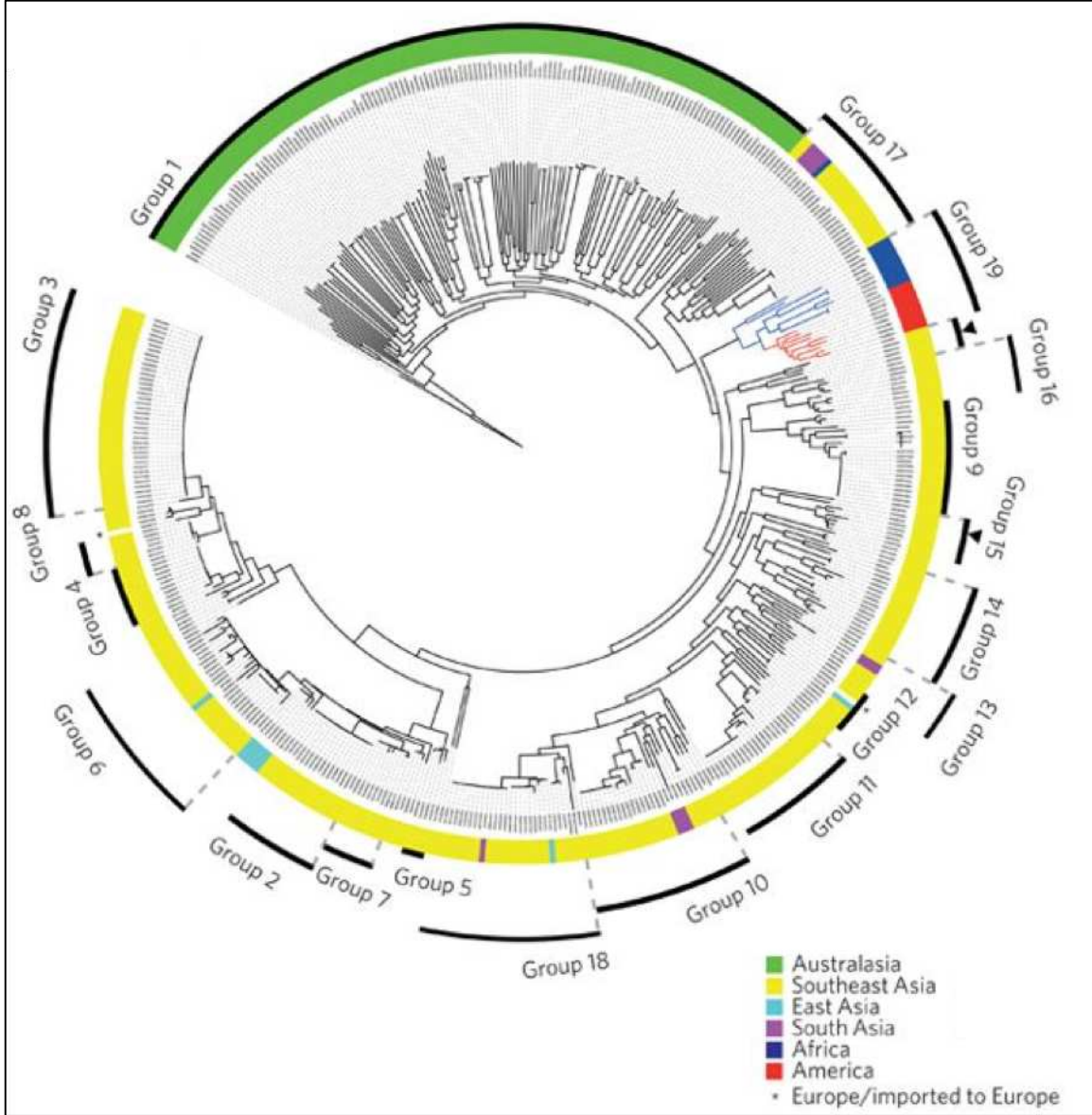
**Figure 1.2 *B. pseudomallei* diversity across worldwide origins.** Taken from Chewapreecha et al. (74), this maximum likelihood phylogeny analysis is based on core genome SNPs of 469 genomes from varying geographical origins. 19 groups are assembled here, rooted on the most genetically distant Australian isolate determined by pairwise SNP divergence. Population clusters are grouped largely according to region of isolation, based on Bayesian Analysis of Population Structure. This figure illustrates the global dissemination of *B. pseudomallei* from the genomic level.
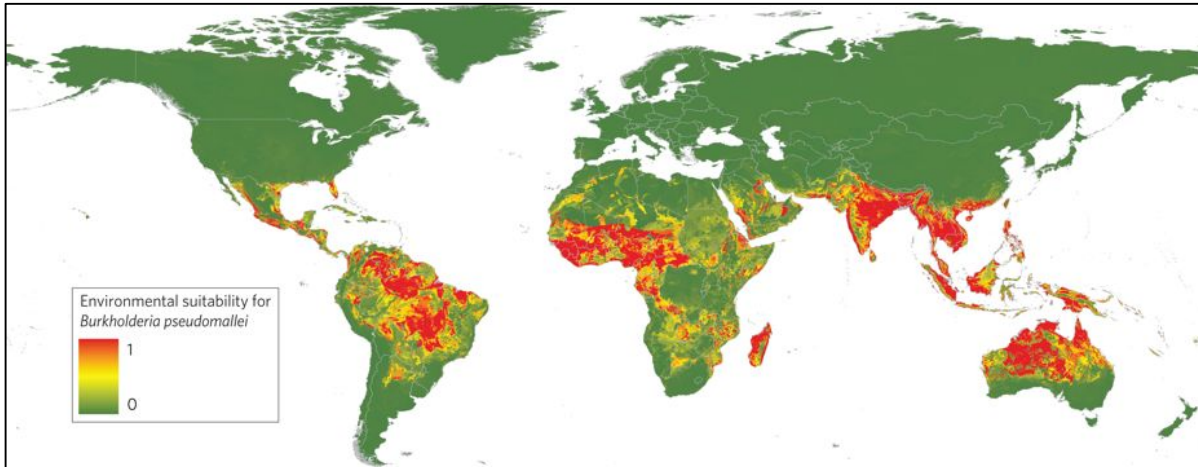
**Figure 1.3 Predicted worldwide environmental suitability for *B. pseudomallei*.** Taken from Limmathurotsakul et al. (73), this assessment is based on a boosted regression tree method linking *B. pseudomallei* environmental occurrences to local environmental covariates. Global environmental data was assembled in 5 x 5 km$^2$ pixels and environmental suitability was determined based on multiple covariates, where red indicates high suitability and green is low.

That *B. pseudomallei* STs have limited dispersal is unexpected for a soil saprophyte that can be carried to new territories in many ways (76). However, there is a significant phylogenetic division between extant *B. pseudomallei* in Southeast Asia compared to the ancestral Australian STs (75, 77, 78). Australian isolates share a characteristic abundance of geographically-distinct virulence-associated genes that may correlate to more common clinical manifestations such as genitourinary and neurological melioidosis in this region (79). Adjacent to the Top End of Australia, recent isolation of *B. pseudomallei* from Papua New Guinea and the Torres Strait archipelago show a more limited diversity, indicating that microbial biogeography is shaped by human activity and globalization (80). Indeed, the identification of an Asian *B. pseudomallei* ST as an increasingly common cause of melioidosis acquired from Australian soil underscores the impact of globalization on emerging *B. pseudomallei* sub-populations despite historic boundaries (81).

The endemicity of *B. pseudomallei* in Southeast Asia has been well documented (74, 82-85) since its characterization by Whitmore and Karishnaswami over 100 years ago. Recent reports confirm those from early melioidosis literature, and events like the 2004 Indian Ocean

earthquake and tsunami off the coast of Sumatra have expanded the endemic regions to include Indonesia, the Indian subcontinent, China, Hong Kong, and Taiwan (86). The burden of *B. pseudomallei* in Southeast Asia is extensive and beyond the scope of this introductory chapter, however it is worth mentioning that the increasing melioidosis cases in this region do not necessarily indicate *B. pseudomallei* emergence but an improvement of surveillance and diagnostic methods (73). The latter sentiment is evident in places such as the Western Indian Ocean where surveillance is underway in Madagascar (84), Indonesia where a recent workshop formed the Indonesia Melioidosis Network (87), and increasing availability of diagnostic facilities in the Philippines (88) and South Asia (89). In Myanmar, where *B. pseudomallei* was first coined, researchers are working to raise awareness of melioidosis that is unknown to most healthcare workers let alone lay persons (90). Indeed, awareness of *B. pseudomallei* and melioidosis in endemic areas continues to be among the most pressing action items on a global scale. In Thailand, where there are over 7500 human melioidosis cases per year, with a nearly 40% case fatality rate (82), only 19% of lay adults have knowledge that the disease exists (91).

Awareness of melioidosis is undoubtedly lower in Africa, South America, Mexico, Central America, and the Caribbean, which do not have extensive history of *B. pseudomallei* research. At present, we know that melioidosis is endemic in these regions (73); however, the public health burden of melioidosis is under-recognized in regions of the world where diagnosing febrile illnesses as malaria may be over-applied (92). Accordingly, there is clinically-relevant value in "searching for old bugs in new places" (92). Recent reports highlight *B. pseudomallei* surveillance efforts in Africa (93, 94), Brazil (95), Mexico and Central America (96, 97). *B. pseudomallei* has been endemic in Puerto Rico since the first reported melioidosis case in 1982, however melioidosis remains relatively rare compared to other endemic areas (98). There are several factors that may contribute to the apparent discrepancy of melioidosis cases in Puerto Rico and the ability of *B. pseudomallei* to persist in this region of the world. Understanding the

physicochemical factors and biological makeup of soils where *B. pseudomallei* is endemic would undoubtedly refine the global ecology and epidemiology of this organism (98).

**1.3 *B. pseudomallei* environmental ecology and factors influencing survival in the soil**

The accurate surveillance of *B. pseudomallei* in the environment depends on several factors including culture media used, animal inoculation detection methods, range of soil depth tested, and attempts at quantification (99). Additionally, there are a variety of factors that influence *B. pseudomallei* distribution in soils, including type of soil, seasonal variability, climactic factors, relative pH, and anthropogenic factors such as man-made fertilizers (99). Understanding the factors that influence *B. pseudomallei* environmental survival is significant in mediating melioidosis in endemic areas, considering that direct acquisition of *B. pseudomallei* bacteria from the environment is the primary mechanism of infection in humans and animals. Based on several ecological surveys, it is evident that *B. pseudomallei* is not evenly distributed in the environment, and has apparent niche preferences such as wet clay soil with oxidized iron components (100). Importantly, the occurrence of *B. pseudomallei* in soil has been linked to anthropogenic disturbances and land management changes such as the incorporation of livestock, farming, and irrigation (101). Anthrosol (human-modified soil), acrisol (clay-rich tropical soil), and high-proportion gravel soils are also significantly associated with *B. pseudomallei* (73).

The physicochemical parameters of soils in sites that were positive for *B. pseudomallei* during a Thailand survey indicate a preference for 10-20% soil water content, low pH between 5.0 – 6.0, and low nutrient availability (102). In Myanmar, a recent analysis of soil properties identified that high iron, clay, and water content (around 11%) were the most important factors related to *B. pseudomallei* occurrence (103). Low pH levels, even down to pH = 2.8, have been linked to *B. pseudomallei* presence (104), which couples with a recent epidemiological study showing significant reduction in melioidosis risk when soil is treated with lime (105). Indeed,

factors such as high water content, low pH, and high temperature, have been extensively studied to identify the optimum natural conditions for *B. pseudomallei* (106-108). In addition to these basic metrics, recent studies have investigated the correlation of nutrient availability and depletion with *B. pseudomallei* frequency.

A recent cross-sectional environmental analysis of three regions of Thailand identified depletion of soil nutrients, except for total nitrogen, sodium, and sulfur, to be positively correlated with *B. pseudomallei* (109). Elevated total nitrogen levels of soils, indicative of nitrate-based fertilizer addition, as well as elevated chemical oxygen demand, have been shown to be significantly associated with sites positive for *B. pseudomallei* in Thailand (102). In contrast to these Thai studies, Northern Australian soil analyses revealed that nutrient-deficient sites with very low nitrogen, nitrate, and organic carbon correlate with the presence of *B. pseudomallei* (110). However, a longitudinal soil microcosm experiment in Northern Australia examined the effects of fertilizer on a naturally positive *B. pseudomallei* field site and determined that nitrates and urea increased bacterial loads in sandy soils characteristic to domestic gardens (111). Thus, although the preferred micro-environments for *B. pseudomallei* can be broad, in part due to the environmental resilience of this bacterium (112, 113), it is possible to reconstruct the suitable natural conditions for soil survival (114). The current known preferences for *B. pseudomallei* include tropical waters and moist soils, with slightly acidic and nutrient-rich conditions (115). Nevertheless, soil sampling and detection methods are not standardized across countries or research groups, thus accurate assessment of *B. pseudomallei* distribution in the environment is dependent on adopting consensus guidelines for surveillance methodology (116).

## 1.4 Occupational and recreational factors related to melioidosis risk

The primary risk factor for melioidosis infection is prolonged exposure to the environments harboring *B. pseudomallei*, which are the wet soils and surface waters of endemic

13

regions throughout the tropics. As such, *B. pseudomallei* is a sapronotic disease agent that is

acquired directly from the environment (29). Melioidosis, the disease caused by *B. pseudomallei*

infection, is considered a sapronosis – "an infectious disease caused by pathogenic

microorganisms that inhabit aquatic ecosystems and/or soil rather than a living host" (26). There

are several clinical risk factors that are associated with a greater risk of melioidosis infection,

including diabetes mellitus, thalassemia, renal disease, excessive alcohol drinking, and

preexisting chronic lung disease such as cystic fibrosis (19, 25, 117). However, this section will

characterize the melioidosis risk factors associated with occupational and recreational activities,

touching on anecdotal evidence that shaped my hypothesis regarding nitrate-biofilm dynamics

in *B. pseudomallei* (as described in **Chapter 3**).

### 1.4.1 Rice agriculture

One of the most frequently associated activities with melioidosis, rice farming has

historically been linked with the disease in endemic areas (99). In rural regions of Thailand that

are endemic for *B. pseudomallei,* rice farmers account for over 80% of melioidosis patients

(118, 119) and it is considered an occupational hazard (120). More recently, a matched case-

control study of melioidosis risk factors in Northeast Thailand revealed that working in a rice

field contributes to a 2.1 odds ratio of acquiring melioidosis, which is higher than potential

exposure through an open wound (2.0 odds ratio) (121). It has been hypothesized that

prolonged submersion of skin in water, which is necessary for fulfilling full-time rice farming

duties, leads to increased percutaneous inoculation of *B. pseudomallei* due to breakdown of

basic physical barriers (122). And while researchers have recommended personal protective

equipment such as rubber boots and gloves be worn on the job for melioidosis prevention (121),

these items are uncomfortable and hinder digital manipulation of rice plants in hot and humid

tropical environments. Furthermore, in rural Northeast Thailand where seasonal rice farmers

make up nearly 80% of the population (123), the burden of melioidosis is also socioeconomic as

treatment is around $15,000 per patient and annual income for outdoor laborers is less than

$5000 (124).  Therefore, given that lowland rice fields are the major cropping system in

Northeast Thailand (125) where the major occupation is rice farming, mitigating melioidosis risk

in this population is of paramount concern.

Another important agricultural aspect in regions endemic for *B. pseudomallei* is the

seasonality of rice farming that corresponds with the monsoon season. Localized flooding is

necessary for planting rice submerged in freshwater (**Figure 1.4**) especially considering that the

rice plant is particularly sensitive to available water levels (126, 127). In the rain-fed lowland

environments that make up almost one fifth of the world's total rice production, physicochemical

properties of soil can be uncertain and planting fields are often managed by land preparation

including addition of reactive nitrogen-based (N) fertilizer (126). Nitrate ($NO_3^-$) leaching under

agricultural lands into the aquifers used for rural drinking water is also a concern (128, 129).

Sampling in the Philippines showed that $NO_3^-$ pollution adjacent to rice farming areas frequently

exceeded the WHO limit of 10 mg/L (128). However, $NO_3^-$ pollution in water is rarely problematic

due to the bacterial denitrification that takes place in anaerobic conditions, such as waterlogged

rice fields (124, 126).



**Figure 1.4 At highest risk for exposure to *B. pseudomallei* and contracting melioidosis, rice paddy workers in Northeast Thailand carry a large portion of the socioeconomic disease burden.** Taken from the University of Nevada Reno School of Medicine Diagnostics Discovery Laboratory (http://medicine.nevada.edu/ddl/research/melioidosis).

*B. pseudomallei* is a facultative anaerobic organism that is capable of growth in anoxic conditions by substituting nitrate as a terminal electron acceptor (130). A survey of *B. pseudomallei* from the Northern Territory, Australia revealed that 98% of soil isolates were capable of nitrate reduction (131), which is also the case for clinical isolates (130). Of interest to the studies described in this dissertation (**Chapter 3** and **Chapter 4**) is the proposition that the use of nitrate-based fertilizers may contribute to *B. pseudomallei* propagation in rice paddy environments (99). Furthermore, anaerobic metabolism of nitrate was previously considered a pathogenicity determinant for *B. pseudomallei* inhabiting irrigated and fertilized rice paddies (108). Anaerobic respiration is important for adapting to environments where oxygen is limited, such as deep soil or host-associated lesions (108). Recently, nitrate concentrations were measured at a study site in Northeast Thailand to determine environmental conditions that correlate to *B. pseudomallei* presence; and although a nitrate threshold was unable to be determined, *B. pseudomallei* was recovered at much higher levels in the rice paddy environment (124). Thus, the well-established association between *B. pseudomallei* and rice agriculture in endemic areas is potentially correlated to the anaerobic metabolism capabilities of this organism.

### 1.4.2   *B. pseudomallei* in domestic gardens

In addition to the occupational exposure risks associated with melioidosis, recreational exposure accounts for a significant risk for *B. pseudomallei* infection, especially where rice agriculture is not as prevalent. The results of a 20-year prospective study from Darwin, Australia analyzed exposure histories of 540 patients and revealed that 75% of melioidosis cases were linked to environmental exposure to *B. pseudomallei* via recreational activities (117). Given that melioidosis is a sapronosis, it is not surprising that exposure to flooded soil and mud in endemic areas is a common method of infection (132-134). According to the Darwin study, 18% of patients had direct occupational exposure to *B. pseudomallei* including construction, military

16

exercises, landscaping, and gardening (117). While there have been several historical reports of military service members acquiring melioidosis after exposure in endemic areas (135-137), this section will focus on the link between the more peaceful activity of recreational gardening and *B. pseudomallei* infection risk.

In Australia, exposure to *B. pseudomallei* is increased in domestic gardens due to irrigation, fertilizer use, and incorporation of imported grasses (79). Melioidosis outbreaks have been linked to contaminated water bores used for irrigation and domestic use in rural parts of the Northern Territory (138, 139), suggesting that unchlorinated water is a source of *B. pseudomallei* for domestic gardens. The proposition that melioidosis is associated with specific land uses and agricultural practices was investigated by Kaestli and colleagues (101), who showed that gardens, farms, and livestock pens are associated with *B. pseudomallei.* Kaestli and colleagues noted that, although classically associated with the monsoon season, *B. pseudomallei* is more prevalent in domestic gardens during the dry season and at disturbed sites including animal pens (101). These observations raise the possibility that anthropogenic soil disturbance such as irrigation, fertilizer, and nitrogen (N) byproducts from animal wastes may support *B. pseudomallei* growth and propagation in these disturbed environments (111).

More recently, a seminal soil microcosm experiment revealed that, in general, irrigation was the only treatment that increased *B. pseudomallei* prevalence across all soils tested (111). Nitrogen phosphate potassium (NPK) fertilizer, urea, and organic fertilizer treatment results were conditional on soil types tested, with nitrate and urea being important for sandy soil but not clay (111). Evidently, land use and anthropogenic modifications of natural environments via irrigation and fertilizer augment natural ecosystems and lead to nutritional imbalances that influence *B. pseudomallei* occurrence. This statement is reinforced by the fact that nonnative grasses, such as mission grass in Australia, are a common habitat for *B. pseudomallei* colonization in both the rhizosphere and aerial sections (115). While the influx of NPK fertilizers can have many agricultural benefits in both domestic gardens and large-scale agriculture, rising

N levels in the environment can have indirect consequences affecting bacterial pathogens (140). The results of the soil microcosm study involving *B. pseudomallei* response to nitrate were inconclusive (111), partly stemming from the complexity of a natural environment with long-term variability in many physical and chemical factors. Nonetheless, the potential for *B. pseudomallei* to respond to nitrate via sensory and metabolic mechanisms (141), raises the possibility that this common anion may drive physiology and subsequently pathogenicity.

## 1.5 Melioidosis epidemiology

In addition to the occupational and recreational risk factors described above, melioidosis disease is correlated with a variety of risk factors that make clinical presentation of the disease variable and diagnosis difficult. The clinical manifestations of melioidosis include but are not limited to: cutaneous abscesses, pulmonary involvement (often mimicking tuberculosis), liver and spleen lesions and enlargements, pericardial and pleural effusions, ocular endophthalmitis, septic arthritis and osteomyelitis, prostatic abscesses and genitourinary involvement, parotid abscesses in children, and CNS involvement with meningitis and encephalitis (17, 25, 142, 143). The complex clinical outcomes of infection with *B. pseudomallei* are ultimately reflective of the bacterium's capacity for invasion and replication in all tissue types tested, including primary endothelial, epithelial, fibroblasts, keratinocytes, monocytes, and mesenchymal stem cells (144). The clinical manifestations of melioidosis in humans are summarized in **Figure 1.5**.

Figure 4 | **Clinical manifestations of melioidosis.** Examples of possible clinical presentations of melioidosis: an MRI of the brainstem and cervical spinal cord with inflammatory changes consistent with encephalomyelitis (arrow, part 1); a ring-enhancing lesion with surrounding oedema in the MRI image indicating cerebral abscesses (arrow, part 2); a CT image of prostatic abscesses (arrow, part 3); a CT image of a mediastinal mass (arrow, part 4); a child with tense parotitis (arrow, part 5); X-ray image of severe pneumonia (arrow, part 6); photo of a subcutaneous abscess (arrow, part 7); and an MRI image of osteomyelitis of the distal femur with surrounding inflammation (arrow, part 8). Clinical images 1–4, 6–8 courtesy of Bart J. Currie, Menzies School of Health, Australia. Clinical image 5 is reproduced with permission from (REF. 249), Elsevier.

**Figure 1.5 Melioidosis a complex infectious disease with no pathognomic clinical syndrome**. Taken from Wiersinga et al. (25). Clinical outcomes of infection with *B. pseudomallei* vary greatly, and can occur throughout the human body. Images illustrate the clinical examples of melioidosis manifestations described in the adjacent boxes.

### 1.5.1   Risk factors

One of the greatest challenges in diagnosing melioidosis accurately is distinguishing the clinical manifestations from other more well-known infectious diseases. Several of the clinical outcomes resemble tuberculosis, namely any pulmonary involvement, pericarditis, and infections of the extremities, manifestations that are also comorbidities of diabetes mellitus (DM) (142). Melioidosis pneumonia can also mimic staphylococcal pneumonia as multiple lobes can be affected (143), and has also been misdiagnosed as metastatic lung cancer (145). The risks associated with misidentifying *B. pseudomallei* can be severe, as evidenced by a recent report that revealed several putative *Acinetobacter* spp. were in fact *B. pseudomallei*, a diagnosis mistake that led to 80% mortality in this case (146). Diagnosis by culture is still the gold standard for melioidosis; however, the sensitivity of culture for *B. pseudomallei* can be as low as

60% with negative predictive value of 62% requiring multiple sampling as bacteremia may be intermittent (147). Even so, *B. pseudomallei* is frequently mistaken for a culture contaminant by laboratory technicians who are unfamiliar with the organism (148). Thus, it is important to consider clinical risk factors that predispose individuals to infection and offer potential clues towards a melioidosis diagnosis.

The most common risk factor associated with melioidosis, besides prolonged exposure to contaminated soil and water in endemic regions, is underlying diabetes mellitus. Over half of all melioidosis patients across the world are diabetic, and individuals with DM have a 12-fold greater relative risk for melioidosis (25). In both Northern Australia (149) and Thailand (118), DM is the most significant clinical risk factor for melioidosis. Diabetes leads to a restricted *B. pseudomallei*-specific cellular response in acute infection (150), as well as dysregulated T cell function, decreased phagocytic capacity in macrophage, defective neutrophils, and dysregulated inflammatory signaling leading to a greater risk of septic shock (25). The diabetic risk profile for melioidosis overlaps with that of tuberculosis (151), and both diseases produce a similar interferon-mediated response (type 2 IFN-$\gamma$ and type 1 IFN-$\alpha\beta$) despite being unrelated organisms with different cell-surface PAMPs (152). Interestingly, the antidiabetic drug metformin has been suggested to improve survival odds in patients with *B. pseudomallei* infections (153), in a similar fashion to its reduction of tuberculosis disease severity (154).  While only indirect evidence links beneficial effects of metformin to boosting autophagy and inflammasome activation, glibenclamide, another antidiabetic drug, has been linked to attenuated inflammatory response and reduced overall mortality in melioidosis patients (155).

Besides the diabetes connection, melioidosis is also associated with advanced age, male gender, aboriginal ethnicity, excessive alcohol consumption, chronic lung disease, and chronic renal disease (149). Based on a whole-population analysis, Currie and colleagues (149) determined the relative risk for each of the above categories and predisposition to melioidosis, noting that only 13% of cases (all resulting in no fatalities) had no discernable risk factor. This

20

observation mirrors a previous epidemiological study from Thailand which noted that 36% of cases were not linked to a pre-existing condition (118). The fact that melioidosis severity often hinges on one or several risk factors and pre-existing conditions is echoed by the sentiment that healthy people rarely die from this disease if diagnosed early and correctly (143). Thus, clinical history in addition to occupational and recreational lifestyles must be considered together so that melioidosis can be readily diagnosed and treated rapidly.

### 1.5.2   Public health concerns

As a sapronosis, melioidosis needs to be considered in the context of One Health (156). While most clinical and research attention is focused on human melioidosis, *B. pseudomallei* infections in animals have been reported in Australia, Thailand, India, the Middle East, South Africa, Brazil, France, and Spain (157). In Thailand, the incidence of melioidosis is highest among goats in areas that also have high rates of human cases (158). The susceptibility of goats to melioidosis is also observed in Australia, where *B. pseudomallei* is a concern not only to humans but livestock like sheep, goats, and pigs (159). The first report of melioidosis in Australia was described during an outbreak in sheep in 1949 (160), a year before the first human case was described in 1950 (79). Although zoonotic transmission to humans is very rare (157), there is a risk for transmission through contaminated milk or animal carcasses that should be considered (159). Thus, in the context of animal products, public health measures include pasteurization and identification of contaminated meat (159). Moreover, it is also important to recognize melioidosis as a natural infection in wild animals, both warm and cold blooded, is an important mode of *B. pseudomallei* dissemination to new environments (26). In general, animals can contribute to the intercontinental spread of *B. pseudomallei* through environmental contamination.

*B. pseudomallei* can be imported to temperate regions where it is not naturally endemic via transportation of infected or subclinical asymptomatic animal carriers, leading to increased

risk of environmental contamination (157). Classic examples of this scenario include an outbreak of melioidosis in France linked to the gift of two infected pandas from the emperor of China in 1975 (161) and an outbreak in the UK linked to imported primates from Southeast Asia (162). More recently, *B. pseudomallei* was transmitted from a biosafety level 3 laboratory at the Tulane National Primate Research Center to macaques in a nearby facility (163), raising the possibility for soil contamination in the southeastern US. The spillover event in Louisiana led to a study of the physiochemical properties of soils in southeastern US, which are highly comparable to optimal *B. pseudomallei* niche conditions (164). Therefore, awareness of melioidosis is important even in areas not traditionally associated with *B. pseudomallei* outside of the tropics, or areas deemed non-endemic due to lack of surveillance (164). In the US, melioidosis is not on the CDC list for National Notifiable Conditions (165), however a case definition exists for human melioidosis (166), which could help increase awareness among clinicians and veterinarians (164).

The lack of awareness and surveillance for *B. pseudomallei* is understandable in the US and Europe, which are not considered endemic or major hotspots of melioidosis. However, in Thailand, where *B. pseudomallei* accounts for nearly 3000 deaths per year, melioidosis has not been a top priority or in the notifiable disease system (82). By not reporting melioidosis accurately, the system of communication between microbiologists, clinicians, and epidemiologists is fundamentally broken, leading to a lack of awareness and prevention in at-risk populations worldwide (72, 122). While melioidosis is a global concern due to the dissemination of *B. pseudomallei* in hospitable environments by the movements of humans, animals, and goods, it is not considered a neglected tropical disease by the World Health Organization (WHO). Coupled with this lack of awareness, an estimated worldwide case fatality rate of 54%, according to the most current modeling study (73), efforts are required in the development of effective vaccines for *B. pseudomallei*.

### 1.5.3 Vaccine prospects

A vaccine for *B. pseudomallei* would be a very valuable tool for reducing melioidosis risk in a bio-threat context as well as a significant step in mitigating the public health risk of naturally acquired infections in endemic areas (167). While the select agent status of *B. pseudomallei* has led to an increase in funding for vaccine development in biodefense endeavors, a vaccine for high-risk populations with DM would be a cost-effective approach for developing countries (167). However, it has been noted that there are differing needs and methods of developing vaccines for military persons versus civilians; a vaccine for the latter population needs to be modified to protect immunocompromised hosts who are infected via skin inoculation rather than inhalation (168). Although there is no currently available melioidosis vaccine, this is an active area of research with several promising candidates that are close to human clinical trials (169). This section will discuss a range of *B. pseudomallei* vaccine candidates including live attenuated vaccines, sub-unit vaccines, and multi-component strategies including polysaccharide antigens and glycoconjugates. Advancement in this area, regardless of complete sterilizing immunity, would likely contribute to reduced disease severity and mitigate the high mortality rate related to death from septic shock within 48 hours for half of all Thai cases (167).

Vaccine development for *B. pseudomallei* must consider the associated public health risks separately from military needs, high-risk individuals with pre-existing conditions, and standardized animal models (71). To date, the most common vaccine strategy explored has been the use of live attenuated *B. pseudomallei* mutants, which have been shown to generate protective immunity in mouse models (170-173). However, live attenuated vaccines pose risks of potential reversion to pathogenic *B. pseudomallei* or establishment of latent infections, especially in immunocompromised patients with pre-existing conditions (167). Even so, research with live attenuated vaccines has characterized important aspects of protective immunity (169), suggesting that coupled with high antibody levels, a robust cell-mediated

response is essential for both protection and clearance of *B. pseudomallei* in mice (174, 175).

Indeed, melioidosis survival in humans is associated with strong CD4+ and CD8+ T-cell

responses, whereas this kind of cellular immunity is impaired in high-risk diabetic patients (150).

One of the first models for T-cell-mediated immunity to *B. pseudomallei* showed that

CD4+ T cells in mice were responsive to a type III secretion system (T3SS) effector protein

BopE and T3SS translocator protein BipD, while CD8+ T cells were less important (176). In

addition to the T3SS clusters, *B. pseudomallei* utilizes type VI secretion systems (T6SS) for

intracellular survival and propagation within a host (44), specifically by inducing cell fusion and

cytotoxicity via a syringe-like structure (177). Recently, a live attenuated mutant with a

disruption in hemolysin-coregulated protein 1 (Hcp1) of the T6SS apparatus as well as a ferric

siderophore complex protein TonB, exhibited full protection against lethal doses of aerosolized

*B. pseudomallei* (178). Interestingly, this vaccine induced a strong humoral response with *B.

pseudomallei*-specific serum IgG antibodies, while CD4+ and CD8+ T cells were less important

for direct immunity (178). The *Δhcp1/ΔtonB* live attenuated vaccine elicited a similar humoral

response that was previously seen in a *purM* mutant strain of *B. pseudomallei* that generated

systemic protection following cutaneous immunization in mice (179). Thus, although a combined

cellular and humoral response was thought to be required for full protection, evidence suggests

that live attenuated vaccine strains may have distinct immune responses that are determined by

other factors (178, 179).

An important factor that determines distinct immune response outcomes to *B.

pseudomallei* challenge is the specific lipopolysaccharide (LPS) type expressed by the bacterial

strain (180). Surface antigens including capsular polysaccharide (CPS) and LPS have been

shown to provide partial protection to *B. pseudomallei* infection (71), with LPS specifically

driving immune response by initiating cytokine production (181). CPS, LPS, and other

membrane antigens can be shuttled in outer membrane vesicles (OMVs) as a platform for

subunit vaccines (182). OMV-based subunit vaccines have been shown to produce protective

humoral responses to *B. pseudomallei* in nonhuman primate experimental melioidosis challenge without any toxicity or risks associated with attenuated vaccines (183, 184). Considering that *B. pseudomallei* OMV-based vaccines provided protection against both inhalational and septicemic melioidosis in mice (182, 183), and their safety in a nonhuman primate model (184), this approach is a promising prospect for clinical human trials.

Most of the current research approaches incorporate several of the above strategies for development of multi-component vaccines that aim to account for the diverse virulence mechanisms and strain heterogeneity of *B. pseudomallei* (185). To optimize protection for a genomic and metabolic diverse pathogen such as *B. pseudomallei*, it may be necessary to incorporate many antigenic epitopes into a multivalent vaccine (186). While none of the current vaccine front-runners provide sterilizing immunity, this effort will likely require a larger array of antigens as well as a standardized approach to vaccine testing and animal models (185, 186). The Steering Group on Melioidosis Vaccine Development (SGMVD) was established specifically for this purpose, aiming to identify candidate vaccines for advancement to early human clinical studies (168). Candidate vaccines are likely to be tested in high-risk populations in areas where melioidosis is endemic and the threat of climate-driven outbreaks is greatest, specifically Southeast Asia and Northern Australia during the monsoon seasons.

### 1.6 Climate factors affecting melioidosis outbreaks

Melioidosis has long been associated with periods of heavy rain and high winds (119, 187-190), the typical monsoon season in tropical Southeast Asia and Northern Australia, where it is advised that at-risk persons stay indoors to avoid aerosolized *B. pseudomallei* (191). In endemic areas, melioidosis cases cluster around rainfall and extreme weather events (192), which are unavoidable in daily life. 75% of Thai melioidosis cases (119) and 85% of Australian cases (193) are associated with the rainy season. Melioidosis cases are correlated to total rainfall in these regions and it has been reported that rainfall in the two weeks before a patient is

admitted to hospital is an independent risk factor for pneumonia, septic shock, and death (190, 193). Aerosolization of *B. pseudomallei* in water droplets during periods of heavy rain likely leads to inhalational melioidosis, which can be more severe than percutaneous inoculation (190, 194). Some of the first indications of the severity of inhalational melioidosis were observed during the Vietnam War, where otherwise healthy soldiers died from septicemic *B. pseudomallei* infections (195). Incidences of melioidosis in soldiers during and after the Vietnam War were more prevalent in helicopter crews, presumably due to the aerosolization of *B. pseudomallei* in water and dust generated by helicopter blades (196). Furthermore, the development of subclinical and chronic melioidosis (197), that can be activated years after exposure (198), has earned *B. pseudomallei* another nickname – the "Vietnamese time bomb" (199). In the modern tropics, with predicted temperature increases, differences in precipitation patterns, and amplified extreme weather events (192), this moniker should be updated to a "tropical time bomb" (199).

Analysis of over two decades of climatic data in relation to melioidosis cases revealed a significant positive correlation between disease and higher groundwater levels (200). Consistent with this correlation is the observation that *B. pseudomallei* is associated with areas of higher soil moisture (115). Additionally, it has been hypothesized that the first heavy rain of the season causes increased microbial activity stimulated by nitrogen mineralization and the conversion to ammonium and nitrate (200). This can cause a rapid metabolic shift in denitrifying bacteria that readily exploit fluctuating resources (201). Interestingly, the seasonality of soil drying and rewetting can drastically influence nutrient cycling, leading to nutrient flushes of C, N, and P, that enhance microbial activity in organisms that are able to resist these stresses (202). Thus, seasonal fluctuations in soil moisture and changing groundwater levels are likely associated with increased incidences of *B. pseudomallei* exposure in endemic areas (200). The association between increasing groundwater and melioidosis was dramatically displayed in the wet season of Northern Australia between 2009 and 2010, which had unusually high early-season rainfall and more melioidosis cases than diagnosed in the previous 20 years (203).

It is predicted that increases in total annual rainfall throughout the tropics will increase melioidosis risk in this region, and that extreme weather events will expand the endemic range of *B. pseudomallei* (192). Tropical cyclones have been shown to leave a trail of melioidosis cases in their tracks along the Northern Territory to Western Australia, carrying specific sequence types across geographical boundaries (192). Similarly, climactic predictors of melioidosis outbreaks in Southeast Asia are dependent on wind speed and wind direction, with respiratory infections more common during windy periods (204). Evidently, climate-driven changes to tropical habitats have impacts on both seasonal incidence of melioidosis as well as the geographical distribution of *B. pseudomallei*; however, it remains to be determined to what extent bacterial strains are transported by weather events and whether they can survive and become endemic in temperate soils (192).

## 1.7 Bioremediation measures

One of the least studied areas related to *B. pseudomallei* is environmental control of the organism through bioremediation measures. Several reports have highlighted the biotechnological capabilities of non-pathogenic *Burkholderia* spp. to promote agriculture and clean contaminated soils via degradation of toxic compounds (205-207). However, research aimed at inhibiting *B. pseudomallei* in soil is scarce, reflecting the tenacity and persistence of this organism in the environment. Early studies tested calcium oxide (quicklime), a strong base and potent disinfectant for increasing soil pH and inhibiting *B. pseudomallei* (208). However, it was determined that only a concentration of 40% (w/w) quicklime was effective to inhibit *B. pseudomallei*, and only for several weeks (208). Physicochemical properties of soils have been also been experimentally modified to increase pH, C/N ratios, and NaCl, however it as determined that *B. pseudomallei* can survive extreme levels of these stressors (209). More recently, chitosan, a chitin-derived biopolymer, was shown to disrupt *B. pseudomallei* cell membrane, with potential for this compound to be tested in soil applications (210). Biological

control agents have also been examined for inhibitory activity against *B. pseudomallei,* suggesting that metabolites from soil bacteria such as *Bacillus amyloliquefaciens* can be used for bio-control purposes (211). And although free-living amoebae have been hypothesized to be reservoirs for *B. pseudomallei* persistence in the environment (212), a recent study showed that an *Acanthamoeba* sp. grazes on *B. pseudomallei*, which promotes amoeba growth in lab co-cultivation conditions (213). The similarities between amoebae and human macrophage may shed light on the success of *B. pseudomallei* as an intracellular pathogen as well as its tenacity in the environment (214).

## 1.8 Conclusion

*B. pseudomallei* is a resilient environmental organism that can survive extreme conditions in tropical regions worldwide. The causative agent of melioidosis can be transported around the globe via human, animal, trade, and weather routes. Anthropogenic disturbances of environments where *B. pseudomallei* is endemic are important determinants of melioidosis epidemiology. Factors such as irrigation, localized nutrient imbalances caused by N-based fertilizers and animal wastes, and introduction of non-native plants are linked to increased *B. pseudomallei* detection from soils. In the environment, *B. pseudomallei* lives in soils and surface waters, existing in biofilm communities rather than mono-dispersed individual cells (112, 114). The propensity for *B. pseudomallei* survival as a biofilm in the environment no doubt influences the ability of this organism to persist as a biofilm in human and animal hosts causing recalcitrant disease (215). One of the most important physiological features of *B. pseudomallei* related to antibiotic tolerance and persistence, biofilm formation is determined by a suite of polysaccharide gene clusters.  The next chapter will discuss components of the extracellular polymeric substance (EPS) matrix that make up the *B. pseudomallei* biofilm structure.

# References

1.	Coenye T, Vandamme P. Diversity and significance of *Burkholderia* species occupying diverse ecological niches. Environ Microbiol. 2003;5(9):719-29.
2.	Yabuuchi E, Kosako Y, Oyaizu H, Yano I, Hotta H, Hashimoto Y, Ezaki T, Arakawa M. Proposal of *Burkholderia* gen. nov. and transfer of seven species of the genus *Pseudomonas* homology group II to the new genus, with the type species *Burkholderia cepacia* (Palleroni and Holmes 1981) comb. nov. Microbiol Immunol. 1992;36(12):1251-75.
3.	Kim M, Kim WS, Tripathi BM, Adams J. Distinct bacterial communities dominate tropical and temperate zone leaf litter. Microb Ecol. 2014;67(4):837-48.
4.	Salles JF, van Veen JA, van Elsas JD. Multivariate analyses of *Burkholderia* species in soil: effect of crop and land use history. Appl Environ Microbiol. 2004;70(7):4012-20.
5.	Estrada-De Los Santos P, Bustillos-Cristales R, Caballero-Mellado J. *Burkholderia*, a genus rich in plant-associated nitrogen fixers with wide environmental and geographic distribution. Appl Environ Microbiol. 2001;67(6):2790-8.
6.	Ramette A, LiPuma JJ, Tiedje JM. Species abundance and diversity of *Burkholderia cepacia* complex in the environment. Appl Environ Microbiol. 2005;71(3):1193-201.
7.	Draghi WO, Degrossi J, Bialer M, Brelles-Marino G, Abdian P, Soler-Bistue A, Wall L, Zorreguieta A. Biodiversity of cultivable *Burkholderia* species in Argentinean soils under no-till agricultural practices. PLoS One. 2018;13(7):e0200651.
8.	Bontemps C, Elliott GN, Simon MF, Dos Reis Junior FB, Gross E, Lawton RC, Neto NE, de Fatima Loureiro M, De Faria SM, Sprent JI, James EK, Young JP. *Burkholderia* species are ancient symbionts of legumes. Mol Ecol. 2010;19(1):44-52.
9.	Compant S, Nowak J, Coenye T, Clement C, Ait Barka E. Diversity and occurrence of *Burkholderia* spp. in the natural environment. FEMS Microbiol Rev. 2008;32(4):607-26.
10.	Estrada-de los Santos P, Rojas-Rojas, F.U., Tapia-Garcia, E.Y., Vasquez-Murrieta, M.S., Hirsch, A.M To split or not to split: an opinion on dividing the genus *Burkholderia*. Annals of Microbiology. 2016;66(3):1303-14.
11.	Sawana A, Adeolu M, Gupta RS. Molecular signatures and phylogenomic analysis of the genus *Burkholderia*: proposal for division of this genus into the emended genus *Burkholderia* containing pathogenic organisms and a new genus *Paraburkholderia* gen. nov. harboring environmental species. Front Genet. 2014;5:429.
12.	Sfeir MM. Burkholderia cepacia complex infections: More complex than the bacterium name suggest. J Infect. 2018;77(3):166-70.
13.	Mahenthiralingam E, Urban TA, Goldberg JB. The multifarious, multireplicon *Burkholderia cepacia* complex. Nat Rev Microbiol. 2005;3(2):144-56.
14.	De Smet B, Mayo M, Peeters C, Zlosnik JE, Spilker T, Hird TJ, LiPuma JJ, Kidd TJ, Kaestli M, Ginther JL, Wagner DM, Keim P, Bell SC, Jacobs JA, Currie BJ, Vandamme P. *Burkholderia stagnalis* sp. nov. and *Burkholderia territorii* sp. nov., two novel *Burkholderia cepacia* complex species from environmental and human sources. Int J Syst Evol Microbiol. 2015;65(7):2265-71.
15.	Whitmore A, Krishnaswami CS. A Hitherto Undescribed Infective Disease in Rangoon. Ind Med Gaz. 1912;47(7):262-7.
16.	Whitmore A. An Account of a Glanders-like Disease occurring in Rangoon. J Hyg (Lond). 1913;13(1):1-34 1.
17.	White NJ. Melioidosis. Lancet. 2003;361(9370):1715-22.
18.	Dance DA. Melioidosis: the tip of the iceberg? Clin Microbiol Rev. 1991;4(1):52-60.

19.	Cheng AC, Currie BJ. Melioidosis: epidemiology, pathophysiology, and management. Clin Microbiol Rev. 2005;18(2):383-416.
20.	Zilinskas RA. A brief history of biological weapons programmes and the use of animal pathogens as biological warfare agents. Rev Sci Tech. 2017;36(2):415-22.
21.	Program FSA. Select Agents and Toxins List https://www.selectagents.gov/SelectAgentsandToxinsList.html2017.
22.	Hemarajata P, Baghdadi JD, Hoffman R, Humphries RM. *Burkholderia pseudomallei*: Challenges for the Clinical Microbiology Laboratory. J Clin Microbiol. 2016;54(12):2866-73.
23.	Stanton AT, Fletcher W. Melioidosis; a new disease of the tropics. Kuala Lumpur,: F. M. S. govt. print. off.; 1921. 1 p.l., 2 p. p.
24.	Yee KC, Lee MK, Chua CT, Puthucheary SD. Melioidosis, the great mimicker: a report of 10 cases from Malaysia. J Trop Med Hyg. 1988;91(5):249-54.
25.	Wiersinga WJ, Virk HS, Torres AG, Currie BJ, Peacock SJ, Dance DAB, Limmathurotsakul D. Melioidosis. Nat Rev Dis Primers. 2018;4:17107.
26.	Dance DA. 'Innocent Bystanders' – Melioidosis, a Model Sapronosis. 8th World Melioidosis Congress; 2016; Cebu, Philippines.
27.	Liu B, Koo GC, Yap EH, Chua KL, Gan YH. Model of differential susceptibility to mucosal *Burkholderia pseudomallei* infection. Infect Immun. 2002;70(2):504-11.
28.	Tuanyok A, Tom M, Dunbar J, Woods DE. Genome-wide expression analysis of *Burkholderia pseudomallei* infection in a hamster model of acute melioidosis. Infect Immun. 2006;74(10):5465-76.
29.	Kuris AM, Lafferty KD, Sokolow SH. Sapronosis: a distinctive type of infectious agent. Trends Parasitol. 2014;30(8):386-93.
30.	Sahl JW, Vazquez AJ, Hall CM, Busch JD, Tuanyok A, Mayo M, Schupp JM, Lummis M, Pearson T, Shippy K, Colman RE, Allender CJ, Theobald V, Sarovich DS, Price EP, Hutcheson A, Korlach J, LiPuma JJ, Ladner J, Lovett S, Koroleva G, Palacios G, Limmathurotsakul D, Wuthiekanun V, Wongsuwan G, Currie BJ, Keim P, Wagner DM. The Effects of Signal Erosion and Core Genome Reduction on the Identification of Diagnostic Markers. MBio. 2016;7(5).
31.	Whitlock GC, Estes DM, Torres AG. Glanders: off to the races with *Burkholderia mallei*. FEMS Microbiol Lett. 2007;277(2):115-22.
32.	Tuanyok A, Mayo M, Scholz H, Hall CM, Allender CJ, Kaestli M, Ginther J, Spring-Pearson S, Bollig MC, Stone JK, Settles EW, Busch JD, Sidak-Loftis L, Sahl JW, Thomas A, Kreutzer L, Georgi E, Gee JE, Bowen RA, Ladner JT, Lovett S, Koroleva G, Palacios G, Wagner DM, Currie BJ, Keim P. *Burkholderia humptydooensis* sp. nov., a New Species Related to *Burkholderia thailandensis* and the Fifth Member of the *Burkholderia pseudomallei* Complex. Appl Environ Microbiol. 2017;83(5).
33.	Holden MTG, Titball RW, Peacock SJ, Cerdeno-Tarraga AM, Atkins T, Crossman LC, Pitt T, Churcher C, Mungall K, Bentley SD, Sebaihia M, Thomson NR, Bason N, Beacham IR, Brooks K, Brown KA, Brown NF, Challis GL, Cherevach I, Chillingworth T, Cronin A, Crossett B, Davis P, DeShazer D, Feltwell T, Fraser A, Hance Z, Hauser H, Holroyd S, Jagels K, Keith KE, Maddison M, Moule S, Price C, Quail MA, Rabbinowitsch E, Rutherford K, Sanders M, Simmonds M, Songsivilai S, Stevens K, Tumapa S, Vesaratchavest M, Whitehead S, Yeats C, Barrell BG, Oyston PCF, Parkhill J. Genornic plasticity of the causative agent of melioidosis, *Burkholderia pseudomallei*. Proc Natl Acad Sci U S A. 2004;101(39):14240-5.
34.	Majerczyk CD, Brittnacher MJ, Jacobs MA, Armour CD, Radey MC, Bunt R, Hayden HS, Bydalek R, Greenberg EP. Cross-species comparison of the *Burkholderia pseudomallei*, *Burkholderia thailandensis*, and *Burkholderia mallei* quorum-sensing regulons. J Bacteriol. 2014;196(22):3862-71.

35. Saikh KU, Mott TM. Innate immune response to *Burkholderia mallei*. Curr Opin Infect Dis. 2017;30(3):297-302.

36. Memisevic V, Zavaljevski N, Pieper R, Rajagopala SV, Kwon K, Townsend K, Yu C, Yu X, DeShazer D, Reifman J, Wallqvist A. Novel *Burkholderia mallei* virulence factors linked to specific host-pathogen protein interactions. Mol Cell Proteomics. 2013;12(11):3036-51.

37. Bochkareva OO, Moroz EV, Davydov, II, Gelfand MS. Genome rearrangements and selection in multi-chromosome bacteria *Burkholderia* spp. BMC Genomics. 2018;19(1):965.

38. Godoy D, Randle G, Simpson AJ, Aanensen DM, Pitt TL, Kinoshita R, Spratt BG. Multilocus sequence typing and evolutionary relationships among the causative agents of melioidosis and glanders, *Burkholderia pseudomallei* and *Burkholderia mallei*. J Clin Microbiol. 2003;41(5):2068-79.

39. Moore RA, Reckseidler-Zenteno S, Kim H, Nierman W, Yu Y, Tuanyok A, Warawa J, DeShazer D, Woods DE. Contribution of gene loss to the pathogenic evolution of *Burkholderia pseudomallei* and *Burkholderia mallei*. Infect Immun. 2004;72(7):4172-87.

40. Maurelli AT, Fernandez RE, Bloch CA, Rode CK, Fasano A. "Black holes" and bacterial pathogenicity: a large genomic deletion that enhances the virulence of *Shigella* spp. and enteroinvasive *Escherichia coli*. Proc Natl Acad Sci U S A. 1998;95(7):3943-8.

41. Sirisinha S, Anuntagool N, Intachote P, Wuthiekanun V, Puthucheary SD, Vadivelu J, White NJ. Antigenic differences between clinical and environmental isolates of *Burkholderia pseudomallei*. Microbiol Immunol. 1998;42(11):731-7.

42. Nierman WC, DeShazer D, Kim HS, Tettelin H, Nelson KE, Feldblyum T, Ulrich RL, Ronning CM, Brinkac LM, Daugherty SC, Davidsen TD, Deboy RT, Dimitrov G, Dodson RJ, Durkin AS, Gwinn ML, Haft DH, Khouri H, Kolonay JF, Madupu R, Mohammoud Y, Nelson WC, Radune D, Romero CM, Sarria S, Selengut J, Shamblin C, Sullivan SA, White O, Yu Y, Zafar N, Zhou L, Fraser CM. Structural flexibility in the *Burkholderia mallei* genome. Proc Natl Acad Sci U S A. 2004;101(39):14246-51.

43. Schell MA, Ulrich RL, Ribot WJ, Brueggemann EE, Hines HB, Chen D, Lipscomb L, Kim HS, Mrazek J, Nierman WC, Deshazer D. Type VI secretion is a major virulence determinant in *Burkholderia mallei*. Mol Microbiol. 2007;64(6):1466-85.

44. Galyov EE, Brett PJ, DeShazer D. Molecular insights into *Burkholderia pseudomallei* and *Burkholderia mallei* pathogenesis. Annu Rev Microbiol. 2010;64:495-517.

45. Podnecky NL, Rhodes KA, Schweizer HP. Efflux pump-mediated drug resistance in *Burkholderia*. Front Microbiol. 2015;6:305.

46. Rhodes KA, Schweizer HP. Antibiotic resistance in *Burkholderia* species. Drug Resist Updat. 2016;28:82-90.

47. Franke J, Ishida K, Hertweck C. Genomics-driven discovery of burkholderic acid, a noncanonical, cryptic polyketide from human pathogenic *Burkholderia* species. Angew Chem Int Ed Engl. 2012;51(46):11611-5.

48. Biggins JB, Ternei MA, Brady SF. Malleilactone, a polyketide synthase-derived virulence factor encoded by the cryptic secondary metabolome of *Burkholderia pseudomallei* group pathogens. J Am Chem Soc. 2012;134(32):13192-5.

49. Losada L, Ronning CM, DeShazer D, Woods D, Fedorova N, Kim HS, Shabalina SA, Pearson TR, Brinkac L, Tan P, Nandi T, Crabtree J, Badger J, Beckstrom-Sternberg S, Saqib M, Schutzer SE, Keim P, Nierman WC. Continuing evolution of *Burkholderia mallei* through genome reduction and large-scale rearrangements. Genome Biol Evol. 2010;2:102-16.

50. Price EP, Sarovich DS, Mayo M, Tuanyok A, Drees KP, Kaestli M, Beckstrom-Sternberg SM, Babic-Sternberg JS, Kidd TJ, Bell SC, Keim P, Pearson T, Currie BJ. Within-host

evolution of *Burkholderia pseudomallei* over a twelve-year chronic carriage infection. MBio. 2013;4(4).

51.     Hayden HS, Lim R, Brittnacher MJ, Sims EH, Ramage ER, Fong C, Wu Z, Crist E, Chang J, Zhou Y, Radey M, Rohmer L, Haugen E, Gillett W, Wuthiekanun V, Peacock SJ, Kaul R, Miller SI, Manoil C, Jacobs MA. Evolution of *Burkholderia pseudomallei* in recurrent melioidosis. PLoS One. 2012;7(5):e36507.

52.     Wuthiekanun V, Amornchai P, Saiprom N, Chantratita N, Chierakul W, Koh GC, Chaowagul W, Day NP, Limmathurotsakul D, Peacock SJ. Survey of antimicrobial resistance in clinical *Burkholderia pseudomallei* isolates over two decades in Northeast Thailand. Antimicrob Agents Chemother. 2011;55(11):5388-91.

53.     Yu Y, Kim HS, Chua HH, Lin CH, Sim SH, Lin D, Derr A, Engels R, DeShazer D, Birren B, Nierman WC, Tan P. Genomic patterns of pathogen evolution revealed by comparison of *Burkholderia pseudomallei*, the causative agent of melioidosis, to avirulent *Burkholderia thailandensis*. BMC Microbiol. 2006;6:46.

54.     Haraga A, West TE, Brittnacher MJ, Skerrett SJ, Miller SI. *Burkholderia thailandensis* as a model system for the study of the virulence-associated type III secretion system of *Burkholderia pseudomallei*. Infect Immun. 2008;76(11):5402-11.

55.     Glass MB, Gee JE, Steigerwalt AG, Cavuoti D, Barton T, Hardy RD, Godoy D, Spratt BG, Clark TA, Wilkins PP. Pneumonia and septicemia caused by *Burkholderia thailandensis* in the United States. J Clin Microbiol. 2006;44(12):4601-4.

56.     Deshazer D. Virulence of clinical and environmental isolates of *Burkholderia oklahomensis* and *Burkholderia thailandensis* in hamsters and mice. FEMS Microbiol Lett. 2007;277(1):64-9.

57.     Brett PJ, Deshazer D, Woods DE. Characterization of *Burkholderia pseudomallei* and *Burkholderia pseudomallei*-like strains. Epidemiol Infect. 1997;118(2):137-48.

58.     Smith MD, Angus BJ, Wuthiekanun V, White NJ. Arabinose assimilation defines a nonvirulent biotype of *Burkholderia pseudomallei*. Infect Immun. 1997;65(10):4319-21.

59.     Ong C, Ooi CH, Wang D, Chong H, Ng KC, Rodrigues F, Lee MA, Tan P. Patterns of large-scale genomic variation in virulent and avirulent *Burkholderia* species. Genome Res. 2004;14(11):2295-307.

60.     Anuntagool N, Intachote P, Wuthiekanun V, White NJ, Sirisinha S. Lipopolysaccharide from nonvirulent Ara+ *Burkholderia pseudomallei* isolates is immunologically indistinguishable from lipopolysaccharide from virulent Ara- clinical isolates. Clin Diagn Lab Immunol. 1998;5(2):225-9.

61.     Trakulsomboon S, Dance DA, Smith MD, White NJ, Pitt TL. Ribotype differences between clinical and environmental isolates of *Burkholderia pseudomallei*. J Med Microbiol. 1997;46(7):565-70.

62.     Ngamdee W, Tandhavanant S, Wikraiphat C, Reamtong O, Wuthiekanun V, Salje J, Low DA, Peacock SJ, Chantratita N. Competition between *Burkholderia pseudomallei* and *B. thailandensis*. BMC Microbiol. 2015;15:56.

63.     Majerczyk C, Brittnacher M, Jacobs M, Armour CD, Radey M, Schneider E, Phattarasokul S, Bunt R, Greenberg EP. Global analysis of the *Burkholderia thailandensis* quorum sensing-controlled regulon. J Bacteriol. 2014;196(7):1412-24.

64.     Tseng BS, Majerczyk CD, Passos da Silva D, Chandler JR, Greenberg EP, Parsek MR. Quorum Sensing Influences *Burkholderia thailandensis* Biofilm Development and Matrix Production. J Bacteriol. 2016;198(19):2643-50.

65.     Garcia EC, Perault AI, Marlatt SA, Cotter PA. Interbacterial signaling via *Burkholderia* contact-dependent growth inhibition system proteins. Proc Natl Acad Sci U S A. 2016;113(29):8296-301.

66. Ocasio AB, Cotter PA. CDI/CDS system-encoding genes of *Burkholderia thailandensis* are located in a mobile genetic element that defines a new class of transposon. PLoS Genet. 2019;15(1):e1007883.

67. Duerkop BA, Varga J, Chandler JR, Peterson SB, Herman JP, Churchill ME, Parsek MR, Nierman WC, Greenberg EP. Quorum-sensing control of antibiotic synthesis in *Burkholderia thailandensis*. J Bacteriol. 2009;191(12):3909-18.

68. Seyedsayamdost MR, Chandler JR, Blodgett JA, Lima PS, Duerkop BA, Oinuma K, Greenberg EP, Clardy J. Quorum-sensing-regulated bactobolin production by *Burkholderia thailandensis* E264. Org Lett. 2010;12(4):716-9.

69. Hantrakun V, Thaipadungpanit J, Rongkard P, Srilohasin P, Amornchai P, Langla S, Mukaka M, Chantratita N, Wuthiekanun V, Dance DAB, Day NPJ, Peacock SJ, Limmathurotsakul D. Presence of *B. thailandensis* and *B. thailandensis* expressing *B. pseudomallei*-like capsular polysaccharide in Thailand, and their associations with serological response to *B. pseudomallei*. PLoS Negl Trop Dis. 2018;12(1):e0006193.

70. Garcia EC, Cotter PA. *Burkholderia thailandensis*: Growth and Laboratory Maintenance. Curr Protoc Microbiol. 2016;42:4C 1 -7.

71. Hatcher CL, Muruato LA, Torres AG. Recent Advances in *Burkholderia mallei* and *B. pseudomallei* Research. Curr Trop Med Rep. 2015;2(2):62-9.

72. Limmathurotsakul D. Burden of melioidosis worldwide was predicted, what we should do next? World Melioidosis Congress; 2016; Cebu, Philippines.

73. Limmathurotsakul D, Golding N, Dance DA, Messina JP, Pigott DM, Moyes CL, Rolim DB, Bertherat E, Day NP, Peacock SJ, Hay SI. Predicted global distribution of *Burkholderia pseudomallei* and burden of melioidosis. Nat Microbiol. 2016;1:15008.

74. Chewapreecha C, Holden MT, Vehkala M, Valimaki N, Yang Z, Harris SR, Mather AE, Tuanyok A, De Smet B, Le Hello S, Bizet C, Mayo M, Wuthiekanun V, Limmathurotsakul D, Phetsouvanh R, Spratt BG, Corander J, Keim P, Dougan G, Dance DA, Currie BJ, Parkhill J, Peacock SJ. Global and regional dissemination and evolution of *Burkholderia pseudomallei*. Nat Microbiol. 2017;2:16263.

75. Pearson T, Giffard P, Beckstrom-Sternberg S, Auerbach R, Hornstra H, Tuanyok A, Price EP, Glass MB, Leadem B, Beckstrom-Sternberg JS, Allan GJ, Foster JT, Wagner DM, Okinaka RT, Sim SH, Pearson O, Wu Z, Chang J, Kaul R, Hoffmaster AR, Brettin TS, Robison RA, Mayo M, Gee JE, Tan P, Currie BJ, Keim P. Phylogeographic reconstruction of a bacterial species with high levels of lateral gene transfer. BMC Biol. 2009;7:78.

76. Chapple SN, Price EP, Sarovich DS, McRobb E, Mayo M, Kaestli M, Spratt BG, Currie BJ. Burkholderia pseudomallei Genotype Distribution in the Northern Territory, Australia. Am J Trop Med Hyg. 2016;94(1):68-72.

77. Vesaratchavest M, Tumapa S, Day NP, Wuthiekanun V, Chierakul W, Holden MT, White NJ, Currie BJ, Spratt BG, Feil EJ, Peacock SJ. Nonrandom distribution of *Burkholderia pseudomallei* clones in relation to geographical location and virulence. J Clin Microbiol. 2006;44(7):2553-7.

78. Dale J, Price EP, Hornstra H, Busch JD, Mayo M, Godoy D, Wuthiekanun V, Baker A, Foster JT, Wagner DM, Tuanyok A, Warner J, Spratt BG, Peacock SJ, Currie BJ, Keim P, Pearson T. Epidemiological tracking and population assignment of the non-clonal bacterium, *Burkholderia pseudomallei*. PLoS Negl Trop Dis. 2011;5(12):e1381.

79. Smith S, Hanson J, Currie BJ. Melioidosis: An Australian Perspective. Trop Med Infect Dis. 2018;3(1).

80. Baker AL, Pearson T, Sahl JW, Hepp C, Price EP, Sarovich DS, Mayo M, Tuanyok A, Currie BJ, Keim P, Warner J. *Burkholderia pseudomallei* distribution in Australasia is linked to paleogeographic and anthropogenic history. PLoS One. 2018;13(11):e0206845.

81. Price EP, Sarovich DS, Smith EJ, MacHunter B, Harrington G, Theobald V, Hall CM, Hornstra HM, McRobb E, Podin Y, Mayo M, Sahl JW, Wagner DM, Keim P, Kaestli M, Currie BJ. Unprecedented Melioidosis Cases in Northern Australia Caused by an Asian *Burkholderia pseudomallei* Strain Identified by Using Large-Scale Comparative Genomics. Appl Environ Microbiol. 2016;82(3):954-63.

82. Hinjoy S, Hantrakun V, Kongyu S, Kaewrakmuk J, Wangrangsimakul T, Jitsuronk S, Saengchun W, Bhengsri S, Akarachotpong T, Thamthitiwat S, Sangwichian O, Anunnatsiri S, Sermswan RW, Lertmemongkolchai G, Tharinjaroen CS, Preechasuth K, Udpaun R, Chuensombut P, Waranyasirikul N, Anudit C, Narenpitak S, Jutrakul Y, Teparrukkul P, Teerawattanasook N, Thanvisej K, Suphan A, Sukbut P, Ploddi K, Sirichotirat P, Chiewchanyon B, Rukseree K, Hongsuwan M, Wongsuwan G, Sunthornsut P, Wuthiekanun V, Sachaphimukh S, Wannapinij P, Chierakul W, Chewapreecha C, Thaipadungpanit J, Chantratita N, Korbsrisate S, Taunyok A, Dunachie S, Palittapongarnpim P, Sirisinha S, Kitphati R, Iamsirithaworn S, Chaowagul W, Chetchotisak P, Whistler T, Wongratanacheewin S, Limmathurotsakul D. Melioidosis in Thailand: Present and Future. Trop Med Infect Dis. 2018;3(2):38.

83. Allou N, Martinet O, Allyn J, Bouchet B, Jaffar-Bandjee MC, Galas T, Traversier N, Belmonte O. Emergence of melioidosis in the Indian Ocean region: Two new cases and a literature review. PLoS Negl Trop Dis. 2017;11(12):e0006018.

84. Rakotondrasoa A, Issack MI, Garin B, Biot F, Valade E, Wattiau P, Allou N, Belmonte O, Bibi J, Price EP, Collard JM. Melioidosis in the Western Indian Ocean and the Importance of Improving Diagnosis, Surveillance, and Molecular Typing. Trop Med Infect Dis. 2018;3(1).

85. Balaji V, Perumalla S, Perumal R, Inbanathan FY, Rajamani Sekar SK, Paul MM, Sahni RD, Prakash JAJ, Iyadurai R. Multi locus sequence typing of *Burkholderia pseudomallei* isolates from India unveils molecular diversity and confers regional association in Southeast Asia. PLoS Negl Trop Dis. 2018;12(6):e0006558.

86. Currie BJ, Dance DA, Cheng AC. The global distribution of *Burkholderia pseudomallei* and melioidosis: an update. Trans R Soc Trop Med Hyg. 2008;102 Suppl 1:S1-4.

87. Tauran PM, Wahyunie S, Saad F, Dahesihdewi A, Graciella M, Muhammad M, Lestari DC, Aryati A, Parwati I, Loho T, Pratiwi DIN, Mutiawati VK, Loesnihari R, Anggraini D, Rahayu SI, Wulan WN, Antonjaya U, Dance DAB, Currie BJ, Limmathuthurotsakul D, Arif M, Aman AT, Budayanti NNS, Iskandriati D. Emergence of Melioidosis in Indonesia and Today's Challenges. Trop Med Infect Dis. 2018;3(1).

88. San Martin PFM, Chua JC, Bautista RLP, Nailes JM, Panaligan MM, Dance DAB. Melioidosis in the Philippines. Trop Med Infect Dis. 2018;3(3).

89. Mukhopadhyay C, Shaw T, Varghese GM, Dance DAB. Melioidosis in South Asia (India, Nepal, Pakistan, Bhutan and Afghanistan). Trop Med Infect Dis. 2018;3(2).

90. Win MM, Ashley EA, Zin KN, Aung MT, Swe MMM, Ling CL, Nosten F, Thein WM, Zaw NN, Aung MY, Tun KM, Dance DAB, Smithuis FM. Melioidosis in Myanmar. Trop Med Infect Dis. 2018;3(1).

91. Chansrichavala P, Wongsuwan N, Suddee S, Malasit M, Hongsuwan M, Wannapinij P, Kitphati R, Day NP, Michie S, Peacock SJ, Limmathurotsakul D. Public awareness of melioidosis in Thailand and potential use of video clips as educational tools. PLoS One. 2015;10(3):e0121311.

92. Birnie E, Wiersinga WJ, Limmathurotsakul D, Grobusch MP. Melioidosis in Africa: should we be looking more closely? Future Microbiol. 2015;10(2):273-81.

93. Sarovich DS, Garin B, De Smet B, Kaestli M, Mayo M, Vandamme P, Jacobs J, Lompo P, Tahita MC, Tinto H, Djaomalaza I, Currie BJ, Price EP. Phylogenomic Analysis Reveals an Asian Origin for African *Burkholderia pseudomallei* and Further Supports Melioidosis Endemicity in Africa. mSphere. 2016;1(2).

94. Steinmetz I, Wagner GE, Kanyala E, Sawadogo M, Soumeya H, Teferi M, Andargie E, Yeshitela B, Yaba Atse-Achi L, Sanogo M, Bonfoh B, Rakotozandrindrainy R, Pongombo Shongo C, Shongoya Pongombo M, Kasamba Ilunga E, Lichtenegger S, Assig K, May J, Bertherat E, Owusu M, Owusu-Dabo E, Adu-Sarkodie Y. Melioidosis in Africa: Time to Uncover the True Disease Load. Trop Med Infect Dis. 2018;3(2).

95. Volpe-Chaves CE, Rodrigues ACS, Lacerda M, Oliveira CTF, Castilho SB, Franciscato C, Santos ICO, Assef A, Roever L, Oliveira S, Paniago AMM. Melioidosis, an emerging infectious disease in the Midwest Brazil: A case report. Medicine (Baltimore). 2019;98(16):e15235.

96. Sanchez-Villamil JI, Torres AG. Melioidosis in Mexico, Central America, and the Caribbean. Trop Med Infect Dis. 2018;3(1).

97. Torres AG, Montufar FE, Gee JE, Hoffmaster AR, Elrod MG, Duarte-Valderrama C, Huertas MG, Blaney DD. Melioidosis is in the Americas: A Call to Action for Diagnosing and Treating the Disease. Am J Trop Med Hyg. 2018;99(3):563-4.

98. Dance DA. Editorial commentary: melioidosis in Puerto Rico: the iceberg slowly emerges. Clin Infect Dis. 2015;60(2):251-3.

99. Dance DA. Ecology of *Burkholderia pseudomallei* and the interactions between environmental *Burkholderia* spp. and human-animal hosts. Acta Trop. 2000;74(2-3):159-68.

100. Kaestli M, Mayo M, Harrington G, Watt F, Hill J, Gal D, Currie BJ. Sensitive and specific molecular detection of *Burkholderia pseudomallei*, the causative agent of melioidosis, in the soil of tropical northern Australia. Appl Environ Microbiol. 2007;73(21):6891-7.

101. Kaestli M, Mayo M, Harrington G, Ward L, Watt F, Hill JV, Cheng AC, Currie BJ. Landscape changes influence the occurrence of the melioidosis bacterium *Burkholderia pseudomallei* in soil in northern Australia. PLoS Negl Trop Dis. 2009;3(1):e364.

102. Palasatien S, Lertsirivorakul R, Royros P, Wongratanacheewin S, Sermswan RW. Soil physicochemical properties related to the presence of *Burkholderia pseudomallei*. Trans R Soc Trop Med Hyg. 2008;102 Suppl 1:S5-9.

103. Musa HI, Hassan L, Shamsuddin ZH, Panchadcharam C, Zakaria Z, Abdul Aziz S. Physicochemical Properties Influencing Presence of *Burkholderia pseudomallei* in Soil from Small Ruminant Farms in Peninsular Malaysia. PLoS One. 2016;11(9):e0162348.

104. Strauss JM, Groves MG, Mariappan M, Ellison DW. Melioidosis in Malaysia. II. Distribution of *Pseudomonas pseudomallei* in soil and surface water. Am J Trop Med Hyg. 1969;18(5):698-702.

105. Musa HI, Hassan L, Shamsuddin ZH, Panchadcharam C, Zakaria Z, Abdul Aziz S, Rachmat RF. Case-control investigation on the risk factors of melioidosis in small ruminant farms in Peninsular Malaysia. J Appl Microbiol. 2015;119(2):331-41.

106. Tong S, Yang S, Lu Z, He W. Laboratory investigation of ecological factors influencing the environmental presence of *Burkholderia pseudomallei*. Microbiol Immunol. 1996;40(6):451-3.

107. Chen YS, Chen SC, Kao CM, Chen YL. Effects of soil pH, temperature and water content on the growth of *Burkholderia pseudomallei*. Folia Microbiol (Praha). 2003;48(2):253-6.

108. Kanai K, Kondo E. Recent advances in biomedical sciences of *Burkholderia pseudomallei* (basonym: *Pseudomonas pseudomallei*). Jpn J Med Sci Biol. 1994;47(1):1-45.

109. Hantrakun V, Rongkard P, Oyuchua M, Amornchai P, Lim C, Wuthiekanun V, Day NP, Peacock SJ, Limmathurotsakul D. Soil Nutrient Depletion Is Associated with the Presence of *Burkholderia pseudomallei*. Appl Environ Microbiol. 2016;82(24):7086-92.

110. Baker AL, Ezzahir J, Gardiner C, Shipton W, Warner JM. Environmental Attributes Influencing the Distribution of *Burkholderia pseudomallei* in Northern Australia. PLoS One. 2015;10(9):e0138953.
111. Kaestli M, Harrington G, Mayo M, Chatfield MD, Harrington I, Hill A, Munksgaard N, Gibb K, Currie BJ. What drives the occurrence of the melioidosis bacterium *Burkholderia pseudomallei* in domestic gardens? PLoS Negl Trop Dis. 2015;9(3):e0003635.
112. Inglis TJ, Sagripanti JL. Environmental factors that affect the survival and persistence of *Burkholderia pseudomallei*. Appl Environ Microbiol. 2006;72(11):6865-75.
113. Pumpuang A, Chantratita N, Wikraiphat C, Saiprom N, Day NP, Peacock SJ, Wuthiekanun V. Survival of *Burkholderia pseudomallei* in distilled water for 16 years. Trans R Soc Trop Med Hyg. 2011;105(10):598-600.
114. Inglis TJJ, Mee BJ, Chang BJ. The environmental microbiology of melioidosis. Reviews in Medical Microbiology. 2001;12(1):13-20.
115. Kaestli M, Schmid M, Mayo M, Rothballer M, Harrington G, Richardson L, Hill A, Hill J, Tuanyok A, Keim P, Hartmann A, Currie BJ. Out of the ground: aerial and exotic habitats of the melioidosis bacterium *Burkholderia pseudomallei* in grasses in Australia. Environ Microbiol. 2012;14(8):2058-70.
116. Limmathurotsakul D, Dance DA, Wuthiekanun V, Kaestli M, Mayo M, Warner J, Wagner DM, Tuanyok A, Wertheim H, Yoke Cheng T, Mukhopadhyay C, Puthucheary S, Day NP, Steinmetz I, Currie BJ, Peacock SJ. Systematic review and consensus guidelines for environmental sampling of *Burkholderia pseudomallei*. PLoS Negl Trop Dis. 2013;7(3):e2105.
117. Currie BJ, Ward L, Cheng AC. The epidemiology and clinical spectrum of melioidosis: 540 cases from the 20 year Darwin prospective study. PLoS Negl Trop Dis. 2010;4(11):e900.
118. Suputtamongkol Y, Chaowagul W, Chetchotisakd P, Lertpatanasuwun N, Intaranongpai S, Ruchutrakool T, Budhsarawong D, Mootsikapun P, Wuthiekanun V, Teerawatasook N, Lulitanond A. Risk factors for melioidosis and bacteremic melioidosis. Clin Infect Dis. 1999;29(2):408-13.
119. Suputtamongkol Y, Hall AJ, Dance DA, Chaowagul W, Rajchanuvong A, Smith MD, White NJ. The epidemiology of melioidosis in Ubon Ratchatani, northeast Thailand. Int J Epidemiol. 1994;23(5):1082-90.
120. Thummakul T, Wilde H, Tantawichien T. Melioidosis, an environmental and occupational hazard in Thailand. Mil Med. 1999;164(9):658-62.
121. Limmathurotsakul D, Kanoksil M, Wuthiekanun V, Kitphati R, deStavola B, Day NP, Peacock SJ. Activities of daily living associated with acquisition of melioidosis in northeast Thailand: a matched case-control study. PLoS Negl Trop Dis. 2013;7(2):e2072.
122. Limmathurotsakul D. *Burkholderia pseudomallei* and the Neglected Tropical Disease Melioidosis with Direk Limmathurotsakul. In: Wolf J. Meet the Microbiologst. asm.org2019.
123. Wiersinga WJ, van der Poll T, White NJ, Day NP, Peacock SJ. Melioidosis: insights into the pathogenicity of *Burkholderia pseudomallei*. Nat Rev Microbiol. 2006;4(4):272-82.
124. Chuah CJ, Tan EKH, Sermswan RW, Ziegler AD. Hydrological connectivity and *Burkholderia pseudomallei* prevalence in wetland environments: investigating rice-farming community's risk of exposure to melioidosis in North-East Thailand. Environ Monit Assess. 2017;189(6):287.
125. Haefele SM, Naklang K, Harnpichitvitaya D, Jearakongman S, Skulkhu E, Romyen P, Phasopa S, Tabtim S, Suriya-Arunroj D, Khunthasuvon S, Kraisorakul D, Youngsuk P, Amarante ST, Wade LJ. Factors affecting rice yield and fertilizer response in rainfed lowlands of northeast Thailand. Field Crops Research. 2006;98(1):39-51.

126. Bouman BAM, Humphreys E, Tuong TP, Barker R. Rice and water. Advances in Agronomy, Vol 92. 2007;92:187-237.
127. Kawasaki J, Herath, S. Impact Assessment of Climate Change on Rice Production in Khon Kaen Province, Thailand. J ISSAAS. 2011;17(2):14-28.
128. Bouman BAM, Castaneda AR, Bhuiyan SI. Nitrate and pesticide contamination of groundwater under rice-based cropping systems: past and current evidence from the Philippines. Agriculture Ecosystems & Environment. 2002;92(2-3):185-99.
129. Pepper IL. The Soil Health-Human Health Nexus. Critical Reviews in Environmental Science and Technology. 2013;43(24):2617-52.
130. Hamad MA, Austin CR, Stewart AL, Higgins M, Vazquez-Torres A, Voskuil MI. Adaptation and antibiotic tolerance of anaerobic *Burkholderia pseudomallei*. Antimicrob Agents Chemother. 2011;55(7):3313-23.
131. Brook MD, Currie B, Desmarchelier PM. Isolation and identification of *Burkholderia pseudomallei* from soil using selective culture techniques and the polymerase chain reaction. J Appl Microbiol. 1997;82(5):589-96.
132. Cheng AC, Wuthiekanun V, Limmathurotsakul D, Chierakul W, Peacock SJ. Intensity of exposure and incidence of melioidosis in Thai children. Trans R Soc Trop Med Hyg. 2008;102 Suppl 1:S37-9.
133. Cheng AC, Hanna JN, Norton R, Hills SL, Davis J, Krause VL, Dowse G, Inglis TJ, Currie BJ. Melioidosis in northern Australia, 2001-02. Commun Dis Intell Q Rep. 2003;27(2):272-7.
134. Issack MI, Bundhun CD, Gokhool H. Melioidosis in Mauritius. Emerg Infect Dis. 2005;11(1):139-40.
135. Kronmann KC, Truett AA, Hale BR, Crum-Cianflone NF. Melioidosis after brief exposure: a serologic survey in US Marines. Am J Trop Med Hyg. 2009;80(2):182-4.
136. Short BH. Melioidosis: an important emerging infectious disease - a military problem? ADF Health. 2002;3:13-21.
137. Clayton AJ, Lisella RS, Martin DG. Melioidosis: a serological survey in military personnel. Mil Med. 1973;138(1):24-6.
138. Mayo M, Kaesti M, Harrington G, Cheng AC, Ward L, Karp D, Jolly P, Godoy D, Spratt BG, Currie BJ. *Burkholderia pseudomallei* in unchlorinated domestic bore water, Tropical Northern Australia. Emerg Infect Dis. 2011;17(7):1283-5.
139. McRobb E, Kaestli M, Mayo M, Price EP, Sarovich DS, Godoy D, Spratt BG, Currie BJ. Melioidosis from contaminated bore water and successful UV sterilization. Am J Trop Med Hyg. 2013;89(2):367-8.
140. McKenzie VJ, Townsend AR. Parasitic and infectious disease responses to changing global nutrient cycles. Ecohealth. 2007;4(4):384-96.
141. Philippot L. Denitrifying genes in bacterial and Archaeal genomes. Biochim Biophys Acta. 2002;1577(3):355-76.
142. Chierakul W. Clinical Manifestations and Treatment: Thailand Experience. 8th World Melioidosis Congress; 2016; Cebu, Philippines.
143. Currie B. The Australian Experience. 8th World Melioidosis Congress; 2016; Cebu, Philippines.
144. Whiteley L, Meffert T, Haug M, Weidenmaier C, Hopf V, Bitschar K, Schittek B, Kohler C, Steinmetz I, West TE, Schwarz S. Entry, Intracellular Survival, and Multinucleated-Giant-Cell-Forming Activity of *Burkholderia pseudomallei* in Human Primary Phagocytic and Nonphagocytic Cells. Infect Immun. 2017;85(10).
145. Overtoom R, Khieu V, Hem S, Cavailler P, Te V, Chan S, Lau P, Guillard B, Vong S. A first report of pulmonary melioidosis in Cambodia. Trans R Soc Trop Med Hyg. 2008;102 Suppl 1:S21-5.

146. Greer RC, Wangrangsimakul T, Amornchai P, Wuthiekanun V, Laongnualpanich A, Dance DAB, Limmathurotsakul D. Misidentification of *Burkholderia pseudomallei* as *Acinetobacter* species in northern Thailand. Trans R Soc Trop Med Hyg. 2019;113(1):48-51.

147. Limmathurotsakul D, Jamsen K, Arayawichanont A, Simpson JA, White LJ, Lee SJ, Wuthiekanun V, Chantratita N, Cheng A, Day NP, Verzilli C, Peacock SJ. Defining the true sensitivity of culture for the diagnosis of melioidosis using Bayesian latent class models. PLoS One. 2010;5(8):e12485.

148. Hoffmaster AR, AuCoin D, Baccam P, Baggett HC, Baird R, Bhengsri S, Blaney DD, Brett PJ, Brooks TJ, Brown KA, Chantratita N, Cheng AC, Dance DA, Decuypere S, Defenbaugh D, Gee JE, Houghton R, Jorakate P, Lertmemongkolchai G, Limmathurotsakul D, Merlin TL, Mukhopadhyay C, Norton R, Peacock SJ, Rolim DB, Simpson AJ, Steinmetz I, Stoddard RA, Stokes MM, Sue D, Tuanyok A, Whistler T, Wuthiekanun V, Walke HT. Melioidosis diagnostic workshop, 2013. Emerg Infect Dis. 2015;21(2).

149. Currie BJ, Jacups SP, Cheng AC, Fisher DA, Anstey NM, Huffam SE, Krause VL. Melioidosis epidemiology and risk factors from a prospective whole-population study in northern Australia. Trop Med Int Health. 2004;9(11):1167-74.

150. Jenjaroen K, Chumseng S, Sumonwiriya M, Ariyaprasert P, Chantratita N, Sunyakumthorn P, Hongsuwan M, Wuthiekanun V, Fletcher HA, Teparrukkul P, Limmathurotsakul D, Day NP, Dunachie SJ. T-Cell Responses Are Associated with Survival in Acute Melioidosis Patients. PLoS Negl Trop Dis. 2015;9(10):e0004152.

151. Stevenson CR, Critchley JA, Forouhi NG, Roglic G, Williams BG, Dye C, Unwin NC. Diabetes and the risk of tuberculosis: a neglected threat to public health? Chronic Illn. 2007;3(3):228-45.

152. Koh GC, Schreiber MF, Bautista R, Maude RR, Dunachie S, Limmathurotsakul D, Day NP, Dougan G, Peacock SJ. Host responses to melioidosis and tuberculosis are both dominated by interferon-mediated signaling. PLoS One. 2013;8(1):e54961.

153. Ketheesan N. Early immune dysregulation in a diabetic host dictates the outcome of *Burkholderia pseudomallei* infection. 8th World Melioidosis Congress; 2016; Cebu, Philippines.

154. Singhal A, Jie L, Kumar P, Hong GS, Leow MK, Paleja B, Tsenova L, Kurepina N, Chen J, Zolezzi F, Kreiswirth B, Poidinger M, Chee C, Kaplan G, Wang YT, De Libero G. Metformin as adjunct antituberculosis therapy. Sci Transl Med. 2014;6(263):263ra159.

155. Kewcharoenwong C, Rinchai D, Utispan K, Suwannasaen D, Bancroft GJ, Ato M, Lertmemongkolchai G. Glibenclamide reduces pro-inflammatory cytokine production by neutrophils of diabetes patients in response to bacterial infection. Sci Rep. 2013;3:3363.

156. Gibbs P. Origins of One Health and One Medicine. Vet Rec. 2014;174(6):152.

157. Sprague LD, Neubauer H. Melioidosis in animals: a review on epizootiology, diagnosis and clinical presentation. J Vet Med B Infect Dis Vet Public Health. 2004;51(7):305-20.

158. Limmathurotsakul D, Thammasart S, Warrasuth N, Thapanagulsak P, Jatapai A, Pengreungrojanachai V, Anun S, Joraka W, Thongkamkoon P, Saiyen P, Wongratanacheewin S, Day NP, Peacock SJ. Melioidosis in animals, Thailand, 2006-2010. Emerg Infect Dis. 2012;18(2):325-7.

159. Choy JL, Mayo M, Janmaat A, Currie BJ. Animal melioidosis in Australia. Acta Trop. 2000;74(2-3):153-8.

160. Cottew GS, Sutherland, A.K., Meehan, J.F. Melioidosis in Sheep in Queensland. Description of an Outbreak. The Australian Veterinary Journal. 1952(May):113-32.

161. Mollaret HH. «L'affaire du jardin des plantesou comment la mélioïdose fit son apparition en France. Medecine et Maladies Infectieuses. 1988;18:643-54.

162. Dance DA, King C, Aucken H, Knott CD, West PG, Pitt TL. An outbreak of melioidosis in imported primates in Britain. Vet Rec. 1992;130(24):525-9.

163. CDC. Conclusion of Select Agent Inquiry into *Burkholderia pseudomallei* Release at Tulane National Primate Research Center: CDC Media Relations; 2015. Available from: https://www.cdc.gov/media/releases/2015/s0313-burkholderia-pseudomallei.html.

164. Portacci K, Rooney AP, Dobos R. Assessing the potential for *Burkholderia pseudomallei* in the southeastern United States. J Am Vet Med Assoc. 2017;250(2):153-9.

165. NIH. Reportable diseases https://medlineplus.gov/ency/article/001929.htm2019.

166. CDC. Melioidosis (*Burkholderia peudomallei*) 2012 Case Definition https://wwwn.cdc.gov/nndss/conditions/melioidosis/case-definition/2012/2012.

167. Peacock SJ, Limmathurotsakul D, Lubell Y, Koh GC, White LJ, Day NP, Titball RW. Melioidosis vaccines: a systematic review and appraisal of the potential to exploit biodefense vaccines for public health purposes. PLoS Negl Trop Dis. 2012;6(1):e1488.

168. Limmathurotsakul D, Funnell SG, Torres AG, Morici LA, Brett PJ, Dunachie S, Atkins T, Altmann DM, Bancroft G, Peacock SJ, Steering Group on Melioidosis Vaccine D. Consensus on the development of vaccines against naturally acquired melioidosis. Emerg Infect Dis. 2015;21(6).

169. Titball RW, Burtnick MN, Bancroft GJ, Brett P. *Burkholderia pseudomallei* and *Burkholderia mallei* vaccines: Are we close to clinical trials? Vaccine. 2017;35(44):5981-9.

170. Atkins T, Prior R, Mack K, Russell P, Nelson M, Prior J, Ellis J, Oyston PC, Dougan G, Titball RW. Characterisation of an acapsular mutant of *Burkholderia pseudomallei* identified by signature tagged mutagenesis. J Med Microbiol. 2002;51(7):539-47.

171. Breitbach K, Kohler J, Steinmetz I. Induction of protective immunity against *Burkholderia pseudomallei* using attenuated mutants with defects in the intracellular life cycle. Trans R Soc Trop Med Hyg. 2008;102 Suppl 1:S89-94.

172. Stevens MP, Haque A, Atkins T, Hill J, Wood MW, Easton A, Nelson M, Underwood-Fowler C, Titball RW, Bancroft GJ, Galyov EE. Attenuated virulence and protective efficacy of a *Burkholderia pseudomallei bsa* type III secretion mutant in murine models of melioidosis. Microbiology. 2004;150(Pt 8):2669-76.

173. Srilunchang T, Proungvitaya T, Wongratanacheewin S, Strugnell R, Homchampa P. Construction and characterization of an unmarked *aroC* deletion mutant of *Burkholderia pseudomallei* strain A2. Southeast Asian J Trop Med Public Health. 2009;40(1):123-30.

174. Barnes JL, Warner J, Melrose W, Durrheim D, Speare R, Reeder JC, Ketheesan N. Adaptive immunity in melioidosis: a possible role for T cells in determining outcome of infection with *Burkholderia pseudomallei*. Clin Immunol. 2004;113(1):22-8.

175. Ulett GC, Ketheesan N, Hirst RG. Macrophage-lymphocyte interactions mediate anti-*Burkholderia pseudomallei* activity. FEMS Immunol Med Microbiol. 1998;21(4):283-6.

176. Haque A, Chu K, Easton A, Stevens MP, Galyov EE, Atkins T, Titball R, Bancroft GJ. A live experimental vaccine against *Burkholderia pseudomallei* elicits CD4+ T cell-mediated immunity, priming T cells specific for 2 type III secretion system proteins. J Infect Dis. 2006;194(9):1241-8.

177. Burtnick MN, Brett PJ, Harding SV, Ngugi SA, Ribot WJ, Chantratita N, Scorpio A, Milne TS, Dean RE, Fritz DL, Peacock SJ, Prior JL, Atkins TP, Deshazer D. The cluster 1 type VI secretion system is a major virulence determinant in *Burkholderia pseudomallei*. Infect Immun. 2011;79(4):1512-25.

178. Khakhum N, Bharaj P, Myers JN, Tapia D, Kilgore PB, Ross BN, Walker DH, Endsley JJ, Torres AG. *Burkholderia pseudomallei ΔtonBΔhcp1* Live Attenuated Vaccine Strain Elicits Full Protective Immunity against Aerosolized Melioidosis Infection. mSphere. 2019;4(1).

179. Silva EB, Goodyear A, Sutherland MD, Podnecky NL, Gonzalez-Juarrero M, Schweizer HP, Dow SW. Correlates of immune protection following cutaneous immunization with an attenuated *Burkholderia pseudomallei* vaccine. Infect Immun. 2013;81(12):4626-34.
180. Norris MH, Schweizer HP, Tuanyok A. Structural diversity of *Burkholderia pseudomallei* lipopolysaccharides affects innate immune signaling. PLoS Negl Trop Dis. 2017;11(4):e0005571.
181. Chantratita N, Tandhavanant S, Myers ND, Seal S, Arayawichanont A, Kliangsa-Ad A, Hittle LE, Ernst RK, Emond MJ, Wurfel MM, Day NP, Peacock SJ, West TE. Survey of innate immune responses to *Burkholderia pseudomallei* in human blood identifies a central role for lipopolysaccharide. PLoS One. 2013;8(11):e81617.
182. Nieves W, Asakrah S, Qazi O, Brown KA, Kurtz J, Aucoin DP, McLachlan JB, Roy CJ, Morici LA. A naturally derived outer-membrane vesicle vaccine protects against lethal pulmonary *Burkholderia pseudomallei* infection. Vaccine. 2011;29(46):8381-9.
183. Nieves W, Petersen H, Judy BM, Blumentritt CA, Russell-Lodrigue K, Roy CJ, Torres AG, Morici LA. A *Burkholderia pseudomallei* outer membrane vesicle vaccine provides protection against lethal sepsis. Clin Vaccine Immunol. 2014;21(5):747-54.
184. Petersen H, Nieves W, Russell-Lodrigue K, Roy CJ, Morici LA. Evaluation of a *Burkholderia pseudomallei* Outer Membrane Vesicle Vaccine in Nonhuman Primates. Procedia Vaccinol. 2014;8:38-42.
185. Morici L, Torres AG, Titball RW. Novel multi-component vaccine approaches for *Burkholderia pseudomallei*. Clin Exp Immunol. 2019;196(2):178-88.
186. Muruato LA, Torres AG. Melioidosis: where do we stand in the development of an effective vaccine? Future Microbiol. 2016;11(4):477-80.
187. Mu JJ, Cheng PY, Chen YS, Chen PS, Chen YL. The occurrence of melioidosis is related to different climatic conditions in distinct topographical areas of Taiwan. Epidemiol Infect. 2014;142(2):415-23.
188. Liu X, Pang L, Sim SH, Goh KT, Ravikumar S, Win MS, Tan G, Cook AR, Fisher D, Chai LY. Association of melioidosis incidence with rainfall and humidity, Singapore, 2003-2012. Emerg Infect Dis. 2015;21(1):159-62.
189. Lo TJ, Ang LW, James L, Goh KT. Melioidosis in a tropical city state, Singapore. Emerg Infect Dis. 2009;15(10):1645-7.
190. Currie BJ, Jacups SP. Intensity of rainfall and severity of melioidosis, Australia. Emerg Infect Dis. 2003;9(12):1538-42.
191. Wiersinga WJ, Currie BJ, Peacock SJ. Melioidosis. N Engl J Med. 2012;367(11):1035-44.
192. Merritt AJ, Inglis TJJ. The Role of Climate in the Epidemiology of Melioidosis. Curr Trop Med Rep. 2017;4(4):185-91.
193. Currie BJ, Fisher DA, Howard DM, Burrow JN, Lo D, Selva-Nayagam S, Anstey NM, Huffam SE, Snelling PL, Marks PJ, Stephens DP, Lum GD, Jacups SP, Krause VL. Endemic melioidosis in tropical northern Australia: a 10-year prospective study and review of the literature. Clin Infect Dis. 2000;31(4):981-6.
194. Cheng AC, Currie BJ, Dance DAB, Funnell SGP, Limmathurotsakul D, Simpson AJH, Peacock SJ. Clinical definitions of melioidosis. Am J Trop Med Hyg. 2013;88(3):411-3.
195. Brundage WG, Thuss CJ, Jr., Walden DC. Four fatal cases of melioidosis in U. S. soldiers in Vietnam. Bacteriologic and pathologic characteristics. Am J Trop Med Hyg. 1968;17(2):183-91.
196. Amadasi S, Dal Zoppo S, Bonomini A, Bussi A, Pedroni P, Balestrieri G, Signorini L, Castelli F. A case of melioidosis probably acquired by inhalation of dusts during a helicopter flight in a healthy traveler returning from Singapore. J Travel Med. 2015;22(1):57-60.

197. Perez JM, Petiot A, Adjide C, Gerry F, Goursaud R, Juminer B. First case report of melioidosis in Guadeloupe, a French West Indies archipelago. Clin Infect Dis. 1997;25(1):164-5.
198. Mackowiak PA, Smith JW. Septicemic melioidosis. Occurrence following acute influenza A six years after exposure in Vietnam. JAMA. 1978;240(8):764-6.
199. Fisher DA, Harris PN. Melioidosis: refining management of a tropical time bomb. Lancet. 2014;383(9919):762-4.
200. Kaestli M, Grist EPM, Ward L, Hill A, Mayo M, Currie BJ. The association of melioidosis with climatic factors in Darwin, Australia: A 23-year time-series analysis. J Infect. 2016;72(6):687-97.
201. Rudaz AO, Davidson EA, Firestone MK. Sources of Nitrous-Oxide Production Following Wetting of Dry Soil. Fems Microbiology Ecology. 1991;85(2):117-24.
202. Gordon H, Haygarth PM, Bardgett RD. Drying and rewetting effects on soil microbial community composition and nutrient leaching. Soil Biology & Biochemistry. 2008;40(2):302-11.
203. Parameswaran U, Baird RW, Ward LM, Currie BJ. Melioidosis at Royal Darwin Hospital in the big 2009-2010 wet season: comparison with the preceding 20 years. Med J Aust. 2012;196(5):345-8.
204. Bulterys PL, Bulterys MA, Phommasone K, Luangraj M, Mayxay M, Kloprogge S, Miliya T, Vongsouvath M, Newton PN, Phetsouvanh R, French CT, Miller JF, Turner P, Dance DAB. Climatic drivers of melioidosis in Laos and Cambodia: a 16-year case series analysis. Lancet Planet Health. 2018;2(8):e334-e43.
205. Andreolli M, Lampis S, Zenaro E, Salkinoja-Salonen M, Vallini G. *Burkholderia fungorum* DBT1: a promising bacterial strain for bioremediation of PAHs-contaminated soils. FEMS Microbiol Lett. 2011;319(1):11-8.
206. O'Sullivan LA, Mahenthiralingam E. Biotechnological potential within the genus *Burkholderia*. Lett Appl Microbiol. 2005;41(1):8-11.
207. Ponce BL, Latorre VK, Gonzalez M, Seeger M. Antioxidant compounds improved PCB-degradation by *Burkholderia xenovorans* strain LB400. Enzyme Microb Technol. 2011;49(6-7):509-16.
208. Na-ngam N, Angkititakul S, Noimay P, Thamlikitkul V. The effect of quicklime (calcium oxide) as an inhibitor of *Burkholderia pseudomallei*. Transactions of the Royal Society of Tropical Medicine and Hygiene. 2004;98(6):337-41.
209. Wang-Ngarm S, Chareonsudjai S, Chareonsudjai P. Physicochemical factors affecting the growth of *Burkholderia pseudomallei* in soil microcosm. Am J Trop Med Hyg. 2014;90(3):480-5.
210. Kamjumphol W, Chareonsudjai P, Chareonsudjai S. Antibacterial activity of chitosan against *Burkholderia pseudomallei*. Microbiologyopen. 2018;7(1).
211. Boottanun P, Potisap C, Hurdle JG, Sermswan RW. Secondary metabolites from *Bacillus amyloliquefaciens* isolated from soil can kill *Burkholderia pseudomallei*. AMB Express. 2017;7(1):16.
212. Inglis TJ, Rigby P, Robertson TA, Dutton NS, Henderson M, Chang BJ. Interaction between *Burkholderia pseudomallei* and *Acanthamoeba* species results in coiling phagocytosis, endamebic bacterial survival, and escape. Infect Immun. 2000;68(3):1681-6.
213. Noinarin P, Chareonsudjai P, Wangsomnuk P, Wongratanacheewin S, Chareonsudjai S. Environmental Free-Living Amoebae Isolated from Soil in Khon Kaen, Thailand, Antagonize *Burkholderia pseudomallei*. PLoS One. 2016;11(11):e0167355.
214. Molmeret M, Horn M, Wagner M, Santic M, Abu Kwaik Y. Amoebae as training grounds for intracellular bacterial pathogens. Appl Environ Microbiol. 2005;71(1):20-8.

215. Ramli NS, Eng Guan C, Nathan S, Vadivelu J. The effect of environmental conditions on biofilm formation of *Burkholderia pseudomallei* clinical isolates. PLoS One. 2012;7(9):e44104.

**CHAPTER 2: The current status of extracellular polymeric substances produced by**
***Burkholderia pseudomallei*[2]**


Extracellular polymeric substances (EPS) that are produced by *Burkholderia pseudomallei* consist of diverse structural components that serve equally diverse protective and antigenic functions. *B. pseudomallei* is a sapronotic disease agent that transitions from the environment to cause severe infection in humans and animals. EPS matrix components are proposed to play a critical role in transmission, dissemination, and protection of the bacteria in these varied environments. However, many of these components remain uncharacterized and there is a lack of consensus regarding classification and nomenclature. The status of *B. pseudomallei* EPS matrix components are presented here; however, the nomenclature regarding extracellular polymeric substances from *Burkholderia* spp. is not consistent. This chapter will discuss these differences and propose unified nomenclature that would facilitate communication for all researchers working with *Burkholderia* spp. Bioinformatics, mutational studies, and transcriptional profiling of biofilms have identified additional EPS components, which include exopolysaccharides, capsular polysaccharides, proteins, and extracellular DNA.


## 2.1 Bacterial biofilms and the EPS matrix

Extracellular polymeric substances (EPS) are composed of extracellular polysaccharides (exopolysaccharides), capsular polysaccharides (CPS), extracellular DNA (eDNA), polypeptide adhesins, extracellular enzymes, lipids, and a variety of polymers (1). The EPS matrix has been metaphorically described as the "house of biofilm cells" because it represents an environment in which microbes are embedded, and as such, is much more complex than the sugar moieties that were once solely labeled as exopolysaccharides (formerly EPS) (1, 2). The EPS matrix is

---

[2] This work is presented in: **Mangalea, M.R.**, Borlee, G.I., and Borlee, B.R. 2017. The current status of extracellular polymeric substances produced by *Burkholderia pseudomallei*. *Current Tropical Medicine Reports*, 4: 117.

conceptually viewed as the encapsulating polymers that contribute to adhesion, aggregation,

biofilm formation, which ultimately protects the bacteria that produce it. EPS matrix components

are most often associated with the biofilm matrix, but it is clear that these components are also

important for bacterial growth and survival. The EPS matrix is paramount for bacterial survival in

various settings, primarily by providing a physical barrier from predation and phagocytosis, but

also protecting against desiccation in the environment (3, 4). During the transition between

planktonic cells to single- and multi-species biofilm communities, the EPS structural

components aid bacteria within the *Burkholderia* genus to survive amid dynamic ecological

conditions in the environment and host-adapted infections.

     *B. pseudomallei* is an opportunistic pathogen capable of biofilm formation, a complex

process that is regulated in a strain-specific manner, in both environmental and clinical settings

(5). In the environment, *B. pseudomallei* is a saprophyte that has been shown to be associated

with the rhizosphere of various rice cultivars and forms biofilms on plant tissues at the interface

where liquids contact plant surfaces (6, 7). Clinical isolates of *B. pseudomallei* that produce

biofilms (5), also exhibit increased antimicrobial tolerance as compared to the same cells grown

planktonically (8), in part by providing a physical barrier to drug diffusion (9). Biofilm formation

has long been implicated with chronic *B. pseudomallei* infection resulting in melioidosis (10)

(although this is still controversial (11)), and has recently been associated with disease relapse

and recurrent melioidosis in humans (12). Thus, *B. pseudomallei* biofilm formation is not only

important for environmental persistence, but a significant consideration for disease progression

and pathogenesis. However, the exact structural components that comprise *B. pseudomallei*

biofilms have yet to be fully elucidated.

     EPS matrix composition is difficult to fully characterize and differentiate from cellular

components or transiently produced macromolecules. Biochemical identification and structural

characterization of the polysaccharides is hindered by the capacity of *Burkholderia* spp. to

produce a diverse array of sugar components with complex linkages (2). The predominant

structures of the EPS matrix identified in *Burkholderia* spp. (**Table 2.1**) are exopolysaccharides (13-23), eDNA (24, 25), and CPS I (26-29), which has been identified as a primary virulence factor in *B. pseudomallei*. Exopolysaccharides or slime polysaccharides (30), are loosely associated with the bacterial cell surface, but are key structural components of *Burkholderia* spp. biofilm communities. CPS are comprised of repeating sugar units with glycosidic linkages that are arranged as diverse molecules intimately associated with the outer cell wall and are distinct from surface-associated lipopolysaccharides (31). Among species within the *Burkholderia pseudomallei* complex (Bpc) the CPS are prominent antigens essential for virulence (27, 32). Both CPS and secreted exopolysaccharides are involved in biofilm formation (20, 33) and thus intrinsic antibiotic resistance and host pathogenicity, yet the biofilm matrix is also composed of contact-dependent growth inhibition (CDI) system proteins and secreted adhesion effector proteins. The *Burkholderia*-specific CDI system *BcpAIOB* gene cluster of *B. thailandensis* (Bpc) is essential not only for biofilm formation, but inter-species antagonism (34, 35). Similarly, secreted outer membrane autotransporter (AT) proteins BoaA and BoaB (36) and the BpaA-BpaF (37) cluster (**Table 2.1**) are also implicated in adhesion and biofilm formation among members of the Bpc. Among Bcc species, a greater diversity of secreted and surface-associated exopolysaccharides has been observed, including a newly characterized PNAG (polysaccharide intracellular adhesin [PIA] or poly-β-1,6-*N*-acetyl-D-glucosamine [PGA]), which plays an important role in biofilm formation and maintenance (38). The structural components and underlying genomic organization of the diverse polysaccharides produced by *Burkholderia* spp. are gradually being characterized; however, there is a lack of consensus nomenclature between Bpc and Bcc researchers. For example, our bioinformatics analyses reveal that the *bce-I* cluster annotated in *B. cepacia* as a prominent functional gene cluster for production of cepacian (20, 21) is referred to as a type III capsular polysaccharide (CPS III) in *B. pseudomallei* (33). Currently, there are four gene clusters annotated to encode for CPS in Bpc (39), yet these clusters are not annotated accordingly in Bcc species. Bcc bacteria are known to

**Table 2.1 Extracellular polymeric substance components of *Burkholderia pseudomallei* complex** Adapted from Mangalea, Borlee, and Borlee, 2017. Gene loci in parentheses are representative of *B. pseudomallei* K96243 *CPS* capsular polysaccharide, *OPS* O-antigen polysaccharide, *bec* biofilm exopolysaccharide gene cluster, *bce B. cepacia* complex exopolysaccharide

| Component | Annotation | Gene Loci | Homology in Bcc | References |
|---|---|---|---|---|
| CPS | CPS I | BP1026b_I0499 – Bp1026b_I0524 | BCAL3246 – BCAL3217 | [27, 39] |
| | CPS II | BP1026b_II0468 – Bp1026b_II0480 | N/A | [33] |
| | CPS III | BP1026b_II1956 – Bp1026b_II1966 | Bcep1808_4200 – Bcep1808_4210 | [20, 33] |
| | CPS IV | BP1026b_I0525 – Bp1026b_I0543 | BCAM0204 – BCAM0214 | [33] |
| CPS or Exopolysaccharide | O-PS | BP1026B_I0633 – Bp1026B_I0656 | BCAL3135 – BCAL3110 | [64] |
| | CPS III/*bceI* | BP1026b_II1956 – Bp1026b_II1966 | Bcep1808_4200 – Bcep1808_4210 | [20] |
| | *becA-R* | BP1026b_I2907 – Bp1026b_I2927 | BCAM1350 – BCAM1336 | [41] |
| Exopolysaccharide | *bceI* | BP1026b_II1956 – Bp1026b_II1966 | Bcep1808_4200 – Bcep1808_4210 | [21] |
| | *bceII* | BP1026b_II1796 – Bp1026b_II1807 | Bcep1808_4480 – Bcep1808_4471 | [20] |
| | Gal-KDO acidic polysaccharide | ? | N/A | [18, 58] |
| | Fucose-containing exopol. | ? | N/A | [54] |
| Proteins | BoaA | BP1026b_II0875A (BPSS0796) | ? | [36, 37, 68, 72] |
| | BoaB | BP1026b_I1654 (BPSL1705) | ? | [37, 68, 69] |
| | BcaA | BP1026b_II1054 (BPSS0962) | ? | [37, 69, 72] |
| | BcaB | BP1026b_II1055 (BPSS0961) | ? | [69] |
| | BatA | BP1026b_I1153 (BPSL2237) | ? | [72] |
| | BcpA | BP1026b_II2207 (BPSS2053) | Bcep1808_3992 (?) | [34, 35, 70] |
| | BpaA | BP1026b_II1526 (BPSS1434) | ? | [37, 72] |
| | BpaB | BP1026b_I2046 (BPSL2063) | ? | [37, 72] |
| | BpaC | BP1026b_I1575 (BPSL1631) | ? | [37, 72] |
| | BpaD | BP1026b_II0095 (BPSS0088) | ? | [37, 72] |
| | BpaE | BP1026b_II0996 (BPSS0908) | ? | [37, 72] |
| | BpaF/BbfA | BP1026b_II1530 (BPSS1439) | ? | [36, 37, 72] |
| eDNA | ? | ? | ? | N/A |
| Lipids | ? | ? | ? | N/A |

produce at least seven exopolysaccharides (14, 16, 18, 19, 40), with cepacian encoded by the

*bce-I* and *bce-II* gene clusters being the most prominent (20).

In contrast, identification and characterization of exopolysaccharides produced by Bpc

species is not as well understood. Recently, our lab identified a novel exopolysaccharide

biosynthesis gene cluster in *B. pseudomallei* 1026b (Bpc), *becA-R* (41), that contributes to

biofilm formation and shares some conservation with a putative exopolysaccharide gene cluster

in *B. cenocepacia* J2315 (Bcc) (22). Thus, there is an apparent overlap between loci predicted

to encode both CPS and exopolysaccharides between Bpc and Bcc species. Given the

antigenic nature of secreted polysaccharides from *Burkholderia* spp., the gaps in

characterization across species in the Bpc and Bcc pose challenges towards their use as

diagnostic markers and potential vaccine candidates. Furthermore, the high plasticity inherent to

*Burkholderia* spp. that possess multireplicon genomes adds to the complexity of identifying the

species-specific genetic loci that encode for these virulence determinants (42-44).

Altogether, the biosynthetic clusters that contribute to the production of *Burkholderia*

EPS are both complex and numerous. There is an immediate need for a more comprehensive

understanding of EPS produced by Bpc and Bcc. The goal of this review is to describe the

current status of EPS produced by bacteria in the genus *Burkholderia* and discuss the need to

develop a consensus annotation in order to better evaluate the roles of EPS as virulence

determinants, surface-expressed antigens, and biofilm structural components.


## 2.2 Status of characterization – exopolysaccharides


### 2.2.1 Exopolysaccharides encoded by the Bpc

Secreted exopolysaccharides that are loosely associated with the cell surface comprise

a key component of the EPS matrix, but are distinct from the more firmly attached CPS (45, 46).

Although abundant in *Burkholderia* spp., the specific gene clusters that encode EPS and the

structural characterization of these components remain largely undefined in *B. pseudomallei*.

Recently, our group has characterized a novel 28-kb exopolysaccharide biosynthetic gene

cluster consisting of 18 genes (Bp1026_I2907 – Bp1026b_I2927) annotated as *becA-R* on

chromosome I from the clinical isolate *B. pseudomallei* 1026b (41). This novel gene cluster from

*B. pseudomallei* 1026b shares some homology (14/18 genes) with a recently identified gene

cluster in *B. cenocepacia* J2315 (BCAM1330 – BCAM1350) (22). The *becA-R* cluster is highly

conserved between *B. pseudomallei, B. mallei*, and *B. thailandensis* (41).Interestingly, the

*becA-R* cluster is adjacent to Bp1026b_I2928, an EAL+GGDEF and PAS domain containing-

protein, which is potentially involved in cyclic di-GMP signaling (47). A transposon insertional

mutant of Bp1026b_I2928 exhibited increased biofilm formation at 37°C but not 30˚C (47). It is

tempting to speculate that this putative hybrid protein Bp1026b_I2928 may also contribute to the

regulation of the *becA-R* gene cluster.

A recent RNA-seq analysis comparing a low biofilm-forming *B. pseudomallei* clinical

isolate and a high biofilm-forming *B. pseudomallei* clinical isolate also identified that some of the

genes in the *becA-R* gene cluster were differentially regulated in concordance with our

transposon mutant analysis (41, 48). The loci identified by Chin et al. are predicted to encode

for polysaccharides (BPSL0603, BPSL0605, BPSL0618, BPSL0619, BPSL0620, BPSL1649,

BPSS1978), and cell surface-associated proteins (BPSS0908, BPSS0909, BPSS1487,

BPSS1434, BPSS1439 (*bbfA*), BPSS2053, BPSL1552, BPSL3094) that are up-regulated and

proposed to contribute to a robust biofilm forming phenotype (48). A mutant of BPSS1439

(*bbfA*), which encodes a trimeric autotransporter adhesin, exhibited a significant decrease in

biofilm formation as compared to the parental wild-type strain, *B. pseudomallei* 10276 (36).

Another recent study using RNA-seq analysis identified a putative polysaccharide biosynthesis

cluster homologous to *becA-R* in *B. thailandensis* E264 (BTH_I0519 – BTH_I0537) that is

regulated by the CDI system protein BcpA, which shares 58% amino acid identity with

BPSS2053 (35). The results from a transposon mutant screen and transcriptional studies

underscore the importance of this exopolysaccharide gene cluster in biofilm formation in at least three species from the Bpc (35, 41, 48).

Mongkolrob et al. postulated a biosynthetic pathway for *B. pseudomallei* exopolysaccharides, in which several sugar transferase enzymes are under transcriptional regulation by the genes *bpsI*, *ppk*, and *rpoS* (49). The exopolysaccharide carbohydrate composition identified via GC-MS in this study identified four monosaccharides: glucose, galactose, mannose, and rhamnose with a ratio of 1.00:1.31:0.82:0.30 (49). The proposed composition of this exopolysaccharide, as determined under different growth conditions and using a different strain, varies from our recent characterization of the polysaccharide produced by the *becA-R* cluster (glucose, galactose, mannose, and rhamnose in a ratio of 0.46:1.41:0.14:0.14, although galactose and glucose remain the most abundant carbohydrates detected (41).

### 2.2.2 Quorum-sensing regulation of EPS

Quorum-sensing (QS) systems are known to contribute to the regulation of biofilm formation in *B. thailandensis* (50) and *B. pseudomallei* (51)*,* which employs three known AHL-signaling molecules (52, 53) that are highly conserved among *B. pseudomallei* and *B. mallei* in the Bpc (54). *bpsI* (Bp1026b_II0974, BPSS0885) encodes for an acylhomoserine lactone (AHL) synthase that has been shown to be required for the formation of a mature biofilm, presumably by regulating EPS matrix components (51). In addition to the AHL-signaling molecules, *B. pseudomallei* also encodes 2-alkyl-4-(1H)-quinolones (AQ) that have recently also been implicated in biofilm growth dynamics (55). QS-regulated genes are also conserved among the Bpc despite different environmental niches and the host-adapted nature of *B. mallei*; and interestingly, the most stringent QS-control is targeted towards genes predicted to encode CPS II (Bp1026b_II0468 – Bp1026b_II0473) (54). A recent study identified a QS-regulated fucose-containing exopolysaccharide from *B. thailandensis* biofilm dome structures (50). This novel

exopolysaccharide that was shown to be regulated by the QS-1 system in *B. thailandensis* is proposed to be temporally associated with aggregate formation and dome production during biofilm development, and hypothesized to mitigate starvation for biofilm cells (50).

### 2.2.3 Exopolysaccharides encoded by the Bcc

Cepacian, which is an important exopolysaccharide produced by members of the Bcc, is a known virulence determinant and important for biofilm formation and is encoded by the *bce-I* and *bce-II* gene clusters (20, 56, 57). The carbohydrate composition of cepacian has been described as a 1:1:1:3:1 ratio of glucose, rhamnose, mannose, galactose, and glucuronic acid (40). Although this exopolysaccharide contains an additional glucuronic acid moiety, it is interesting to note that the proportion of galactose is similar in composition to the exopolysaccharide produced by BecA-R in *B. pseudomallei* (41, 49). The cepacian biosynthesis genes have been examined in several clinical isolates of the Bcc and locus tags have been assigned for the *B. vietnamiensis* G4 genome (20). The *bce-I* gene cluster includes 11 ORFs encoding *bceA-K* (Bcep1808_4200 – Bcep1808_4210) while the *bce-II* gene cluster includes 9 ORFs encoding *bceM-U* (Bcep1808_4471 – Bcep1808_4480), separated by roughly 155-314 kb depending on the strain (20).

Interestingly, the homologous cluster of *bce-I* from the Bcc group is encoded in *B. pseudomallei* 1026b by Bp1026b_II1956 – Bp1026b_II1966 (CPS III) while the *bce-II* cluster is represented by loci Bp1026b_II1796 – Bp1026b_II1807 (**Table 2.2**). There is an obvious overlap of annotation among the *bce-I* cluster in the Bcc and CPS III loci in the Bpc, which highlights a need for additional characterization of these genes as they relate to EPS production and biofilm formation. Recently, a transposon insertional mutant in a predicted glycosyltransferase (Bp1026b_II1959, BPSS1828) within the homologous *bce-I* cluster exhibited a reduction of roughly 60% in biofilm formation (41). These data suggest that *bce-I* and *bce-II* clusters may also be involved in biofilm formation in *B. pseudomallei*. Members of both the Bcc

and Bpc have the coding capacity for the cepacian biosynthesis genes encoded by *bce-I* and *bce-II* with the exception of *B. mallei* (**Table 2.2**). Furthermore, our recent bioinformatics analyses revealed a high level of sequence conservation among *B. pseudomallei* 1026b, *B. vietnamiensis* G4, *B. cenocepacia* J2315, and *B. thailandensis* E264 for the *bce-I* cluster and included *B. mallei* ATCC 23344 for *bce-II* (41). Such a high level of conservation across the Bps, particularly in *B. mallei*, underscores the fact that some exopolysaccharide clusters are more important for pathogenesis than others, given that *bce-I* is absent in the host-adapted *B. mallei.*

Although *B. cenocepacia* J2315 encodes the *bce-I* and *bce-II* clusters, an 11-bp deletion causes a frameshift mutation in BCAM0856 so this strain does not produce cepacian (57); however, other gene clusters are involved in exopolysaccharide biosynthesis in this strain (22). One of these recently described putative exopolysaccharide clusters is encoded by 12 loci spanning BCAM1330 – 1341 in *B. cenocepacia* J2315 and has been shown to be essential for biofilm formation (22). Additionally, Fazli et al. demonstrated that a gene downstream of this newly-described cluster, BCAM1349, binds the second messenger cyclic di-GMP and regulates biofilm formation in *B. cenocepacia* J2315 (22, 56). It is not surprising that c-di-GMP signaling is involved in the regulation of exopolysaccharide production and biofilm development (58). Characterization of 23 transposon insertional mutant in genes involved in c-di-GMP signaling in *B. pseudomallei* demonstrated that temperature plays a role in biofilm formation (47), however there is a need to identify the c-di-GMP binding domains in protein from Bpc and Bcc that regulate EPS synthesis similar to BCAM1349.

Another type of exopolysaccharide produced by Bcc bacteria is PNAG (poly- β-1,6-*N*-acetylglucosamine) encoded by the *pga*ABCD operon, which has been shown to be important for biofilm formation (38), yet it has not been examined in the Bpc. Altogether, the Bcc have an impressive repertoire capable of producing seven exopolysaccharides in addition to cepacian, with galactose, glucose, and most recently fucose residues (14). In light of the recent discovery

**Table 2.2 *bce I* (*bceA – bceK*) and *bce II* (*bceM – bceU*) coding loci among Bcc and Bpc.** Adapted from Mangalea, Borlee, and Borlee, 2017.

| | *Burkholderia cepacia* complex | | | | |
|---|---|---|---|---|---|
| Cluster | ***B. vietnamiensis* G4** | ***B. cenocepacia* J2315** | ***B. multivorans* ATCC 17616** | ***B. cepacia* ATCC 25416** | ***B. dolosa* AU0158** |
| ***bce I*** (*bceA – K*) | Bcep1808_4200– Bcep1808_4210 | BCAM0854 – BCAM0864[3] | Bmul4920 – Bmul4910 | BURCEP_RS0128365[4] – BURCEP_RS0128415 | AK34_4592 – AK34_4582 |
| ***bce II*** (*bceM – U*) | Bcep1808_4471 – Bcep1808_4480 | BCAM1003 – BCAM1011 | Bmul4613 – Bmul4604 | BURCEP_RS0129130 – BURCEP_RS0129180 | AK34_4461 – AK34_4452 |

| | *Burkholderia pseudomallei* complex | | | | |
|---|---|---|---|---|---|
| Cluster | ***B. vietnamiensis* G4** | ***B. pseudomallei* 1026b** | ***B. thalandensis* E264** | ***B. oklahomensis* E0147** | ***B. mallei* ATCC 23344** |
| ***bce I*** (*bceA – K*) | Bcep1808_4200 – Bcep1808_4210 | BP1026b_II1966[5] – BP1026b_II1956 | BTH_II0542 – BTH_II0552 | DM82_RS30795 – DM82_RS30745 | N/A |
| ***bce II*** (*bceM – U*) | Bcep1808_4471 – Bcep1808_4480 | BP1026b_II1807 – BP1026b_II1796 | BTH_II0689 – BTH_II0700 | DM82_RS29900 – DM82_RS29930 | BMA1710 – BMA1701 |

---

[3] *B. cenocepacia* J2315 does not produce cepacian; an 11-bp deletion in BCAM0856 causes a frameshift mutation in the *bceI* cluster [56]
[4] *bceI* cluster encoded by 12 genes on chromosome 2, originally identified from clinically isolated *B. cepacia* IST408 [21]
[5] CPS III is encoded by 11 genes spanning Bp1026b_II1956 – Bp1026b_II1966 [33]

of a novel fucose-containing exopolysaccharide in *B. thailandensis* (Bpc) via lectin-binding experiments (50), it will be interesting to determine what similarities, if any, exist between the fucose-rich moieties produced by Bpc and Bcc bacteria. The progress made in characterization of Bcc exopolysaccharides thus far provides a valuable resource for identifying homologous functional gene clusters in Bpc bacteria, given the observed level of conservation for polysaccharide genetic organization (**Tables 2.1 and 2.2**).

### 2.2.4 The acidic exopolysaccharide

The first exopolysaccharide to be isolated and structurally identified in *B. pseudomallei* is described as the acidic polysaccharide and is composed of repeating galactose residues with an ulosonic acid (Kdo) residue: [→3)-β-D-Galp2Ac-(1→4)-A-D-Galp-(1→3)-β-D-Galp-(1→5)-β-Kdo-(2→]n (59). Kdo, or 3-Deoxy-D-*manno*-oct-2-ulosonic acid, was originally identified as a component of the LPS but is now recognized to be an important element of CPS in many species including Bpc bacteria (59). The Gal-Kdo has also recently been isolated from the Georgian strain of *B. oklahomensis* E0147 (60). Interestingly, an identical polysaccharide structure comprised of repeating galacatose residues, an *o*-acetyl group, and the Kdo residue has been characterized in a clinically isolated strain of *B. cepacia*, indicating that the acidic polysaccharide is equally important for Bcc species (16). In addition to *B. cepacia,* the galactose-Kdo extracellular structure has been isolated from *B. stabilis, B. dolosa, B. ambifaria* (18), as well as clinical strains of *B. multivorans* and *B. cenocepacia* (19) comprising the Bcc group. Thus, while cepacian is recognized as the primary extracellular polysaccharide among the Bcc, it is worth investigating the acidic polysaccharide in infection, based on its high conservation.

### 2.3 Status of characterization – capsular polysaccharides

## 2.3.1 CPS encoded by the Bpc

The bacterial capsule is defined as a hydrated polysaccharide layer that surrounds and may be covalently attached to the cell surface (31). The first *B. pseudomallei* capsular polysaccharide (CPS I) described was originally reported as a type I O-polysaccharide moiety, an unbranched homopolymer encoded by 21 genes on chromosome I: [→3)-2-*O*-acetyl-6-deoxy- β-D-*manno*-heptopyranose-(1→] (27). More recently, CPS I from *B. pseudomallei* K96243 was expanded to include 25 genes (BPSL2786 – BPSL2810) and one pseudogene (BPSL2806a), encoded by a 34.5 kb locus (39). An original bioinformatics analysis of this cluster identified putative glycosyltransferases, transporters, sugar and lipid biosynthesis genes, among loci of unknown function (39). Of these previously undefined loci, BPSL2799 (*wcbI*), has been recently characterized to encode a functional acetyltransferase essential for CPS I biosynthesis (61). At least four CPS clusters – CPS I, II, II, and IV – have been proposed with homologous clusters across the Bpc bacteria with the exception of *B. mallei* (Table 1). *B. mallei,* whose genome has been reduced during host-adapted evolution (42), completely lacks CPS II, CPS III, and CPS IV, although a couple of remnants remain at loci BMA0274 (*wcaJ*, CPS III) and BMA2284.1 (hypothetical gene, CPS IV). CPS III, encoded by an 11-gene cluster (BPSS1825 – BPSS1835), has been functionally characterized as a distinct polysaccharide cluster in *B. pseudomallei* K96243 that is not involved in pathogenesis in an acute model of melioidosis using Syrian hamsters (33). Much less is known about CPS II and CPS IV, encoded by BPSS0417 – BPSS0419 and BPSL2769 – BPSL2785: however, these genetic clusters are well conserved among Bpc members (**Table 2.1**).

Interestingly, a CPS I mutant of *B. pseudomallei* 1026b exhibits enhanced biofilm formation as compared to wild type (41, 62). This enhancement of biofilm formation of the CPS I mutant suggests that perhaps there is a reallocation of resources in the bacterium which allows for compensation when one polysaccharide biosynthetic pathway is nonfunctional. Ultimately,

these data indicate the regulation of polysaccharide biosynthetic pathways in *Burkholderia* spp. is complex.

### 2.3.2 Structural characterization of *B. pseudomallei* capsular polysaccharides

Initially described as the O-antigen (type I O-PS) of the lipopolysaccharide in *B. pseudomallei*, the primary capsular polysaccharide is composed of D-*manno*-heptopyranoside residues (63). Currently this structure is defined as CPS I in *B. pseudomallei* and *B. mallei*, and encoded by the largest known locus responsible for biosynthesis of a bacterial repeating sugar unit (39). The CPS I antigen has been repeatedly characterized as an unbranched homopolymer with the following structure: [→3)-2-*O*-acetyl-6-deoxy-β-D-*manno*-heptopyranose-(1→] (27-29, 63). To date, three varieties of OPS have been described and annotated in *B. pseudomallei* (64): the predominant type A (BPSL2672 – BPSL2687; Bp K96264), type B (BUC_3392 – 3416; Bp 576), and type B2 (BURP840_LPSb01 – BURP840_LPSb21; Bp MSHR840). In the Bcc, the O-antigen of the lipopolysaccharide has been described in *B. cenocepacia* (although strain J2315 is O-antigen deficient) as a 29-kb region of 24 loci including *rmlBACD*, predicted to encode for dTDP-rhamnose synthesis, and *wbiI*, predicted to encode for UDP-GalNAc synthesis (65) (BCAL3135 – BCAL3110, Table 1).

*B. pseudomallei* type A OPS (formerly type II O-PS), is reported as an unbranched disaccharide with repeating units in the following structure: [→3)-β -D-glucopyranose-(1-3)-α-L-6-deoxy-talopyranose-(1→], with either 2-O-methyl, 4-O-acetyl, or 2-O-acetyl modifications to the 6-deoxy-talose residues (63, 66). This predominant OPS moiety is produced almost identically in *B. mallei*, however the 4-O-acetyl modification is missing in this close relative (67). Interestingly, *B. thailandensis* synthesizes a nearly identical OPS moiety, but uses an additional 3-O-methyl modification to the 6dTal residue to terminate the oligopolysaccharide elongation (68). The 3-O-methylated 6dTal residue has also been identified in both *B. pseudomallei* and *B. mallei* suggesting that this mechanism is important for O-antigens across Bpc species (66).

### 2.3.3 CPS encoded by the Bcc

Given the importance in pathogenesis and environmental survival in the majority of Bpc, CPS antigens have not been fully characterized in the Bcc, despite the apparent coding capacity for CPS clusters. CPS I is encoded by 28 genes in *B. cenocepacia* J2315 (BCAL3217 – BCAL3246) based on previously published reports and our bioinformatics analyses; however, expression of this cluster is most likely impeded by the insertion of an IS element in gene responsible for export (57). Interestingly, CPS III from the Bpc is homologous to the *bce-I* 16.2 kb gene cluster originally implicated in cepacian biosynthesis in *B. cepacia and B. cenocepacia* (21). The genetic organization of the *bce-I*/bce-*II* clusters suggests that the functional homologs of these loci can encode cepacian even in Bpc strains, whereas *bce-I* clusters are annotated as capsular polysaccharides (**Table 2.2**).

### 2.4 *Burkholderia* adhesins, trimeric autotransporters, CDI systems, and eDNA

An important function of the EPS matrix in *Burkholderia* spp. is cell-cell adherence to environmental surfaces and host tissues. Several extracellular proteins that comprise EPS components have been recently identified in *B. pseudomallei* and the Bpc, including the BoaA and BoaB adhesins (69), the BcaA autotransporter outer membrane protein (BPSL2237) (70), as well as BcpA toxin and the contact-dependent growth inhibition (CDI) system encoded by *bcpAIOB* (34, 35, 71). Within a community of bacteria living as a biofilm, CDI systems act to modulate group behaviors, and the extracellular activity of BcpA has recently been characterized in *B. thailandensis* (Bpc) to promote biofilm formation and autoaggregation (34, 71). Secreted autotransporter (AT) proteins in *B. pseudomallei* are equally important for adherence as well as cellular invasion and dissemination during infection (36, 37, 69, 70, 72). Of note, the recently identified AT adhesins in *B. pseudomallei:* BbfA (36), BoaA/B (69), BcaA (70), and BcpA (34) warrant further investigation within the context of larger EPS matrix components and potential interactions with other secreted polysaccharides and eDNA. To date, eleven loci

that are predicted to encode autotransporters have been identified in *B. pseudomallei* (**Table 2.1**) (73). Recently, the predicted *B. pseudomallei* autotransporters were assessed for pathogenesis-associated phenotypes such as adhesion and invasion via transposon mutagenesis studies (73). While such mutagenesis studies are valuable for autotransporter characterization in *Burkholderia* spp., the mechanisms by which these proteins modulate components within the EPS matrix in relation to pathogenesis are largely undetermined.

eDNA is an important contributing factor for EPS matrix stabilization that forms a network with the above-mentioned adhesins and polysaccharide moieties (3, 74). Much of what is known about the role of eDNA in biofilm formation has been elucidated in model organisms such as *P. aeruginosa* (74). Unfortunately, very little is known about the role of eDNA in *B. pseudomallei*, although a recent study suggests eDNA is produced via extrusion from live cells and is controlled by the transcriptional regulator BPSL1887 (75). eDNA has also recently been shown to enhance biofilm formation (34) and autoaggregation (71) in *B. thailandensis* and to contribute to antimicrobial resistance as part of the EPS matrix in *B. cepacia* (24). Thus, it is evident that in addition to the polysaccharide EPS components, proteins and eDNA may also serve additional important functional roles for the EPS matrix secreted by *B. pseudomallei* and warrant further investigation in persistence and host pathogenicity.

### 2.5 Conclusions

*Burkholderia pseudomallei*, the causative agent of melioidosis, is a sapronotic disease agent and a top-priority public health risk throughout tropical and subtropical regions worldwide. *B. pseudomallei* can produce a variety of capsular and extracellular polysaccharides, in addition to other EPS components that contribute to its ability to survive in the environment as well as host phagocytic cells and serum during infection. Given the importance of the EPS for *B. pseudomallei* survival and establishment of infection, there is a critical need to functionally characterize and agree to a consensus regarding the annotation and classification of these EPS

components. To that end, the information presented here seeks to illuminate the discrepancies between annotations in the Bpc and Bcc fields of research, and we propose a call to action for a clear consensus of the already muddled EPS "slime". Identification and functional characterization of EPS matrix components will undoubtedly facilitate the development of new strategies to detect and treat melioidosis infections as more cases are being readily identified in endemic areas. While CPS I (76) and type A OPS are current frontrunners for the development of diagnostics (77), there are additional polysaccharides and EPS components encoded by Bpc that may serve as markers for variant serotypes or different manifestations of disease progression (e.g. persistent vs. acute infection). Similarly, vaccine candidates could also be selected to provide protection from the multiple routes of infection and the natural diversity of the O-antigen *B. pseudomallei* LPS (78).

To date, four CPS gene clusters have been identified in *B. pseudomallei* of which CPS I is widely considered as the most important virulence determinant for the development of non-invasive diagnostics (76, 79, 80) and vaccine therapeutics (29). Much less is known regarding the diversity of exopolysaccharides produced by *B. pseudomallei* and the Bpc, although up to seven different exopolysaccharides have been characterized for bacteria in the Bcc. We have observed that the *B. pseudomallei* CPS-III is in fact the same gene cluster assigned to *bce-I* in *B. vietnamiensis* and other Bcc species, thus there is ambiguity regarding the differentiation between exopolysaccharide and CPS in this case. It is also evident there is a need for more comprehensive analyses regarding the EPS matrix components produced by *B. pseudomallei* that contribute to host colonization, survival, and biofilm formation. Our lab has characterized a novel exopolysaccharide biosynthetic gene cluster in *B. pseudomallei* (41), but these and additional EPS biosynthetic loci warrant further functional characterization and comparison between pathogenic and environmental isolates across the Bpc and Bcc. Additional functional analyses of the EPS matrix components produced by *B. pseudomallei* will undoubtedly aid in

the development of novel diagnostics and therapeutics for identifying and treating the various disease manifestations associated with melioidosis.

## 2.6 Summary of Aims

### <u>Aim I Chapter 3</u>

To evaluate biofilm formation in response to nitrate, and identify specific loci as well as genetic mechanisms responsible for altering biofilm dynamics.

**Hypothesis:**

Exogenous nitrate, a component of fertilizer and a byproduct of animal waste, inhibits *B. pseudomallei* biofilms by potentially modulating the intracellular concentration of the secondary messenger cyclic di-GMP.

### <u>Aim II Chapter 4</u>

**Part 1:** To characterize the global transcriptional response of nitrate and nitrite in *B. pseudomallei*, identify functional clusters related to biofilm formation and physiology, cyclic di-GMP and nitrate signaling cascades.

**Hypothesis:**

Biofilm inhibition in response to exogenous N-oxides results in transcriptional reduction in key exopolysaccharide biosynthesis clusters and capsular polysaccharide clusters, and is mediated by upregulation of nitrate and cyclic di-GMP metabolic loci.

**Part 2:** To evaluate *B. pseudomallei* intracellular replication and survival *in vivo* and determine if the nitrate sensing two-component system NarX-NarL is required for intracellular survival.

**Hypothesis:**

Reduction of N-oxides promotes intracellular survival and disruption of the nitrate-sensing components NarX and NarL will impede intracellular growth in *B. pseudomallei*.

## 2.7 A Look Back

Before beginning to describe the relationship between *Burkholderia pseudomallei* biofilm dynamics and N-oxide sensing and metabolism, it is worthwhile to orient the reader with the scientific consensus on these topics. At the onset of my graduate studies, the biofilm mode of growth of *B. pseudomallei* had been well established several years prior. One of the first studies to define bacterial biofilm formation in both laboratory media and animal tissue described micro-colonies of *B. pseudomallei* encased in large amounts of exopolysaccharide (81). At the same time, *B. pseudomallei* biofilms were characterized by the degree of resistance to the most common antibiotics used for melioidosis and mechanisms of persistence and chronic infections were hypothesized to hinge on biofilm formation (10). Since the 1990s, many studies have confirmed *B. pseudomallei* biofilm formation as a mechanism of survival and persistence in the environment as well as in human and animal hosts (7, 81-83). As an environmental saprophyte and a facultative intracellular pathogen, *B. pseudomallei* has been shown to withstand several stressors, leading to numerous explorations into factors that influence its survival across niches.

It has been hypothesized that *B. pseudomallei* has a selective advantage over other species in disturbed and eutrophic ecosystems partly due to its faculties for polyphosphate accumulation and denitrification (84). Among the factors that drive its environmental persistence (see **Chapter 1**), anaerobic metabolism via denitrification has long been considered a potential pathogenicity determinant for *B. pseudomallei* (82); however, a clear link between denitrification and biofilm dynamics was missing. A putative description of denitrification clusters has been described in *B. pseudomallei* in relation to other proteobacteria (85), however their specificity or functional redundancy between the two chromosomes has not been addressed. Likewise, a role for the predicted nitrate-sensing system NarX-NarL in *B. pseudomallei* biofilm formation has yet to be established. The bis-molybdopterin biosynthetic pathway, which is required for the nitrate reductase enzyme activity, had been characterized in relation to anaerobic growth, biofilm formation, and motility in *B. thailandensis* a year prior to the start of this work (86). Thus, despite

the apparent connections between nitrogen byproducts and *Burkholderia* biology, a clear role for N-oxide effects on *B. pseudomallei* biofilms and the use of nitrate or nitrite as respiratory substrates remained to be determined.

Prior to this work, several studies in *Pseudomonas aeruginosa* characterized the importance of the free radical nitric oxide (NO) as a biofilm dispersal signaling molecule (87-90). NO is a ubiquitous signaling molecule in the natural world and its role in bacterial signaling is considerably complex due to its versatility and toxicity (91). The use of nitrogen byproducts as biofilm inhibitory agents has been demonstrated mainly in the context of cystic fibrosis pathogens, where the use of acidified sodium nitrite has been proposed as a biocide against mucoid *P. aeruginosa* (92-94). Indeed, sodium nitrite, whether acidified or not, has been shown to inhibit growth of several species including *Helicobacter pylori* (95), *Clostridium difficile* (96), *Staphylococcus aureus* (97), in addition to *P. aeruginosa* (98). Evidently, nitrite and its derivative nitrous acid have strong bactericidal effects; nitrate and nitrite have been historically used to cure meats, fish, and cheeses for these reasons (99). However, the goals of the studies presented here are not to pile onto a previous mountain of work describing nitrate- and nitrite-derived compounds that can be used as medical or commercial biocides.

The big question addressed in the studies presented here is "how do bacterial pathogens transition from an environmental reservoir to establish persistent infections and ultimately disseminate within a host?" *Burkholderia pseudomallei* is an ideal candidate for these studies because it is a sapronotic disease agent that transitions from the environment to cause multiple types of infections (acute, chronic, and latent) that are difficult to treat. I propose that the ability to sense and acquire nitrate from the environment enables *B. pseudomallei* to adapt to anaerobic respiration, shifting from biofilm to planktonic cells that promote propagation via a global transcriptional response. The data presented in the next two chapters will shed light on the response to exogenous N-oxides in relation to biofilm formation and pathogenicity in *B. pseudomallei* and ultimately improve our understanding of this organism's complex biology.

# References

1.	Flemming HC. EPS-Then and Now. Microorganisms. 2016;4(4).
2.	Flemming HC, Neu TR, Wozniak DJ. The EPS matrix: the "house of biofilm cells". J Bacteriol. 2007;189(22):7945-7.
3.	Gunn JS, Bakaletz LO, Wozniak DJ. What's on the Outside Matters: The Role of the Extracellular Polymeric Substance of Gram-negative Biofilms in Evading Host Immunity and as a Target for Therapeutic Intervention. J Biol Chem. 2016;291(24):12538-46.
4.	Roberson EB, Firestone MK. Relationship between Desiccation and Exopolysaccharide Production in a Soil *Pseudomonas* sp. Appl Environ Microbiol. 1992;58(4):1284-91.
5.	Ramli NS, Eng Guan C, Nathan S, Vadivelu J. The effect of environmental conditions on biofilm formation of *Burkholderia pseudomallei* clinical isolates. PLoS One. 2012;7(9):e44104.
6.	Prasertsincharoen N, Constantinoiu C, Gardiner C, Warner J, Elliman J. Effects of Colonization of the Roots of Domestic Rice (*Oryza sativa* L. cv. Amaroo) by *Burkholderia pseudomallei*. Appl Environ Microbiol. 2015;81(13):4368-75.
7.	Inglis TJ, Sagripanti JL. Environmental factors that affect the survival and persistence of *Burkholderia pseudomallei*. Appl Environ Microbiol. 2006;72(11):6865-75.
8.	Sawasdidoln C, Taweechaisupapong S, Sermswan RW, Tattawasart U, Tungpradabkul S, Wongratanacheewin S. Growing *Burkholderia pseudomallei* in biofilm stimulating conditions significantly induces antimicrobial resistance. PLoS One. 2010;5(2):e9196.
9.	Pibalpakdee P, Wongratanacheewin S, Taweechaisupapong S, Niumsup PR. Diffusion and activity of antibiotics against *Burkholderia pseudomallei* biofilms. Int J Antimicrob Agents. 2012;39(4):356-9.
10.	Vorachit M, Lam K, Jayanetra P, Costerton JW. Resistance of *Pseudomonas pseudomallei* growing as a biofilm on silastic discs to ceftazidime and co-trimoxazole. Antimicrob Agents Chemother. 1993;37(9):2000-2.
11.	Taweechaisupapong S, Kaewpa C, Arunyanart C, Kanla P, Homchampa P, Sirisinha S, Proungvitaya T, Wongratanacheewin S. Virulence of *Burkholderia pseudomallei* does not correlate with biofilm formation. Microb Pathog. 2005;39(3):77-85.
12.	Limmathurotsakul D, Paeyao A, Wongratanacheewin S, Saiprom N, Takpho N, Thaipadungpanit J, Chantratita N, Wuthiekanun V, Day NP, Peacock SJ. Role of *Burkholderia pseudomallei* biofilm formation and lipopolysaccharide in relapse of melioidosis. Clin Microbiol Infect. 2014;20(11):O854-6.
13.	Steinmetz I, Rohde M, Brenneke B. Purification and characterization of an exopolysaccharide of *Burkholderia* (*Pseudomonas*) *pseudomallei*. Infect Immun. 1995;63(10):3959-65.
14.	Cescutti P, Cuzzi B, Herasimenka Y, Rizzo R. Structure of a novel exopolysaccharide produced by *Burkholderia vietnamiensis*, a cystic fibrosis opportunistic pathogen. Carbohydr Polym. 2013;94(1):253-60.
15.	Cescutti P, Impallomeni G, Garozzo D, Rizzo R. O-Acetyl location on cepacian, the principal exopolysaccharide of *Burkholderia cepacia* complex bacteria. Carbohydr Res. 2011;346(18):2905-12.
16.	Cescutti P, Impallomeni G, Garozzo D, Sturiale L, Herasimenka Y, Lagatolla C, Rizzo R. Exopolysaccharides produced by a clinical strain of *Burkholderia cepacia* isolated from a cystic fibrosis patient. Carbohydr Res. 2003;338(23):2687-95.
17.	Chiarini L, Cescutti P, Drigo L, Impallomeni G, Herasimenka Y, Bevivino A, Dalmastri C, Tabacchioni S, Manno G, Zanetti F, Rizzo R. Exopolysaccharides produced by *Burkholderia cenocepacia recA* lineages IIIA and IIIB. J Cyst Fibros. 2004;3(3):165-72.

18. Cuzzi B, Herasimenka Y, Silipo A, Lanzetta R, Liut G, Rizzo R, Cescutti P. Versatility of the *Burkholderia cepacia* complex for the biosynthesis of exopolysaccharides: a comparative structural investigation. PLoS One. 2014;9(4):e94372.

19. Herasimenka Y, Cescutti P, Impallomeni G, Campana S, Taccetti G, Ravenni N, Zanetti F, Rizzo R. Exopolysaccharides produced by clinical strains belonging to the *Burkholderia cepacia* complex. J Cyst Fibros. 2007;6(2):145-52.

20. Ferreira AS, Leitao JH, Silva IN, Pinheiro PF, Sousa SA, Ramos CG, Moreira LM. Distribution of cepacian biosynthesis genes among environmental and clinical *Burkholderia* strains and role of cepacian exopolysaccharide in resistance to stress conditions. Appl Environ Microbiol. 2010;76(2):441-50.

21. Moreira LM, Videira PA, Sousa SA, Leitao JH, Cunha MV, Sa-Correia I. Identification and physical organization of the gene cluster involved in the biosynthesis of *Burkholderia cepacia* complex exopolysaccharide. Biochem Biophys Res Commun. 2003;312(2):323-33.

22. Fazli M, McCarthy Y, Givskov M, Ryan RP, Tolker-Nielsen T. The exopolysaccharide gene cluster Bcam1330-Bcam1341 is involved in *Burkholderia cenocepacia* biofilm formation, and its expression is regulated by c-di-GMP and Bcam1349. Microbiologyopen. 2013;2(1):105-22.

23. Laroussarie A, Barycza B, Andriamboavonjy H, Tamigney Kenfack M, Bleriot Y, Gauthier C. Synthesis of the Tetrasaccharide Repeating Unit of the beta-Kdo-Containing Exopolysaccharide from *Burkholderia pseudomallei* and *B. cepacia* Complex. J Org Chem. 2015;80(20):10386-96.

24. Messiaen AS, Nelis H, Coenye T. Investigating the role of matrix components in protection of *Burkholderia cepacia* complex biofilms against tobramycin. J Cyst Fibros. 2014;13(1):56-62.

25. Novotny LA, Amer AO, Brockson ME, Goodman SD, Bakaletz LO. Structural stability of *Burkholderia cenocepacia* biofilms is reliant on eDNA structure and presence of a bacterial nucleic acid binding protein. PLoS One. 2013;8(6):e67629.

26. Dando SJ, Ipe DS, Batzloff M, Sullivan MJ, Crossman DK, Crowley M, Strong E, Kyan S, Leclercq SY, Ekberg JA, St John J, Beacham IR, Ulett GC. *Burkholderia pseudomallei* Capsule Exacerbates Respiratory Melioidosis but Does Not Afford Protection against Antimicrobial Signaling or Bacterial Killing in Human Olfactory Ensheathing Cells. Infect Immun. 2016;84(7):1941-56.

27. Reckseidler SL, DeShazer D, Sokol PA, Woods DE. Detection of bacterial virulence genes by subtractive hybridization: identification of capsular polysaccharide of *Burkholderia pseudomallei* as a major virulence determinant. Infect Immun. 2001;69(1):34-44.

28. Reckseidler-Zenteno SL, DeVinney R, Woods DE. The capsular polysaccharide of *Burkholderia pseudomallei* contributes to survival in serum by reducing complement factor C3b deposition. Infect Immun. 2005;73(2):1106-15.

29. Marchetti R, Dillon MJ, Burtnick MN, Hubbard MA, Kenfack MT, Bleriot Y, Gauthier C, Brett PJ, AuCoin DP, Lanzetta R, Silipo A, Molinaro A. *Burkholderia pseudomallei* Capsular Polysaccharide Recognition by a Monoclonal Antibody Reveals Key Details toward a Biodefense Vaccine and Diagnostics against Melioidosis. ACS Chem Biol. 2015;10(10):2295-302.

30. Whitfield C. Bacterial extracellular polysaccharides. Can J Microbiol. 1988;34(4):415-20.

31. Roberts IS. The biochemistry and genetics of capsular polysaccharide production in bacteria. Annu Rev Microbiol. 1996;50:285-315.

32. Warawa JM, Long D, Rosenke R, Gardner D, Gherardini FC. Role for the *Burkholderia pseudomallei* capsular polysaccharide encoded by the *wcb* operon in acute disseminated melioidosis. Infect Immun. 2009;77(12):5252-61.

33. Reckseidler-Zenteno SL, Viteri DF, Moore R, Wong E, Tuanyok A, Woods DE. Characterization of the type III capsular polysaccharide produced by *Burkholderia pseudomallei*. J Med Microbiol. 2010;59(Pt 12):1403-14.
34. Garcia EC, Anderson MS, Hagar JA, Cotter PA. Burkholderia BcpA mediates biofilm formation independently of interbacterial contact-dependent growth inhibition. Mol Microbiol. 2013;89(6):1213-25.
35. Garcia EC, Perault AI, Marlatt SA, Cotter PA. Interbacterial signaling via *Burkholderia* contact-dependent growth inhibition system proteins. Proc Natl Acad Sci U S A. 2016;113(29):8296-301.
36. Lazar Adler NR, Dean RE, Saint RJ, Stevens MP, Prior JL, Atkins TP, Galyov EE. Identification of a predicted trimeric autotransporter adhesin required for biofilm formation of *Burkholderia pseudomallei*. PLoS One. 2013;8(11):e79461.
37. Campos CG, Byrd MS, Cotter PA. Functional characterization of *Burkholderia pseudomallei* trimeric autotransporters. Infect Immun. 2013;81(8):2788-99.
38. Yakandawala N, Gawande PV, LoVetri K, Cardona ST, Romeo T, Nitz M, Madhyastha S. Characterization of the poly-beta-1,6-N-acetylglucosamine polysaccharide component of *Burkholderia* biofilms. Appl Environ Microbiol. 2011;77(23):8303-9.
39. Cuccui J, Milne TS, Harmer N, George AJ, Harding SV, Dean RE, Scott AE, Sarkar-Tyson M, Wren BW, Titball RW, Prior JL. Characterization of the *Burkholderia pseudomallei* K96243 capsular polysaccharide I coding region. Infect Immun. 2012;80(3):1209-21.
40. Cescutti P, Bosco M, Picotti F, Impallomeni G, Leitao JH, Richau JA, Sa-Correia I. Structural study of the exopolysaccharide produced by a clinical isolate of *Burkholderia cepacia*. Biochem Biophys Res Commun. 2000;273(3):1088-94.
41. Borlee GI, Plumley, B. A., Martin, K. H., Somprasong, N., Mangalea, M. R., Islam, M. N., Burtnick, M. N., Brett, P. J., Steinmetz, I., AuCoin, D. P., Belisle, J. T., Crick, D. C., Schweizer, H. P., Borlee, B. R. Genome-scale analysis of the genes that contribute to *Burkholderia pseudomallei* biofilm formation identifies a crucial exopolysaccharide biosynthesis gene cluster. PLoS Negl Trop Dis. 2017;11(6).
42. Holden MT, Titball RW, Peacock SJ, Cerdeno-Tarraga AM, Atkins T, Crossman LC, Pitt T, Churcher C, Mungall K, Bentley SD, Sebaihia M, Thomson NR, Bason N, Beacham IR, Brooks K, Brown KA, Brown NF, Challis GL, Cherevach I, Chillingworth T, Cronin A, Crossett B, Davis P, DeShazer D, Feltwell T, Fraser A, Hance Z, Hauser H, Holroyd S, Jagels K, Keith KE, Maddison M, Moule S, Price C, Quail MA, Rabbinowitsch E, Rutherford K, Sanders M, Simmonds M, Songsivilai S, Stevens K, Tumapa S, Vesaratchavest M, Whitehead S, Yeats C, Barrell BG, Oyston PC, Parkhill J. Genomic plasticity of the causative agent of melioidosis, *Burkholderia pseudomallei*. Proc Natl Acad Sci U S A. 2004;101(39):14240-5.
43. Sahl JW, Vazquez AJ, Hall CM, Busch JD, Tuanyok A, Mayo M, Schupp JM, Lummis M, Pearson T, Shippy K, Colman RE, Allender CJ, Theobald V, Sarovich DS, Price EP, Hutcheson A, Korlach J, LiPuma JJ, Ladner J, Lovett S, Koroleva G, Palacios G, Limmathurotsakul D, Wuthiekanun V, Wongsuwan G, Currie BJ, Keim P, Wagner DM. The Effects of Signal Erosion and Core Genome Reduction on the Identification of Diagnostic Markers. MBio. 2016;7(5).
44. Sim SH, Yu Y, Lin CH, Karuturi RK, Wuthiekanun V, Tuanyok A, Chua HH, Ong C, Paramalingam SS, Tan G, Tang L, Lau G, Ooi EE, Woods D, Feil E, Peacock SJ, Tan P. The core and accessory genomes of *Burkholderia pseudomallei*: implications for human melioidosis. PLoS Pathog. 2008;4(10):e1000178.
45. Kumar AS, Mody K, Jha B. Bacterial exopolysaccharides--a perception. J Basic Microbiol. 2007;47(2):103-17.
46. Flemming HC, Wingender J. The biofilm matrix. Nat Rev Microbiol. 2010;8(9):623-33.

47.     Plumley BA, Martin KH, Borlee GI, Marlenee NL, Burtnick MN, Brett PJ, AuCoin DP, Bowen RA, Schweizer HP, Borlee BR. Thermoregulation of Biofilm Formation in *Burkholderia pseudomallei* Is Disrupted by Mutation of a Putative Diguanylate Cyclase. J Bacteriol. 2017;199(5).

48.     Chin CY, Hara Y, Ghazali AK, Yap SJ, Kong C, Wong YC, Rozali N, Koh SF, Hoh CC, Puthucheary SD, Nathan S. Global transcriptional analysis of *Burkholderia pseudomallei* high and low biofilm producers reveals insights into biofilm production and virulence. BMC Genomics. 2015;16:471.

49.     Mongkolrob R, Taweechaisupapong S, Tungpradabkul S. Correlation between biofilm production, antibiotic susceptibility and exopolysaccharide composition in *Burkholderia pseudomallei bpsI*, *ppk*, and *rpoS* mutant strains. Microbiol Immunol. 2015;59(11):653-63.

50.     Tseng BS, Majerczyk CD, Passos da Silva D, Chandler JR, Greenberg EP, Parsek MR. Quorum Sensing Influences *Burkholderia thailandensis* Biofilm Development and Matrix Production. J Bacteriol. 2016;198(19):2643-50.

51.     Gamage AM, Shui G, Wenk MR, Chua KL. N-Octanoylhomoserine lactone signalling mediated by the BpsI-BpsR quorum sensing system plays a major role in biofilm formation of *Burkholderia pseudomallei*. Microbiology. 2011;157(Pt 4):1176-86.

52.     Chandler JR, Duerkop BA, Hinz A, West TE, Herman JP, Churchill ME, Skerrett SJ, Greenberg EP. Mutational analysis of *Burkholderia thailandensis* quorum sensing and self-aggregation. J Bacteriol. 2009;191(19):5901-9.

53.     Majerczyk C, Brittnacher M, Jacobs M, Armour CD, Radey M, Schneider E, Phattarasokul S, Bunt R, Greenberg EP. Global analysis of the *Burkholderia thailandensis* quorum sensing-controlled regulon. J Bacteriol. 2014;196(7):1412-24.

54.     Majerczyk CD, Brittnacher MJ, Jacobs MA, Armour CD, Radey MC, Bunt R, Hayden HS, Bydalek R, Greenberg EP. Cross-species comparison of the *Burkholderia pseudomallei*, *Burkholderia thailandensis*, and *Burkholderia mallei* quorum-sensing regulons. J Bacteriol. 2014;196(22):3862-71.

55.     Butt A, Halliday N, Williams P, Atkins HS, Bancroft GJ, Titball RW. *Burkholderia pseudomallei kynB* plays a role in AQ production, biofilm formation, bacterial swarming and persistence. Res Microbiol. 2016;167(3):159-67.

56.     Fazli M, O'Connell A, Nilsson M, Niehaus K, Dow JM, Givskov M, Ryan RP, Tolker-Nielsen T. The CRP/FNR family protein Bcam1349 is a c-di-GMP effector that regulates biofilm formation in the respiratory pathogen *Burkholderia cenocepacia*. Mol Microbiol. 2011;82(2):327-41.

57.     Holden MT, Seth-Smith HM, Crossman LC, Sebaihia M, Bentley SD, Cerdeno-Tarraga AM, Thomson NR, Bason N, Quail MA, Sharp S, Cherevach I, Churcher C, Goodhead I, Hauser H, Holroyd N, Mungall K, Scott P, Walker D, White B, Rose H, Iversen P, Mil-Homens D, Rocha EP, Fialho AM, Baldwin A, Dowson C, Barrell BG, Govan JR, Vandamme P, Hart CA, Mahenthiralingam E, Parkhill J. The genome of *Burkholderia cenocepacia* J2315, an epidemic pathogen of cystic fibrosis patients. J Bacteriol. 2009;191(1):261-77.

58.     Romling U, Galperin MY, Gomelsky M. Cyclic di-GMP: the first 25 years of a universal bacterial second messenger. Microbiol Mol Biol Rev. 2013;77(1):1-52.

59.     Nimtz M, Wray V, Domke T, Brenneke B, Haussler S, Steinmetz I. Structure of an acidic exopolysaccharide of *Burkholderia pseudomallei*. Eur J Biochem. 1997;250(2):608-16.

60.     Stone JK, Heiss C, Wang Z, Black I, Grasso SA, Koppisch AT, Azadi P, Keim P, Tuanyok A. Structural characterization of polysaccharides expressed by *Burkholderia oklahomensis* E0147. Carbohydr Res. 2014;386:68-72.

61.     Vivoli M, Ayres E, Beaumont E, Isupov MN, Harmer NJ. Structural insights into WcbI, a novel polysaccharide-biosynthesis enzyme. IUCrJ. 2014;1(Pt 1):28-38.

62.     Wikraiphat C, Charoensap J, Utaisincharoen P, Wongratanacheewin S, Taweechaisupapong S, Woods DE, Bolscher JG, Sirisinha S. Comparative *in vivo* and *in vitro* analyses of putative virulence factors of *Burkholderia pseudomallei* using lipopolysaccharide, capsule and flagellin mutants. FEMS Immunol Med Microbiol. 2009;56(3):253-9.

63.     Perry MB, MacLean LL, Schollaardt T, Bryan LE, Ho M. Structural characterization of the lipopolysaccharide O antigens of *Burkholderia pseudomallei*. Infect Immun. 1995;63(9):3348-52.

64.     Tuanyok A, Stone JK, Mayo M, Kaestli M, Gruendike J, Georgia S, Warrington S, Mullins T, Allender CJ, Wagner DM, Chantratita N, Peacock SJ, Currie BJ, Keim P. The genetic and molecular basis of O-antigenic diversity in *Burkholderia pseudomallei* lipopolysaccharide. PLoS Negl Trop Dis. 2012;6(1):e1453.

65.     Ortega X, Hunt TA, Loutet S, Vinion-Dubiel AD, Datta A, Choudhury B, Goldberg JB, Carlson R, Valvano MA. Reconstitution of O-specific lipopolysaccharide expression in *Burkholderia cenocepacia* strain J2315, which is associated with transmissible infections in patients with cystic fibrosis. J Bacteriol. 2005;187(4):1324-33.

66.     Heiss C, Burtnick MN, Roberts RA, Black I, Azadi P, Brett PJ. Revised structures for the predominant O-polysaccharides expressed by *Burkholderia pseudomallei* and *Burkholderia mallei*. Carbohydr Res. 2013;381:6-11.

67.     Burtnick MN, Brett PJ, Woods DE. Molecular and physical characterization of *Burkholderia mallei* O antigens. J Bacteriol. 2002;184(3):849-52.

68.     Heiss C, Burtnick MN, Black I, Azadi P, Brett PJ. Detailed structural analysis of the O-polysaccharide expressed by *Burkholderia thailandensis* E264. Carbohydr Res. 2012;363:23-8.

69.     Balder R, Lipski S, Lazarus JJ, Grose W, Wooten RM, Hogan RJ, Woods DE, Lafontaine ER. Identification of *Burkholderia mallei* and *Burkholderia pseudomallei* adhesins for human respiratory epithelial cells. BMC Microbiol. 2010;10:250.

70.     Campos CG, Borst L, Cotter PA. Characterization of BcaA, a putative classical autotransporter protein in *Burkholderia pseudomallei*. Infect Immun. 2013;81(4):1121-8.

71.     Anderson MS, Garcia EC, Cotter PA. The *Burkholderia bcpAIOB* genes define unique classes of two-partner secretion and contact dependent growth inhibition systems. PLoS Genet. 2012;8(8):e1002877.

72.     Muangman S, Korbsrisate, S., Muangsombut, V., Srinon, V., Adler, N.L., Schroeder, G.N., Frankel, G. and Galyov, E.E. BopC is a type III secreted effector protein of *Burkholderia pseudomallei*. FEMS Microbiol Lett. 2011;323(1):75-82.

73.     Adler NRL, Stevens MP, Dean RE, Saint RJ, Pankhania D, Prior JL, Atkins TP, Kessler B, Nithichanon A, Lertmemongkolchai G, Galyov EE. Systematic Mutagenesis of Genes Encoding Predicted Autotransported Proteins of *Burkholderia pseudomallei* Identifies Factors Mediating Virulence in Mice, Net Intracellular Replication and a Novel Protein Conferring Serum Resistance. PLoS One. 2015;10(4).

74.     Gloag ES, Turnbull L, Huang A, Vallotton P, Wang H, Nolan LM, Mililli L, Hunt C, Lu J, Osvath SR, Monahan LG, Cavaliere R, Charles IG, Wand MP, Gee ML, Prabhakar R, Whitchurch CB. Self-organization of bacterial biofilms is facilitated by extracellular DNA. Proc Natl Acad Sci U S A. 2013;110(28):11541-6.

75.     Austin CR, Goodyear AW, Bartek IL, Stewart A, Sutherland MD, Silva EB, Zweifel A, Vitko NP, Tuanyok A, Highnam G, Mittelman D, Keim P, Schweizer HP, Vazquez-Torres A, Dow SW, Voskuil MI. A *Burkholderia pseudomallei* colony variant necessary for gastric colonization. MBio. 2015;6(1).

76.     Nualnoi T, Kirosingh A, Pandit SG, Thorkildson P, Brett PJ, Burtnick MN, AuCoin DP. In vivo Distribution and Clearance of Purified Capsular Polysaccharide from *Burkholderia pseudomallei* in a Murine Model. PLoS Negl Trop Dis. 2016;10(12):e0005217.

77.    Pumpuang A, Dunachie SJ, Phokrai P, Jenjaroen K, Sintiprungrat K, Boonsilp S, Brett PJ, Burtnick MN, Chantratita N. Comparison of O-polysaccharide and hemolysin co-regulated protein as target antigens for serodiagnosis of melioidosis. PLoS Negl Trop Dis. 2017;11(3):e0005499.

78.    Titball RW, Burtnick MN, Bancroft GJ, Brett P. *Burkholderia pseudomallei* and *Burkholderia mallei* vaccines: Are we close to clinical trials? Vaccine. 2017.

79.    Suttisunhakul V, Chantratita N, Wikraiphat C, Wuthiekanun V, Douglas Z, Day NP, Limmathurotsakul D, Brett PJ, Burtnick MN. Evaluation of Polysaccharide-Based Latex Agglutination Assays for the Rapid Detection of Antibodies to *Burkholderia pseudomallei*. Am J Trop Med Hyg. 2015;93(3):542-6.

80.    Houghton RL, Reed DE, Hubbard MA, Dillon MJ, Chen H, Currie BJ, Mayo M, Sarovich DS, Theobald V, Limmathurotsakul D, Wongsuvan G, Chantratita N, Peacock SJ, Hoffmaster AR, Duval B, Brett PJ, Burtnick MN, Aucoin DP. Development of a prototype lateral flow immunoassay (LFI) for the rapid diagnosis of melioidosis. PLoS Negl Trop Dis. 2014;8(3):e2727.

81.    Vorachit M, Lam K, Jayanetra P, Costerton JW. Electron microscopy study of the mode of growth of *Pseudomonas pseudomallei in vitro* and *in vivo*. J Trop Med Hyg. 1995;98(6):379-91.

82.    Kanai K, Kondo E. Recent advances in biomedical sciences of *Burkholderia pseudomallei* (basonym: *Pseudomonas pseudomallei*). Jpn J Med Sci Biol. 1994;47(1):1-45.

83.    Kamjumphol W, Chareonsudjai S, Chareonsudjai P, Wongratanacheewin S, Taweechaisupapong S. Environmental factors affecting *Burkholderia pseudomallei* biofilm formation. Southeast Asian J Trop Med Public Health. 2013;44(1):72-81.

84.    Kaestli M, Harrington G, Mayo M, Chatfield MD, Harrington I, Hill A, Munksgaard N, Gibb K, Currie BJ. What drives the occurrence of the melioidosis bacterium *Burkholderia pseudomallei* in domestic gardens? PLoS Negl Trop Dis. 2015;9(3):e0003635.

85.    Philippot L. Denitrifying genes in bacterial and Archaeal genomes. Biochim Biophys Acta. 2002;1577(3):355-76.

86.    Andreae CA, Titball RW, Butler CS. Influence of the molybdenum cofactor biosynthesis on anaerobic respiration, biofilm formation and motility in *Burkholderia thailandensis*. Res Microbiol. 2014;165(1):41-9.

87.    Barnes RJ, Bandi RR, Wong WS, Barraud N, McDougald D, Fane A, Kjelleberg S, Rice SA. Optimal dosing regimen of nitric oxide donor compounds for the reduction of *Pseudomonas aeruginosa* biofilm and isolates from wastewater membranes. Biofouling. 2013;29(2):203-12.

88.    Barraud N, Hassett DJ, Hwang SH, Rice SA, Kjelleberg S, Webb JS. Involvement of nitric oxide in biofilm dispersal of *Pseudomonas aeruginosa*. J Bacteriol. 2006;188(21):7344-53.

89.    Barraud N, Schleheck D, Klebensberger J, Webb JS, Hassett DJ, Rice SA, Kjelleberg S. Nitric oxide signaling in *Pseudomonas aeruginosa* biofilms mediates phosphodiesterase activity, decreased cyclic di-GMP levels, and enhanced dispersal. J Bacteriol. 2009;191(23):7333-42.

90.    Barraud N, Storey MV, Moore ZP, Webb JS, Rice SA, Kjelleberg S. Nitric oxide-mediated dispersal in single- and multi-species biofilms of clinically and industrially relevant microorganisms. Microb Biotechnol. 2009;2(3):370-8.

91.    Poole RK. Nitric oxide and nitrosative stress tolerance in bacteria. Biochem Soc Trans. 2005;33(Pt 1):176-80.

92.    Major TA, Panmanee W, Mortensen JE, Gray LD, Hoglen N, Hassett DJ. Sodium nitrite-mediated killing of the major cystic fibrosis pathogens *Pseudomonas aeruginosa*,

*Staphylococcus aureus*, and *Burkholderia cepacia* under anaerobic planktonic and biofilm conditions. Antimicrob Agents Chemother. 2010;54(11):4671-7.

93. Yoon SS, Coakley R, Lau GW, Lymar SV, Gaston B, Karabulut AC, Hennigan RF, Hwang SH, Buettner G, Schurr MJ, Mortensen JE, Burns JL, Speert D, Boucher RC, Hassett DJ. Anaerobic killing of mucoid *Pseudomonas aeruginosa* by acidified nitrite derivatives under cystic fibrosis airway conditions. J Clin Invest. 2006;116(2):436-46.

94. Zemke AC, Shiva S, Burns JL, Moskowitz SM, Pilewski JM, Gladwin MT, Bomberger JM. Nitrite modulates bacterial antibiotic susceptibility and biofilm formation in association with airway epithelial cells. Free Radic Biol Med. 2014;77:307-16.

95. Dykhuizen RS, Fraser A, McKenzie H, Golden M, Leifert C, Benjamin N. *Helicobacter pylori* is killed by nitrite under acidic conditions. Gut. 1998;42(3):334-7.

96. Cunningham R, Mustoe E, Spiller L, Lewis S, Benjamin N. Acidified nitrite: a host defence against colonization with *C. difficile* spores? J Hosp Infect. 2014;86(2):155-7.

97. Schlag S, Nerz C, Birkenstock TA, Altenberend F, Gotz F. Inhibition of staphylococcal biofilm formation by nitrite. J Bacteriol. 2007;189(21):7911-9.

98. Zemke AC, Gladwin MT, Bomberger JM. Sodium nitrite blocks the activity of aminoglycosides against *Pseudomonas aeruginosa* biofilms. Antimicrob Agents Chemother. 2015;59(6):3329-34.

99. Cammack R, Joannou CL, Cui XY, Torres Martinez C, Maraj SR, Hughes MN. Nitrite and nitrosyl compounds in food preservation. Biochim Biophys Acta. 1999;1411(2-3):475-88.

**CHAPTER 3: Nitrate sensing and metabolism inhibit biofilm formation in the opportunistic pathogen *Burkholderia pseudomallei* by reducing the intracellular concentration of c-di-GMP[6]**

The work presented in this chapter and published research article describes a genetic mechanism for nitrate-mediated biofilm inhibition in the clinical isolate *B. pseudomallei* 1026b. We identified genes encoding a nitrate-sensing two-component system *narX/narL* adjacent to genetic elements of the primary nitrate reductase *narGHJI-1* that are linked to biofilm formation in the presence of exogenous nitrate. Additionally, we quantified the intracellular concentration of the second messenger molecule cyclic di-GMP and showed its significant decrease in response to exogenous nitrate, corresponding to an increase in the phosphodiesterase *cdpA*.

## 3.1 Summary

The opportunistic pathogen *Burkholderia pseudomallei* is a saprophytic bacterium and the causative agent of melioidosis, an emerging infectious disease associated with high morbidity and mortality. Although melioidosis is most prevalent during the rainy season in endemic areas, domestic gardens and farms can also serve as a reservoir for *B. pseudomallei* during the dry season, in part due to irrigation and fertilizer use. In the environment, *B. pseudomallei* forms biofilms and persists in soil near plant root zones. Biofilms are dynamic bacterial communities whose formation is regulated by extracellular cues and corresponding changes in the nearly universal secondary messenger cyclic di-GMP. Recent studies suggest *B. pseudomallei* loads are increased by irrigation and the addition of nitrate-rich fertilizers, whereby such nutrient imbalances may be linked to the transmission epidemiology of this important

---

[6] This work is presented in: **Mangalea, M.R.**, Plumley, B.A., and Borlee, B.R. 2017. Nitrate sensing and metabolism inhibit biofilm formation in the opportunistic pathogen *Burkholderia pseudomallei* by reducing the intracellular concentration of c-di-GMP. *Frontiers in Microbiology*, 8: 1353.

pathogen. We hypothesized that exogenous nitrate inhibits *B. pseudomallei* biofilms by reducing the intracellular concentration of c-di-GMP. Bioinformatics analyses revealed *B. pseudomallei* 1026b has the coding capacity for nitrate sensing, metabolism, and transport distributed on both chromosomes. Using a sequence-defined library of *B. pseudomallei* 1026b transposon insertion mutants, we characterized the role of denitrification genes in biofilm formation in response to nitrate. Our results indicate that the denitrification pathway is implicated in *B. pseudomallei* biofilm growth dynamics and biofilm formation is inhibited by exogenous addition of sodium nitrate. Genomics analysis identified transposon insertional mutants in a predicted two-component system (*narX*/*narL*), a nitrate reductase (*narGH*), and a nitrate transporter (*narK-1*) required to sense nitrate and alter biofilm formation. Additionally, the results presented here show that exogenous nitrate reduces intracellular levels of the bacterial second messenger c-di-GMP. These results implicate the role of nitrate sensing in the regulation of a c-di-GMP phosphodiesterase and the corresponding effects on c-di-GMP levels and biofilm formation in *B. pseudomallei* 1026b.

## 3.2 Introduction

Biofilms are dynamic natural communities of adherent bacteria encased in an extracellular polymeric matrix with signal-sensing systems primed to detect and respond to a variety of cues and environmental stimuli (1, 2). Biofilm formation in many pathogenic species is coordinated and positively regulated by the universal bacterial second messenger cyclic dimeric GMP (c-di-GMP), which facilitates the transition from free-swimming planktonic bacteria to sessile adherent communities (3). *Burkholderia pseudomallei* is a Gram-negative motile bacillus and saprophyte inhabiting tropical and subtropical soils and surface waters (4). This bacterium has been shown to persist in the environment as a pellicle (a biofilm that forms at the air-liquid interface) and as surface-associated biofilms on plants and in the rhizosphere of rice in endemic areas (5-7). As an opportunistic pathogen, *B. pseudomallei* is acquired directly from the

70

environment and can cause multiple types of infections in humans and a range of animal hosts (4). For a sapronotic disease agent such as *B. pseudomallei* (8), it is important to understand the unique epidemiology related to its transition from the environment to establish persistent infections within susceptible hosts.

*B. pseudomallei* is found primarily within Southeast Asia and Northern Australia, where it is a prominent cause of bacterial pneumonia and sepsis, respectively (9). However, a recent report estimates the global distribution of *B. pseudomallei* is much larger than previously recognized and predicts environmental suitability across the tropics worldwide (10). *B. pseudomallei* infection results in melioidosis, a febrile illness whose clinical manifestations reflect the route of inoculation. Infection most commonly results from cutaneous exposure to contaminated soil or water, but also ingestion and respiratory inhalation (11). Occupational exposure while working in rice fields is a primary source for acquisition of infection, but recreational activities such as gardening also expose individuals to *B. pseudomallei* in endemic areas (12, 13). Anthropogenic manipulation of garden soils through irrigation and application of urea- and nitrate-rich fertilizers increases *B. pseudomallei* populations across different soil types (12). Nitrates are naturally occurring salts and byproducts of animal wastes, as well as artificial components of fertilizers, the use of which can lead to an imbalance in nutrient-limited soils (12). *B. pseudomallei* is associated with soil that contains elevated levels of nitrates and total nitrogen (14), anthrosol soil (10), as well as livestock and animal housing (14). This association with nitrogen levels is an apparent exception to the general negative association between *B. pseudomallei* and soil nutrient levels (15).

Given the association of increased *B. pseudomallei* abundance in disturbed soils with elevated nitrate and organic materials, there is a critical need to understand the effects of exogenous nitrogen derivatives on *B. pseudomallei* physiology and epidemiology. Members of the *Burkholderia* genus, including the clinical isolate *B. pseudomallei* K96243, can grow in anaerobic conditions using nitrate as an alternative terminal electron acceptor, much like other

facultative anaerobic bacteria (16, 17). The effects of anaerobic growth using nitrate on the

physiology of *B. pseudomallei* biofilms remains largely undetermined. Interestingly, genes

associated with nitrate reduction are implicated in biofilm formation in *B. thailandensis*, yet a

mechanism of action has not been determined (18). Nitrate sensing and metabolism have also

been shown to influence biofilm formation and virulence in *Pseudomonas aeruginosa* (19, 20)

and nitrite is known to inhibit biofilm formation in *Staphylococcus aureus* (21). Additionally,

nitrite metabolism is implicated in modulating antibiotic susceptibility in *P. aeruginosa* (22, 23).

To address the effects of exogenous nitrate on *B. pseudomallei* biofilms, transposon

insertional mutants in predicted nitrate metabolism, regulatory, and sensory genes were

identified and assessed for their ability to form biofilms in the presence of sodium nitrate.

Inhibition of biofilm formation by sodium nitrate was not observed in five of the 21 transposon

mutants tested: Bp1026b_I1013::T24 (*narL*), Bp1026b_I1014::T24 (*narX*), Bp1026b_I1017::T24

(*narH-1*), Bp1026b_I1018::T24 (*narG-1*), and Bp1026b_I1020::T24 (*nark-1*). The dissimilatory

nitrate reductase encoded by the *narGHJI* operon, which is conserved among both facultative

and obligate anaerobes, is a membrane-bound enzyme complex comprised of four subunits

responsible for nitrate reduction in the absence of oxygen (24, 25). The *narX/narL* system is

instrumental in nitrate metabolism and regulation as it has been shown to activate nitrate-

specific enzymes and repress unnecessary anaerobic respiration genes in response to

exogenous nitrate (26, 27). In this study, we show that the alpha and beta subunits of the major

nitrate reductase *narGHJI-1* along with the *narX/narL* two-component regulatory system and the

nitrate/nitrite transporter *narK-1* are responsible for biofilm inhibition based on nitrate availability.

These data demonstrate that nitrate sensory cascades and metabolism are linked to

biofilm growth dynamics in *B. pseudomallei* 1026b. Moreover, we show a significant reduction in

c-di-GMP levels in *B. pseudomallei* grown in the presence of nitrate. We hypothesize that nitrate

sensing and nitrate-dependent anaerobic respiration promote a planktonic lifestyle transition in

*B. pseudomallei* that is ultimately a result of depletion of intracellular levels of c-di-GMP and a corresponding decrease in biofilm formation.

## 3.3 Materials and Methods

### 3.3.1 Bacterial strains and growth conditions

All experiments were performed in biosafety level 3 (BSL-3) facilities within the Regional Biocontainment Laboratory at Colorado State University with approvals from the Center for Disease Control and Prevention and the Colorado State University Institutional Biosafety Committee. *B. pseudomallei* strain 1026b, a clinical isolate from a human case of septicemic melioidosis in Thailand (28), was used in this study. Transposon (T24) mutant strains used in this study were generated during the production of a comprehensive two-allele sequence defined transposon mutant library (manuscript in preparation). T24 is a Tn5-derived transposon containing a kanamycin resistance selection marker approved for use in *B. pseudomallei* that was constructed in Colin Manoil's laboratory at the University of Washington. Briefly, the two-allele library was assembled via random transposon insertion into gene loci spanning both chromosomes of *B. pseudomallei* 1026b, resulting in insertions into 4,931 of 6,070 (81.2%) total predicted genes. In total, the library contains two copies of 4,415 genetic mutants that were re-sequenced. All transposon insertion mutants were verified by additional sequencing for these studies. Bacterial strains were grown in Lysogeny Broth (LB) media consisting of 10 g/L tryptone (Fisher Scientific), 5 g/L yeast extract (Becton, Dickinson and Company), and 5 g/L NaCl (Fisher Scientific) as previously described (29). For experiments involving media with sodium nitrate, LB was supplemented with a final concentration of 10 mM sodium nitrate (Sigma), unless otherwise stated. Transposon mutants were grown in LB with 300 µg/mL kanamycin (Gold Biotechnology).

**3.3.2 Identification of putative nitrogen metabolism genes in *B. pseudomallei* 1026b**

A combination of open-access genomic databases were used to assess the comparative identity of genetic orthologs in closely related *Burkholderia* spp*.* as well as *P*. *aeruginosa* strain PAO1. Predicted nucleotide sequences in the *B. pseudomallei* 1026b (taxid: 884204) genome for chromosomes I and II (accession numbers NC_017831.1 and NC_017832.1, respectively), were acquired from the NCBI GenBank database using the BLASTN program under default parameters to identify sequences similar to the PAO1 reference genome (GenBank assembly accession: GCA_000414275.1). Functional nitrogen metabolism pathways were evaluated using the Kyoto Encyclopedia of Genes and Genomes (KEGG) (30). Further comparative genomic analyses, as well as gene annotations and locus positions were deduced using the Burkholderia Genome Database (31) in conjunction with the Pseudomonas Genome Database (32). Sequence comparison among nitrogen metabolism genes was analyzed with the following: *B. pseudomallei* K96243 (taxid: 272560), *B. thailandensis* E264 (taxid: 271848), and *P. aeruginosa* PAO1 (taxid: 208964). Percent identity between genetic orthologs was calculated using the Multiple Sequence Comparison by Log-Expectation (MUSCLE) tool provided by the European Bioinformatics Institute (EMBL-EBI), which calculates a percent identity matrix using Clustal 2.1 (33). Gene names and functional descriptions were not entirely available for *B. pseudomallei* 1026b, and in such cases, were assigned based on consensus among the better annotated species detailed above.

**3.3.3 Comparative analysis of predicted nitrogen metabolism clusters**

Sequence analyses for the predicted nitrogen metabolism clusters encoded on chromosome I and II from the sequenced genome of *B. pseudomallei* 1026b (taxid: 884204) were visualized using open-source bioinformatics platforms and genomic sequence databases. We used BLASTN (BLAST, NCBI) under default parameters in conjunction with the Burkholderia Orthologous Groups cataloging system from the Burkholderia Genome Database

([http://burkholderia.com](http://burkholderia.com)) (31) to identify homologous regions. Sequences for *B. pseudomallei* 1026b chromosome I (accession number: NC_017831.1) and chromosome II (accession number: NC_017832.1) were downloaded from the GenBank database (NCBI, NIH). Sequence fragments were extracted with Geneious version 7.1.7 ([http://geneious.com](http://geneious.com)) (34) and visualized with EasyFig version 2.23 (35) using Python version 2.7 ([http://python.org](http://python.org)). To calculate homology between input sequences, command line parameters for EasyFig included a minimum identity cutoff for BLASTN of 0.60 and a threshold E-value of 1E-3.

### 3.3.4 Pellicle biofilm assays

Overnight cultures were grown in LB medium (kanamycin as indicated for transposon mutants) and sub-cultured 1:50 in 2 mL LB with or without 10 mM sodium nitrate. Pellicles were grown in 17 x 100 mm polystyrene tubes (#1485-2810, USA Scientific) at 37°C for 24 hours before incubation at room temperature for 14 days without disturbance then photographed.

### 3.3.5 Static biofilm assays

Overnight cultures were grown in LB and diluted to $OD_{600}$ of 0.1 in LB with or without 10 mM sodium nitrate. Experiments using sodium nitrite were performed in the same manner as those using sodium nitrate. Gradient concentrations {0, 1, 2, 3, 5, 8, 10, 20, 50, and 100 mM} of sodium nitrate, sodium nitrite, or sodium chloride in LB were evaluated as indicated. 100 μL was added, in replicates of six, to individual wells of a 96-well polystyrene plate (Nunc™ Microwell™ 96-well microplates #243656, Thermo Scientific) and incubated at 37°C for 24 hours. Static biofilms were processed as previously described (29). Briefly, bacterial supernatant was removed from the biofilms and wells were washed once with PBS to remove non-adherent cells. The wells were stained with 0.05% crystal violet (Sigma-Aldrich, St. Louis, MO) and incubated at room temperature for 15 minutes. Stain was removed and wells were washed again with PBS. Adherent crystal violet was solubilized by addition of 95% EtOH and incubated for 30

minutes. The solubilized dye was transferred to a new 96-well polystyrene plate and the absorbance was measured at $OD_{600}$ on a Synergy HT plate reader (BioTek Instruments, Winooski, VT). Significance was calculated with an unpaired Student's t-test using the Holm-Sidak method to account for multiple comparisons.

### 3.3.7 Complementation of Bp1026b_I1013::T24 (*narL*) and Bp1026b_I1014::T24 (*narX*) mutants

Complementation constructs were designed for conditional expression of re-integrated genes via IPTG induction from the *tac* promoter, following select-agent-compliant methods for genetic modification in *B. pseudomallei* (29, 36). The full-length sequences of Bp1026b_I1013 (*narL*) and Bp1026b_I1014 (*narX*) were amplified using the following PCR primer pairs: (5' – NNNCCCGGGAGGAGGATATTCATGACCATACGGGTACTGTT – 3') and (5' – NNNAAGCTTTTATGCCTCGGCCGGATGCG – 3') for Bp1026b_I1013, and (5' – NNNCCCGGGAGGAGGATATTCATGGCTCCCGCCCTCCCCGA – 3') and (5' – NNNAAGCTTCTATGCCGCCTGTCGCGCGT – 3') for Bp1026b_I1014. Cloned genes were ligated into pUC18T-mini-Tn7T-Km-LAC, which uses the *tac* promoter from *E. coli* to drive gene expression (37). 5 mM IPTG was used to induce expression from the *tac* promoter. 5 mM $NaNO_3$ was used to stimulate biofilm inhibition.

### 3.3.8 Growth curves

Overnight cultures were grown in LB and diluted to $OD_{600}$ of 0.1 in LB supplemented with increasing concentrations of sodium nitrate or sodium chloride as indicated. Sodium chloride was supplemented in addition to the original 170 mM NaCl concentration in LB. Each experimental growth condition was repeated in six replicates. 100 μL of each culture was added to a 96-well polystyrene plate (Nunc™ Microwell™ 96-well microplates #243656, Thermo Scientific) in triplicate. Plates were incubated at 37°C shaking aerobically at 250 rpm for 48

hours. Absorbance (OD$_{600}$) was measured hourly on a Synergy HT plate reader (BioTek Instruments).

### 3.3.9 Extraction and quantification of c-di-GMP

Nucleotide extraction methods using formic acid were adapted from Massie et al. (38). Overnight cultures of *B. pseudomallei* 1026b were grown in LB at 37°C shaking (250 rpm). Cultures were diluted 1:50 in 4 mL of M9 Salts minimal medium with or without 10 mM sodium nitrate supplemented and grown statically at 37°C for 18 hours in six-well Costar polystyrene plates (#3516, Corning). Cells from 1 mL culture including the pellicle biofilm were collected and resuspended in 100 µL of cold 40% (vol/vol) acetonitrile/ 40% (vol/vol) methanol/ 20% (vol/vol) LC-MS-grade water/ 1% formic acid. An internal control of 2-chloro-adenosine-5'-O-monophosphate (2-Cl-5'-AMP, Axxora, LLC) was used at a final concentration of 100 nM (39). The buffer, cells, and matrix were incubated at 65°C for 10 minutes and then immediately transferred to -20°C for 30 minutes to ensure complete lysis. Samples were then centrifuged at 16,000 X g at 4°C for 5 minutes and the supernatant fraction containing c-di-GMP was collected and neutralized with 20 µL 1 M KOH, followed by another spin at 16,000 X g at 4°C for 5 minutes. A calibration curve using known standards of chemically synthesized c-di-GMP (Axxora, LLC) and 2-Cl-5'-AMP was generated and extracted in identical conditions to experimental samples. Absolute quantification of c-di-GMP was calculated using the linear regression equation generated from known standards and peak areas normalized to the internal standard. Analysis was performed on an Acquity M-Class UPLC (Waters) coupled to a Xevo TQ-S triple quadrupole mass spectrometer (Waters) for LC-MS/MS. A Waters Atlantis dC18 stationary phase column (300 µm x 150 mm, 3.0 µM) was used for chromatographic separations. Protein pellets from the initial cell collection were analyzed for total protein concentration using the Pierce 660 nm Protein Assay (Thermo Scientific) for normalization of the absolute concentration of c-di-GMP. Nucleotide extraction experiments were repeated on

two different days using four biological replicate cultures with three technical replicates each. Statistical significance was determined using an unpaired T-test in GraphPad Prism.

### 3.3.10 RNA isolation and quantitative real-time PCR

*B. pseudomallei* 1026b was grown statically in M9 Salts minimal media with or without 10 mM sodium nitrate supplemented at 37°C in six well Costar polystyrene plates (Corning). After 18 hours of static growth, 1 mL of culture was collected and cells were centrifuged at 12,000 X g for 2 minutes at 4°C. Bacterial pellets were resuspended in 350 μL RNAprotect Bacteria Reagent (Qiagen) before centrifuging at 5,000 X g for 10 minutes at 4°C. Bacterial pellets were resuspended in 1 mL QIAzol Lysis Reagent (Qiagen), incubated for 5 minutes at room temperature, and transferred to screwcap tubes containing 250 μL of 0.1 mm glass disruption beads (RPI Corp.) on ice. Cells were lysed using a TissueLyser II homogenizer (Qiagen) using three rounds of 60 second pulses at 30 Hz with 60 seconds on ice between each lysis round. After lysis, the cell mixture was incubated at room temperature for 5 minutes before adding 200 μL chloroform and vortexing for 5 seconds. Samples were incubated again at room temperature for 5 minutes before centrifugation at 13,000 X g for 10 minutes. The aqueous phase was collected and RNA was purified with an RNeasy Mini Kit (Qiagen) using the protocol recommended by the manufacturer. RNA samples were treated with two rounds of TURBO DNase (Ambion) before cDNA was synthesized using the Transcriptor First Strand cDNA Synthesis Kit (Roche). qRT-PCR was performed on a LightCycler 480 System with SYBR Green I Master (Roche) using 10 ng total cDNA and the following cycling conditions: pre-incubation at 95°C for 10 minutes; three-step amplification at 95°C for 10 seconds, 55°C for 15 seconds, 72°C for 15 seconds; melting curve at 95°C for 5 seconds, 65°C for 1 minute, and 97°C for continuous acquisitions per 5°C. Primers for Bp1026b_I2284 (*cdpA*) were designed using the PrimerQuest tool (IDT DNA Technologies). For a housekeeping reference gene, we used published 23S rRNA primers (40). Both sets of primers were validated for amplification

78

efficiency in a standard curve. The primer set used for *cdpA* was as follows: forward (5' – AAGCTGGCTGGAGCAAA – 3') and reverse (5' – GCAGATAGTCGCGGTGATAA – 3'). The primer set used for Bp1026b_II2523 was as follows: forward (5' – GCAAGATCGAGAGCGTGTT – 3') and reverse (5' – GTGATCGAAGCGGAACAGATAC – 3'). The primer set used for Bp1026b_II0885 was as follows: forward (5' – CTGCACCTACCGCTTCTT – 3') and reverse (5' – AAGCACAGCGAGAAGTAGTC – 3'). The primer set used for Bp1026b_II3148 was as follows: forward (5' – CGCTGCATCTGGAGAACTT – 3') and reverse (5' – CCTGAAACGGATCGGTGAG – 3'). Transcript abundance was measured using the Pfaffl method (41), taking into account primer amplification efficiency, including three independent biological samples performed in technical triplicates.

## 3.4 Results

### 3.4.1 Nitrate inhibits *B. pseudomallei* biofilm formation

While the effectors of biofilm dispersal and inhibition are extensive and diverse, nitrogenous compounds have been shown to modulate biofilm formation in both Gram-negative and Gram-positive bacteria (19, 21, 23). Sodium nitrate ($NaNO_3$), a naturally-occurring salt compound and a synthetic agricultural additive, inhibits biofilm formation in a dose-dependent manner (**Figure 3.1A**). Likewise, sodium nitrite also inhibits biofilm formation following a similar trend, although the effect is not as robust initially (**Figure 3.1A**). To assess the impact of nitrate/nitrite on biofilm formation, wild-type *B. pseudomallei* 1026b was grown statically for 24 hours with increasing concentrations of sodium nitrate or sodium nitrite (**Figure 3.1A**).

Biofilm inhibition effects were first noted at 1 mM while the most significant biofilm inhibition occurred with the addition of 10 mM sodium nitrate/nitrite. There were no additional inhibitory effects on biofilm formation with treatment concentrations greater than 10 mM $NaNO_3$. As such, concentrations of 10 mM $NaNO_3$ were used for all subsequent experiments. To

evaluate the effects of sodium concentration on biofilm formation, experiments with only sodium

chloride (NaCl) indicated that biofilm inhibition was not significantly altered during biofilm

formation under the same conditions (**Figure 3.1A**). Viability was also tested by measuring

growth kinetics in media supplemented with NaCl (**Figure 3.1B**) and $NaNO_3$ (**Figure 3.1C**).

Growth inhibition was observed only when cells were grown in media supplemented with 100

mM of $NaNO_3$ and 100 mM NaCl, concentrations that are well beyond those used in this study.

No significant differences in growth dynamics were observed at 10 mM $NaNO_3$ suggesting that

nitrate dosing at this concentration does not affect cell viability. These results suggest that

nitrate sensing and metabolism, and not sodium, is responsible for biofilm inhibition in *B.

seudomallei* 1026b and the observed inhibition is not the result of decreased cellular viability.
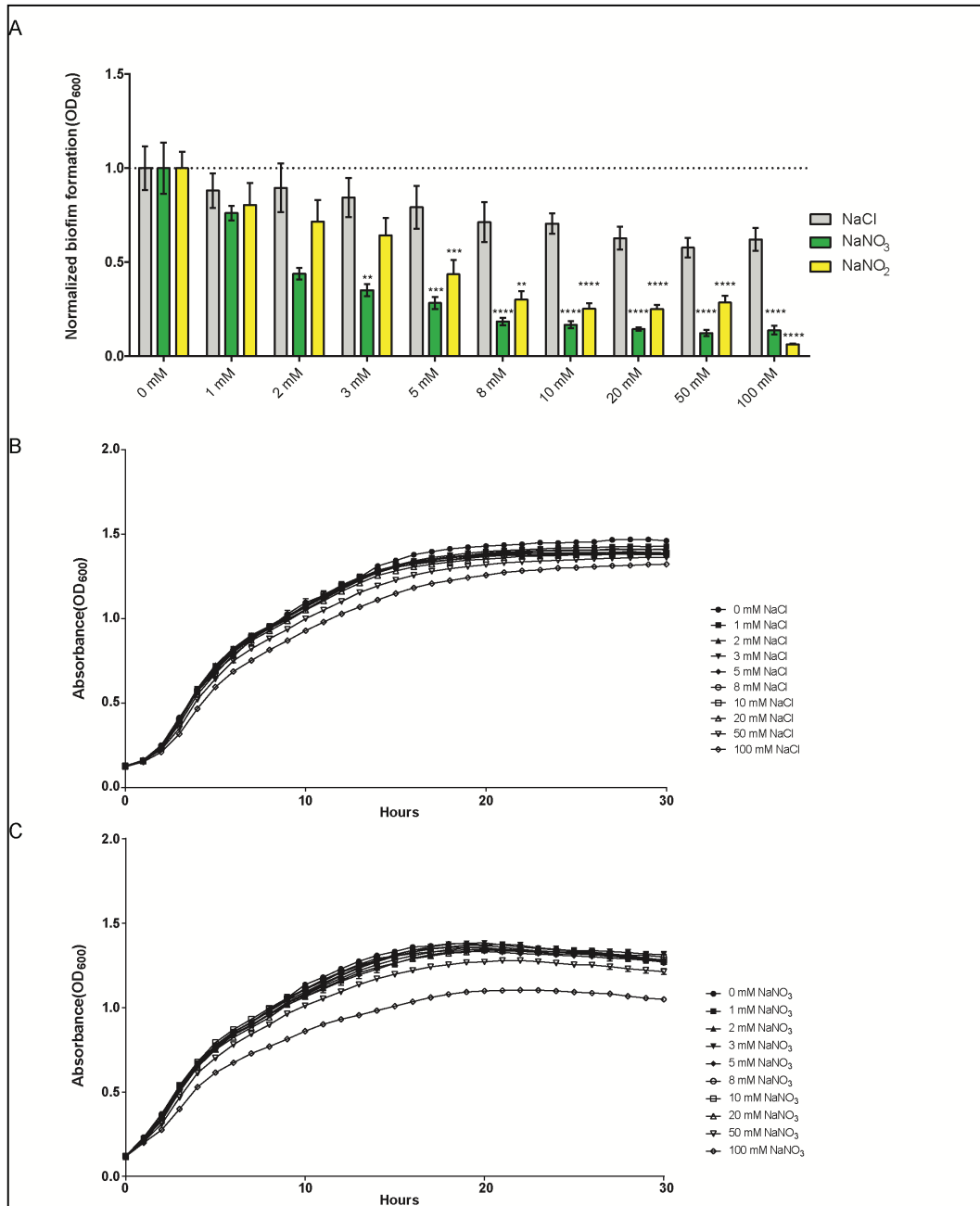
**Figure 3.1 Sodium nitrate and sodium nitrite, but not sodium chloride, inhibit biofilm formation in *B. pseudomallei* 1026b.** (A) Biofilm inhibition was assessed for static biofilm cultures growing at 37°C in the presence of sodium chloride, sodium nitrate, or sodium nitrite at 1, 2, 3, 5, 8, 10, 20, 50, and 100 mM. All experiments were performed with wild-type *B. pseudomallei* 1026b and inhibition was evaluated relative to wild-type biofilm formation in LB without additional salts added. Asterisks indicate a significant difference (** = p<0.01, *** = p<0.001, **** = p<0.0001) calculated with an unpaired Student's t-test using the Holm-Sidak method to account for multiple comparisons (n=12). Growth curves were generated from cultures grown with shaking at 37°C in the presence of either sodium chloride **(B)** or sodium nitrate **(C)** using concentrations as indicated for the biofilm inhibition assay. Absorbance (OD$_{600}$) measurements were taken hourly for 30 continuous hours.

### 3.4.2 Bioinformatics analysis of predicted nitrogen metabolism genes

Bioinformatics analyses identified 25 *B. pseudomallei* 1026b genes predicted to be involved in nitrogen metabolism (**Table 3.1**), of which 21 were included in this study based on the availability from a two-allele sequence defined transposon library. The genes included in this study were selected based on sequence homology among closely related *Burkholderia* spp. to *P. aeruginosa* PAO1, which has an extensively annotated reference genome that has been biochemically validated for the nitrogen metabolism genes. Within the *proteobacteria* phylum, the *β-proteobacteria,* which contains the genus *Burkholderia,* is closely related to the genus *Pseudomonas,* which is a *γ-proteobacteria* (42), thus inter-genus comparisons described in this study will provide insights into the functions among these conserved nitrogen metabolism proteins.

While *B. pseudomallei* 1026b encodes many genes predicted to encode enzymes in the denitrification pathway, there is a need for more comprehensive functional annotation in this relatively new clinically isolated strain. Therefore, nucleotide sequence identity was analyzed across three *Burkholderia* species in relation to *P. aeruginosa* PAO1 (**Table 3.1** and **Table 3.2**). Orthologs of the denitrification enzymes in *B. pseudomallei* 1026b presented here share 99-100% nucleotide identity to the fully sequenced genome of *B. pseudomallei* K96243, 90-97% nucleotide identity to *B. thailandensis* E264, and 60-78% nucleotide identity to the more distant relative *P. aeruginosa* PAO1 (**Table 3.2**). This underscores the highly conserved nature of the genes constituting the essential denitrification pathway among these soil-dwelling bacteria.

**Table 3.1 Predicted nitrogen metabolism genes identified in this study.** Gene annotations and predicted functions were assembled using the Burkholderia Genome Database in conjunction with the Pseudomonas Genome Database. Sequence homologies were compared between *B. pseudomallei* 1026b and *P. aeruginosa* PAO1. Locus identification for all genomes was determined using the NCBI GenBank database. Percent identities were calculated using the open-source MUSCLE alignment program from EMBL-EBI.

| Name and predicted function | Putative annotation | *B. pseudomallei* | *P. aeruginosa* | Nucleotide Similarity (%) |
|---|---|---|---|---|
| DNA-binding response regulator | *narL* | Bp1026b_I1013 | PA3879 | 65.12 |
| Nitrate/nitrite sensor protein | *narX* | Bp1026b_I1014 | PA3878 | 65.00 |
| Nitrate reductase (1) | | | | |
|     Gamma subunit | *narI-1* | Bp1026b_I1015 | PA3872 | 64.50 |
|     Delta subunit | *narJ-1* | Bp1026b_I1016 | PA3873 | 72.54 |
|     Beta subunit | *narH-1* | Bp1026b_I1017 | PA3874 | 75.88 |
|     Alpha subunit | *narG-1* | Bp1026b_I1018 | PA3875 | 75.20 |
| Nitrate/nitrite transporter | *narK-2* | Bp1026b_I1019 | PA3876 | 73.90 |
| Nitrate/nitrite transporter | *narK-1* | Bp1026b_I1020 | PA3877 | 69.76 |
| Nitric oxide reductase | *norB* | Bp1026b_I0974 | PA0524 | 68.37 |
| Nitrous oxide reductase | *nosZ* | Bp1026b_I1546 | PA3392 | 68.47 |
| Assimilatory nitrite reductase (NAD(P)H) (1) | | | | |
|     Large subunit | *nirB-1* | Bp1026b_I2984 | PA1781 | 76.39 |
|     Small subunit | *nirD-1* | Bp1026b_I2985 | PA1780 | 69.23 |
| Assimilatory nitrate reductase (1) | | | | |
|     Molybdopterin oxidoreductase family protein | *nasA-1* | Bp1026b_I2986 | PA1779 | 67.45 |
| Nitrate/nitrite transporter | *narK* | Bp1026b_II1220 | PA3870 | 59.89 |
| Nitrate reductase (2) | | | | |
|     Gamma subunit | *narI-2* | Bp1026b_II1222 | PA3872 | 65.45 |
|     Delta subunit | *narJ-2* | Bp1026b_II1223 | PA3873 | 65.60 |
|     Beta subunit | *narH-2* | Bp1026b_II1224 | PA3874 | 78.55 |
|     Alpha subunit | *narG-2* | Bp1026b_II1225 | PA3875 | 74.14 |
| Assimilatory nitrate reductase (2) | | | | |
|     Large subunit | *nasA-2* | Bp1026b_II1316 | PA1779 | 66.77 |
| Assimilatory nitrite reductase (NAD(P)H) (2) | | | | |
|     Small subunit | *nirD-2* | Bp1026b_II1317 | PA1780 | 64.53 |
|     Large subunit | *nirB-2* | Bp1026b_II1318 | PA1781 | 62.74 |
| Nitrate regulator | *nasT* | Bp1026b_II1319 | PA1783 | 61.92 |
| Nitrate transport ATP-binding protein | *nasS* | Bp1026b_II1322 | PA1786 | 68.54 |
| Nitrite reductases | | | | |
|     Multicopper oxidase domain-containing protein | *nirS* | Bp1026b_II1540 | PA0519 | 60.60 |
|     Anaerobically induced outer membrane protein | *nirK* | Bp1026b_II1580 | N/A | N/A |

**Table 3.2 Predicted nitrogen metabolism genes in *Burkholderia* spp. in relation to *P. aeruginosa* PAO1.** Gene annotations and predicted functions were assembled using the Burkholderia Genome Database in conjunction with the Pseudomonas Genome Database. Sequence homologies were compared between *Burkholderia spp*. and *P. aeruginosa* PAO1. Locus identification for all genomes was determined using the NCBI GenBank database. Percent identities were calculated using the open-source MUSCLE alignment program from EMBL-EBI.

| Name and predicted function | Putative Annotation | *B. pseudomallei* 1026b (old number) | *B. pseudomallei* 1026b (new number) | *B. pseudomallei* K96243 (% similarity) | *B. thailandensis* E264 (% similarity) | *P. aeruginosa* PA01 (% similarity) |
|---|---|---|---|---|---|---|
| DNA-binding response regulator | *narL* | BP1026b_I1013 | BP1026B_RS05050 | BPSL2314 (99.86) | BTH_I1849 (95.87) | PA3879 (65.12) |
| Nitrate/nitrite sensor protein | *narX* | BP1026b_I1014 | BP1026B_RS05055 | BPSL2313 (99.74) | BTH_I1850 (95.30) | PA3878 (65.00) |
| Nitrate reductase (1) | | | | | | |
| Gamma subunit | *narI-1* | BP1026b_I1015 | BP1026B_RS05060 | BPSL2312 (99.56) | BTH_I1851 (95.34) | PA3872 (64.50) |
| Delta subunit | *narJ-1* | BP1026b_I1016 | BP1026B_RS05065 | BPSL2311 (99.56) | BTH_I1852 (95.28) | PA3873 (72.54) |
| Beta subunit | *narH-1* | BP1026b_I1017 | BP1026B_RS05070 | BPSL2310 (99.87) | BTH_I1853 (97.30) | PA3874 (75.88) |
| Alpha subunit | *narG-1* | BP1026b_I1018 | BP1026B_RS05075 | BPSL2309 (99.87) | BTH_I1854 (97.13) | PA3875 (75.20) |
| Nitrate/nitrite transporter | *narK-2* | BP1026b_I1019 | BP1026B_RS05080 | BPSL2308 (99.57) | BTH_I1855 (96.32) | PA3876 (73.90) |
| Nitrate/nitrite transporter | *narK-1* | BP1026b_I1020 | BP1026B_RS05085 | BPSL2307 (99.77) | BTH_I1856 (96.96) | PA3877 (69.76) |
| Nitrous-oxide reductase | *nosZ* | BP1026b_I1546 | BP1026B_RS07765 | BPSL1607 (100) | BTH_I2325 (95.45) | PA3392 (68.47) |
| Assimilatory nitrite reductase (NAD(P)H) (1) | | | | | | |
| Large subunit | *nirB-1* | BP1026b_I2984 | BP1026B_RS14915 | BPSL0512 (99.63) | BTH_I0464 (95.83) | PA1781 (76.39) |
| Small subunit | *nirD-1* | BP1026b_I2985 | BP1026B_RS14920 | BPSL0511 (99.24) | BTH_I0463 (96.72) | PA1780 (69.23) |
| Assimilatory nitrate reductase (1) | | | | | | |
| Molybdopterin oxidoreductase family | *nasA-1* | BP1026b_I2986 | BP1026B_RS14925 | BPSL0510 (99.68) | BTH_I0462 (95.80) | PA1779 (67.45) |
| Nitrate/nitrite transporter | *narK* | BP1026b_II1220 | BP1026B_RS24705 | BPSS1154 (99.92) | BTH_II1254 (92.78) | PA3870 (59.89) |
| Nitrate reductase (2) | | | | | | |
| Gamma subunit | *narI-2* | BP1026b_II1222 | BP1026B_RS24715 | BPSS1156 (100) | BTH_II1252 (92.54) | PA3872 (65.45) |
| Delta subunit | *narJ-2* | BP1026b_II1223 | BP1026B_RS24720 | BPSS1157 (99.13) | BTH_II1251 (91.88) | PA3873 (65.60) |
| Beta subunit | *narH-2* | BP1026b_II1224 | BP1026B_RS24725 | BPSS1158 (99.61) | BTH_II1250 (94.44) | PA3874 (78.55) |
| Alpha subunit | *narG-2* | BP1026b_II1225 | BP1026B_RS24730 | BPSS1159 (99.61) | BTH_II1249 (94.37) | PA3875 (74.14) |
| Assimilatory nitrate reductase (2) | | | | | | |
| Large subunit | *nasA-2* | BP1026B_II1316 | BP1026B_RS25170 | BPSS1241 (99.65) | BTH_II1172 (94.28) | PA1779 (66.77) |
| Nitrite reductase (NAD(P)H) (2) | | | | | | |
| Small subunit | *nirD-2* | BP1026B_II1317 | BP1026B_RS25175 | BPSS1242 (100) | BTH_II1171 (94.59) | PA1780 (64.53) |
| Large subunit | *nirB-2* | BP1026B_II1318 | BP1026B_RS25180 | BPSS1243 (99.92) | BTH_II1170 (95.31) | PA1781 (62.74) |
| Nitrate transporter | *nasT* | BP1026B_II1319 | BP1026B_RS25185 | BPSS1244 (99.77) | BTH_II1169 (96.23) | PA1783 (61.92) |
| Nitrate transport ATP-binding protein | *nasS* | BP1026B_II1322 | BP1026B_RS25200 | BPSS1247 (99.34) | BTH_II1166 (90.87) | PA1786 (68.54) |
| Nitrite reductases | | | | | | |
| Multicopper oxidase domain-containing | *nirS* | BP1026b_II1540 | BP1026B_RS26370 | BPSS1452 (99.86) | BTH_II0944 (86.48) | PA0519 (60.6) |
| Anaerobically induced outer membrane | *nirK* | BP1026b_II1580 | BP1026B_RS26570 | BPSS1487 (99.49) | BTH_II0881 (95.16) | N/A |

Interestingly, bioinformatics analysis revealed duplications of specific genes implicated in the denitrification pathway in *B. pseudomallei* 1026b, which is consistent with the predicted genetic supplementation and metabolic redundancy of *B. pseudomallei* (43). The major nitrate reductases are encoded on chromosome I at Bp1026b_I1015 – Bp1026b_I1018 and on chromosome II at Bp1026b_II1222 – Bp1026b_II1225, and share sequence homology of 69 – 79% (**Table 3.3**). Additionally, the major nitrite reductase is encoded on chromosome I at Bp1026b_I2984 – Bp1026b_I2985 and on chromosome II at Bp1026b_II1317 – Bp1026b_II1318, sharing only 65% nucleotide identity (**Table 3.3**).

**Table 3.3 Percent nucleotide identity of homologous nitrate metabolism genes between chromosomes I and II from *B. pseudomallei* 1026b**

| chromosome 1 | chromosome 2 | Nucleotide Percent Identity |
| --- | --- | --- |
| I1015 | II1222 | 69.70 |
| I1016 | II1223 | 70.79 |
| I1017 | II1224 | 78.74 |
| I1018 | II1225 | 75.65 |
| I1019 | II1221 | 69.20 |
| I1020 | II1220 | 70.71 |
| I2984 | II1318 | 65.17 |
| I2985 | II1317 | 64.58 |
| I2986 | II1316 | 68.51 |

Bioinformatics analyses also identified putative nitrogen metabolism genes with no clear annotations across *Burkholderia* spp. Therefore, Bp1026b_I1019, Bp1026b_I1020, Bp1026b_II1319, and Bp1026b_II1540 were assigned genetic annotations based on the *P. aeruginosa* PAO1 reference genome. Two genes were identified as assimilatory nitrate reductases (Bp1026b_I2986 and Bp1026b_II1316) based on sequence homology to PAO1; however, no annotated homologs were available throughout *Burkholderia* spp., thus the annotation was assigned to be consistent with *P. aeruginosa* PAO1. Lastly, Bp1026b_II1580, which is predicted to encode an anaerobically induced outer membrane nitrite reductase, was specific to *Burkholderia* spp. with no representative homolog in *P. aeruginosa*.

Based on the information available from the previously described open source genome

databases and the genetic functional pathway predictions provided by the KEGG database, we

mapped and compared the genetic arrangement of the predicted nitrogen metabolism enzymes

across both chromosomes (**Figure 3.2 A-B**). The *narX/narL* predicted two-component signaling

system lies upstream and adjacent to the primary nitrate reductase on chromosome I, which is

flanked by the cytoplasmic membrane-associated nitrate/nitrite transporters (**Figure 3.2A**).

Another gene cluster of interest for these studies is the assimilatory nitrite reductase on

chromosome I, with the adjacent molybdopterin oxidoreductase *nasA,* which is predicted to

function as an assimilatory nitrate reductase (44) (**Figure 3.2B**).  Interestingly, the nitrate

metabolism gene clusters found on chromosome I are replicated in similar configurations on

chromosome II. The relatively equal distribution of denitrification-associated loci across both *B.*

*pseudomallei* chromosomes is not surprising considering that chromosome II is not an

accessory genome and also encodes for essential and central metabolism genes (43); however,

the predicted nitrate metabolism loci on chromosome II are not directly homologous to those on

chromosome I. This disparity in sequence identity among similarly annotated gene loci with

parallel genetic arrangements indicates that the nitrate metabolism clusters are not direct

paralogs and may be required for specific metabolic functions based on extracellular cues.
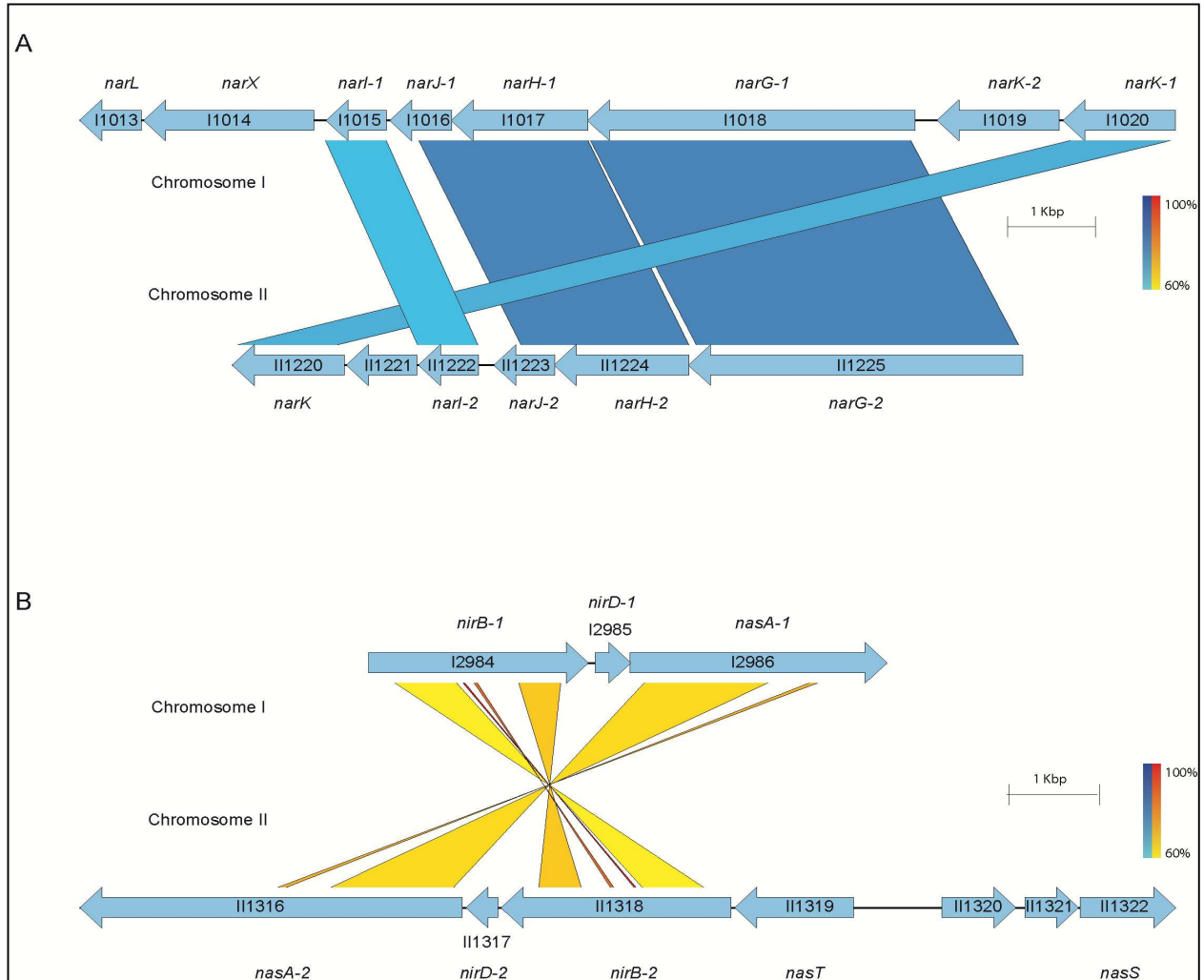
**Figure 3.2 Predicted nitrogen metabolism gene clusters in *B. pseudomallei* 1026b.** The putative nitrate and nitrite reductases, transporters, and nitrate-sensing gene clusters from the sequenced genome of *B. pseudomallei* 1026b are shown. A total of 21 loci spanning *B. pseudomallei* chromosomes I and II included in this study are illustrated here. Bp1026b_I1546, Bp1026b_II1540, and Bp1026b_II1580 were excluded. Coding sequences for the represented nitrate metabolism loci are depicted by arrows in relation to positive or negative strand orientation with open reading frames and intergenic regions illustrated to scale. The results of BLASTN annotations are depicted by color coded bars spanning gene loci across the two chromosomes with a minimum percent identity of 0.60 and a threshold E-value of 1E-3. Blue bars depict direct sequence homology and yellow-to-red bars depict homology amid sequence inversion, on a color density gradient indicating the percent homology. **(A)** The major predicted nitrate reductase *narGHJI* is encoded on chromosome I (Bp1026b_I1015 – 1018) as well as on chromosome II (Bp1026b_II1222 – 1225). Adjacent to the nitrate reductases are predicted nitrate transporters (Bp1026b_I1019, Bp1026b_I1020, Bp1026b_II1220) and the predicted two-component signaling system (Bp1026b_I1013 – I1014). **(B)** The major nitrite reductase *nirBD* is encoded on chromosome I (Bp1026b_I2984 – 2985) as well as on chromosome II (Bp1026b_II1317 – 1318). Adjacent to the nitrite reductase is the predicted assimilatory nitrate reductase *nasA* encoded by Bp1026b_I2986 on chromosome I and Bp1026b_II1316 on chromosome II. The predicted nitrate regulator, *nasT*, and nitrate transport ATP-binding loci, *nasS*, are encoded on chromosome II at Bp1026b_II1319 and Bp1026b_II1322, respectively.

### 3.4.3 Five genes within the denitrification pathway contribute to pellicle biofilm inhibition in the presence of exogenous nitrate in *B. pseudomallei*

We hypothesized that pellicle biofilms cannot form in the presence of exogenous nitrate under the conditions tested. Pellicle biofilms have been historically well characterized in the Gram-positive soil-dwelling bacterium *Bacillus subtilis* (45), as well as pathogenic Gram-negative species such as *P. aeruginosa* (46) and *Burkholderia cenocepacia* (47). *B. pseudomallei* forms pellicle biofilms in static cultures *in vitro* and at the surface-liquid interface near the root zone of plants. Wild-type and transposon insertional mutants of genes in the denitrification pathway were grown statically with or without sodium nitrate to assess the impact of nitrate on pellicle formation. The wild type did not form a pellicle biofilm in the presence of 10 mM $NaNO_3$, while a robust pellicle biofilm was observed in LB without nitrate (**Figure 3.3**). Furthermore, pellicle formation was inhibited by sodium nitrate in 16 of 21 transposon insertional mutants (**Figure 3.4**). Interestingly, five transposon insertional mutants in the denitrification pathway were resistant to inhibition of pellicle formation by exogenous nitrate (**Figure 3.3** and **Figure 3.4**). Transposon insertions in *narL*, a DNA-binding response regulator, and *narX*, a
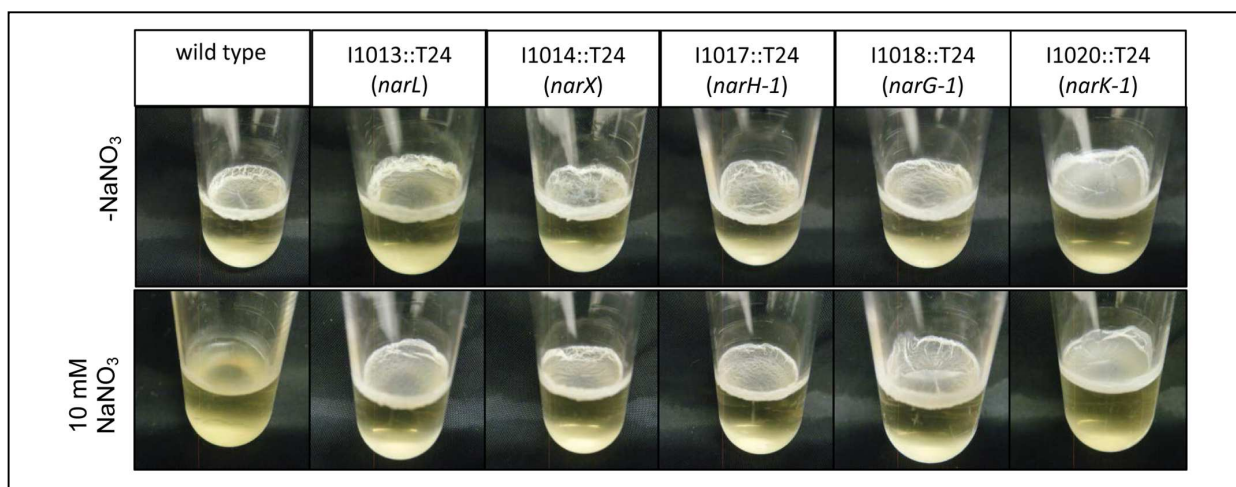


**Figure 3.3 Five transposon insertions in the predicted nitrate metabolism pathway do not respond to inhibition of pellicle biofilm formation mediated by the addition of sodium nitrate.** Wild-type *B. pseudomallei* 1026 forms a distinct pellicle biofilm when grown statically in liquid culture; however, it is unable to form a pellicle biofilm in the presence of 10 mM $NaNO_3$. Transposon insertion mutants in the following genes {Bp1026b_I1013::T24 (*narL*), Bp1026b_I1014::T24 (*narX*), Bp1026b_I1017::T24 (*narH-1*), Bp1026b_I1018::T24 (*narG-1*), and

Bp1026b_I1020::T24 (*nark-1*)} were identified that form pellicle biofilms growing statically in LB + 10 mM NaNO$_3$. Pellicles were grown in 3 mL media at room temperature, with or without 10 mM NaNO$_3$ supplemented, and photographed at 14 days.
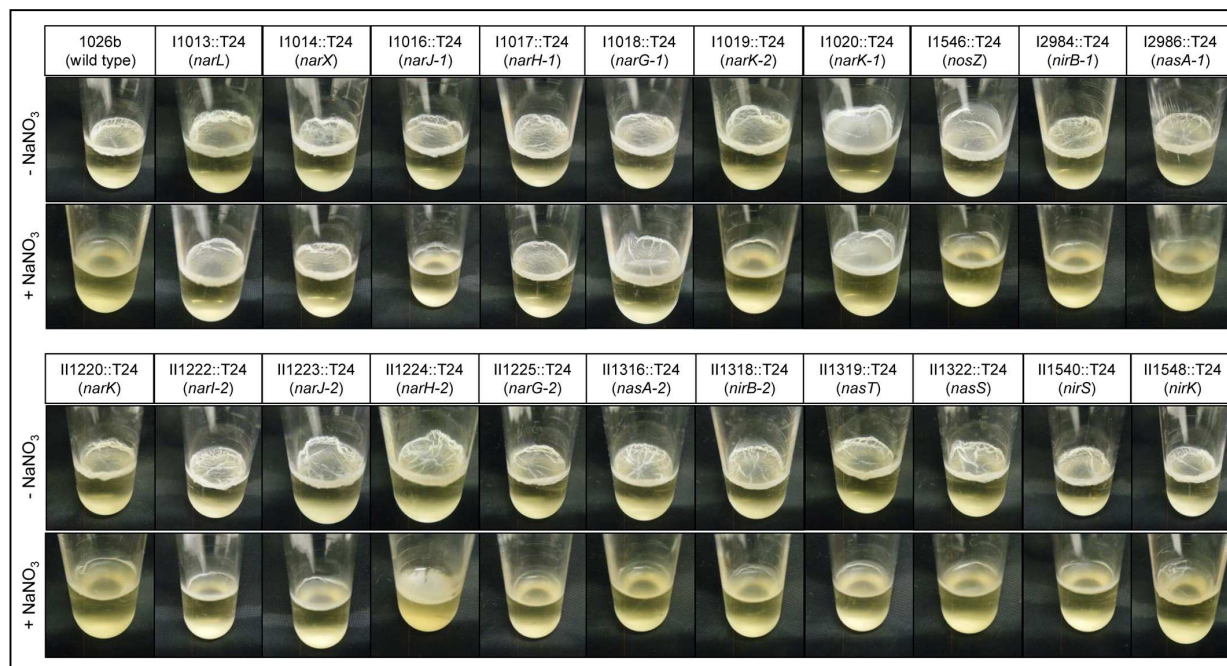


**Figure 3.4 Assessment of pellicle biofilm formation for all 21 transposon insertional mutants used in this study.** Pellicle biofilms were grown statically in 3 mL LB medium, with or without 10 mM NaNO$_3$ supplemented, and photographed at 14 days.

nitrate sensor protein, which comprise a two-component signaling system regulated by nitrate, were resistant to pellicle inhibition by nitrate. Similarly, transposon mutants with insertions in *narG-1* and *narH-1*, which are predicted to be the major nitrate reductase alpha and beta subunits were also insensitive to inhibition of pellicle formation by nitrate. Interestingly, transposon mutations into *narG-1* and *narH-1* did not confer resistance to biofilm inhibition by sodium nitrite (**Figure 3.5**), indicating that nitrite may inhibit biofilm formation independently of the major nitrate reductase. It is curious that only the cytoplasmic subunits of the major nitrate reductase were hit during our transposon screen for the biofilm inhibitory phenotype via sodium nitrate, an observation that may provide insights into the respiratory electron transfer pathway in *B. pseudomallei*. Additionally, it is worth noting that the membrane-anchored *narI* gamma subunit of the nitrate reductase was not available in our transposon mutant library, and as such,

its relation to biofilm dynamics remains uncharacterized. We identified a fifth transposon mutant

with an insertion in *narK-1*, encoding a predicted nitrate/nitrite transporter that was also

insensitive to pellicle biofilm inhibition by nitrate. These results suggest that this genetic quintet

{Bp1026b_I1013 (*narL*), Bp1026b_I1014 (*narX*), Bp1026b_I1017 (*narH-1*), Bp1026b_I1018

(*narG-1*), Bp1026b_I1020 (*nark-1*)} contributes to the regulation and formation of *B.*

*pseudomallei* biofilms when exogenous nitrate is encountered.
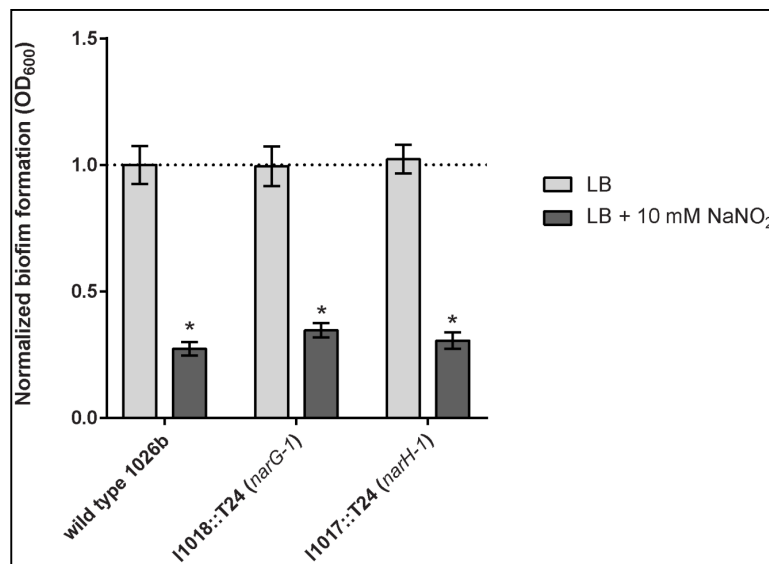


**Figure 3.5 Biofilm inhibition by sodium nitrite does not require *narG-1* or *narH-1*.** Asterisks
indicate a significant difference (p<0.0001) calculated with an unpaired Student's t-test.

### 3.4.4 Quantification of biofilm formation

Biofilm inhibition by nitrate was assessed in the same array of transposon insertion

mutants using the quantitative biofilm growth method (48) to calculate results from static biofilm

assays. In conjunction with the direct observation of pellicle formation, the static biofilm assay

provides quantitative analysis on the biofilm forming capabilities for each strain in this study.

Biofilm formation was significantly abolished with nitrate treatment in 16 of the 21 transposon

mutants; however, biofilm formation of transposon mutants in *narL*, *narX*, *narG-1*, *narH-1*, and

*narK-1* was not significantly altered in the presence of nitrate (**Figure 3.6A**). These results

corroborated the qualitative observations of the pellicle biofilm assay, as the same five mutants
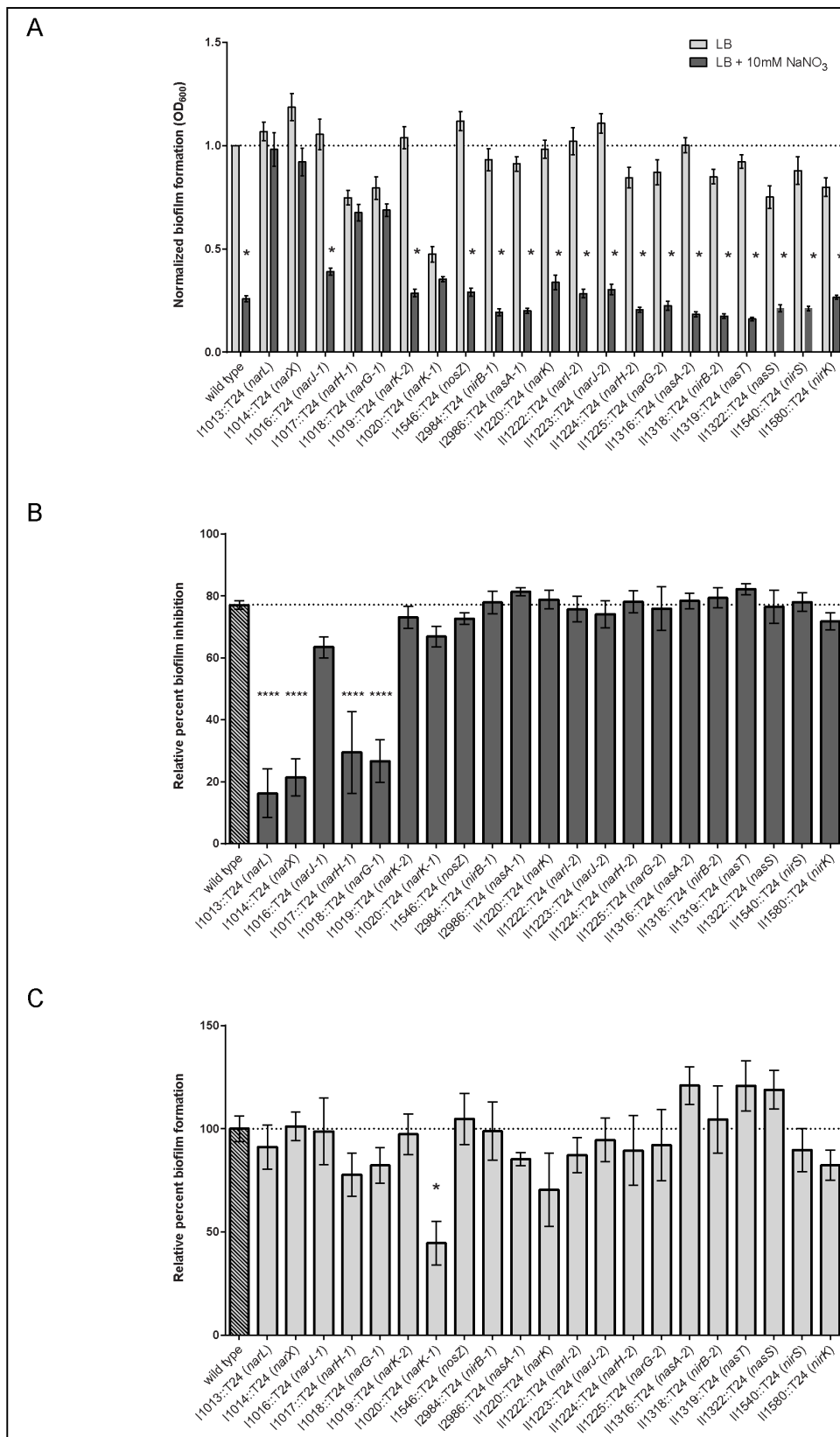
**Figure 3.6 Quantitative evaluation of relative biofilm formation and biofilm inhibition in**

**the presence and absence of sodium nitrate. (**A) Biofilm formation was evaluated when grown statically in the presence of 10 mM $NaNO_3$. Biofilm formation of the wild type and 16 of the 21 transposon mutants identified in this study were inhibited by treatment with $NaNO_3$, while five mutants {Bp1026b_I1013::T24 (*narL)*, Bp1026b_I1014::T24 (*narX*), Bp1026b_I1017::T24 (*narH-1)*, Bp1026b_I1018::T24 (*narG-1*), and Bp1026b_I1020::T24 (*nark-1*)} were not inhibited by treatment with $NaNO_3$. Bars are representative of the means for individually normalized values for biofilm formation relative to the wild type. Asterisks indicate a significant difference (p<0.0001) calculated with an unpaired Student's t-test using the Holm-Sidak method to account for multiple comparisons (n=12). **(B)** Percent biofilm inhibition for all mutants was calculated relative to inhibition of the wild type in the presence of 10 mM $NaNO_3$. Bars are representative of the means for each mutant relative to the mean for wild type. **(C)** Biofilm formation for all mutants was calculated relative to wild-type biofilm formation in LB medium. Bars are representative of the means for each mutant relative to the mean for wild type.

were similarly resistant to the biofilm inhibitory effects of nitrate in both assays. Planktonic

growth for *narL*, *narX*, *narG-1*, *narH-1*, and *narK-1* was similar when compared to wild-type *B.*

*pseudomallei* 1026b (**Figure 3.7**).
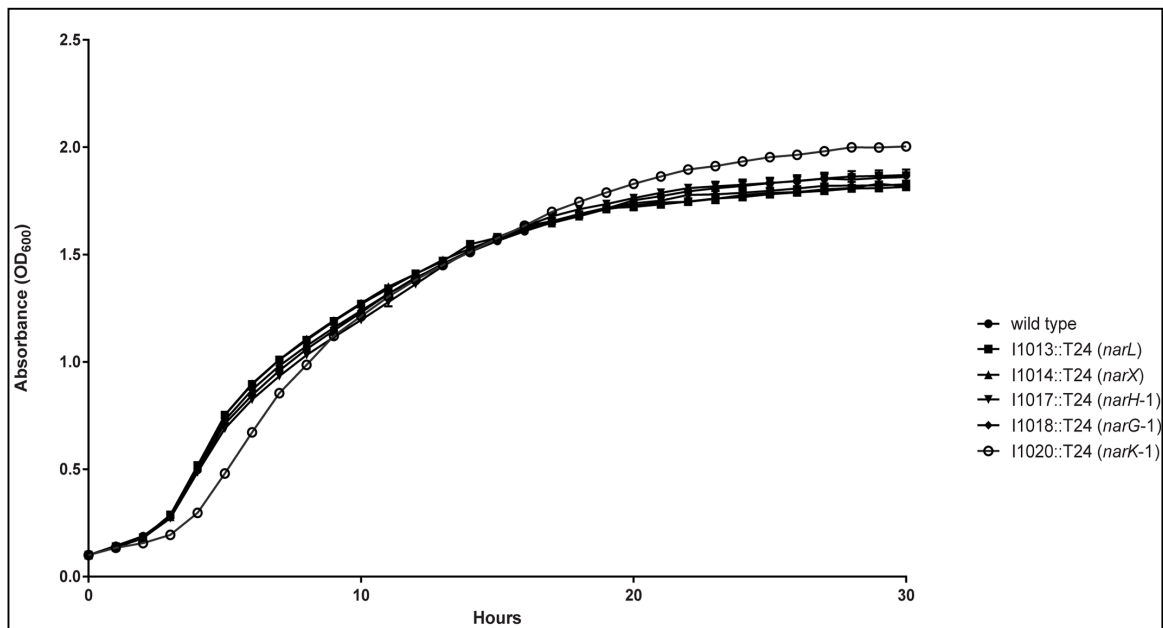


**Figure 3.7 Growth curves for transposon insertion mutants in denitrification genes that no longer respond to nitrate mediated biofilm inhibition.** Growth curves were generated for cultures grown with shaking at 37C and absorbance ($OD_{600}$) readings were taken for 30 continuous hours.

To further assess the effects of nitrate metabolism genes on biofilm inhibition, we

calculated the percent of relative biofilm inhibition for all mutant strains in this study (**Figure**

**3.6B**). While wild-type biofilm formation was reduced by nearly 80% when sodium nitrate is

encountered, transposon insertions in *narL*, *narX*, *narG-1*, and *narH-1* did not respond to the

inhibitory effects of treatment with sodium nitrate. The decrease in the percentage of relative

biofilm formation for the transposon-inactivated *narK-1* mutant (**Figure 3.6C**) indicates that this

mutant is affected by nitrate more so than the *narL*, *narX*, *narG-1*, and *narH-1* mutants, and is

also reflective of a fundamental biofilm-forming defect in the *narK-1* mutant. Taken together,

these results provide quantitative measurements of biofilm inhibition and formation in the

presence of exogenous nitrate, and support our conclusions regarding the role of these

functionally-inactivated genetic loci as observed in the pellicle biofilm assay.

To validate the transposon-inactivated mutants identified through the T24-mutagenesis

approach, we complemented the inactive versions of *narL* (Bp1026b_I1013::T24) and *narX*

(Bp1026b_I1014::T24) with full-length versions that are expressed via an IPTG-inducible

promoter. Complementation of both genes reversed the mutant phenotype that was resistant to

biofilm inhibition by nitrate (**Figure 3.8**). Complemented versions of *narL* (Bp1026b_I1013::T24

(*narL*)P$_{tac}$-I1013) and *narX* (Bp1026b_I1014::T24 (*narX*)P$_{tac}$-I1014) react to exogenous nitrate in

a similar manner as the wild-type empty-vector (EV), that is biofilm formation is inhibited by

roughly 50% with the addition of 5 mM NaNO$_3$ (**Figure 3.8**). These data provide further support

to the hypothesis that the *narX-L* two-component signaling system, which is predicted to

respond to nitrate sensing, is implicated in biofilm growth dynamics in *B. pseudomallei*.
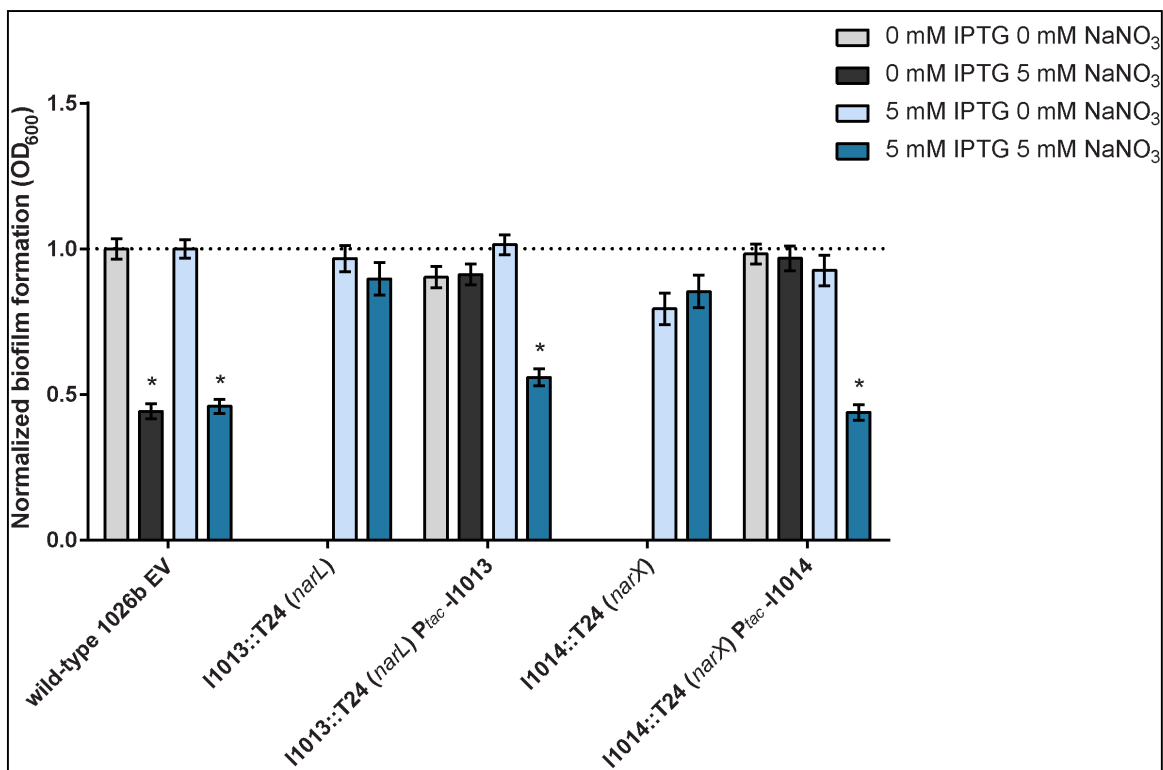
**Figure 3.8 Complementation of the I1013::T24 (*narL*) and I1014::T24 (*narX*) mutants that are resistant to the inhibitory effects of exogenous nitrate.** Mutants of the predicted nitrate-sensing two-component system *narX/narL* were complemented with full-length Bp1026b_I1013 (*narL*) and Bp1026b_I1014 (*narX*). The genes were re-introduced in the T24-mutant background at a neutral site and expression was conditionally induced using 5 mM IPTG. Biofilm formation was assessed in the presence and absence of 5 mM NaNO$_3$.

### 3.4.5 Exogenous nitrate reduces intracellular c-di-GMP in a static biofilm assay

Biofilm formation and dispersal mechanisms are ultimately dependent on the level of intracellular c-di-GMP in many pathogenic bacteria (3), thus we hypothesized that biofilm inhibition via exogenous nitrate sensing regulates c-di-GMP concentrations in *B. pseudomallei* 1026b. We analyzed the intracellular concentration of c-di-GMP via liquid chromatography tandem-mass spectrometry (LC-MS/MS) using a triple quadrupole mass spectrometer. The intracellular concentration of c-di-GMP in wild-type bacteria grown statically in minimal media with 10 mM sodium nitrate was reduced by 38% as compared to biofilms cultivated statically in the absence of nitrate (**Figure 3.9A**). For static biofilms cultivated without sodium nitrate, we observed an average concentration of 80.46 nmol c-di-GMP per mg of total protein and for

biofilms cultivated in the presence of 10 mM nitrate the average concentration was 50.19 nmol

c-di-GMP per mg total protein (**Figure 3.9A**). These results suggest that nitrate metabolism

regulates intracellular c-di-GMP levels in *B. pseudomallei* 1026b biofilms.
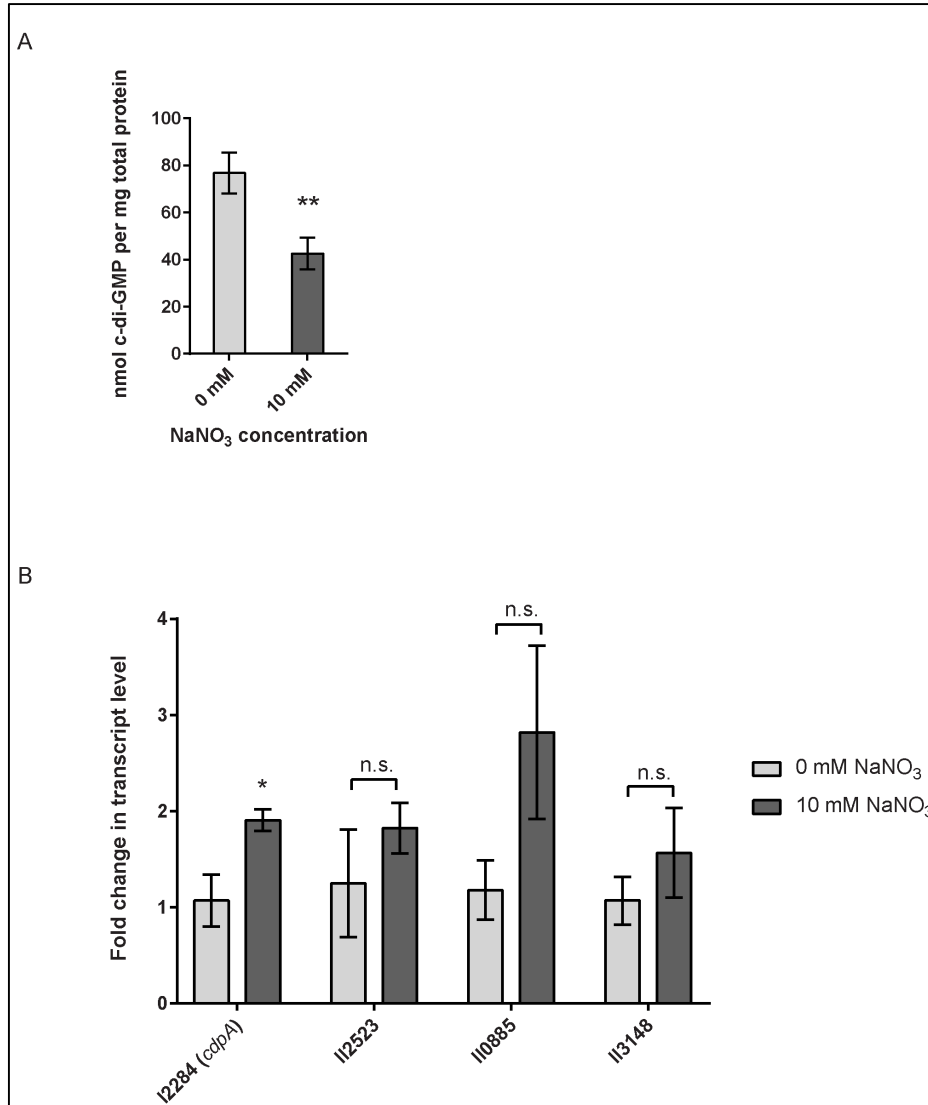


**Figure 3.9 Quantification of cyclic dimeric GMP (c-di-GMP) in response to sodium nitrate and relative transcript abundance of *cdpA*, the major phosphodiesterase in *B. pseudomallei*.** (A) The intracellular concentration of the bacterial second messenger c-di-GMP is significantly reduced in *B. pseudomallei* 1026b grown statically in nitrate-supplemented media. Error bars indicate standard error for four biological replicates extracted on different days. Statistical significance was determined using the Sidak-Bonferroni method across multiple T-tests (** = p<0.01). (B) *cdpA* transcript level is upregulated nearly 2-fold in *B. pseudomallei* 1026b grown statically in nitrate-supplemented media. Three additional transcripts that encode for a phosphodiesterase (I3148), a diguanylate cyclase (II2523), and a composite diguanylate

cyclase/phosphodiesterase (II0885) did not show statistical differences in the levels of transcript. Fold change in transcript level was calculated using the Pfaffl method considering primer amplification efficiency and normalized to the reference transcript for 23S rRNA. Statistical significance was determined using a one-tailed heteroscedastic Student's T-test (* = $p < 0.05$).

### 3.4.6 The phosphodiesterase *cdpA* is upregulated in response to nitrate in a static biofilm assay

In a simplified model of c-di-GMP regulation, a decrease in intracellular c-di-GMP levels suggests either decreased diguanylate cyclase activity or increased phosphodiesterase activity. We chose to evaluate the expression of previously described diguanylate cyclase and phosphodietsersases that are known to alter biofilm dynamics in *B. pseudomallei* (29, 49). C-di-GMP metabolism in bacteria, including *B. pseudomallei* 1026b, is classically mediated by diguanlyate cyclases and phosphodiesterases that contain conserved GG(D/E)EF and EAL catalytic domains, respectively (3, 29). *B. pseudomallei* 1026b contains six predicted proteins with conserved EAL domains and five predicted GGDEF-EAL composite proteins; however, only one of these predicted proteins, Bp1026b_I2284, has been shown to potentially function as a classical phosphodiesterase (Plumley et al., 2017). Bp1026b_I2284 (*cdpA*) is a previously described phosphodiesterase and known regulator of c-di-GMP levels in *B. pseudomallei* KHW (49). Recently, Bp1026b_I2284 (*cdpA*) has also been shown to contribute to motility and is therefore potentially implicated in reducing c-di-GMP levels in *B. pseudomallei* 1026b during planktonic growth (29). Thus, we hypothesized that *cdpA* transcript expression is regulated during nitrate metabolism in *B. pseudomallei* 1026b, leading to a decrease in intracellular c-di-GMP and inhibition of biofilm formation.

Since more than one phosphodiesterase may be expressed simultaneously during stimulatory conditions, we also evaluated transcription of phosphodiesterase genes with conserved catalytic domains previously identified (29). Of the GGDEF-EAL composite proteins, Bp1026b_II0885 was chosen for analysis based on the conservation of the EAL domain with

*cdpA* as well as conservation of the GGDEF catalytic domain (29). An EAL-containing gene locus, Bp1026b_I3148, was also chosen based on a similarly high level of consensus among the EAL domain containing proteins in *B. pseudomallei* 1026b (29). To evaluate the effects on diguanylate cyclase activity, we chose to analyze the GG(D/E)EF-containing gene locus, Bp1026b_II2523, based on its conserved GGEEF domain and its previously observed role in the regulation of biofilm growth dynamics (29).

To assess the impact of exogenous nitrate on the expression of c-di-GMP phosphodiesterases and diguanylate cyclases, wild-type *B. pseudomallei* 1026b was grown statically under biofilm-inducing conditions in minimal media with or without 10 mM $NaNO_3$. The expression of *cdpA* was significantly higher, representing a nearly two-fold increase in cells grown in 10 mM $NaNO_3$-supplemented minimal media when normalized to 23S rRNA (**Figure 3.6B**). Interestingly, the expression values for the additional two transcripts that potentially encode c-di-GMP phosphodiesterases showed a similar trend to that of *cdpA*; however, these analyses lacked statistical significance (**Figure 3.9B**). The expression of Bp1026b_II2523, a putative diguanylate cyclase showed no significant response to nitrate, which indicates it may not be involved in the nitrate-dependent biofilm inhibition cascade under the conditions tested. Thus, while nitrate has a clear regulatory effect on *cdpA*, it is possible that other phosphodiesterases and diguanylate cyclases that remain to be tested also contribute to the intracellular concentration of c-di-GMP. Moreover, we showed that *cdpA* is not required for nitrate- or nitrite-dependent biofilm inhibition (**Figure 3.10**). Nonetheless, these results indicate that nitrate can potentially increase phosphodiesterase activity in *B. pseudomallei* 1026b and can explain the significant decrease in c-di-GMP concentration during growth under identical conditions. Taken together with the absolute quantification of c-di-GMP, these data support our hypothesis that exogenous nitrate inhibits *B. pseudomallei* 1026b biofilms by reducing the intracellular concentration of c-di-GMP.
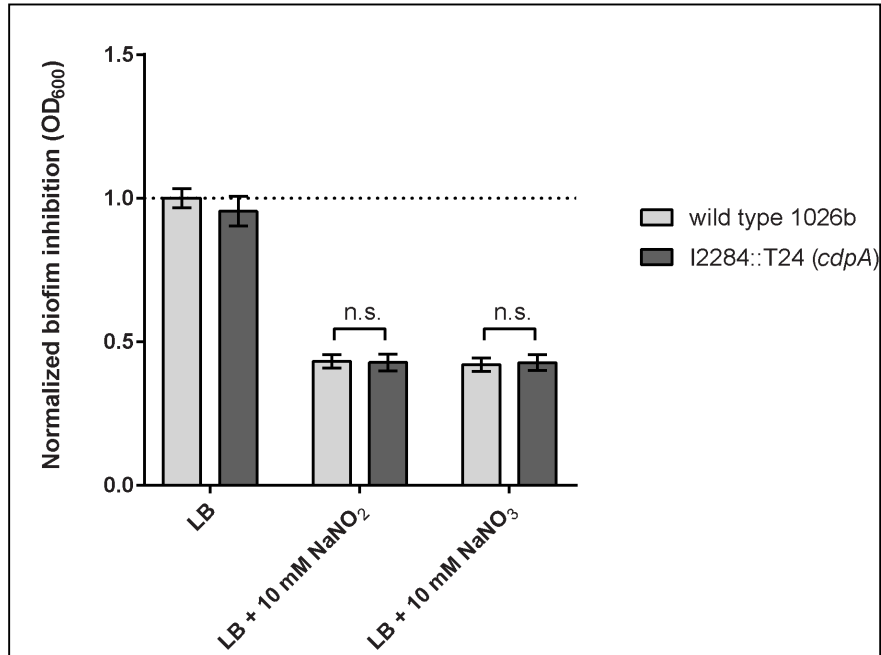
**Figure 3.10 Biofilm inhibition by sodium nitrate or sodium nitrite does not require *cdpA*.**

### 3.5 Conclusions

Environmental acquisition of opportunistic pathogens such as *B. pseudomallei* requires a lifestyle transition that prompts a shift from the natural reservoir to establish infections in susceptible human and animal hosts. Biofilm communities serve as a predominant natural habitat for the saprophytic *B. pseudomallei*, which colonizes and persists in the rhizosphere of plants in wet soils of endemic areas (6), thus efforts to better understand the dissemination from this environment would serve to mitigate public health risks related to the emerging infectious disease melioidosis. The particular effectors that serve as biofilm inhibition signals and dispersal cues for *B. pseudomallei* are poorly understood, although previous studies link anthropogenic disturbances to increased bacterial presence in endemic areas (10, 13, 50). Notably, and of particular interest to our present study, are the observations by Kaestli et al. (12) that addition of nitrate-rich fertilizer increased *B. pseudomallei* bacterial loads across a variety of soils. Since nitrate ($NO_3^-$) and nitrite ($NO_2^-$) can serve as terminal electron acceptors for anaerobic

respiration in denitrifying bacteria (25) and the *Burkholderia* genera are capable of denitrification (12), we tested the hypothesis that nitrate inhibits biofilm formation in *B. pseudomallei* 1026b.

The results presented in this study indicate that exogenous addition of nitrate, and to a lesser extent, nitrite, inhibit biofilm formation. While both nitrate and nitrite have been shown to repress biofilm formation in *P. aeruginosa* (19) and *S. aureus* (21), respectively, this is the first study to address the effects of nitrate on *B. pseudomallei* biofilm formation. We identified a total of 21 genes, which were predicted to encode nitrate metabolism enzymes in the denitrification pathway, of which five transposon mutants no longer responded to biofilm inhibition by nitrate. This analysis identified the predicted two-component signaling system *narX/narL*, and implicates this conserved regulatory system in nitrate metabolism as well as control of biofilm growth dynamics in *B. pseudomallei*. The nitrate sensing two-component system, which is conserved among aerobes and anaerobes alike, mediates gene expression when *narX* senses environmental nitrate, thereby stimulating a phosphorylation cascade that causes *narL* to bind and regulate DNA transcription (51). Thus, the *narX/narL* system acts as a primary sensor of exogenous nitrate, and our observations implicate this system in the genetic control of biofilm formation. Given the genetic arrangement of this two-component system adjacent to the predicted major nitrate reductase on chromosome I (**Figure 3.2**), future studies will address whether the DNA-binding and regulatory effects of NarL are targeted to the upstream *narGHJI-1* operon.

Our results also indicate that two subunits in the major dissimilatory nitrate reductase *narGHJI-1*, which is tasked with reducing nitrate to nitrite inside the bacterial cell, contributes to exogenous nitrate sensing and control of biofilm formation when nitrate is present. Biofilm formation is also inhibited by nitrite (**Figure 3.1A**), and although this genetic mechanism has not been investigated in the present study, our results indicate that this phenotype occurs independently of the alpha and beta subunits of the primary nitrate reductase *narGH-1* (**Figure 3.5**). Additionally, biofilm formation of a transposon mutant insertion in one of the four

nitrate/nitrite transporter genes, *narK-1*, was no longer inhibited in the presence of nitrate.

These results suggest that the five genes *narL*, *narX*, *narG-1*, *narH-1*, and *narK-1* are implicated

in mediating the biofilm growth dynamics of *B. pseudomallei* when exogenous nitrate is

encountered in the environment. Given that the *narX/narL* two-component system is adjacent to

the major nitrate reductase encoded by the *narGHJI-1* operon, a prominent hypothesis is that

this system is required for transcriptional regulation of the nitrate reductase, similar to the nitrate

regulatory network of *P. aeruginosa* (52). Interestingly, while there is another predicted

dissimilatory nitrate reductase encoded on chromosome II by the *narGHJI-2* operon, transposon

mutant insertions within these loci do not function like *narGHJI-1* under the conditions tested.

Moreover, we did not find evidence for homologs of the *narX/narL* two-component signaling

system for nitrate sensing on chromosome II in our bioinformatics analyses.

 *B. pseudomallei* is a facultative anaerobe that is found in soils approximately 30 cm

deep (14), a depth which becomes relatively hypoxic in rice paddy soils (18), and nitrate

becomes increasingly more important as a terminal electron acceptor for anaerobic respiration.

Similarly, biofilms are intrinsically hypoxic microenvironments as oxygen and nutrient diffusion

are physically limited, leading to increased dependence on nitrate anions as an alternative

terminal electron acceptor (18). Based on our *in vitro* results, our working hypothesis is that

excessive environmental nitrate triggers dispersal of hypoxic, nutrient-limited sessile cells

residing in the biofilm community leading to increased abundance of planktonic bacteria. This

working model is illustrated in the context of the denitrification pathway for *B. pseudomallei*

1026b and its potential connection to c-di-GMP metabolic regulatory cascades (**Figure 3.11**). It

is important to mention that the information regarding c-di-GMP signaling and metabolism in *B.*

*pseudomallei* is scarce, given the importance of this second messenger molecule in the

regulation of biofilm dynamics (29). Given the well-established connection between c-di-GMP

and biofilm formation in many bacterial species, and the important transition from biofilm to

planktonic cells in a variety of natural and host environments, it is vital to further identify and

characterize the environmental cues that modulate c-di-GMP levels in the Tier 1 Select Agent *B. pseudomallei*.
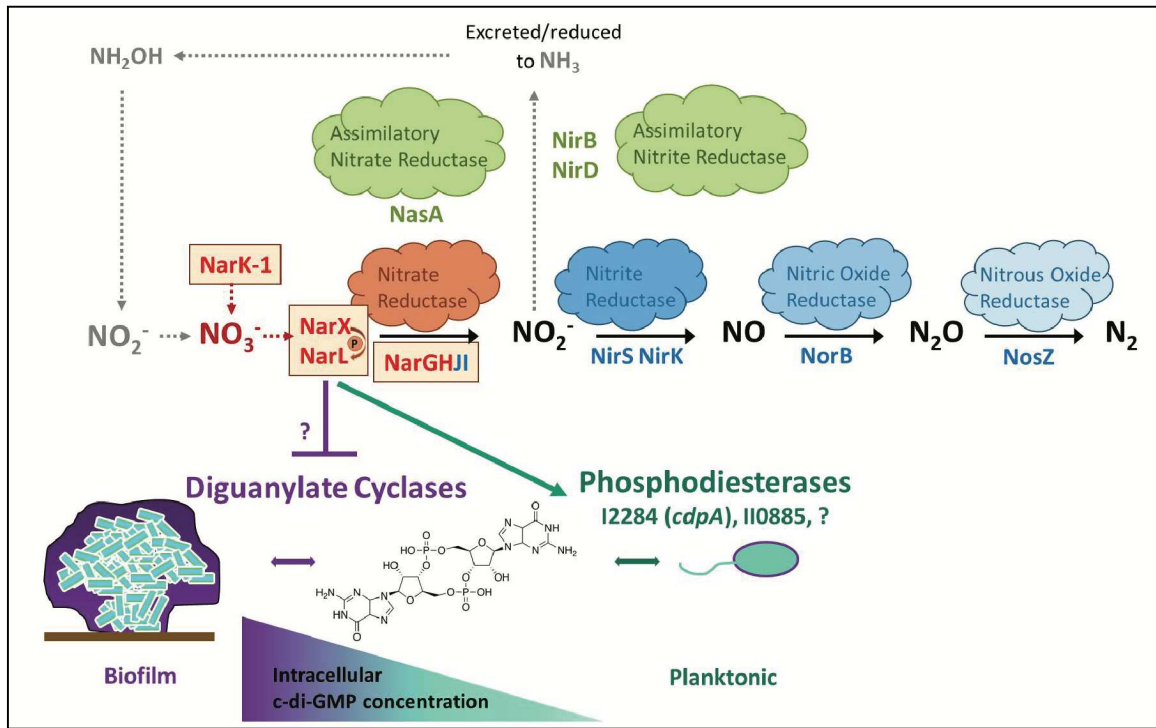


**Figure 3.11 Working model for nitrate sensing and metabolism in relation to biofilm dynamics in *B. pseudomallei*.** This model serves to illustrate nitrate metabolism in the context of biofilm dynamics for *B. pseudomallei*. The process of denitrification is carried out by four individual enzyme complexes: nitrate reductase, nitrite reductase, nitric oxide reductase, and nitrous oxide reductase. Additionally, *B. pseudomallei* encodes assimilatory nitrate and assimilatory nitrite reductases. The process of nitrification, depicted by grey arrows, is not intrinsic to *B. pseudomallei*; however, it is a relevant source of nitrate in the environment, produced by nitrifying bacteria. The five genes identified in this study are highlighted in bold red with surrounding boxes, in proximity to the major nitrate reductase (also highlighted in red). The biofilm life-cycle is illustrated as a state of constant flux mediated by intracellular c-di-GMP concentration. A proposed mechanism by which the NarX/NarL two-component nitrate-sensing system modulates c-di-GMP is illustrated, although the connection to diguanlyate cyclases and additional phosphodiesterases remains to be determined.

The results presented here provide evidence that a primary mechanism for control of *B. pseudomallei* biofilm formation is through the regulation of the intracellular concentration of the bacterial second messenger, c-di-GMP, via nitrate sensing and metabolism. The role of c-di-GMP in the regulation of bacterial behaviors, which include biofilm formation, is known to have significant implications on the ability of pathogenic bacteria to cause disease (3). The model of c-di-GMP flux inside a cell generally dictates that more intracellular c-di-GMP molecules

corresponds to a biofilm and sessile state, while a reduced intracellular concentration stimulates motility and favors a planktonic lifestyle; however, many of the extracellular cues that activate these signaling cascades remain uncharacterized (**Figure 3.11**) (3). Quantification of intracellular c-di-GMP levels in response to exogenous nitrate revealed that nitrate metabolism can affect the levels of this secondary messenger in *B. pseudomallei* 1026b. We hypothesize that the signaling transduction cascade initiated by nitrate sensing as controlled by the *narX/narL* two-component system activates not only dissimilatory nitrate reduction through the *narGHJI-1* complex but also regulates phosphodiesterase enzymes tasked with rapidly reducing intracellular concentrations of c-di-GMP. Our results indicate a significant reduction of c-di-GMP levels in static cultures grown in the presence of sodium nitrate, in addition to increased expression of *cdpA*, which encodes a known phosphodiesterase. These findings collectively indicate that the mechanism of nitrate sensing is linked to control of c-di-GMP levels in the cell.

Modulation of c-di-GMP levels is a primary mechanism bacteria use to respond to extracellular signals and cues as they relate to control autoaggregation, biofilm formation, and motility during the transition from sessile to planktonic growth states. Therefore, such a mechanism is at the crux of controlling bacterial dissemination from environmental reservoirs to host-associated infections for sapronotic disease agents such as *B. pseudomallei.* CdpA, which has been characterized as a key phosphodiesterase enzyme in *B. pseudomallei* KHW (49) and at the gene level in *B. pseudomallei* 1026b (29), has also been implicated in the regulatory control of biofilm formation in *B. cepacia* J2315 (53). Our assessment of *cdpA* expression from *B. pseudomallei* 1026b revealed significant upregulation of this transcript in response to elevated nitrate availability, with a corresponding decrease of intracellular c-di-GMP levels. These data reveal an important connection between increased phosphodiesterase activity and reduction of this key second messenger molecule in response to the addition of nitrate. We expect global c-di-GMP metabolic cascades to be simultaneously activated by an exogenous nitrate signal, and given that we have previously identified 23 gene loci predicted to encode c-di-

GMP metabolic or binding enzymes, there is undoubtedly more complex regulation in addition to *cdpA* activity (29). Future studies will address nitrate's global transcriptional regulation of c-di-GMP metabolism in addition to exopolysaccharide, capsule, pili, flagellar, quorum sensing, and antibiotic efflux machinery, among other mechanisms pertinent to the biofilm-to-planktonic transition.

The complexity of the regulatory network for denitrifying growth in hypoxic conditions has been extensively examined across several bacterial species (54), implicating several transcriptional regulators of nitrate metabolism such as the *narX/narL* system in addition to quorum sensing and nutrient availability. Our study implicates nitrate metabolism in biofilm growth dynamics in *B. pseudomallei*, and identifies specific gene loci that may be targeted for regulation by a combination of systems. Furthermore, we provide evidence that the second messenger, c-di-GMP, is involved in biofilm inhibition in response to exogenous addition of nitrate. Future analyses will assess the regulation of the enzymes described in this study and investigate the effects of denitrification on c-di-GMP metabolism as it relates to the pathogenesis of *B. pseudomallei*.

# References

1.    McDougald D, Rice SA, Barraud N, Steinberg PD, Kjelleberg S. Should we stay or should we go: mechanisms and ecological consequences for biofilm dispersal. Nat Rev Microbiol. 2011;10(1):39-50.
2.    O'Toole G, Kaplan HB, Kolter R. Biofilm formation as microbial development. Annu Rev Microbiol. 2000;54:49-79.
3.    Tamayo R, Pratt JT, Camilli A. Roles of cyclic diguanylate in the regulation of bacterial pathogenesis. Annu Rev Microbiol. 2007;61:131-48.
4.    Dance DA. Melioidosis as an emerging global problem. Acta Trop. 2000;74(2-3):115-9.
5.    Inglis TJ, Sagripanti JL. Environmental factors that affect the survival and persistence of *Burkholderia pseudomallei*. Appl Environ Microbiol. 2006;72(11):6865-75.
6.    Prasertsincharoen N, Constantinoiu C, Gardiner C, Warner J, Elliman J. Effects of Colonization of the Roots of Domestic Rice (*Oryza sativa* L. cv. Amaroo) by *Burkholderia pseudomallei*. Appl Environ Microbiol. 2015;81(13):4368-75.
7.    Ramli NS, Eng Guan C, Nathan S, Vadivelu J. The effect of environmental conditions on biofilm formation of *Burkholderia pseudomallei* clinical isolates. PLoS One. 2012;7(9):e44104.
8.    Kuris AM, Lafferty KD, Sokolow SH. Sapronosis: a distinctive type of infectious agent. Trends Parasitol. 2014;30(8):386-93.
9.    Hatcher CL, Muruato LA, Torres AG. Recent Advances in *Burkholderia mallei* and *B. pseudomallei* Research. Curr Trop Med Rep. 2015;2(2):62-9.
10.   Limmathurotsakul D, Golding N, Dance DA, Messina JP, Pigott DM, Moyes CL, Rolim DB, Bertherat E, Day NP, Peacock SJ, Hay SI. Predicted global distribution of *Burkholderia pseudomallei* and burden of melioidosis. Nat Microbiol. 2016;1(1).
11.   Wiersinga WJ, Currie BJ, Peacock SJ. Melioidosis. N Engl J Med. 2012;367(11):1035-44.
12.   Kaestli M, Harrington G, Mayo M, Chatfield MD, Harrington I, Hill A, Munksgaard N, Gibb K, Currie BJ. What drives the occurrence of the melioidosis bacterium *Burkholderia pseudomallei* in domestic gardens? PLoS Negl Trop Dis. 2015;9(3):e0003635.
13.   Limmathurotsakul D, Kanoksil M, Wuthiekanun V, Kitphati R, deStavola B, Day NP, Peacock SJ. Activities of daily living associated with acquisition of melioidosis in northeast Thailand: a matched case-control study. PLoS Negl Trop Dis. 2013;7(2):e2072.
14.   Palasatien S, Lertsirivorakul R, Royros P, Wongratanacheewin S, Sermswan RW. Soil physicochemical properties related to the presence of *Burkholderia pseudomallei*. Trans R Soc Trop Med Hyg. 2008;102 Suppl 1:S5-9.
15.   Hantrakun V, Rongkard P, Oyuchua M, Amornchai P, Lim C, Wuthiekanun V, Day NP, Peacock SJ, Limmathurotsakul D. Soil Nutrient Depletion Is Associated with the Presence of *Burkholderia pseudomallei*. Appl Environ Microbiol. 2016;82(24):7086-92.
16.   Hamad MA, Austin CR, Stewart AL, Higgins M, Vazquez-Torres A, Voskuil MI. Adaptation and antibiotic tolerance of anaerobic *Burkholderia pseudomallei*. Antimicrob Agents Chemother. 2011;55(7):3313-23.
17.   Yabuuchi E, Kosako Y, Oyaizu H, Yano I, Hotta H, Hashimoto Y, Ezaki T, Arakawa M. Proposal of *Burkholderia* gen. nov. and transfer of seven species of the genus *Pseudomonas* homology group II to the new genus, with the type species *Burkholderia cepacia* (Palleroni and Holmes 1981) comb. nov. Microbiol Immunol. 1992;36(12):1251-75.

18.     Andreae CA, Titball RW, Butler CS. Influence of the molybdenum cofactor biosynthesis on anaerobic respiration, biofilm formation and motility in *Burkholderia thailandensis*. Res Microbiol. 2014;165(1):41-9.

19.     Van Alst NE, Picardo KF, Iglewski BH, Haidaris CG. Nitrate sensing and metabolism modulate motility, biofilm formation, and virulence in *Pseudomonas aeruginosa*. Infect Immun. 2007;75(8):3780-90.

20.     Zemke A, Lashua L, Gladwin M, Bomberger J. Sodium nitrite disrupts biotic biofilm formation by *Pseudomonas aeruginosa* on polarized human airway epithelial cells. Nitric Oxide-Biology and Chemistry. 2013;31:S13-S4.

21.     Schlag S, Nerz C, Birkenstock TA, Altenberend F, Gotz F. Inhibition of staphylococcal biofilm formation by nitrite. J Bacteriol. 2007;189(21):7911-9.

22.     Zemke AC, Gladwin MT, Bomberger JM. Sodium nitrite blocks the activity of aminoglycosides against *Pseudomonas aeruginosa* biofilms. Antimicrob Agents Chemother. 2015;59(6):3329-34.

23.     Zemke AC, Shiva S, Burns JL, Moskowitz SM, Pilewski JM, Gladwin MT, Bomberger JM. Nitrite modulates bacterial antibiotic susceptibility and biofilm formation in association with airway epithelial cells. Free Radic Biol Med. 2014;77:307-16.

24.     Sodergren EJ, Hsu PY, DeMoss JA. Roles of the *narJ* and *narI* gene products in the expression of nitrate reductase in *Escherichia coli*. J Biol Chem. 1988;263(31):16156-62.

25.     Payne WJ. Denitrification. New York, NY: John Wiley & Sons, Inc.; 1981.

26.     Goh EB, Bledsoe PJ, Chen LL, Gyaneshwar P, Stewart V, Igo MM. Hierarchical control of anaerobic gene expression in *Escherichia coli* K-12: the nitrate-responsive NarX-NarL regulatory system represses synthesis of the fumarate-responsive DcuS-DcuR regulatory system. J Bacteriol. 2005;187(14):4890-9.

27.     Egan SM, Stewart V. Mutational analysis of nitrate regulatory gene *narL* in *Escherichia coli* K-12. J Bacteriol. 1991;173(14):4424-32.

28.     DeShazer D, Brett PJ, Carlyon R, Woods DE. Mutagenesis of *Burkholderia pseudomallei* with Tn5-OT182: isolation of motility mutants and molecular characterization of the flagellin structural gene. J Bacteriol. 1997;179(7):2116-25.

29.     Plumley BA, Martin KH, Borlee GI, Marlenee NL, Burtnick MN, Brett PJ, AuCoin DP, Bowen RA, Schweizer HP, Borlee BR. Thermoregulation of Biofilm Formation in *Burkholderia pseudomallei* Is Disrupted by Mutation of a Putative Diguanylate Cyclase. J Bacteriol. 2017;199(5).

30.     Ogata H, Goto S, Sato K, Fujibuchi W, Bono H, Kanehisa M. KEGG: Kyoto Encyclopedia of Genes and Genomes. Nucleic Acids Res. 1999;27(1):29-34.

31.     Winsor GL, Khaira B, Van Rossum T, Lo R, Whiteside MD, Brinkman FSL. The Burkholderia Genome Database: facilitating flexible queries and comparative analyses. Bioinformatics. 2008;24(23):2803-4.

32.     Winsor GL, Griffiths EJ, Lo R, Dhillon BK, Shay JA, Brinkman FS. Enhanced annotations and features for comparing thousands of *Pseudomonas* genomes in the Pseudomonas Genome Database. Nucleic Acids Res. 2016;44(D1):D646-53.

33.     Edgar RC. MUSCLE: multiple sequence alignment with high accuracy and high throughput. Nucleic Acids Res. 2004;32(5):1792-7.

34.     Kearse M, Moir R, Wilson A, Stones-Havas S, Cheung M, Sturrock S, Buxton S, Cooper A, Markowitz S, Duran C, Thierer T, Ashton B, Meintjes P, Drummond A. Geneious Basic: an integrated and extendable desktop software platform for the organization and analysis of sequence data. Bioinformatics. 2012;28(12):1647-9.

35.     Sullivan MJ, Petty NK, Beatson SA. Easyfig: a genome comparison visualizer. Bioinformatics. 2011;27(7):1009-10.

36. Choi KH, Mima T, Casart Y, Rholl D, Kumar A, Beacham IR, Schweizer HP. Genetic tools for select-agent-compliant manipulation of *Burkholderia pseudomallei*. Appl Environ Microbiol. 2008;74(4):1064-75.

37. Rholl DA, Papp-Wallace KM, Tomaras AP, Vasil ML, Bonomo RA, Schweizer HP. Molecular Investigations of PenA-mediated beta-lactam Resistance in *Burkholderia pseudomallei*. Front Microbiol. 2011;2:139.

38. Massie JP, Reynolds EL, Koestler BJ, Cong JP, Agostoni M, Waters CM. Quantification of high-specificity cyclic diguanylate signaling. Proc Natl Acad Sci U S A. 2012;109(31):12746-51.

39. Irie Y, Parsek MR. LC/MS/MS-based quantitative assay for the secondary messenger molecule, c-di-GMP. Methods Mol Biol. 2014;1149:271-9.

40. Mima T, Schweizer HP. The BpeAB-OprB efflux pump of *Burkholderia pseudomallei* 1026b does not play a role in quorum sensing, virulence factor production, or extrusion of aminoglycosides but is a broad-spectrum drug efflux system. Antimicrob Agents Chemother. 2010;54(8):3113-20.

41. Pfaffl MW. A new mathematical model for relative quantification in real-time RT-PCR. Nucleic Acids Res. 2001;29(9):e45.

42. Estrada-de los Santos P, Vinuesa P, Martinez-Aguilar L, Hirsch AM, Caballero-Mellado J. Phylogenetic analysis of *Burkholderia* species by multilocus sequence analysis. Curr Microbiol. 2013;67(1):51-60.

43. Holden MT, Titball RW, Peacock SJ, Cerdeno-Tarraga AM, Atkins T, Crossman LC, Pitt T, Churcher C, Mungall K, Bentley SD, Sebaihia M, Thomson NR, Bason N, Beacham IR, Brooks K, Brown KA, Brown NF, Challis GL, Cherevach I, Chillingworth T, Cronin A, Crossett B, Davis P, DeShazer D, Feltwell T, Fraser A, Hance Z, Hauser H, Holroyd S, Jagels K, Keith KE, Maddison M, Moule S, Price C, Quail MA, Rabbinowitsch E, Rutherford K, Sanders M, Simmonds M, Songsivilai S, Stevens K, Tumapa S, Vesaratchavest M, Whitehead S, Yeats C, Barrell BG, Oyston PC, Parkhill J. Genomic plasticity of the causative agent of melioidosis, *Burkholderia pseudomallei*. Proc Natl Acad Sci U S A. 2004;101(39):14240-5.

44. Ogawa K, Akagawa E, Yamane K, Sun ZW, LaCelle M, Zuber P, Nakano MM. The *nasB* operon and *nasA* gene are required for nitrate/nitrite assimilation in *Bacillus subtilis*. J Bacteriol. 1995;177(5):1409-13.

45. Armitano J, Mejean V, Jourlin-Castelli C. Gram-negative bacteria can also form pellicles. Environ Microbiol Rep. 2014;6(6):534-44.

46. Cole EC, Rutala WA, Carson JL, Alfano EM. *Pseudomonas* pellicle in disinfectant testing: electron microscopy, pellicle removal, and effect on test results. Appl Environ Microbiol. 1989;55(2):511-3.

47. Fazli M, McCarthy Y, Givskov M, Ryan RP, Tolker-Nielsen T. The exopolysaccharide gene cluster Bcam1330-Bcam1341 is involved in *Burkholderia cenocepacia* biofilm formation, and its expression is regulated by c-di-GMP and Bcam1349. Microbiologyopen. 2013;2(1):105-22.

48. O'Toole GA, Kolter R. Initiation of biofilm formation in *Pseudomonas fluorescens* WCS365 proceeds via multiple, convergent signalling pathways: a genetic analysis. Mol Microbiol. 1998;28(3):449-61.

49. Lee HS, Gu F, Ching SM, Lam Y, Chua KL. CdpA is a *Burkholderia pseudomallei* cyclic di-GMP phosphodiesterase involved in autoaggregation, flagellum synthesis, motility, biofilm formation, cell invasion, and cytotoxicity. Infect Immun. 2010;78(5):1832-40.

50. Kaestli M, Mayo M, Harrington G, Ward L, Watt F, Hill JV, Cheng AC, Currie BJ. Landscape changes influence the occurrence of the melioidosis bacterium *Burkholderia pseudomallei* in soil in northern Australia. PLoS Negl Trop Dis. 2009;3(1):e364.

51.  Walker MS, DeMoss JA. Phosphorylation and dephosphorylation catalyzed in vitro by purified components of the nitrate sensing system, NarX and NarL. J Biol Chem. 1993;268(12):8391-3.

52.  Schobert M, Jahn D. Anaerobic physiology of *Pseudomonas aeruginosa* in the cystic fibrosis lung. Int J Med Microbiol. 2010;300(8):549-56.

53.  Ferreira AS, Silva IN, Oliveira VH, Becker JD, Givskov M, Ryan RP, Fernandes F, Moreira LM. Comparative transcriptomic analysis of the *Burkholderia cepacia* tyrosine kinase *bceF* mutant reveals a role in tolerance to stress, biofilm formation, and virulence. Appl Environ Microbiol. 2013;79(9):3009-20.

54.  Campbell RE. Microbial ecology. Oxford: Blackwell Scientific; 1977. 148 p. p.

**CHAPTER 4: The NarX/NarL two-component system is a global regulator of biofilm formation, natural product biosynthesis, and pathogenicity in *Burkholderia pseudomallei***

The work presented in this chapter and prepared manuscript describes the global transcriptional response to the N-oxides nitrate ($NO_3^-$) and nitrite ($NO_2^-$) and the NarX and NarL regulons under the conditions tested. Using in-frame deletions of the nitrate sensing histidine kinase, *narX*, and the DNA-binding nitrate regulator, *narL*, we characterized this predicted two-component system in relation to *B. pseudomallei* biofilm dynamics.  We isolated RNA from our nitrate and nitrite-dependent biofilm inhibitory model and generated cDNA libraries for next generation sequencing. Using the Illumina NextSeq, we compiled raw transcript read counts and analyzed the differentially regulated transcripts associated with nitrate and nitrite biofilm inhibition. Differential expression profiles of biofilm-associated exopolysaccharides, general metabolism, virulence, antibiotic resistance, and secondary metabolite biosynthetic clusters are described here. Furthermore, we demonstrated *narX* and *narL* mutants are deficient in intracellular growth in mouse macrophage cells.

## 4.1 Summary

The roles of inorganic nitrogen (N) containing compounds in the biological processes of bacteria are well established and broadly effect a range of activities which include essential agricultural mechanisms (nitrogen fixation, ammonification, and nitrification) and regulation of immune responses involved in host-pathogen interactions. *Burkholderia pseudomallei* is a sapronotic disease agent that can cause complex disease in human and animal hosts in part due to its intracellular lifecycle. In the environment, *B. pseudomallei* exists as a saprophyte of soils and surface waters where denitrification is important for anaerobic respiration. We have previously shown that *B. pseudomallei* responds to nitrate and nitrite in part by inhibiting biofilm formation by altering cyclic di-GMP signaling. Here, we describe the global transcriptomic

response to nitrate and nitrite and characterize the nitrosative stress response relative to biofilm inhibition. To better understand the roles of nitrate-sensing in the biofilm inhibitory phenotype of *B. pseudomallei*, we created in-frame deletions of *narX* (Bp1026b_I1014) and *narL* (Bp1026b_I1013), which are separate components of the conserved nitrate-sensing two-component system. Through differential expression analysis of RNA-seq data, we observed that key components of the biofilm matrix are downregulated in response to nitrate and nitrite. Nonribosomal peptide synthase clusters encoding bactobolin, malleilactone, syrbactin, and the cryptic cluster 16 were among the most highly differentially expressed genes. In addition, several gene loci associated with the stringent response, central metabolism dysregulation, antibiotic tolerance, and pathogenicity determinants were significantly altered in their expression. Reduced expression of ribosomal structure and biogenesis loci, as well as translation and DNA replication are indicative of a lower growth rate under nitrosative stress conditions. The differences in expression observed under nitrosative stress were reversed in *narX* and *narL* mutants, suggesting that nitrate sensing is an important checkpoint for regulating the diverse metabolic changes occurring in the biofilm inhibitory phenotype. Furthermore, in a macrophage infection model, *narX* and *narL* mutants were attenuated in intracellular replication, suggesting that nitrate sensing is important for host survival. We propose a model in which nitrate sensing and metabolism in *B. pseudomallei* regulates not only biofilm formation but secondary metabolism and the stringent response. Given that nitrate metabolism in *B. pseudomallei* is important for environmental as well as host survival, the global transcriptomic characterization of the nitrosative stress response serves as a foundation for identifying biochemical targets necessary for survival as a biofilm and inside of a host cell.

## 4.2 Introduction

The ability of many bacteria, including bacilli and pseudomonads, to substitute nitrate as a terminal electron acceptor in oxygen-limited environments offers various benefits for niche

adaptation at comparable free energy changes (1). Metabolism of N-oxides, inorganic ions comprised of oxygen and nitrogen, derived from exogenous sources in the environment or endogenous metabolic byproducts, preferentially follows the denitrification pathway (2). N-oxides, such as nitrate ($NO_3^-$) and nitrite ($NO_2^-$), can be derived from anthropogenic environmental contamination or host innate immune cells during host-pathogen interactions. *Burkholderia pseudomallei*, an environmental saprophyte (3) and sapronotic disease agent (4), is an opportunistic pathogen that transitions between environments where nitrate metabolism can influence bacterial physiology and biofilm dynamics (5). Biofilms are comprised of extracellular polymeric substances that represent a protective matrix in which bacteria can reside; the formation and degradation of which is dependent on extracellular cues and intrinsic bacterial signal transduction mechanisms. *B. pseudomallei* 1026b, a clinical isolate (6), encodes a complete denitrification pathway and responds to exogenous nitrate to some extent by inhibiting biofilm formation and reducing intracellular cyclic di-GMP (5). The denitrification pathway in *B. pseudomallei* 1026b aligns with the conservation of denitrification genes among the β-proteobacteria, including *B. mallei* and *B. pseudomallei* (7). Utilizing a transposon library in *B. pseudomallei* 1026b, we have recently identified a predicted two-component nitrate-sensing system (*narX-narL*) that produces biofilm in the presence of nitrate (5). However, the global regulatory drivers of biofilm dynamics associated with the signal transduction of exogenous nitrate and cyclic di-GMP turnover in *B. pseudomallei* are poorly understood.

The NarX and NarL proteins comprise a conserved two-component regulatory system whereby NarX responds to nitrate and nitrite ligands to initiate phosphorylation of the NarL response regulator receiver domain (8, 9). The *narXL* operon, as initially described in *Escherichia coli*, regulates transcription of gene clusters involved in fermentation and anaerobic respiration (10-13), and specifically activates *narGHJI* (membrane-associated nitrate reductase) and *narK* (nitrate/nitrite transporter) promoters to which it is adjacent (9) (**Figure 1A**). *Pseudomonas* and *Burkholderia* spp. contain a *narXL* system for nitrate and nitrite sensing (9),

which directs hierarchical control of anaerobic respiration and general cellular physiology (14). The *narXL* system has been shown to regulate anaerobic metabolism in *P. stutzeri* (15) and *P. aeruginosa* (16), in which nitrate chemotaxis has recently been demonstrated and speculated to play a role in virulence gene regulation (17). Relatively little is known regarding nitrate sensing and metabolism in *Burkholderia* spp., although the *narX-narL* genes have recently been implicated in the global regulation of *B. thailandensis* biosynthetic gene clusters via hierarchical control of host survival and anaerobic respiration genes (18).

*B. pseudomallei* is a facultative anaerobe that can adapt to oxygen tension in plant-associated rhizospheres (19) or to an intracellular lifestyle in animal immune cells (20); environments that are rich in N-oxides and reactive nitrogen intermediates (RNI). Given the broad environmental distribution of *B. pseudomallei* (21) and its propensity to cause persistent chronic infections in immunocompromised individuals, we hypothesize that this organism possesses the molecular machinery to sense and resist various nitrosative stressors. Although stimulated macrophages can inhibit intracellular growth of *B. pseudomallei* through RNI-dependent bactericidal mechanisms, *B. pseudomallei* has the ability to survive and replicate in phagocytes (22). One approach for identifying resistance mechanisms for RNI is to induce the expression of these mechanisms via sub-lethal levels of the stressor (23). Using concentrations of sodium nitrate and sodium nitrite that we have previously shown to be inhibitory to biofilm formation but not bactericidal (5), we identified gene loci that are involved in resistance to RNI and therefore potentially relevant for intracellular survival of *B. pseudomallei*.

Here we describe global transcriptome profiling of gene expression in *B. pseudomallei* under nitrosative stress as it is coordinated by the two-component nitrate-sensing system *narX-narL*. RNA-seq analysis of the Δ*narX* and Δ*narL* mutants revealed a global network of genes involved in nitrate and nitrite signal transduction and identified key elements of biofilm formation, virulence and antibiotic resistance markers, as well as the differential regulation of key natural product biosynthetic gene clusters. Interestingly, the nitrosative stress response is alleviated by

111

the absence of either *narX* or *narL*. Additionally, we characterized the intracellular replication

kinetics of *B. pseudomallei* lacking nitrate-sensing capabilities thereby linking *narX* and *narL* to

the pathogenicity and survival of this pathogen in the host. These results provide a framework

for biofilm inhibition mediated by the nitrosative stress response and nitrate metabolism, and link

secondary metabolism biosynthesis to the stringent response and antimicrobial tolerance in *B.*

*pseudomallei*.


## 4.3 Materials and Methods

### 4.3.1 Bacterial strains and growth conditions

*B. pseudomallei* 1026b, a clinical isolate from a human septicemic infection (24), was

grown in Lysogeny Broth (LB) at 37°C with aeration as described previously (5), unless

otherwise indicated. *E. coli* DH5α and RHO3 strains were grown at 37°C with aeration. *B.*

*pseudomallei* experiments were carried out in biosafety level 3 (BSL-3) in the Regional

Biocontainment Laboratory at Colorado State University (5). For anaerobic growth, LB was

supplemented with 0.75% glucose (LBG) and experiments were performed inside a 2.5L

anaerobic jar (AnaeroPack) using one sachet of Anaerobic Gas Generator (AnaeroPack). For

experiments involving media with nitrate or nitrite, LB was supplemented with a final

concentration of 10 mM sodium nitrate (Sigma) or 10 mM sodium nitrite (Matheson Coleman

and Bell) as described previously (5), unless otherwise indicated.


### 4.3.2 Mutant strain construction and complementation

*B. pseudomallei* Bp82 (25) (Select Agent exempt auxotroph) genomic DNA was used as

a template for PCR fragment generation, grown with 80 μg/mL adenine (Sigma) supplemented.

DNA restriction enzymes were purchased from New England Biolabs. Primers used for mutant

strain construction and complementation are in **Table 4.1**. In-frame deletion constructs were
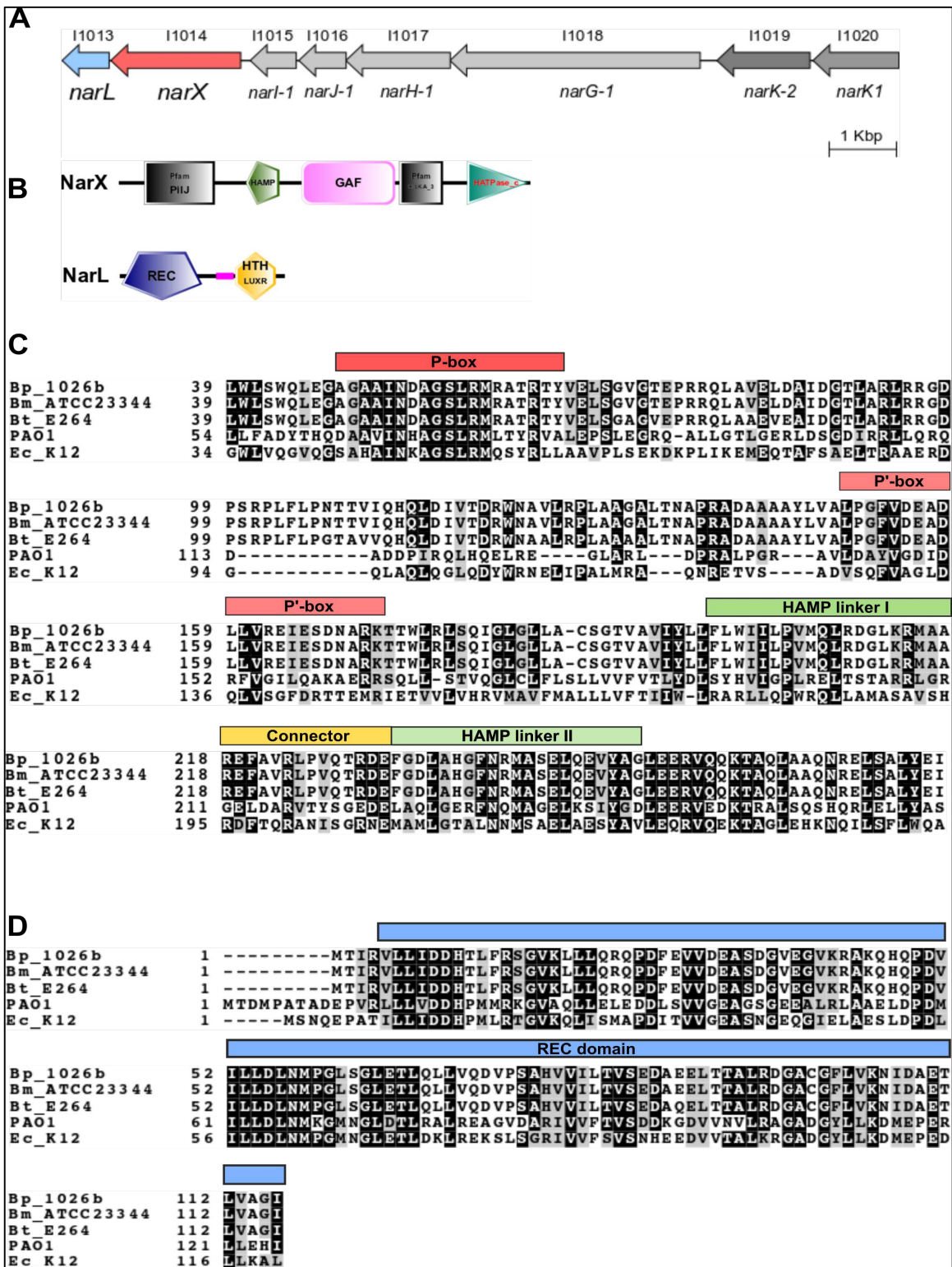
**Figure 4.1 Orientation and conservation of the *narXL-narGHJI₁-narK₂narK₁* cluster.** (A) Genomic orientation of the NarX-NarL regulatory system (red and blue, respectively), NarGHJI-1 dissimilatory nitrate reductase (light grey), and NarK-2 and NarK-1 nitrate/nitrite transporters (dark grey) in *B. pseudomallei* 1026b (coding sequences to scale). (B) Simple Modular Architecture Research Tool (SMART) protein domain analysis of NarX (Bp1026b_I1014) and

113

NarL (Bp1026b_I1013). (C) Amino acid conservation of key residues in the sensory module of NarX (Bp1026b_I1014), including periplasmic domain sequences (P and P' boxes) and HAMP (linker I, linker II, and connector) linker elements of *B. pseudomallei* 1026b (Bp_1026b), *B. mallei* ATCC 23344 (Bm_ATCC23344), *B. thailandensis* E264 (Bt_E264), *P. aeruginosa* PAO1 (PAO1), and *E. coli* K12 (Ec_K12). (D) Amino acid conservation of key residues of the receiver domain of NarL (Bp1026b_I1013) including the same organisms as above. Multiple sequence alignments were generated using Clustal Omega and visualized using BoxShade v3.2 where black boxes indicate identical residues and grey boxes indicate similar sequences.

generated using Splicing Overlap Extension (SOE) PCR (26). Flanking sequences on both

sides (~1Kb each) of Bp1026b_I1014 (*narX*) and Bp1026b_I1013 (*narL*) were amplified from

Bp82 template DNA, and spliced via amplification of a fragment excluding the gene coding

regions. Spliced overlap fragments were cloned into pEXKm5 (27) and electroporated into *E.

coli* RHO3. *E. coli* RHO3 pEXKm5::Δ*narX* and pEXKm5::Δ*narL* were grown in LB supplemented

with diaminophilic acid (400 μg/mL) and kanamycin (35 μg/mL) at 37°C. Tri-parental mating with

*B. pseudomallei* 1026b was facilitated with *E. coli* RHO3 pTNS3 grown in LB supplemented with

ampicillin (100 μg/mL) and diaminophilic acid (400 μg/mL). Transconjugants were selected for

using kanamycin (1000 μg/mL) and X-Gluc (100 μg/mL) screening. Merodiploids were resolved

using yeast-tryptone (YT) media supplemented with 15% sucrose. In-frame deletion constructs

were verified via internal and flanking primers (**Table 4.1**). For complementation, full-length

copies of Bp1026b_I1014 (*narX*) and Bp1026b_I1013 (*narL*) were cloned into pUC18T-mini-

Tn*7*T-km-LAC for IPTG-inducible expression (28). 5 mM IPTG was used to induce downstream

gene expression from the *tac* promoter, and 5 mM NaNO$_3$ was used to stimulate biofilm

conditions for complementation assays.


### 4.3.3 Static biofilm and motility assays

Static biofilm and motility assays were performed as described previously (5, 29). All

experiments were performed in LB supplemented with 10 mM sodium nitrate or 10 mM sodium

nitrite unless otherwise specified, grown at 37°C, in either aerobic or anaerobic conditions.

**Table 4.1 Primers used in this study for in-frame deletions, complementation, and quantitative real-time PCR.**

| Primers | Sequence (5' → 3') | Use | Ref |
|---|---|---|---|
| Δ*narX* A | NNNCCCGGGTCATGGATTATCTGAATACG | SOE Δ*narX* fragment 1 | This study |
| Δ*narX* B | CTATGCCGCCTGTCGCGCGTCGTCGGGGGAGGGCGGGAGCCAT | SOE Δ*narX* fragment 1 | This study |
| Δ*narX* C | ATGGCTCCCGCCCTCCCCGACGACGCGCGACAGGCGGCATAG | SOE Δ*narX* fragment 2 | This study |
| Δ*narX* D | NNNGAATTCGACGCCGTTGTAGGTTTTCT | SOE Δ*narX* fragment 2 | This study |
| Δ*narL* A | NNNCCCGGGAGGACAATTGTCATGT | SOE Δ*narX* fragment 1 | This study |
| Δ*narL* B | TTATGCCTCGGCCGGATGCGAACAGTACCCGTATGGTCAT | SOE Δ*narX* fragment 1 | This study |
| Δ*narL* C | ATGACCATACGGGTACTGTTCGCATCCGGCCGAGGCATAA | SOE Δ*narL* fragment 2 | This study |
| Δ*narL* D | NNNGAATTCCAGTTCTATCGCGTG | SOE Δ*narL* fragment 2 | This study |
| *narX* FWD | NNNCCCGGGATGGCTCCCGCCCTCCCCGACT | Complementing Δ*narX* | (5) |
| *narX* REV | NNNAAGCTTCTATGCCGCCTGTCGCGCGT | Complementing Δ*narX* | (5) |
| *narL* FWD | NNNCCCGGGATGACCATACGGGTACTGTT | Complementing Δ*narL* | (5) |
| *narL* REV | NNNAAGCTTTTATGCCTCGGCCGGATGCG | Complementing Δ*narL* | (5) |
| I1018 FWD | CGAGATGGTGAAATTCG | *narG-1* qPCR | This study |
| I1018 REV | TACTGCTTCACGTAGTC | *narG-1* qPCR | This study |
| II1965 FWD | CAGATTCACCGGATCGTCAC | CPSIII qPCR | This study |
| II1965 REV | CTCGATGACCTCCTGATTGAAG | CPSIII qPCR | This study |
| I1913 FWD | CGGACATCAAGGATTGCTACAC | *relA* qPCR | This study |
| I1913 REV | GACCGTATGCAGCGATTGT | *relA* qPCR | This study |
| II1245 FWD | GACGCTCGGCTACGAATAC | *btaR2* qPCR | This study |
| II1245 REV | GGGATAGTTGGACACCATGAG | *btaR2* qPCR | This study |
| II1353 FWD | ATTACGCGGCCACGATTAC | *syrA* qPCR | This study |
| II1353 REV | CGTTCAACGCGACCTTCA | *syrA* qPCR | This study |
| I0189 FWD | ACGAAGTGACGATCGATTTCC | *hcp-1* qPCR | This study |
| I0189 REV | GATCACGTACTTCAGCTTGATCT | *hcp-1* qPCR | This study |
| II0386 FWD | GTAGACCCGAAACCAGGTGA | 23S qPCR | (30) |
| II0386 REV | CACCCCTATCCACAGCTCAT | 23S qPCR | (30) |

Biofilms were assayed in replicates of six individual wells of 96-well polystyrene plates (Nunc™ Microwell™ 96-well microplates #243656, Thermo Scientific) and processed as previously described (5). Motility was measured by inoculating strains of interest into 0.3% semisolid LB agar, supplemented with sodium nitrate as indicated, and measuring visible diameter of bacterial spread over the specified time.

### 4.3.4 Nitrite ion measurement

Nitrite ion ($NO_2^-$) from bacterial cultures was measured using the Griess Reagent system (Promega) following the protocol recommended by the manufacturer. Briefly, a nitrite standard reference curve was generated and included on each 96-well plate (Nunc) used for experimental samples. The Griess reaction was performed using room-temperature Sulfanilamide Solution and NED Solution and the resulting azo compound density was measured at $OD_{550}$. These experiments were performed in aerobic as well as anaerobic conditions with wild type, Δ*narX*, and Δ*narL* mutant strains grown statically for 24 hours at 37°C in biological triplicates and technical triplicates. Aerobic cultures were cultivated in LB media supplemented with 10 mM $NaNO_3$ and anaerobic cultures were cultivated in LBG media (LB 0.75% glucose) and supplemented with 25 mM $NaNO_3$.

### 4.3.5 RNA isolation and RNA-seq library preparation

Total RNA was isolated from static-growth cultures as described previously (5), with a few modifications. LB media was used due to previous observations of pellicle biofilm formation, in either aerobic or anaerobic conditions as indicated. Pellicle biofilms were grown in six-well Costar polystyrene plates (Corning) for 24 hours at 37°C, at which point 1.5 mL of culture samples were collected and resuspended in RNAprotect Bacteria Reagent (Qiagen) and then QIAzol Lysis Reagent (Qiagen) before storage at -80°C. RNA samples were purified and

depleted of genomic DNA as described previously (5), before depletion of ribosomal RNA with Ribo-Zero rRNA Removal Kit for bacteria (Illumina) and purification using magnetic beads (AMPure). RNA-seq libraries of cDNA were generated using ScriptSeq™ Complete v2 RNA-seq Library Preparation Kit (Illumina) and purified using Monarch DNA cleanup kit (New England Biolabs). Unique barcodes were added to each sample library using ScriptSeq™ Index PCR Primers (Illumina). Libraries were analyzed on a Tapestation using HS D1000 tapes and reagents (Agilent) to determine average sizes and concentrations of the libraries. Size and molarity estimates were used to pool all libraries in equimolar concentrations. Final quality control and library quantification analyses were completed at the Colorado State University Next Generation Sequencing Core Facility.

### 4.3.6 Illumina sequencing and differential expression quantification

A NextSeq run was completed on the pooled libraries using the NextSeq 500 hi-output v2 75-cycle kit and Buffer Cartridge (Illumina). Sequence files were downloaded from the NGS server, de-multiplexed according to index primers, and converted to FastQ files before initial quality control using FastQC (31). Adapter sequences were trimmed using Trimmomatic before another quality control round using FastQC. Bowtie2 was used to align sequencing reads to the reference genome GCF_000260515.1_ASM26051v1 (NCBI) and TopHat was used for transcriptome assembly. HTseq was used to count accepted hits before the DEseq2 package was employed in R for comprehensive differential expression analysis. Raw read count coverage values were used to compare the differential gene expression between temperature treatments, mutants, and untreated controls. Using a negative binomial distribution to estimate variance and a Bayesian method for variance shrinkage, the DEseq2 package (32)produced logarithmic fold-change values between the conditions tested. Wald tests were used to calculate p-value and the Benjamini-Hochberg multiple testing correction was used to correct for the false discovery rate.

### 4.3.7 Gene expression and quantitative real-time PCR

Genomic DNA-depleted RNA samples, isolated in quadruplicate, were pooled and cDNA was synthesized using 1 µg total RNA, using the Transcriptor First Strand cDNA Synthesis kit (Roche). Primers for Bp1026b_I1018 (*narG-1*), Bp1026b_II1965 (CPS III) Bp1026b_I1913 (*relA*), Bp1026b_II1245 (*btaR2*), Bp1026b_II1353 (*syrA*), and Bp1026b_I0189 (*hcp-1*), were designed using the PrimerQuest tool (IDT DNA Technologies), and primer efficiencies were calculated using dilutions of cDNA samples. The 23S rRNA reference gene (30) was used as a housekeeping control for normalization, due to its consistent expression profile for all cDNA samples of total RNA. qRT-PCR was performed using 10 ng total cDNA and the same cycling conditions described previously (5). Relative transcript abundance was measured in biological triplicate and technical duplicate using the Pfaffl method (33).

### 4.3.8 Infection of murine macrophage cells

Murine macrophage cells (RAW 264.7 cell line, ATCC) were propagated in Dulbecco's Modified Eagle Medium (DMEM, Gibco) supplemented with 10% fetal bovine serum at 37°C with 5% $CO_2$ and 80-90% relative humidity in T-75 flasks (Corning). *B. pseudomallei* 1026b strains were grown overnight at 37°C with aeration to stationary phase, and diluted to an appropriate $OD_{600}$ for an infection inoculum of ~$1x10^6$ CFU/mL. RAW 264.7 cells were seeded in 12-well cell culture dishes (Corning) at a density of ~$5x10^5$ cells. Bacteria were resuspended in DMEM and added to eukaryotic cells at an MOI of ~2 and incubated at 37°C for 1 hour. Macrophage cells were washed with PBS and culture medium was replaced with fresh medium supplemented with kanamycin (750 µg/mL) before a 2-hour incubation at 37°C to kill extracellular bacteria. RAW 264.7 cells were washed and lysed in PBS containing 0.2% Triton X-100 for 2.5 min and serially diluted and plated on LB agar to quantify intracellular bacteria.

### 4.3.9 Antibiotic tolerance assay

Wild-type *B. pseudomallei* 1026b was grown overnight at 37°C with aeration before being diluted 1:50 in 4 mL of LB media in six-well Costar polystyrene plates (Corning). LB media was supplemented with 10 mM NaNO$_3$ for three experimental wells per plate to stimulate the biofilm inhibitory phenotype while the other three wells were allowed to grow pellicles in plain LB as previously described. After inoculation, the six-well plates were incubated statically at 37°C in oxic conditions for the duration of the experiment. At 2h, 6h, and 20h after sub-culturing and beginning static growth, 2x MIC (4μg/mL) of ceftazidime hydrate (Sigma) was added to each experimental well, dosing each culture in biological triplicate, with or without supplemented nitrate. After dosing with antibiotic at 2h, 6h, and 20h time-points, cultures were incubated for an additional 24h at 37°C, after which 250 μL from each well was sampled and diluted in a 10-fold dilution series for CFU quantification. Ceftazidime-treated cells were plated on LB agar and incubated for another 24h at 37°C before colonies were counted at the appropriate dilutions.

### 4.4 Results

### 4.4.1 NarX-NarL comprise a nitrate-sensing two-component system in *B. pseudomallei*

The NarX-NarL two-component system (TCS) has been described extensively in γ-proteobacteria (9), in which it was discovered to regulate nitrate respiration in coordination with an additional NarQ-NarP TCS depending on environmental nitrate availability (34-36). In β-proteobacteria, *Burkholderia* and *Ralstonia* spp. encode only the NarX-NarL system, a feature shared with Pseudomonadaceae in the γ-proteobacteria clade but not Neisseriaceae (also β-proteobacteria) (9). The NarX-NarL TCS is often part of a larger regulon including the dissimilatory nitrate reductase NarGHJI-1 and the transporters/permeases NarK-1 and NarK-2, as is the case in *B. pseudomallei* 1026b (**Figure 4.1A**). Analysis of this system via the SMART algorithm revealed a predicted HAMP domain in NarX and a predicted REC domain in NarL

(**Figure 4.1B**), indicative of two-component signal transduction capabilities. NarX (*E. coli*) is a

sensory histidine kinase with a periplasmic sensor domain that is dimeric when bound to its

ligand, nitrate ($NO_3^-$) (37). The NarX (*E. coli*) sensory module (**Figure 4.1C**) contains conserved

periplasmic domains (P-box and P'-box) that are necessary for ligand binding and response, yet

only $Gly^{51}$ and $Met^{55}$ (numbering with respect to $NarX_{Ec\_K12}$) have been found to be invariant (9).

The HAMP linker-connector-linker domains are common to sensor kinases and are required for

signal transduction (38, 39). The *B. pseudomallei* complex (Bpc) which includes *B. mallei* ATCC

23344, an obligate intracellular pathogen, and *B. thailandensis* E264, a non-pathogenic soil

saprophyte, share conserved NarX sensory module (**Figure 4.1C**) and NarL receiver domain

(**Figure 4.1D**) sequences with *P. aeruginosa* PAO1 and *E. coli* K12. Additionally, the complete

*narX-narL-narGHJI$_1$-narK$_1$-narK$_2$* regulon is conserved in its entirety in *B. mallei* ATCC 23344

and *B. thailandensis* E264 based on *in silico* sequence alignment (**Figure 4.2**). Collectively,

these bioinformatics analyses suggest that the NarX-NarL system functions as an archetypal

signal-response regulatory system in *B. pseudomallei* 1026b, and that organisms across the

Bpc share this functional genomic element.
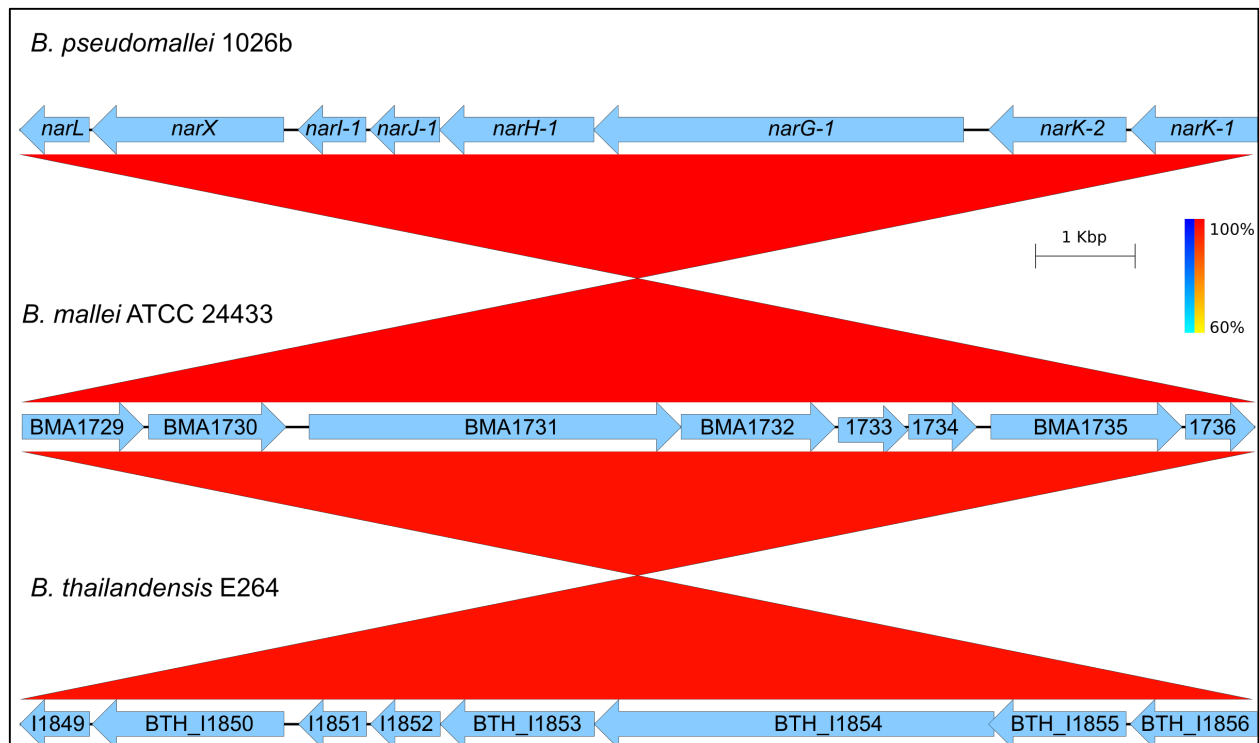
**Figure 4.2 Genomic conservation of the Nar regulon in the Bpc.** *Burkholderia pseudomallei* 1026b*, B. mallei* ATCC23344*,* and *B. thailandensis* E264 nitrate reduction regulons are compared here. Orthologous sequences were extracted and aligned using EasyFig in Python v2.7. Illustrations depict results of blastn annotations represented by colored bars spanning chromosomal segments, with minimum percent identity of 0.60 and a threshold E-value of 1E-3. Yellow-to-red bars depict sequence homology amid inverted sequences on a color density gradient indicating percent homology, whereby dark red indicates the most homology.

### 4.4.2 NarX and NarL respond to nitrate but not nitrite to inhibit biofilm formation

Previously, we have shown that both sodium nitrate and sodium nitrite inhibit *B. pseudomallei* 1026b biofilm formation in a dose-dependent fashion (5). Five genes, *narX, narL, narH_1, narG_1,* and *narK_2,* were implicated in the regulation of biofilm dynamics in response to exogenous nitrate and nitrite (5). Deletion mutants Δ*narX* and Δ*narL* and the wild type were grown statically in LB supplemented with either 10 mM $NaNO_3$ or 10 mM $NaNO_2$ for 24 hr (**Figure 4.3A**). Biofilm inhibition via nitrate and nitrite supplementation was observed for the wild type while both Δ*narX* and Δ*narL* mutants were resistant to nitrate biofilm inhibition but not nitrite. Nitrite inhibited biofilm formation in the nitrate sensing-deficient mutants at similar levels to wild type (**Figure 4.3A**). Nitrate-mediated biofilm inhibition of Δ*narX* and Δ*narL* mutants was

restored by complementation of Bp1026b_I1014 (*narX*) and Bp1026b_I1013 (*narL*)) with IPTG-induction and was comparable to the wild type (**Figure 4.3B**). Consistent with our previous transposon insertional mutants (5), both components of the NarX-NarL system respond to nitrate by biofilm inhibition, however this system is not similarly affected by nitrite at the concentration tested. These results suggest that the NarX-NarL system has specificity for nitrate sensing in the regulation of biofilm dynamics in *B. pseudomallei* 1026b.
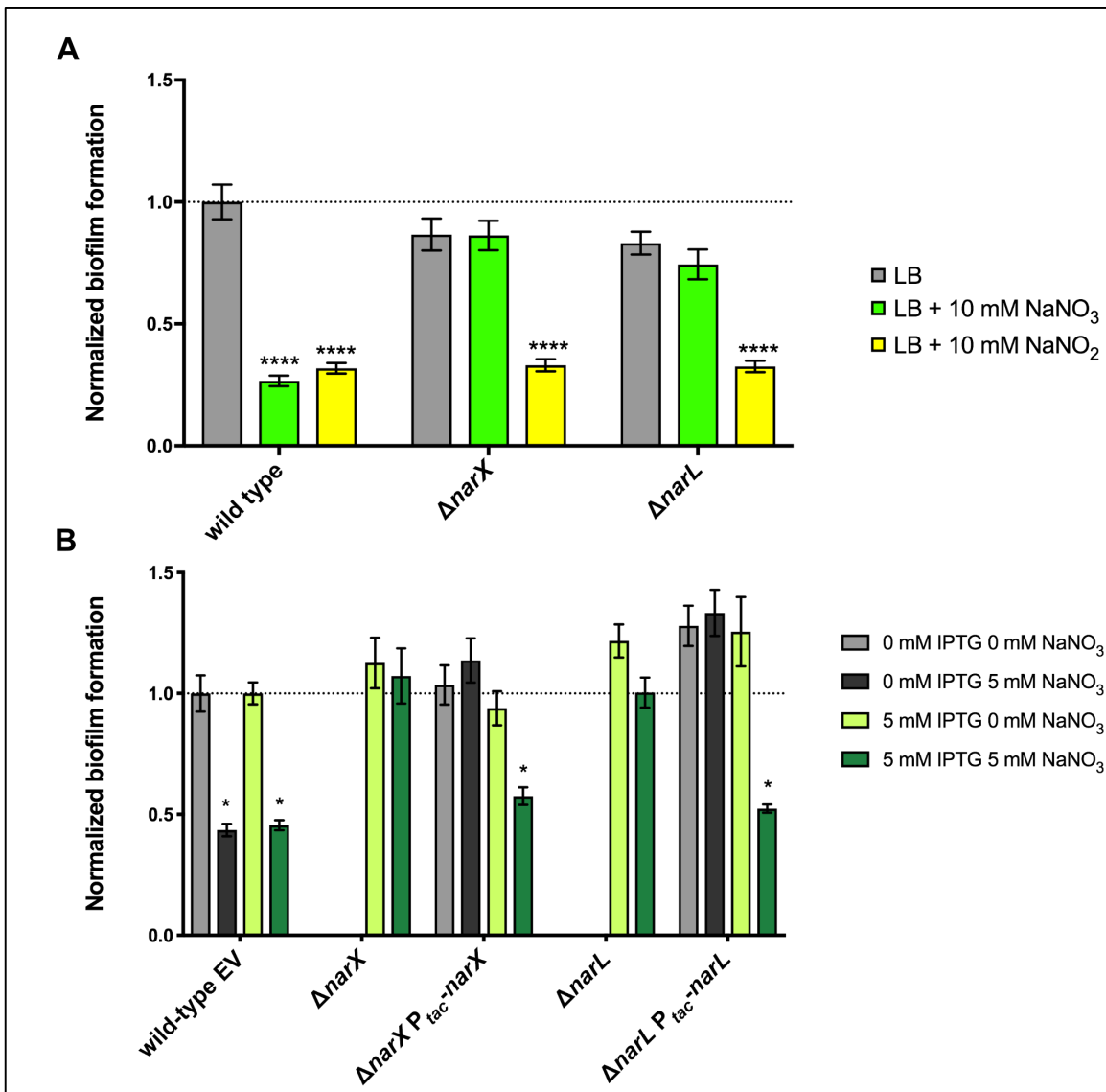


**Figure 4.3 Biofilm formation analysis of *B. pseudomallei* mutant strains and their complements, relative to the wild type, grown at 37 °C for 24 hours.** (A) Wild type, Δ*narX*, and Δ*narL* biofilms were grown in LB media (grey) with supplemented either 10 mM NaNO$_3$ (green) or 10 mM NaNO$_2$ (yellow). Asterisks indicate significant differences (**** = p < 0.0001) calculated with an unpaired Student's T-test using the Bonferonni method to account for multiple

comparisons (n = 12). (B) Complements of $\Delta narX$ and $\Delta narL$ mutants were grown in LB media (light grey) supplemented with 5 mM $NaNO_3$ (dark grey), 5 mM IPTG (light green), or 5 mM IPTG and 5 mM $NaNO_3$ (dark green), and compared to wild-type *B. pseudomallei* 1026b containing an empty complementation vector (EV). Asterisks indicate significant differences (* = $p < 0.0001$) calculated with an unpaired Student's T-test using the Bonferonni method to account for multiple comparisons (n = 12).

### 4.4.3 Nitrite, but not nitrate, suppresses static anaerobic growth in *B. pseudomallei*

To examine the effects of nitrate and nitrite on oxygen-deprived bacterial cells, as commonly found in tissue-associated biofilm (40) or intracellular infections (41), we adapted an anaerobic growth model for *B. pseudomallei* (42). Static biofilm growth was initiated in an oxygen-deprived anaerobic jar with the addition of an added carbon source (0.75% glucose) and enhanced via supplemented nitrate, which increased anaerobic growth capacity starting at 10 mM (**Figure 4.4A**). Surprisingly, in contrast to the beneficial effect of nitrate, the addition of sodium nitrite had an inhibitory effect on anaerobic biofilm growth (**Figure 4.4B**). Significant growth defects were observed starting with the addition of 10 mM $NaNO_2$, while subsequent concentration increases favored growth in $NaNO_3$-supplemented media (**Figure 4.4B**). The observed ceasing of growth in the nitrite treatment condition corresponds to a similar phenotype involving mycobacterial growth repression due to endogenous nitrite accumulation (41). Interestingly, the addition of exogenous nitrate for anaerobic swim motility assays showed a robust increase in flagellar motility in response to nitrate sensing, considering that absence of both *narX* and *narL* inhibited swimming even with nitrate present (**Figure 4.4C**).These results suggest that *B. pseudomallei* uses nitrate but not nitrite as an alternative terminal electron acceptor during anaerobic growth, and that nitrite may inhibit anaerobic biofilm growth, suggesting hierarchical control during the shift to anaerobiosis.

To analyze relative function of the primary nitrate reductase in *B. pseudomallei* under both aerobic and anaerobic conditions, we next examined the production of nitrite in culture media using the Griess test. Using Griess reagent, which enables colorimetric quantification of nitrite ion in solution, we measured 1.4 mM $NO_2$ and 3 mM $NO_2$ in anaerobic (**Figure 4.4D**) and

aerobic (**Figure 4.4E**) culture conditions. For Griess tests, we supplemented LB medium with 10 mM NaNO$_3$ and 25 mM NaNO$_3$ in aerobic and anaerobic conditions, respectively, to account for both biofilm inhibition and anaerobic growth models. In both conditions, absence of either *narX* or *narL* significantly inhibited the production of nitrite ion in solution (**Figures 4.4D and 4.4E**), indicating that the predicted nitrate-sensing two-component system activates nitrate-nitrite respiration via the primary nitrate reductase in both aerobic and anaerobic conditions. Altogether, these results demonstrate a disparity between exogenous nitrate or nitrite supplementation regarding biofilm growth in *B. pseudomallei*; while both nitrate and nitrite inhibit aerobic biofilm growth, nitrite suppresses anaerobic biofilm growth.  Both components of the nitrate-sensing system, *narX* and *narL*, respond to exogenous nitrate and nitrite in a similar fashion by facilitating nitrate-nitrite respiration, motility, and biofilm inhibition.



**Figure 4.4 Anaerobic growth kinetics of *B. pseudomallei* utilizing an alternative terminal electron acceptor.** (A) Static growth of wild-type *B. pseudomallei* was measured after 24 hours of anaerobic growth at 37 °C with increasing concentrations (0, 10, 25, 50, and 100 mM) of NaNO$_3$ in LB media (light blue) or LB media supplemented with 0.75% glucose (dark blue). Asterisks indicate significant differences (* = p < 0.05, **** = p <0.0001) calculated with an unpaired Student's T-test using the Bonferonni method to account for multiple comparisons (n = 12). (B) Static growth of wild-type *B. pseudomallei* was measured after 24 hours of anaerobic

growth at 37 °C grown in LBG (LB 0.75% glucose) media supplemented with either $NaNO_3$ (green) or $NaNO_2$ (yellow) at increasing concentrations (0, 10, 25, 50, and 100 mM). Asterisks indicate significant differences (* = $p < 0.05$, **** = $p < 0.0001$) calculated using a Dunnett's multiple comparison 2way ANOVA test. (C) Swimming motility of wild type, $\Delta narX$, and $\Delta narL$ strains in 0.3% semi-solid LBG agar (grey) supplemented with 25 mM $NaNO_3$ (green) and incubated at 37 °C for 24 hours. Asterisks indicate significant differences (*** = $p < 0.001$) calculated with an unpaired Student's T-test using the Bonferonni method to account for multiple comparisons (n = 6). Griess reaction results measuring nitrite ion produced by wild type, $\Delta narX$, and $\Delta narL$ strains anaerobically (D) after growth in LBG with 25 mM $NaNO_3$ or aerobically (E) after growth in LB with 10 mM $NaNO_3$ at 37 °C for 24 hours. Asterisks indicate significant differences (* = $p < 0.05$, *** = $p < 0.001$, **** = $p < 0.0001$) calculated with an unpaired Student's T-test using the Bonferonni method to account for multiple comparisons (n = 12).

### 4.4.4 Analyses of global responses to nitrate/nitrite-mediated biofilm inhibition reveals divergent responses

Because of the observed disparities between nitrate- and nitrite-mediated biofilm inhibition (**Figure 4.3A**), as well as our previous observations involving cyclic di-GMP metabolism in response to nitrate, we next aimed to characterize the global transcriptional response to nitrate/nitrite sensing in *B. pseudomallei* 1026b. To assess the impacts of nitrosative stress on the *B. pseudomallei* transcriptome, wild type, $\Delta narX$, and $\Delta narL$ strains were grown statically in LB media or supplemented with either 10 mM $NaNO_3$ or 10 mM $NaNO_2$, in biological quadruplicates. RNA from technical triplicates were collected and pooled on separate days for each biological sample to minimize batch effect, then treated with DNase I, depleted of ribosomal RNA, chemically fragmented, and reverse transcribed into indexed cDNA libraries (**Figure 4.5**). Illumina sequencing using a NextSeq 500 hi-output flow cell, followed by read quality assessment and subsequent mapping and alignment to the *B. pseudomallei* 1026b genome, and statistical analysis of differentially regulated transcripts via DESeq2 revealed divergent transcriptome datasets (**Figure 4.6**). The minimal genetic relatedness between these populations of cells responding to differing environmental conditions is supported by the hierarchical clustering and ordination of rlog-transformed data for each transcript Z-score that is linked by sample and treatment condition (**Figure 4.6A, 4.6B**). When comparing wild-type

cultures grown in LB supplemented with or without 10 mM $NaNO_3$, principal component analysis

reveals unrelated populations with 79% of variance explained by one principal component

(**Figure 4.6C**). Similar results were observed when comparing wild-type cultures grown in LB

supplemented with or without 10 mM $NaNO_2$ (**Figure 4.6D**). However, when exploring the

transcriptome data comparing nitrate and nitrite effects on wild type, most differentially regulated

transcripts are affected similarly by nitrate and nitrite (**Figure 4.7**). Venn diagrams display 181

up-regulated genes with fold changes greater than two and 203 down-regulated genes with fold

changes less than two and false discovery thresholds below $q < 0.01$ that share expression

profiles between nitrate- and nitrite-treated sample groups (**Figure 4.7**). These data analyses on

the global transcriptome datasets suggest that although substantial differences exist in the

response to growth supplemented with either nitrate or nitrite, these genetic differences are

mitigated when comparing nitrate and nitrite treatments to each other.
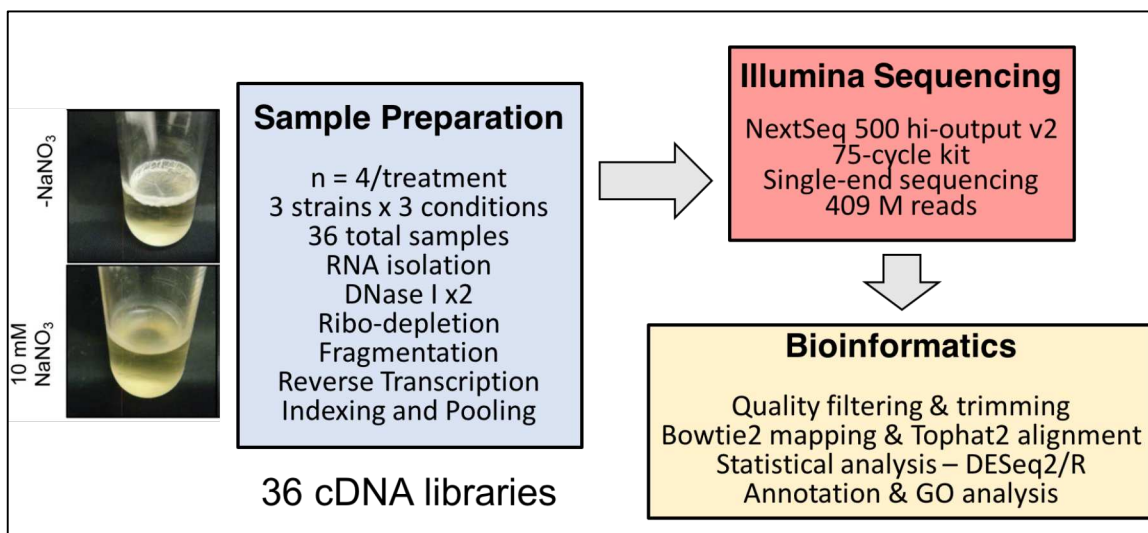


**Figure 4.5 Overview of the transcriptomic analysis of nitrate/nitrite-mediated biofilm inhibition of *B. pseudomallei* strains used in this study.** 36 individual cDNA libraries were generated from total RNA (Sample Processing), before single-end sequencing (Illumina Sequencing) and statistical analysis (Bioinformatics). 409 million reads were generated, from which statistically significant differential expression analysis was derived. Following quality assessment of reads, mapping and alignment to the *B. pseudomallei* 1026b genome, DESeq2 statistical analysis was performed in R.
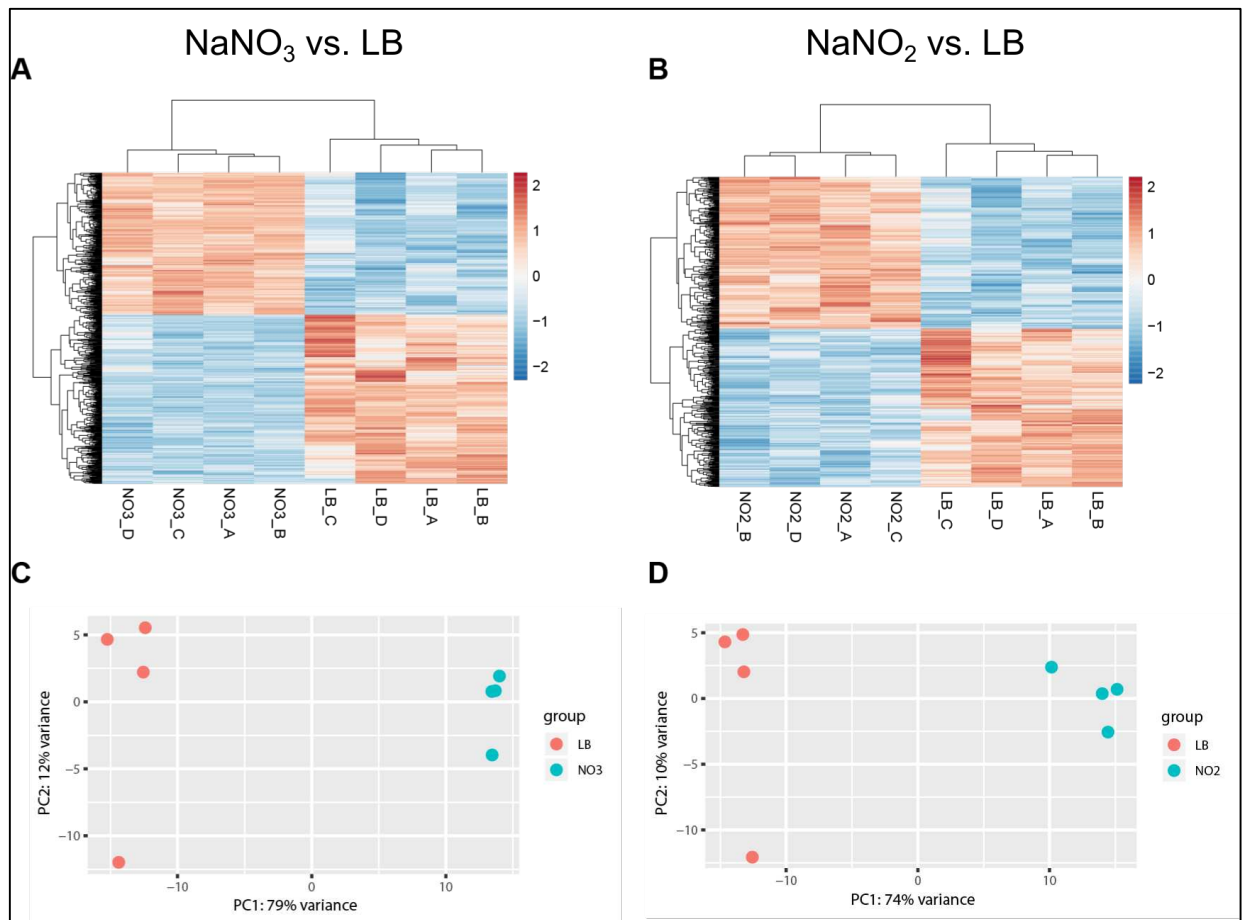
**Figure 4.6 Data analysis reveals divergent datasets in the differential expression patterns among wild-type *B. pseudomallei* samples in both $NO_3^-$ and $NO_2^-$ treatment conditions.** Z-score analysis of all differentially regulated transcripts for $NO_3^-$ vs. LB (A) and for $NO_2^-$ vs. LB (B). Principal component analysis of entire datasets for $NO_3^-$ vs. LB (C) and for $NO_2^-$ vs. LB (D). Total RNA was purified from biological samples cultured on separate days to mitigate batch effects. Hierarchical clustering of all significantly expressed transcripts are presented in panels A and B while complete transcriptomes of all samples are depicted in panels C and D.
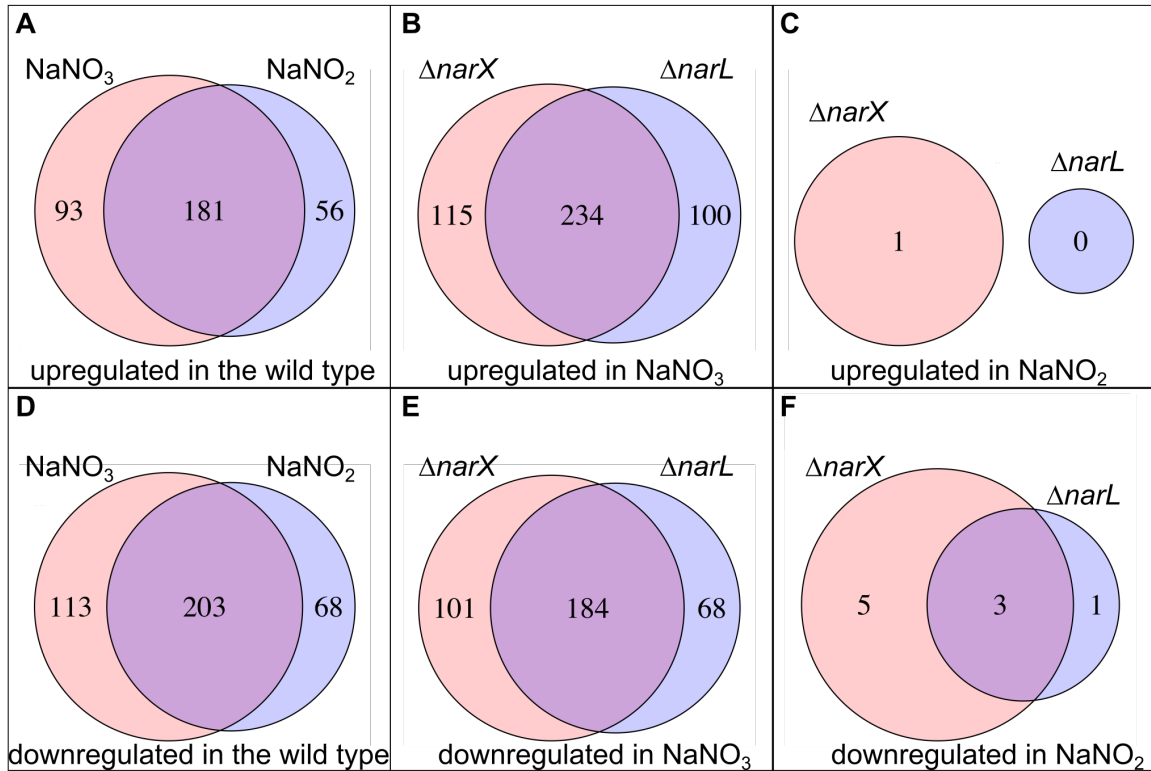
**Figure 4.7 Nitrate and nitrite treatments differentially regulate similar transcripts in wild-type *B. pseudomallei,* while *narXL* mutants respond comparably to nitrate but not nitrite treatments.** (A, D) Wild-type *B. pseudomallei* in either the nitrate ($NO_3^-$) or nitrite ($NO_2^-$) treatment condition. (A) Upregulated transcripts: nitrate vs. LB = 274, nitrite vs LB = 237; (D) downregulated transcripts: nitrate vs. LB = 316, nitrite vs LB = 271. (B, E) Δ*narX* and Δ*narL* strains in the nitrate ($NO_3^-$) treatment condition. (B) Upregulated transcripts: Δ*narX* vs. wild type = 349, Δ*narL* vs. wild type = 334; (E) downregulated transcripts: Δ*narX* vs. wild type = 285, Δ*narL* vs. wild type = 252. (C, F) Δ*narX* and Δ*narL* strains in the nitrite ($NO_2^-$) treatment condition; (C) upregulated transcripts: Δ*narX* vs. wild type = 1, Δ*narL* vs. wild type = 0; (F) downregulated transcripts: Δ*narX* vs. wild type = 8, Δ*narL* vs. wild type = 4.

## 4.4.5 Differential expression profiles reveal key metabolic processes, biofilm components, respiratory pathways, and biosynthetic clusters that are globally regulated in response to nitrate and nitrite

To analyze the global gene expression profiles of wild-type cells grown in the presence of nitrate or nitrite, Illumina single-end sequencing reads using the DESeq2 modeling and statistical package for RNA-seq data were analyzed (32). Differential expression analysis was performed using pair-wise comparisons across the three strains (wild type, Δ*narX*, and Δ*narL*)

and the three treatment conditions (LB, LB 10 mM $NaNO_3$, and LB 10 mM $NaNO_2$), with four biological samples per group. In total, 36 samples were assembled into cDNA libraries, indexed with individual barcodes, and pooled for NextSeq Illumina Sequencing, resulting in 408.8 M reads passing initial filtering. Following further filtering, trimming, mapping, and alignments, transcript count matrices for each sample were compiled using the HTseq Python package (43). Un-normalized count matrices were then imported into RStudio and the DESeq2 differential expression pipeline with thresholds and outputs specified in R. For significantly differentially expressed genes, we set thresholds of $log_2$Fold-Change < -1 or > 1 and adjusted *p*-value < 0.001. Overall, 274 up-regulated genes and 316 down-regulated genes in the nitrate condition versus LB for wild type (**Figure 4.7A**). 237 genes were up-regulated and 271 were down-regulated in the nitrite-supplemented condition versus LB for the wild type as well (**Figure 4.7B**). However, when comparing the Δ*narX* mutant to the wild type in the nitrate supplemented condition, the trends are reversed (**Figure 4.7C**), suggesting that nitrate sensing is required for biofilm inhibitory phenotype. We identified key differences and similarities regarding the effects of nitrate and nitrite on the differential regulation of metabolic, respiratory, biofilm, virulence, and biosynthetic gene clusters in *B. pseudomallei* 1026b. Given the significant overlap in transcripts regulated similarly by both nitrate and nitrite, we explored the genome-wide regulation of gene clusters of proximal genes with the same differential regulation and visualized the effect of exogenous nitrate on the *B. pseudomallei* 1026b genome as detailed below (**Figure 4.8**). Using the Webserver for Position Related data analysis of gene Expression in Prokaryotes (WoPPER) (44), we considered the transcriptional regulation of exogenous nitrate to identify differentially expressed regions on each chromosome of *B. pseudomallei* 1026b. By identifying and mapping physically contiguous clusters of genes along both chromosomes that respond similarly to nitrate, we can provide a visual validation of the differential expression statistical output provided by DESeq2. While there is no visual difference between the regulation profiles among both chromosomes, this graphical representation of the gene expression data set highlights
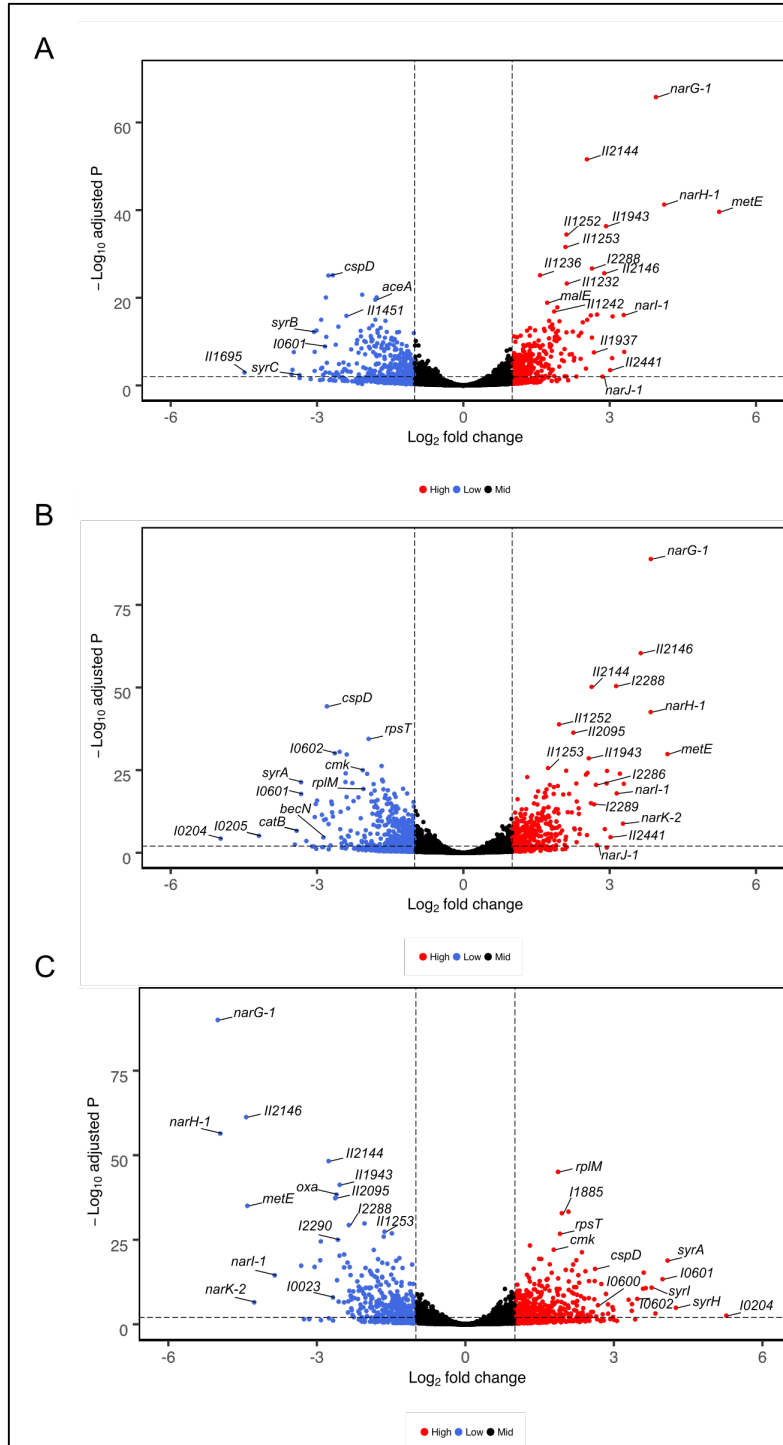
**Figure 4.8 Trends in transcript fold changes in relation to statistical significance for comparably regulated datasets under nitrate and nitrite stress are reversed in the Δ*narX* mutant.** NO$_3^-$ vs. LB (A) and NO$_2^-$ vs. LB (B), and Δ*narX* vs. wild type in the NO$_3^-$ condition (C). Transcripts are depicted as colored circles; unchanged or middle expression (black), upregulated or high expression (red), downregulated or low expression (blue). Log$_2$ fold change values are distributed along the X-axes and Log$_{10}$ adjusted p-values (as determined by the Wald test) are distributed along the Y-axes.
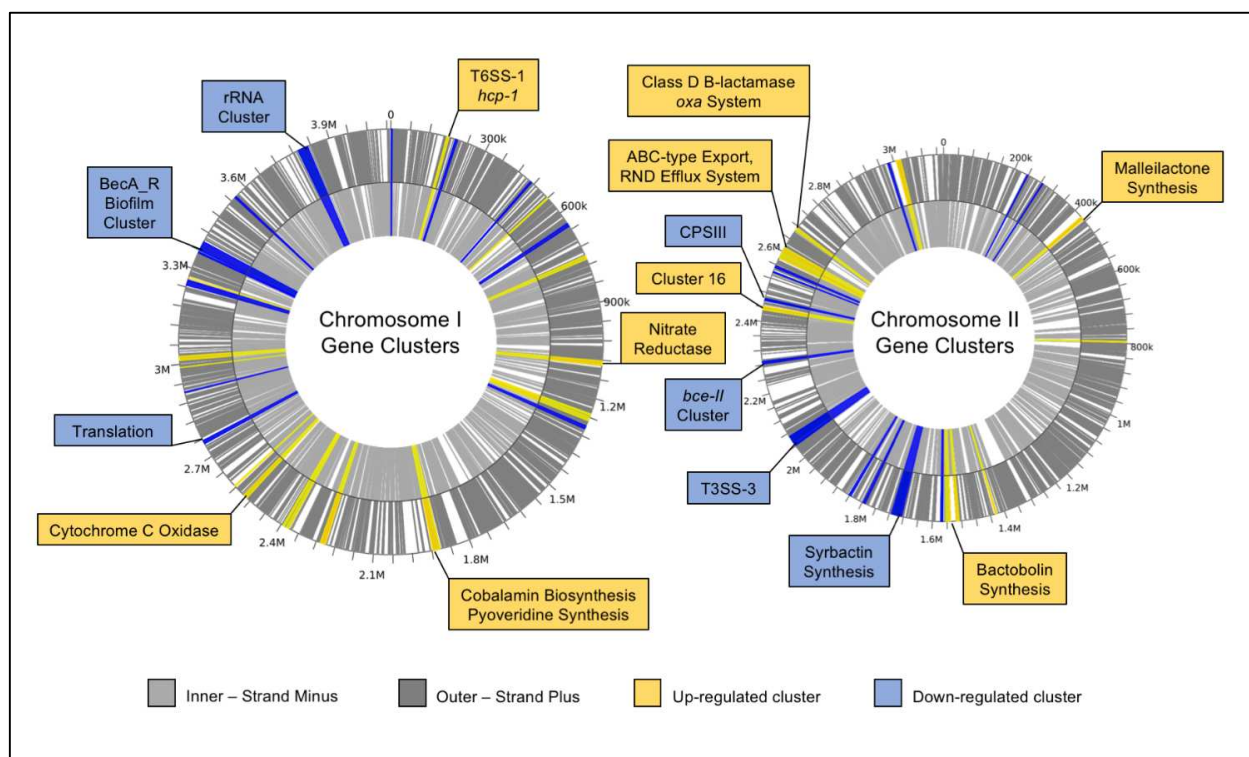
**Figure 4.9 Differentially regulated transcripts comprise clusters of genes distributed across both chromosomes in *B. pseudomallei* 1026b.** WoPPER analysis reveals biofilm-associated gene clusters, secondary metabolic biosynthetic clusters, general metabolism and respiration, and virulence-associated clusters are differentially regulated in response to nitrate treatment.

important biofilm-associated clusters, antibiotic resistance-associated clusters, and interestingly, the confinement of secondary metabolite biosynthetic gene clusters on chromosome II. In total, WoPPER analysis identified 27 clusters on chromosome I (**Table 4.2**) and 21 clusters on chromosome II (**Table 4.3**) as differentially regulated in response to exogenous nitrate. The following sections explore the trends described above (**Figures 4.6 – 4.9**) in more detail, considering distinct loci in relation to their metabolic and biosynthetic functions.

**Table 4.2 Expression trends for differentially regulated transcripts on Chromosome I in response to 10 mM NaNO$_3$**

| ID | No. Genes | Genes in Cluster | Log2 FC Mean | Log2 FC SD | Expression Trend |
|---|---|---|---|---|---|
| 1 | 4 | I0001, I0002, I0003, I0004 | -0.9207 | 0.2024 | Down |
| 2 | 11 | I0180, I0181, I0182, I0183, I0184, I0185, I0186, I0187, I0188, I0189, I0190 | 0.5888 | 0.0309 | Up |
| 3 | 8 | I0202, I0203, I0204, I0205, I0206, I0207, I0208, I0209 | -0.8623 | 0.0823 | Down |
| 4 | 7 | I0449, I0450, I0451, I0452, I0453, I0454, I0455 | -0.7196 | 0.0333 | Down |
| 5 | 5 | I0506, I0507, I0509, I0508, I0510 | 0.5304 | 0.0081 | Up |
| 6 | 10 | I0597, I0598, I0599, I0600, I0601, I0602, I0603, I0604, I0605, I0606 | -0.9851 | 0.1576 | Down |
| 7 | 12 | I0703, I0704, I0705, I0706, I0707, I0708, I0709, I0710, I0711, I0712, I0713, I0714 | 0.7376 | 0.1338 | Up |
| 8 | 11 | I1012, I1013, I1014, I1015, I1016, I1017, I1018, I1019, I1020, I1021, I1023 | 1.475 | 0.6393 | Up |
| 9 | 7 | I1162, I1163, I1164, I1165, I1166, I1167, I1168 | 0.5481 | 0.0204 | Up |
| 10 | 11 | I1173, I1172, I1174, I1175, I1176, I1177, I1178, I1179, I1180, I1182, I1183 | 0.6515 | 0.0872 | Up |
| 11 | 10 | I1202, I1203, I1204, I1205, I1206, I1207, I1208, I1209, I1211, I1212 | -0.9315 | 0.1395 | Down |
| 12 | 11 | I1725, I1726, I1727, I1728, I1729, I1730, I1731, I1732, I1733, I1734, I1735 | 0.6804 | 0.0494 | Up |
| 13 | 15 | I2017, I2018, I2019, I2020, I2021, I2022, I2023, I2024, I2025, I2026, I2027, I2028, I2029, I2030, I2031 | 0.6847 | 0.0724 | Up |
| 14 | 15 | I2133, I2134, I2135, I2136, I2137, I2138, I2139, I2140, I2141, I2142, I2145, I2146, I2148, I2149, I2150 | 0.6509 | 0.0806 | Up |
| 15 | 8 | I2159, I2160, I2161, I2163, I2165, I2167, I2168, I2169 | 0.5869 | 0.0531 | Up |
| 16 | 13 | I2282, I2283, I2284, I2285, I2286, I2287, I2288, I2289, I2290, I2291, I2292, I2293, I2294 | 1.3565 | 0.4006 | Up |
| 17 | 3 | I2330, I2331, I2332 | 0.5236 | 0.0017 | Up |
| 18 | 11 | I2467, I2468, I2469, I2470, I2471, I2473, I2474, I2475, I2476, I2479, I2480 | -1.2768 | 0.2544 | Down |
| 19 | 3 | I2626, I2627, I2628 | -0.6907 | 0.0096 | Down |
| 20 | 2 | I2695, I2696 | 0.523 | 0.0042 | Up |
| 21 | 13 | I2716, I2718, I2719, I2720, I2721, I2722, I2723, I2724, I2725, I2726, I2727, I2728, I2729 | 0.7016 | 0.0889 | Up |
| 22 | 13 | I2914, I2915, I2916, I2918, I2917, I2919, I2920, I2921, I2922, I2923, I2924, I2925, I2926 | -1.274 | 0.3835 | Down |
| 23 | 3 | I2930, I2931, I2932 | 0.5643 | 0.003 | Up |
| 24 | 4 | I3001, I3002, I3003, I3004 | -0.7224 | 0.0377 | Down |
| 25 | 27 | I3006, I3007, I3008, I3009, I3010, I3011, I3012, I3013, I3014, I3015, I3016, I3017, I3018, I3019, I3020, I3021, I3022, I3024, I3023, I3025, I3026, I3027, I3028, I3029, I3030, I3031, I3032 | -1.2112 | 0.2934 | Down |
| 26 | 5 | I3183, I3184, I3185, I3186, I3187 | -0.6895 | 0.0187 | Down |
| 27 | 40 | I3419, I3420, I3421, I3422, I3423, I3424, I3425, I3426, I3427, I3428, I3429, I3430, I3431, I3432, I3433, I3434, I3435, I3436, I3437, I3438, I3439, I3440, I3441, I3442, I3443, I3444, I3445, I3446, I3447, I3448, I3449, I3450, I3451, I3453, I3454, I3455, I3456, I3457, I3458, I3460 | -0.927 | 0.102 | Down |

**Table 4.3 Differentially regulated gene clusters on Chromosome II in response to 10 mM NaNO₃**

| ID | No. Genes | Genes in Cluster | Log2 FC Mean | Log2 FC SD | Expression Trend |
|---|---|---|---|---|---|
| 1 | 3 | II0199, II0201, II0200 | -0.9365 | 0.011 | Down |
| 2 | 4 | II0232, II0233, II0234, II0235 | -0.9472 | 0.0139 | Down |
| 3 | 5 | II0336, II0337, II0338, II0339, II0340 | 1.1898 | 0.0388 | Up |
| 4 | 4 | II0639, II0640, II0641, II0642 | 1.1602 | 0.0365 | Up |
| 5 | 4 | II1137, II1138, II1139, II1140 | 1.3533 | 0.1301 | Up |
| 6 | 7 | II1231, II1232, II1233, II1234, II1235, II1236, II1237 | 1.3228 | 0.0763 | Up |
| 7 | 14 | II1241, II1242, II1243, II1244, II1245, II1246, II1247, II1248, II1249, II1251, II1250, II1252, II1253, II1254 | 1.6048 | 0.1707 | Up |
| 8 | 3 | II1261, II1262, II1263 | -1.0715 | 0.0498 | Down |
| 9 | 14 | II1342, II1343, II1344, II1345, II1346, II1347, II1348, II1349, II1350, II1351, II1352, II1353, II1354, II1355 | -2.0991 | 0.6582 | Down |
| 10 | 6 | II1414, II1415, II1416, II1417, II1418, II1419 | -1.0476 | 0.0779 | Down |
| 11 | 9 | II1447, II1448, II1449, II1450, II1451, II1452, II1454, II1455, II1456 | -1.1587 | 0.0947 | Down |
| 12 | 29 | II1612, II1615, II1616, II1617, II1618, II1619, II1620, II1621, II1622, II1623, II1624, II1625, II1626, II1627, II1628, II1629, II1630, II1631, II1632, II1633, II1634, II1635, II1636, II1637, II1638, II1639, II1640, II1641, II1642 | -1.1798 | 0.1661 | Down |
| 13 | 6 | II1799, II1800, II1801, II1802, II1803, II1804 | -1.0501 | 0.06 | Down |
| 14 | 13 | II1931, II1932, II1933, II1934, II1935, II1936, II1937, II1938, II1939, II1940, II1941, II1942, II1943 | 1.8051 | 0.3416 | Up |
| 15 | 6 | II1959, II1960, II1961, II1962, II1963, II1964 | -0.9653 | 0.0242 | Down |
| 16 | 5 | II2030, II2031, II2032, II2033, II2034 | -1.0977 | 0.0339 | Down |
| 17 | 8 | II2043, II2042, II2044, II2045, II2046, II2047, II2048, II2049 | -1.1748 | 0.0985 | Down |
| 18 | 30 | II2068, II2069, II2070, II2071, II2072, II2073, II2074, II2075, II2076, II2077, II2078, II2079, II2080, II2082, II2081, II2083, II2084, II2085, II2086, II2087, II2088, II2089, II2090, II2091, II2092, II2093, II2094, II2095, II2096, II2097 | 1.3065 | 0.1232 | Up |
| 19 | 8 | II2141, II2142, II2144 II2145, II2146, II2147, II2148, II2149 | 1.6808 | 0.3017 | Up |
| 20 | 5 | II2418, II2419, II2420, II2421, II2422 | -1.0116 | 0.0618 | Down |
| 21 | 13 | II2437, II2438, II2439, II2440, II2441, II2442, II2443, II2444, II2445, II2446, II2447, II2449, II2448 | 1.3985 | 0.1535 | Up |

## 4.4.6 Nitrate metabolism

Not surprisingly, among the most highly expressed transcripts in both nitrate and nitrite treatment groups compared to LB were genes in the *narXL-narGHJI-narK$_2$-narK$_1$* regulon. Bp1026b_I1015 (*narI-1*), I1016 (*narJ-1*), I1017 (*narH-1*), I1018 (*narG-1*), I1019 (*narK-2*), and I1020 (*narK-1*) were collectively up-regulated at mean fold change of 9.7 in the nitrate treatment group, and at mean fold change of 10.5 in the nitrite group. Among these loci, the $\alpha$- and $\beta$-subunits of the dissimilatory nitrate reductase *narG-1*, and *narH-1*, respectively, were the most highly and significantly expressed in the nitrate (**Tables 4.4, 4.5**) and nitrite (**Tables 4.6, 4.7**) groups. Noticeably, only loci in the *narXL-narGHJI- narK$_2$-narK$_1$* regulon were significantly regulated in response to either nitrate or nitrate, omitting loci on chromosome II and the duplicate dissimilatory nitrate reductase *narGHJI-2.* Genes encoding assimilatory nitrate and nitrite reductases, nitrite reductases, nitric oxide, and nitrous oxide reductases were all absent from our expression data. The absence of other nitrate metabolism genes in this analysis suggests that the normoxic experimental conditions did not stimulate anaerobic respiration and potentially implicate the nar*XL* regulon in nitrate-nitrite respiration.

Bp1026b_I1014 (*narX*) was conspicuously down-regulated in both treatment groups; -2.5-fold in the nitrate group and -2.9-fold in the nitrite group. This seeming discrepancy can be explained by the fact that the snapshot into global regulatory mechanisms provided by these RNA-seq data are reflective of a 24-hour time-point, at which point nitrate sensing has ceased and nitrate metabolism is well underway. The response regulator and transcription factor Bp1026b_I1013 (*narL*) was also noticeably absent from this differential expression analysis. Bp1026b_0861 (*mobA*), encoding for the final molybdoenzyme responsible for generating the molybdenum guanine dinucleotide cofactor required for nitrate reductase function (45) was also down-regulated in both nitrate and nitrite treatment groups; -2.9-fold and -2.2-fold, respectively. The down-regulation of key genes associated with activation of nitrate reduction can be explained by the sampling time after prolonged exposure to the nitrosative treatments.

**Table 4.4 Top 50 up-regulated genes in wild-type *B. pseudomallei* 1026b grown in the presence of 10 mM NaNO₃ relative to LB.** Locus tags, gene annotations (if available), putative gene product names, fold changes and adjusted p-values are presented.

| Locus tag | Gene | Burkholderia Genome Database product name | Fold change | Adj. P-value |
|---|---|---|---|---|
| BP1026B_I0767 | *metE* | 5- methyltetrahydropteroyltriglutamate/homocysteine S-methyltransferase | 18.3 | 1.04E-30 |
| BP1026B_I1018 | *narG-1* | Nitrate reductase subunit alpha | 14.4 | 7.26E-91 |
| BP1026B_I1017 | *narH-1* | Nitrate reductase subunit beta | 14.4 | 1.38E-43 |
| BP1026B_II2146 | | Hypothetical protein | 12.5 | 9.67E-62 |
| BP1026B_II2147 | | Lipoprotein | 9.8 | 1.06E-21 |
| BP1026B_I1019 | *nark-2* | Nitrate/nitrite transporter NarK | 9.7 | 1.41E-09 |
| BP1026B_II1137 | | Hypothetical protein | 9.3 | 7.59E-25 |
| BP1026B_I1015 | *narI-1* | Respiratory nitrate reductase subunit gamma | 8.9 | 7.60E-19 |
| BP1026B_I2288 | | Cytochrome C oxidase subunit II | 8.8 | 1.21E-51 |
| BP1026B_II2441 | | Flavin reductase domain-containing protein | 8.2 | 1.84E-05 |
| BP1026B_I2290 | | Cytochrome C | 7.7 | 9.54E-26 |
| BP1026B_II1255 | | Shikimate transporter | 7.7 | 7.12E-22 |
| BP1026B_II1936 | | Hypothetical protein | 7.5 | 6.62E-08 |
| BP1026B_I1016 | *narJ-1* | Nitrate reductase subunit delta | 6.7 | 0.00491 |
| BP1026B_I2286 | | Cytochrome C protein | 6.6 | 1.89E-21 |
| BP1026B_I2289 | | Hypothetical protein | 6.5 | 1.68E-15 |
| BP1026B_II2144 | | Hypothetical protein | 6.2 | 2.11E-51 |
| BP1026B_II1937 | *mhpE* | 4-hydroxy-2-ketovalerate aldolase | 6.2 | 7.18E-16 |
| BP1026B_II1943 | | Deoxygenase | 6.0 | 8.27E-30 |
| BP1026B_I2220 | | Hypothetical protein | 5.9 | 3.19E-25 |
| BP1026B_II0639 | | Hypothetical protein | 5.8 | 4.43E-06 |
| BP1026B_I2168 | | PAP2 family protein | 5.7 | 1.13E-24 |
| BP1026B_I0706 | | Hypothetical protein | 5.3 | 6.38E-08 |
| BP1026B_I2141 | | gp54 | 5.2 | 1.99E-06 |
| BP1026B_II0722 | | Hypothetical protein | 5.2 | 1.37E-12 |
| BP1026B_II1938 | *mhpF* | Acetaldehyde dehydrogenase | 5.2 | 2.58E-14 |
| BP1026B_II1940 | | Branched-chain amino acid aminotransferase | 5.0 | 2.02E-16 |
| BP1026B_I1505 | | Hypothetical protein | 5.0 | 0.00063 |
| BP1026B_II0064 | | Hypothetical protein | 5.0 | 5.33E-22 |
| BP1026B_II1939 | | Thioesterase | 4.9 | 7.56E-08 |
| BP1026B_II1249 | | Hypothetical protein | 4.9 | 3.81E-08 |
| BP1026B_II2095 | | Poly-beta-hydroxybutyrate polymerase | 4.8 | 1.21E-37 |
| BP1026B_II1935 | | Hypothetical protein | 4.7 | 4.79E-13 |

| Locus tag | Gene | Product name | Fold change | Adj. P-value |
|---|---|---|---|---|
| BP1026B_I2287 | | Cytochrome c oxidase subunit 1 | 4.5 | 8.15E-19 |
| BP1026B_II2438 | | Nitrilotriacetate monooxygenase | 4.4 | 3.99E-13 |
| BP1026B_II2145 | oxa | Class D beta-lactamase | 4.3 | 6.80E-26 |
| BP1026B_II2065 | | Sulfotransferase domain-containing protein | 4.3 | 1.36E-05 |
| BP1026B_I1342 | | Carboxymuconolactone decarboxylase familyprotein | 4.3 | 0.00010 |
| BP1026B_I1797 | cysT | Sulfate ABC transporter, permease protein CysT | 4.3 | 0.00358 |
| BP1026B_II1244 | | Hypothetical protein | 4.2 | 1.32E-18 |
| BP1026B_I1020 | nark-1 | Nitrate/nitrite transporter, NarK | 4.1 | 1.62E-07 |
| BP1026B_I3675 | | Long-chain fatty acid CoA ligase (AMP-binding) | 4.0 | 1.19E-06 |
| BP1026B_I1566 | | N/A | 4.0 | 3.98E-12 |
| BP1026B_I2602 | | Class II aldolase/adducin domain-containing protein | 3.9 | 7.51E-09 |
| BP1026B_II1252 | | Acyl carrier protein | 3.9 | 2.19E-40 |
| BP1026B_II0643 | pchC | Pyochelin biosynthetic protein | 3.9 | 0.00025 |
| BP1026B_II2071 | | ABC transporter ATP-binding protein | 3.9 | 8.73E-13 |
| BP1026B_I2291 | | Cytochrome C | 3.8 | 2.63E-21 |
| BP1026B_II2082 | | Methyl-accepting chemotaxis transducer transmembrane protein | 3.8 | 4.72E-14 |
| BP1026B_II1942 | | Thioesterase | 3.8 | 1.04E-30 |

**Table 4.5 Top 50 down-regulated genes in wild-type *B. pseudomallei* 1026b grown in the presence of 10 mM NaNO₃ relative to LB.** Locus tags, gene annotations (if available), putative gene product names, fold changes and adjusted p-values are presented.

| Locus tag | Gene | Burkholderia Genome Database product name | Fold change | Adj. P-value |
|---|---|---|---|---|
| BP1026B_I0204 | | Hypothetical protein | -31.3 | 5.27E-05 |
| BP1026B_I0205 | | Hypothetical protein | -18.1 | 7.55E-06 |
| BP1026B_I2778 | | tRNA-Met | -15.4 | 1.38E-08 |
| BP1026B_II2421 | | Glycosyl transferase family protein | -10.9 | 0.00328 |
| BP1026B_II2030 | catB | Muconate cycloisomerase | -10.6 | 2.26E-07 |
| BP1026B_I0601 | | Hypothetical protein | -10.0 | 2.12E-18 |
| BP1026B_II1353 | syrA | AMP-binding domain-containing protein | -10.0 | 5.84E-22 |
| BP1026B_II1346 | syrH | MbtH-like protein | -9.3 | 0.00029 |
| BP1026B_I1836 | | tRNA-Leu | -9.3 | 2.23E-43 |
| BP1026B_I1199 | | tRNA-Asp | -9.3 | 2.25E-06 |
| BP1026B_II1345 | syrI | Nonribosomal peptide synthetase DhbF | -8.2 | 1.98E-11 |
| BP1026B_II1351 | syrC | Acyl-CoA dehydrogenase domain-containing protein | -8.1 | 2.39E-15 |
| BP1026B_II1352 | syrB | Acyl-CoA dehydrogenase domain-containing protein | -7.9 | 2.19E-16 |
| BP1026B_II2043 | benA | Benzoate 1,2-dioxygenase alpha subunit | -7.4 | 4.17E-12 |
| BP1026B_I2923 | becN | Glycoside hydrolase family protein | -7.3 | 2.58E-05 |

| BP1026B_I2625 | rpmG | 50S ribosomal protein L33 | -7.2 | 5.04E-31 |
|---|---|---|---|---|
| BP1026B_II0247 | | N/A | -7.1 | 2.50E-06 |
| BP1026B_I2473 | infA | Translation initiation factor IF-1 | -7.0 | 2.45E-10 |
| BP1026B_II1347 | syrG | Major facilitator superfamily transporter | -7.0 | 9.20E-11 |
| BP1026B_I2571 | | Hypothetical protein | -6.8 | 2.36E-09 |
| BP1026B_I1198 | | tRNA-Glu | -6.8 | 6.72E-25 |
| BP1026B_I0996 | | tRNA-Val | -6.8 | 1.23E-17 |
| BP1026B_I1195 | | tRNA-Ala | -6.7 | 6.25E-33 |
| BP1026B_I0903 | | tRNA-Cys | -6.7 | 4.58E-11 |
| BP1026B_II1695 | | agmatinase | -6.6 | 0.00642 |
| BP1026B_I0218 | cspD | Cold shock transcription regulator protein | -6.5 | 8.41E-44 |
| BP1026B_I3494 | | Transcriptional regulator | -6.5 | 4.33E-16 |
| BP1026B_I1849 | | Hypothetical protein | -6.4 | 7.48E-13 |
| BP1026B_I0914 | | Hypothetical protein | -6.3 | 1.28E-11 |
| BP1026B_I0602 | | Serine-type carboxypeptidase family protein | -6.2 | 8.68E-31 |
| BP1026B_I0850 | | tRNA-Asn | -6.2 | 1.15E-09 |
| BP1026B_I1901 | | Hypothetical protein | -6.1 | 8.72E-14 |
| BP1026B_I0265 | | tRNA-Ala | -6.1 | 7.45E-22 |
| BP1026B_II1451 | | Cold shock transcription regulator protein | -5.8 | 2.84E-31 |
| BP1026B_II1348 | syrF | Hybrid NRPS(L-Lys - L-Ala)/PKS | -5.7 | 5.16E-13 |
| BP1026B_II1350 | syrD | Acyl carrier protein | -5.7 | 8.72E-08 |
| BP1026B_II2168 | | tRNA-Val | -5.6 | 4.67E-24 |
| BP1026B_II1644 | bsaN | MxiH protein | -5.6 | 0.00157 |
| BP1026B_I2839 | | Hypothetical protein | -5.6 | 2.67E-05 |
| BP1026B_I3021 | | Acyl-CoA dehydrogenase domain-containing protein | -5.4 | 0.00037 |
| BP1026B_I2257 | osmB | Lipoprotein | -5.4 | 0.00018 |
| BP1026B_II1699 | | Hypothetical protein | -5.3 | 9.86E-25 |
| BP1026B_II1452 | rpsU | 30S ribosomal protein S21 | -5.3 | 4.74E-22 |
| BP1026B_I1314 | | tRNA-Leu | -5.3 | 2.09E-23 |
| BP1026B_I1197 | | tRNA-Asp | -5.3 | 1.06E-18 |
| BP1026B_I1209 | | ATP-dependent RNA helicase | -5.2 | 2.04E-30 |
| BP1026B_I2922 | becM | PAP2 superfamily protein | -5.2 | 0.00358 |
| BP1026B_I1837 | | tRNA-Leu | -5.2 | 3.11E-14 |
| BP1026B_I2624 | rpmB | 50S ribosomal protein L28 | -5.1 | 4.04E-14 |
| BP1026B_I0600 | | Hypothetical protein | -5.1 | 7.35E-06 |

**Table 4.6 Top 50 up-regulated genes in wild-type *B. pseudomallei* 1026b grown in the presence of 10 mM NaNO$_2$ relative to LB**. Locus tags, gene annotations (if available), putative gene product names, fold changes and adjusted p-values are presented.

| Locus tag | Gene | Burkholderia Genome Database product name | Fold change | Adj. P-value |
|---|---|---|---|---|
| BP1026B_I0767 | *metE* | 5- methyltetrahydropteroyltriglutamate/homocysteine S-methyltransferase | 37.9 | 1.82E-40 |
| BP1026B_I1017 | *narH-1* | nitrate reductase subunit beta | 17.4 | 4.47E-42 |
| BP1026B_I1018 | *narG-1* | nitrate reductase subunit alpha | 15.4 | 1.55E-66 |
| BP1026B_I1019 | *nark-2* | nitrate/nitrite transporter NarK | 9.8 | 2.36E-08 |
| BP1026B_I1015 | *narJ-1* | respiratory nitrate reductase subunit gamma | 9.8 | 9.61E-17 |
| BP1026B_II1137 | | hypothetical protein | 8.3 | 1.88E-16 |
| BP1026B_II1936 | | hypothetical protein | 8.3 | 6.02E-07 |
| BP1026B_II2441 | | flavin reductase domain-containing protein | 8.1 | 0.00033 |
| BP1026B_II1943 | | deoxygenase | 7.6 | 4.30E-37 |
| BP1026B_II2146 | | hypothetical protein | 7.4 | 2.74E-26 |
| BP1026B_I1016 | *narI-1* | nitrate reductase subunit delta | 7.2 | 0.00976 |
| BP1026B_I2290 | | cytochrome C | 6.7 | 5.77E-17 |
| BP1026B_I0706 | | hypothetical protein | 6.4 | 3.05E-08 |
| BP1026B_I2288 | | cytochrome c oxidase subunit II | 6.2 | 2.43E-27 |
| BP1026B_II1937 | | 4-hydroxy-2-ketovalerate aldolase | 6.2 | 1.36E-11 |
| BP1026B_II2438 | | nitrilotriacetate monooxygenase | 6.1 | 1.13E-16 |
| BP1026B_II1940 | | branched-chain amino acid aminotransferase | 5.8 | 1.22E-15 |
| BP1026B_II2144 | | hypothetical protein | 5.8 | 3.53E-52 |
| BP1026B_II0639 | | hypothetical protein | 5.7 | 0.00015 |
| BP1026B_I2220 | | hypothetical protein | 5.5 | 3.98E-15 |
| BP1026B_II1935 | | hypothetical protein | 5.3 | 1.08E-12 |
| BP1026B_II1249 | | hypothetical protein | 5.3 | 8.81E-07 |
| BP1026B_II1938 | | acetaldehyde dehydrogenase | 5.2 | 4.76E-12 |
| BP1026B_I1797 | *cysT* | sulfate ABC transporter, permease protein CysT | 5.0 | 0.00928 |
| BP1026B_I2603 | | dihydrodipicolinate synthase | 4.8 | 5.19E-07 |
| BP1026B_II1939 | | Thioesterase | 4.8 | 2.04E-06 |
| BP1026B_II1255 | | shikimate transporter | 4.7 | 5.11E-13 |
| BP1026B_I2289 | | hypothetical protein | 4.7 | 7.75E-08 |
| BP1026B_I1726 | *cobW* | cobalamin biosynthesis protein CobW | 4.5 | 8.91E-08 |
| BP1026B_II1232 | | TauD/TfdA family dioxygenase | 4.3 | 5.28E-24 |
| BP1026B_I3221 | | hypothetical protein | 4.3 | 0.00903 |
| BP1026B_II1252 | | acyl carrier protein | 4.3 | 4.71E-35 |
| BP1026B_II2449 | | 2-oxoisovalerate dehydrogenase subunit alpha | 4.3 | 7.45E-13 |

| Locus tag | Gene | | Product name | Fold change | Adj. P-value |
|---|---|---|---|---|---|
| BP1026B_II1253 | | | deoxygenase | 4.3 | 2.75E-32 |
| BP1026B_I1505 | | | hypothetical protein | 4.2 | 0.00837 |
| BP1026B_I2286 | | | cytochrome c protein | 4.2 | 5.04E-09 |
| BP1026B_I1795 | | | sulfate ABC transporter ATP-binding protein | 4.2 | 3.09E-06 |
| BP1026B_I2602 | *cysA* | | class II aldolase/adducin domain-containing protein | 4.1 | 1.73E-06 |
| BP1026B_II1942 | | | Thioesterase | 4.0 | 5.90E-08 |
| BP1026B_I0711 | | | ABC transporter permease | 3.9 | 2.14E-15 |
| BP1026B_II1941 | | | transferase | 3.9 | 5.41E-05 |
| BP1026B_II0334 | | | ketol-acid reductoisomerase | 3.9 | 2.13E-11 |
| BP1026B_II0339 | | | hypothetical protein | 3.8 | 3.33E-13 |
| BP1026B_II2145 | *oxa* | | class D beta-lactamase | 3.8 | 1.58E-18 |
| BP1026B_I2287 | | | cytochrome c oxidase subunit 1 | 3.8 | 5.61E-12 |
| BP1026B_II1945 | | | Peptide synthetase | 3.8 | 7.40E-11 |
| BP1026B_II1772 | | | hypothetical protein | 3.7 | 9.63E-13 |
| BP1026B_II1244 | | | hypothetical protein | 3.7 | 8.86E-12 |
| BP1026B_I0390 | | | hypothetical protein | 3.7 | 5.10E-11 |
| BP1026B_II2444 | | | hypothetical protein | 3.6 | 0.00725 |

**Table 4.7. Top 50 down-regulated genes in wild-type *B. pseudomallei* 1026b grown in the presence of 10 mM NaNO$_2$ relative to LB.** Locus tags, gene annotations (if available), putative gene product names, fold changes and adjusted p-values are presented.

| Locus tag | Gene | Burkholderia Genome Database product name | Fold change | Adj. P-value |
|---|---|---|---|---|
| BP1026B_II1695 | | agmatinase | -22.4 | 0.00118 |
| BP1026B_II2184 | | short chain dehydrogenase/reductase family oxidoreductase | -11.5 | 0.00327 |
| BP1026B_II1414 | | major facilitator family transporter | -11.3 | 0.00027 |
| BP1026B_II1345 | | nonribosomal peptide synthetase DhbF | -11.1 | 2.45E-08 |
| BP1026B_II1351 | | acyl-CoA dehydrogenase domain-containing protein | -10.3 | 0.00449 |
| BP1026B_II1352 | | acyl-CoA dehydrogenase domain-containing protein | -8.4 | 5.85E-13 |
| BP1026B_II2043 | | Benzoate 1,2-dioxygenase alpha subunit | -8.3 | 2.22E-08 |
| BP1026B_I3493 | | ISBma1, transposase | -8.3 | 0.00049 |
| BP1026B_II1353 | | AMP-binding domain-containing protein | -8.1 | 2.69E-13 |
| BP1026B_II2288 | | fumarylacetoacetate hydrolase family protein | -7.6 | 0.00016 |
| BP1026B_II1348 | | thiotemplate mechanism natural product synthetase | -7.5 | 9.77E-16 |
| BP1026B_II2030 | | muconate cycloisomerase | -7.4 | 8.97E-05 |
| BP1026B_I1497 | | hypothetical protein | -7.3 | 0.00402 |
| BP1026B_II1699 | | hypothetical protein | -7.1 | 8.51E-21 |
| BP1026B_I2923 | | glycoside hydrolase family protein | -7.1 | 0.00110 |

| | | | | |
|---|---|---|---|---|
| BP1026B_I0601 | | hypothetical protein | -7.1 | 1.25E-09 |
| BP1026B_II0676 | | short chain dehydrogenase | -7.0 | 7.22E-06 |
| BP1026B_I3494 | | transcriptional regulator | -7.0 | 8.86E-12 |
| BP1026B_I0218 | | cold shock transcription regulator protein | -6.8 | 7.80E-26 |
| BP1026B_I2839 | | hypothetical protein | -6.7 | 0.00129 |
| BP1026B_II0306 | | Rieske iron-sulfur protein | -6.4 | 0.00344 |
| BP1026B_I0602 | | serine-type carboxypeptidase family protein | -6.4 | 7.50E-26 |
| BP1026B_II1418 | | MerR family transcriptional regulator | -6.2 | 0.00708 |
| BP1026B_II1628 | | BipB protein | -6.1 | 0.00103 |
| BP1026B_I1849 | | hypothetical protein | -6.1 | 4.84E-10 |
| BP1026B_I2476 | | hypothetical protein | -5.9 | 1.34E-05 |
| BP1026B_I1324 | | endonuclease Nuc | -5.9 | 0.00316 |
| BP1026B_II1413 | | transcriptional regulator | -5.9 | 4.20E-14 |
| BP1026B_II1643 | | type III secretion system protein PrgH/EprH | -5.6 | 0.00080 |
| BP1026B_II1347 | | major facilitator superfamily transporter | -5.5 | 5.87E-06 |
| BP1026B_II2042 | | benzoate 1,2-dioxygenase subunit beta | -5.4 | 0.00018 |
| BP1026B_II1451 | csd | cold shock transcription regulator protein | -5.3 | 1.18E-16 |
| BP1026B_II1350 | | phosphopantetheine attachment site domain-containing protein | -5.3 | 0.00022 |
| BP1026B_I3034 | | hypothetical protein | -5.2 | 0.00062 |
| BP1026B_I1560 | | hypothetical protein | -5.1 | 1.92E-05 |
| BP1026B_II1124 | | FecR family protein | -5.0 | 0.00077 |
| BP1026B_I1901 | | hypothetical protein | -4.9 | 6.28E-09 |
| BP1026B_I3716 | | phenylalanine 4-monooxygenase | -4.6 | 2.96E-10 |
| BP1026B_II0750 | | asparagine synthase | -4.5 | 3.98E-11 |
| BP1026B_I2473 | | translation initiation factor IF-1 | -4.5 | 9.98E-06 |
| BP1026B_II0765 | | 4-hydroxyphenylacetate degradation bifunctional isomerase/decarboxylase, subunit A | -4.4 | 0.00304 |
| BP1026B_I2257 | | lipoprotein | -4.4 | 0.00702 |
| BP1026B_II1916 | | molybdenum ABC transporter periplasmic molybdate-binding protein | -4.4 | 3.63E-08 |
| BP1026B_I1559 | | hypothetical protein | -4.3 | 3.47E-09 |
| BP1026B_II1422 | | YeeE/YedE family protein | -4.3 | 6.48E-12 |
| BP1026B_II1419 | | hypothetical protein | -4.3 | 3.67E-13 |
| BP1026B_II1885 | | 30S ribosomal protein S21 | -4.2 | 2.09E-21 |
| BP1026B_I2625 | | 50S ribosomal protein L33 | -4.1 | 6.72E-11 |
| BP1026B_I2814 | | cholesterol oxidase | -4.1 | 7.58E-05 |
| BP1026B_II0062 | | hypothetical protein | -4.0 | 8.04E-08 |

Altogether, under the conditions tested in these transcriptomic analyses, the primary nitrate reductase, which is activated at 10 mM $NO_3^-$ or above (46), along with the *narX-narL* system and the *narK* extrusion genes are the key elements of nitrate metabolism in *B. pseudomallei*.

### 4.4.7 General Metabolism

In addition to nitrate metabolism, several transcripts associated with amino acid and energy metabolism were identified as being significantly regulated in response to nitrate and nitrite via differential expression. The highest and most significantly expressed transcript for both treatment groups, Bp1026b_I0767 (*metE*), (**Figure 8A, 8B**) is a cobalamin-independent methionine synthase that produces methionine from homocysteine (47, 48). *metE* was up-regulated 18.3-fold in the nitrate group and 37.9-fold in the nitrite group. *metE* has been shown to be strongly induced in *R. solanacearum* during plant cell infection (43) and implicated in homocysteine turnover in *S. typhimurium* during infection where other methionine metabolism enzymes are candidate RNI resistance genes (23, 49). In addition to methionine metabolism, sulfate metabolic loci (Bp1026b_I1794 – I1798) were up-regulated a mean 3.1-fold and 4.0-fold in the nitrate and nitrite treatment groups, respectively. A genetic cluster containing 12 loci involved propionate metabolism (Bp1026b_II1934 – II1945) was up-regulated by a mean 4.5-fold and 5.0-fold in the nitrate and nitrite treatment groups, respectively. The gene cluster containing the predicted propionate metabolism loci is also annotated as a non-ribosomal peptide synthase cluster (Cluster 16) of unknown biosynthetic functionality in both *B. pseudomallei* and *B. thailandensis* (50, 51), with Bp1026b_II1945 in *B. pseudomallei* 1026b annotated as a predicted peptide synthase. However, two loci within this cluster are analogous to the *mhpE* aldolase (II1937) and *mhpF* dehydrogenase (II1938) loci in *E. coli* with putative aromatic cleavage function (52). Propionate is an important carbon source in proteobacteria that

is intricately linked to central metabolism and the TCA cycle, as it can be converted to pyruvate via *prpB* and the PrpR sigma factor (53).

Correspondingly, Bp1026b_II0229 (*prpB*) and Bp1026b_II0228 (*prpR*) were both down-regulated 2- to 3-fold in in both the nitrate and nitrite treatment groups. Bp1026b_I1208 (*aceA*, isocitrate lyase) and Bp1026b_I1204 (*aceB*, malate synthase), genes involved in the glyoxylate cycle of central metabolism and carbohydrate synthesis, were also significantly down-regulated 2- to 4-fold in both treatment groups. Collectively, these data suggest dysregulation in the TCA cycle due to nitrosative stress and present intriguing possibilities regarding bacterial defense from RNI using essential metabolic enzymes such as *metE*. These data also complement a recent transcriptomic analysis comparing a *B. pseudomallei* Δ*gvmR* (globally acting virulence and metabolism regulator) mutant relative to the wild type (54). In our analysis, Bp1026b_I0113 (*gvmR*) is significantly down-regulated -2.7-fold in both the nitrate and nitrite treatment groups; however, a pairwise comparison with Δ*narX* versus the wild type under nitrate treatment reverses this trend and *gvmR* is up-regulated 2-fold. Thus, the general nitrosative stress response in *B. pseudomallei* involves significant shifts in central metabolic processes as well as differential regulation of several virulence determinants.

### 4.4.8 Virulence-associated genes

Several antigens and secretion systems were differentially regulated in response to nitrate and nitrite treatment in *B. pseudomallei* 1026b. Notably, the type VI secretion system (T6SS) gene *hcp-1* from T6SS cluster 1 was significantly upregulated 2.3-fold in the nitrate condition and 2.5-fold in the nitrite condition. Organisms in the Bpc, including *B. pseudomallei, B. mallei,* and *B. thailandensis* variably encode six separate T6SS clusters, with *B. pseudomallei* having the coding capacity for all six (55). Of these six, T6SS-1 has been shown to be a virulence determinant in *B. mallei* (55), and hemolysin co-regulated protein-1 (*hcp-1*) has been shown to be important for eukaryotic cell replication and multinucleated giant cell (MNGC)

formation in *B. pseudomallei* (56). However, T6SS eukaryotic effectors such as Hcp-1 are tightly regulated for infection and are usually not expressed or produced in laboratory growth conditions (56, 57). While *hcp-1* expression has been shown to be negatively regulated by zinc and iron (57), our results indicate positive regulation by nitrate and nitrite that requires an intact NarX-NarL sensing system (*hcp-1* is down-regulated in Δ*narX* under nitrosative stress). In contrast, expression of genes in the type III secretion system (T3SS) cluster 3 was significantly reduced in the nitrate and nitrite conditions. Comprised of 37 genes, T3SS-3 is a major virulence determinant in *B. pseudomallei* (58) and has been shown to participate in intracellular spread and actin-based motility in macrophage-like cells (59, 60). Our analysis identified three genes within this cluster, Bp1026b_II1628 (*bipB*), II1643 (*bsaM*), and II1644 (*bsaN*) that were significantly down-regulated at a mean fold change ratio of -4.5 in the nitrate condition and -5.8 in the nitrite condition. *bsaN* has been shown to encode a positive transcriptional regulator of the T3SS-3 cluster in *B. pseudomallei* that is down-regulated in response to arabinose (61). In a similarly indirect fashion, growth with supplemental nitrate and nitrite suggest that exogenous N-oxides have implications for *B. pseudomallei*, in this inhibiting T3SS-3-mediated pathogenesis.

Again, these changes are dependent on a functional NarX-NarL system, as four T3SS-3 loci in Δ*narX* were up-regulated at a mean 4.2-fold compared to the wild type in the nitrate condition. In addition to these secretion system-associated gene loci, our analysis identified two loci within the capsular polysaccharide 1 (CPS I) cluster as being positively regulated in both nitrate and nitrite treatment groups. Bp1026b_I0505 (*wzt*), a putative ATP-binding ABC transporter capsular polysaccharide export protein, and Bp1026b_I0503 (*wcbD*), capsular polysaccharide export system inner membrane protein, were up-regulated at a mean fold change ratio of 2.0 in the nitrate-supplemented condition and 2.3 in the nitrite condition. CPS I is a prominent antigen and virulence determinant that allows for survival in host blood and protection from opsonization and is required for acute virulence in *B. pseudomallei* (62).

Additionally, the CPS I antigen is a current frontrunner for melioidosis diagnostic development (63), along with the previously mentioned antigen Hcp1 (64). Thus, the nitrosative stress response in *B. pseudomallei* involves activation of some classical virulence determinants for successful eukaryotic infection while at the same time a reduction of T3SS-3 *bsa* cluster expression under the conditions and time points evaluated.

### 4.4.9 Antibiotic resistance-associated genes

A hallmark of *Burkholderia* spp. infections is multidrug resistance via intrinsic mechanisms in these adaptable organisms. In *B. pseudomallei*, resistance mechanisms are chromosomally encoded and provide antibiotic protection via physical exclusion, enzymatic inactivation, target mutation, and importantly, many RND efflux pumps (65). Our transcriptomic analysis revealed significant differential regulation of several antibiotic resistance-associated loci in *B. pseudomallei* 1026b in the conditions tested. A putative RND efflux system spanning Bp1026b_II2076 – II2080 was significantly upregulated in its entirety, with a mean fold change ratio of 3.0 in the nitrate treatment and 2.5 in the nitrite treatment groups. However, this cluster has yet to be characterized in *B. pseudomallei* as a classical RND efflux relevant to clinical antibiotics (66), thus this expression may not be associated to increased drug resistance. Interestingly, this putative RND efflux cluster is encoded adjacent to an ABC-type export system spanning Bp1026b_II2069 – II2072 that is similarly upregulated in its entirety, 3.1-fold in the nitrate condition and 2.2-fold in the nitrite treatment group. These two export clusters are separated by a universal stress protein locus (Bp1026b_II2074) and a TetR transcriptional regulator (Bp1026b_II2075), which are similarly expressed and suggest that activation of the export systems may be an artifact of the general stress response (67, 68).

Several gene loci that are directly correlated to antimicrobial resistance via enzymatic and genetic mechanisms were also identified in our analysis. Most notably, the class D $\beta$-lactamase, OXA-57 (69) encoded by Bp1026b_II2145 (*oxa*), was significantly expressed at a

ratio of 4.3-fold and 3.8-fold for the nitrate and nitrite conditions, respectively. Transcription of

class D β-lactamases such as OXA-57 has been shown to be increased in *B. pseudomallei* that

are resistant to ceftazidime, a frontline antibiotic (70). Strikingly, the operon Bp1026b_II2141 –

Bp1026b_II2145, which has been shown to be transcriptionally activated *in vivo* in response to

ceftazidime treatment (71) was significantly upregulated as an entire unit (except for the

response regulator *irlR2*) with an average fold change ratio of 4.2 in the nitrate condition. This

operon encodes a putative regulator of the stress response (Bp1026b_II2144) and a response

regulator implicated in imipenem resistance (Bp1026b_II2142, *irlR2*) in addition to the *oxa* β-

lactamase amid genes for hypothetical proteins (71). Our transcriptional analyses revealed

Bp1026b_II2144 to be upregulated 6.2-fold and 5.8-fold in the nitrate and nitrite conditions,

respectively. Following this trend, another locus encoding a hypothetical protein of unknown

function, Bp1026b_II2146, adjacent to *oxa*, was significantly upregulated 12.5-fold and 7.4-fold

in the nitrate and nitrite conditions, respectively.

Additionally, the locus encoding DNA gyrase subunit A, *gyrA* (Bp1026b_I0792) was

significantly downregulated -2-fold in both conditions, indicating a restriction of active cell

division under the conditions tested. Furthermore, the locus encoding for dihydrofolate

reductase (72), *folA* (Bp1026b_I0834) is also downregulated -2.7-fold and -2.2-fold in the nitrate

and nitrite conditions, respectively, although the latter did not pass our stringent statistical

threshold. In addition to the RND efflux, periplasmic β-lactamases, and LPS, among other

mechanisms, *Burkholderia* spp. have been shown to acquire resistance to fluoroquinolones and

trimethroprim via targeted mutations in *gyrA* and *folA*, respectively (73). Thus, our observations

of significant differential regulation of key antibiotic resistance-associated gene loci implicate the

nitrosative stress response in regulation of these resistance mechanisms in *B. pseudomallei*.

## 4.4.10 Polysaccharide components

In conjunction with the biofilm inhibitory phenotype resulting from nitrate and nitrite dose responses in wild type (**Figure 4.3A,** (5)), our analysis revealed significant downregulation of several gene clusters associated with polysaccharide biosynthesis. The extracellular polymeric substance (EPS) matrix in *Burkholderia* spp*.* encompasses numerous polysaccharides, adhesins, lipids, and extracellular DNA that contribute to aggregation and biofilm formation (63). To date, four capsular polysaccharide (CPS) gene clusters have been characterized in *B. pseudomallei* (63); CPS I: Bp1026b_I0499 – Bp1026b_I0524, CPS II: Bp1026b_II0468 – Bp1026b_II0480, CPS III: Bp1026b_II1956 – Bp1026b_II1966, and CPS IV: Bp1026b_I0525 – Bp1026b_I0543. Exopolysaccharide clusters homologous to *bce-I* (Bp1026b_II1956 – Bp1026b_I1966, also annotated as CPS III) and *bce-II* (Bp1026b_II1795 – Bp1026b_II1807) cepacian biosynthesis in the *Burkholderia cepacia* complex (Bcc) (74) have also been described in *B. pseudomallei* (63). Additionally, we have recently described a novel biofilm-associated biosynthesis gene cluster, *becA-R* (Bp1026b_I2097 – Bp1026b_I2927) (75). Our analysis revealed significant downregulation of CPS III/*bce-I*, *bce-II*, and *becA-R* biofilm-associated gene clusters, with varying degrees of cluster coverage, among the differentially expressed datasets from both the nitrate and nitrite conditions.

The CPS III cluster displayed a reduced expression of -2.2 mean fold change for six transcripts in the nitrate comparison, and -2.7 mean fold change for seven transcripts in the nitrite comparison. Similarly, the *bce-II* cluster displayed reduced expression of -2.5 mean fold change for seven transcripts in the nitrate comparison, and -2.9 mean fold change for six transcripts in the nitrite comparison. Within the *becA-R* biofilm cluster, Bp1026b_I2922 (*becM*) was downregulated -5.2-fold and Bp1026b_I2923 (*becN*) -7.3-fold in the nitrate condition, with *becN* also down -7.1-fold in the nitrite condition. Lastly, Bp1026b_II0477, encoding a predicted ADP-heptose-LPS-heptosyltransferase in CPSII was downregulated -2.3-fold in the nitrate condition. Altogether, these results demonstrate the transcript level reduction of key EPS matrix

components, notably exopolysaccharide clusters, that go hand in hand with the biofilm inhibition response to both nitrate and nitrite supplementation in *B. pseudomallei*. The reduction of expression in these biofilm-associated clusters is also dependent on the intact NarX-NarL system, as all the above trends are reversed in pairwise comparisons of Δ*narX* and Δ*narL* to the wild type under nitrate treatment.

### 4.4.11 Secondary metabolite biosynthetic gene clusters

In addition to polysaccharide biosynthetic clusters, *Burkholderia* spp. encode several gene clusters that produce antimicrobial natural products (76). *B. pseudomallei* 1026b encodes a combination of 15 nonribosomal peptide synthetase (NRPS) and polyketide synthase (PKS) biosynthetic gene clusters residing on both chromosomes (50). Our analysis identified four clusters on chromosome II in which all loci were similarly differentially regulated in both the nitrate and nitrite stress comparisons (**Figure 4.10**).
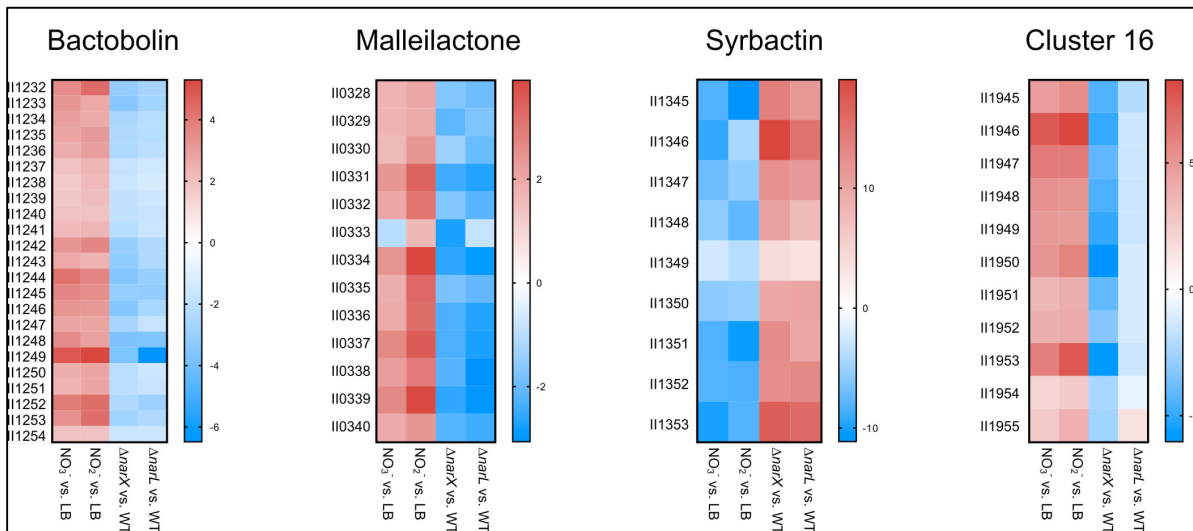


**Figure 4.10 Key clusters associated with antibiotic production, cytotoxic siderophore synthesis, and proteasome inhibition are positively regulated by nitrate and nitrite in a similar fashion.** Differential regulation of secondary metabolite synthesis clusters, Bactobolin, Malleilactone, Syrbactin, and the cryptic Cluster 16. Data was extracted from DESeq2 analysis of significantly regulated gene loci, pooled as mean fold change values, are visualized here. Uniform regulation is evident among the treatment conditions, with nitrate and nitrite conditions similarly regulating clusters opposed by Δ*narX* and Δ*narL* mutant trends in the nitrate treatment condition. Color density gradients represent up-regulation (red), down-regulation (blue), and no differential regulation (white).

Bactobolin is an antibiotic encoded by a 120-Kb DNA element in *B. pseudomallei* and *B. thailandensis* that is responsive to an ASL quorum-sensing system (77). The bactobolin biosynthetic cluster, encoded by loci Bp1026b_II1232 – Bp1026b_II1251 (*btaA – btaU*) (78), was markedly upregulated at a mean fold change of 3.1 in the nitrate treatment group and 3.0 in the nitrite treatment group. In both comparisons, all gene loci in the bactobolin cluster were among the most significantly expressed with consistently low false discovery rates. Another biosynthetic gene cluster that was identified in our analysis as significantly upregulated in both nitrate and nitrite stress conditions encodes for malleilactone, a cytotoxic siderophore (79). Malleilactone contains 13 ORFs (Bp1026b_II0330 – Bp1026b_II0341), including two large polyketide synthase gene loci (*malA* and *malF*) and a LuxR-type transcription factor (*malR*), indicating that its expression is mediated by an AHL quorum-sensing system (79). When comparing wild type in the nitrate-supplemented condition versus regular media, 7/13 of the malleilactone genes were significantly upregulated by a mean fold change ratio of 2.4, and in the nitrite condition versus regular media, 11/13 loci are significantly expressed at a fold change ratio of 3.1. Interestingly, malleilactone is among the few PKS/NRPS clusters that is conserved among the Bpc, including *B. mallei* and *B. thailandensis*, the latter of which has been shown to be important for virulence (50, 79). Thus, in apparent coordination with bactobolin antibiotic expression, *B. pseudomallei* similarly regulates the transcription of the malleilactone siderophore biosynthetic genes in response to the biofilm-inhibitory doses of nitrate and nitrite.

In stark contrast to bactobolin and malleilactone upregulation in these conditions, a cluster of genes from Bp1026b_II1345 – Bp1026b_II1353 (*syrA – syrI*) encoding syrbactin (50), was significantly downregulated in both the nitrate and nitrite treatment groups. Syrbactin is a proteasome inhibitor produced by a hybrid PKS/NRPS cluster comprised of nine genes. All nine genes in the syrbactin cluster were downregulated at a mean fold change of -7.1 in the nitrate treatment group and -7.5 in the nitrite treatment group. For both treatment groups, syrbactin biosynthetic cluster genes were among the most downregulated genes in the differential

expression analysis. However, analysis of Δ*narX* and Δ*narL* under nitrate stress compared to the wildtype reversed this trend, implicating the NarX-NarL system in regulation of secondary metabolism in *B. pseudomallei* 1026b. Further supporting this hypothesis, a homolog of the recently described global regulator of secondary metabolism (80), Bp1026b_I0582 (*scmR*), is significantly downregulated -2.0-fold in the nitrate treatment group and -1.7-fold in the nitrite group. ScmR is a LysR-type transcriptional regulator that represses many biosynthetic gene clusters in the Bpc (80). In both analyses of Δ*narX* and Δ*narL* under nitrate stress, *scmR* is notably upregulated, 2.6-fold and 2.9-fold, respectively. Collectively, these results suggest that nitrosative stress induces transcription of bactobolin antibiotic and malleilactone siderophore biosynthesis and represses transcription of the syrbactin proteasome inhibitor via the global regulator *scmR,* which is dependent on a functioning NarX-NarL two-component system.

### 4.4.12 Genes associated with the stringent response

The growth conditions tested in these experiments causing nitrosative stress in sessile cells resulted in the activation of several genes associated with the stringent response. In β- and γ-proteobacteria, enzymes RelA and SpoT regulate production of (p)ppGpp, a messenger molecule that signals nutritional stress and regulates transcription and cell physiology (81), including biofilm formation (82). Importantly, *B. pseudomallei* encodes homologs of both these ppGpp-metabolism loci, the deletion of which have been considered for vaccine candidacy due to attenuation in both acute and chronic melioidosis models (83). Our results comparing sessile *B. pseudomallei* cells subject to elevated nitrate and nitrite levels revealed significant upregulation of the *relA* homolog (Bp1026b_I1913) as well as several loci associated with oxidative stress, destabilization of rRNA/tRNAs, reduction of DNA replication, and general stasis survival genes. The *relA* locus, encoding the GTP hydrolase associated with (p)ppGpp alarmone production (84), was significantly upregulated at a fold change ratio of 2.1 in both the

149

nitrate and nitrite treatment conditions. The relative expression of *relA*, along with several other key transcripts identified in this study (**Figure 4.11**), matched observed trends from the larger DESeq2 analysis.

Several rRNA loci encoding 50S and 30S subunits were significantly downregulated in both conditions and tRNA encoding-loci were among the most significantly downregulated in the nitrate treatment group. The downregulation of rRNA/tRNA loci in response to nitrate and nitrite treatment corresponds to potential markers of *in vivo* infections as described in a recent transcriptomic profile of *B. pseudomallei* (71). Similarly, the locus encoding for the translation initiation factor IF1, Bp1026b_I2473, was significantly downregulated -7.0-fold in the nitrate-supplemented condition and -4.5-fold in the nitrite-supplemented condition. Collectively, these data indicate a general downregulation of nonessential genes associated with bacterial replication and protein synthesis, reminiscent of the stringent response in *E. coli* (85).
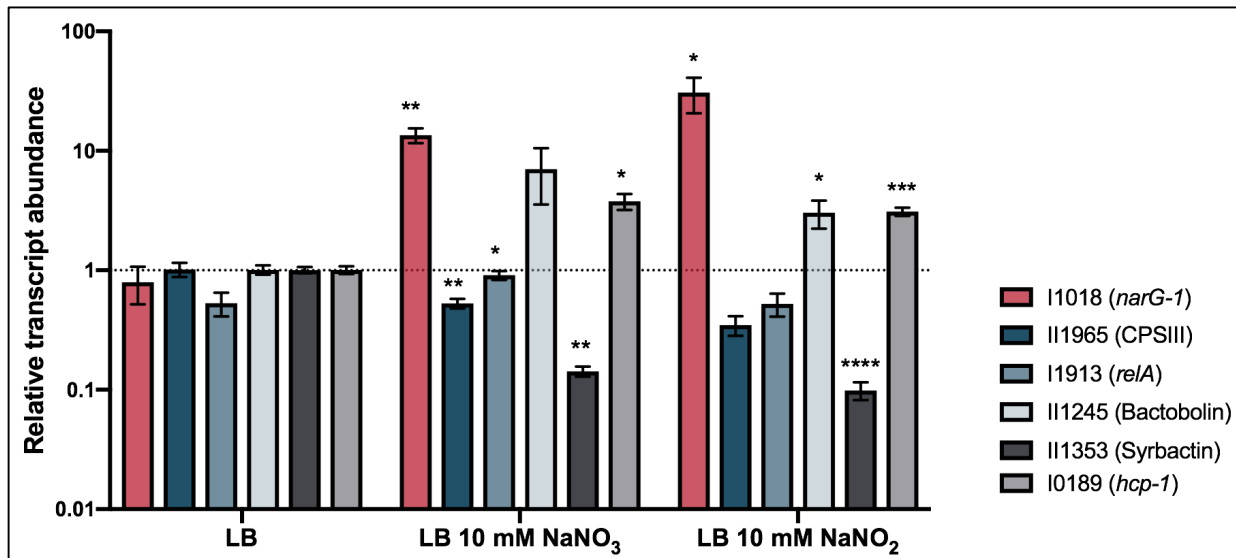


**Figure 4.11 Quantitative evaluation of key transcripts confirms trends in the DESeq2 data set.** Relative abundance of transcripts differentially regulated by both nitrate and nitrite treatment conditions as compared to baseline expression in LB. Fold change in transcript level was calculated using the Pfaffl method and normalized to the housekeeping transcript for 23S rRNA. Statistical significance was determined using a one-tailed heteroscedastic Student's T-test (* = $p < 0.05$, ** = $p < 0.01$, *** = $p < 0.001$).

**4.4.13 *B. pseudomallei* nitrate sensing mutants are deficient in intracellular replication in murine macrophages**

Successful intracellular pathogens require the ability to survive within phagocytic cells such as macrophage that bombard intruders with reactive oxygen and nitrogen intermediates (20, 22). To determine the ability of the nitrate sensing-deficient mutants to infect and survive in a hostile macrophage environment amid nitrosative stress, a murine macrophage cell line (RAW 246.7) was co-incubated with to wild-type, Δ*narX,* and Δ*narL* strains at an MOI of ~2. The number of intracellular bacteria was determined after 2h, 6h, and 20h post-exposure when eukaryotic cells were lysed and plated to count bacterial colony forming units (CFU). At 2h, there was a notable increase in bacterial internalization into the murine macrophage cells; however, at 6h and 20h Δ*narX* and Δ*narL* mutants were significantly impaired at intracellular replication (**Figure 4.12**). Two hours after infection, the wild type was recovered at lower titers than either of the two mutant strains (**Figure 4.12B**). Δ*narX* and Δ*narL* were internalized at 166% and 168% compared to the wild type, respectively, suggesting possible preferential uptake of these mutant bacteria by the murine macrophage. At 6h post-infection, Δ*narX* colony forming units were recovered at 56%, and Δ*narL* at 33% compared to the wild type, indicating an early-onset defect in intracellular replication. After 20h of infection, the observed Δ*narX* and Δ*narL* defects were maintained and CFU were recovered at 51% and 33% compared to wild type, respectively (**Figure 4.12A**). When comparing Δ*narX* and Δ*narL* mutants to wild type infection dynamics, CFU values were statistically significant at all three time-points of infection, however Δ*narL* was more drastically attenuated in this model. Thus, these results indicate that although attachment and internalization of the mutant strains tested are elevated at 2h post-infection, there are significant defects in *B. pseudomallei* lacking the NarX sensor kinase and the NarL DNA-binding regulator during intracellular replication and long-term survival.
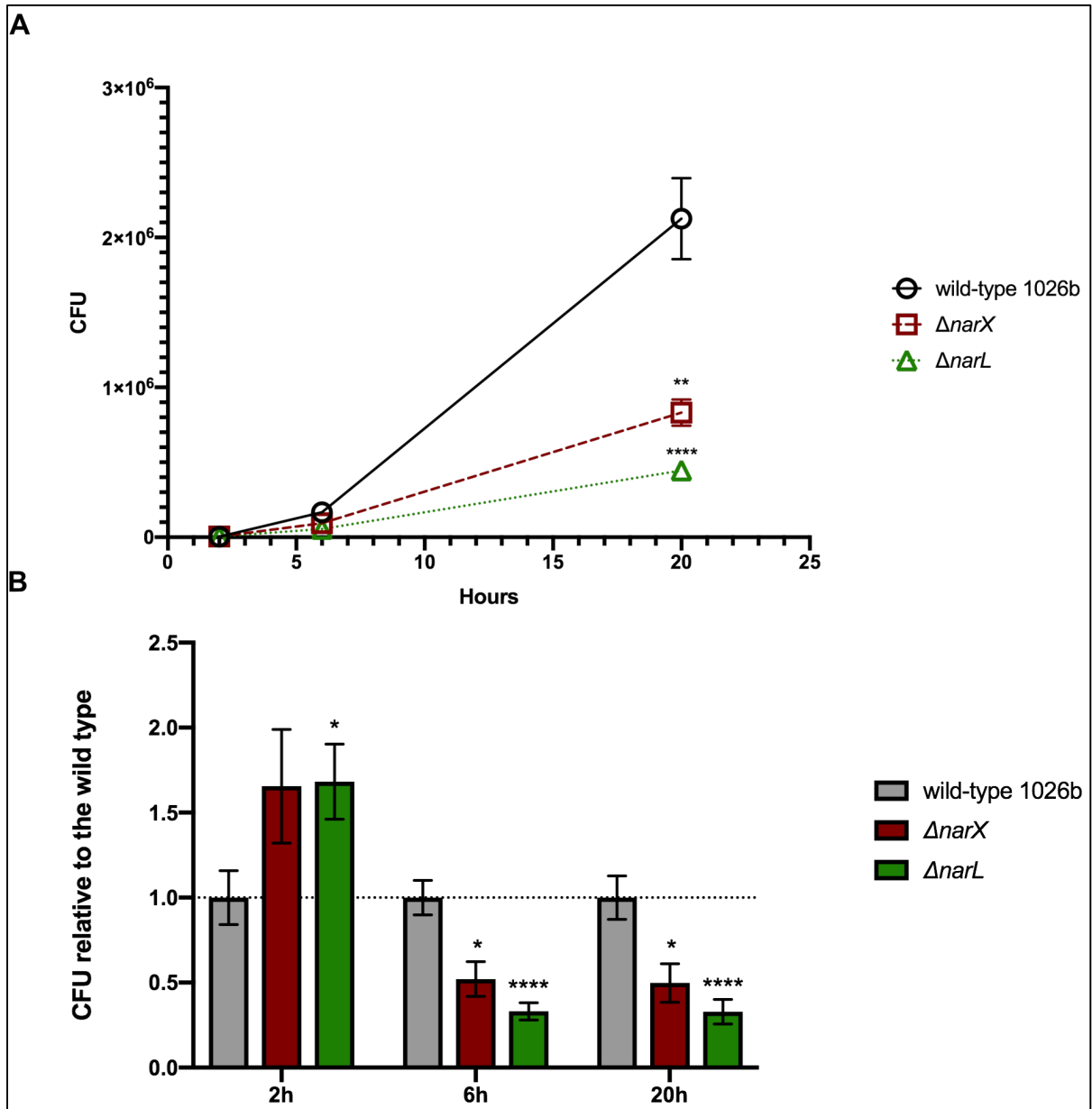
**Figure 4.12** *B. pseudomallei* **1026b mutants lacking NarX and NarL components of the nitrate sensing two-component system are deficient in intracellular replication despite being internalized at a higher rate than the wild type.** RAW264.7 cell monolayers were infected at an MOI of ~2 with three strains (wild-type 1026b, Δ*narX*, and Δ*narL*) and intracellular survival was measured at 2h, 6h, and 20h post-infection. At 1h post-infection, cells were treated with 750 $\mu$g/mL kanamycin to kill extracellular bacteria. Total CFU levels were calculated (A) as well as CFU relative to the wild type (B) at all time-points. The internalization efficiency of the mutants is evident at 2h post-infection, yet the intracellular replication efficiency is hindered at 6h and infection is attenuated at 20h (B). Statistical significance was determined using the Holm-Sidak method across multiple Student's T-tests (* = p<0.05, ** = p<0.01, **** = p<0.0001).

**4.5 Discussion**

Understanding the biofilm dynamics of *B. pseudomallei* in the context of environmental sensing of nitrate and nitrite has broad implications for transmission epidemiology as well as the pathogenicity and clinical mitigation of this facultative intracellular organism. The metabolic versatility and adaptability of *B. pseudomallei* underscores its success as a ubiquitous tropical saprophyte (21) as well as a human pathogen capable of infecting all tissue types tested (86). The present study is based on characterization of the response to exogenous nitrate and nitrite in *B. pseudomallei* as it relates to biofilm inhibition via the NarX-NarL two component nitrate-sensing regulatory system. Using comparative transcriptome analyses between conditions of nitrate and nitrite treatments, we identified the global regulatory mechanisms of nitrate sensing that are intimately linked to both physiology and pathogenicity in *B. pseudomallei*. Our previous study identified a link between genes in the *narL-narX-narGHJI$_1$-narK$_1$-narK$_2$* regulon, biofilm inhibition and reduction of cyclic di-GMP (5). We further characterized the *narX-narL* system in conjunction with biofilm inhibition and discovered a complex regulatory system encompassing key elements of the stringent response, secondary metabolism, virulence and antibiotic tolerance (**Figure 4.13**).

Our initial observation of a biofilm inhibition phenotype that is comparable in both nitrate and nitrite treatment in oxic conditions is complicated by the fact that nitrite-dependent biofilm inhibition does not require the NarX-NarL system (**Figure 4.3A**). This disparity leads us to hypothesize that the NarX-NarL system in *B. pseudomallei* can discriminate between nitrate and nitrite ligands, with clear preference towards nitrate, as evidenced by NarX protein classification studies in *E. coli* (9). This evident ligand preference is further demonstrated in our transcriptomic analyses including ∆*narX* and ∆*narL* mutants in the presence of either nitrate and nitrite (**Figure 4.6**). In response to nitrate, both mutants activate and upregulate 683 transcripts (11% of *B. pseudomallei* coding sequences), with 234 of those shared among them (**Figure 4.7B**), and downregulate 537 (9% of coding sequences), with 184 overlapping in regulation. Conversely,
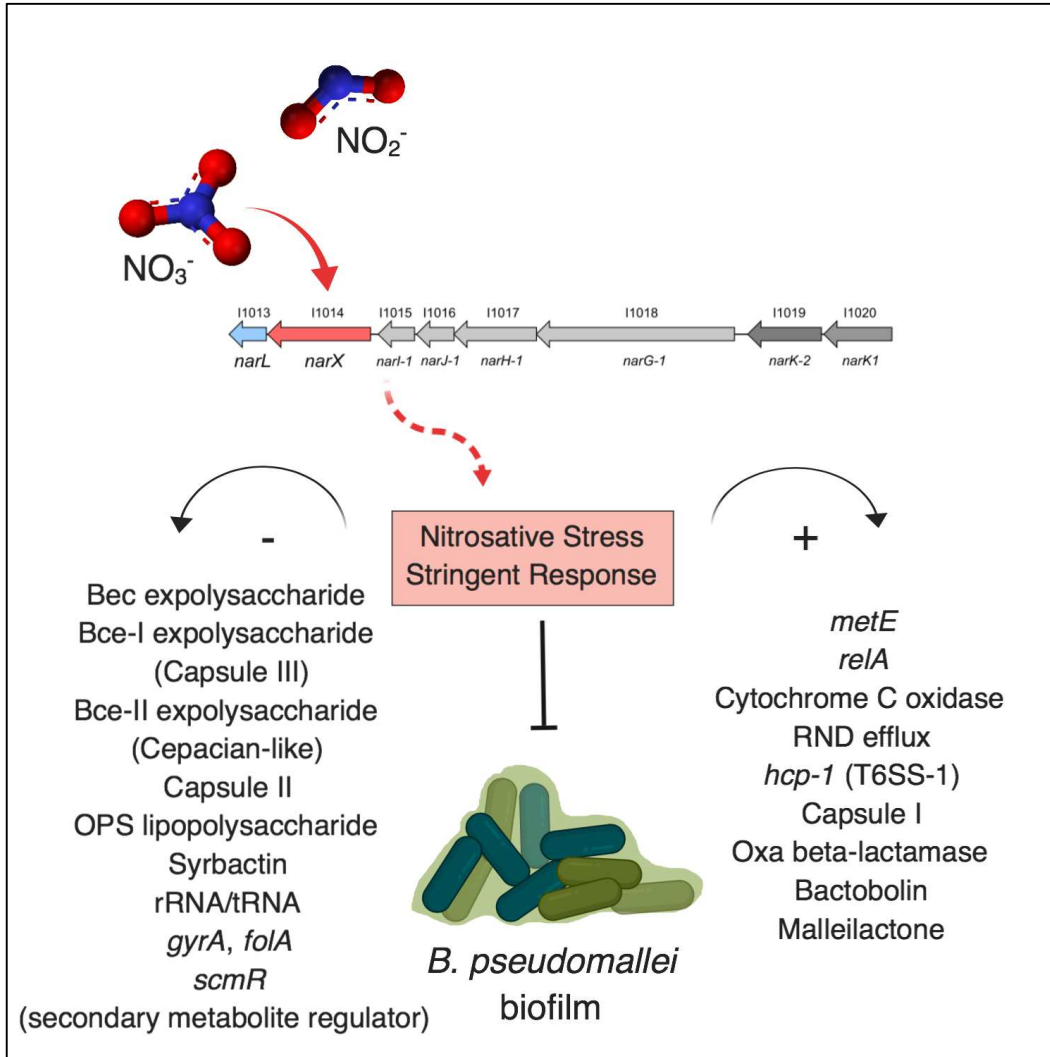
**Figure 4.13 Working model of nitrate-dependent biofilm inhibition and activation of the stringent response in *B. pseudomallei*.** Nitrate, and to a lesser extent nitrite, activate the *narXL* sensing mechanism in *B. pseudomallei* which leads to metabolism of N-oxides, activation of nitrosative stress and stringent responses, and indirectly inhibiting biofilm formation. Several biofilm-associated gene clusters such as capsules, exopolysaccharides, and lipopolysaccharides are down-regulated along with several housekeeping genes that are necessary for growth and division. On the other hand, secondary metabolic biosynthesis clusters are up-regulated in conjunction with pathogenicity-associated genes, an alternative respiration mechanism, as well as the classical indicator for stringent response, *relA*, and methionine metabolism gene *metE*.

$\Delta narX$ and $\Delta narL$ mutants compared to the wild type in the presence of nitrite only differentially regulated 10 transcripts in either a positive or a negative manner, further suggesting that exogenous nitrite is not regulated by NarX-NarL (**Figure 4.7C, 4.7F**). Future studies are required to characterize the complex regulatory systems that facilitate both nitrate and nitrite

signals in *B. pseudomallei*, although this is beyond the scope of the current study. Similarly, the conditions required for activation of the cryptic nitrate reductase encoded on chromosome II (5, 45) were not identified in this study and remain unclear. Sensing of similar N-oxides, nitrate and nitrite, are facilitated by twin two-component systems NarXL and NarQP (87), of which *B. pseudomallei* only encodes NarXL (9). Given that our previous *in silico* analyses did not discover a duplication of the NarXL system on chromosome II in *B. pseudomallei* (5), and given the data presented here, we propose that the NarXL system preferentially binds nitrate as a ligand.

The NarX-NarL system regulates biofilm formation in a nitrate-dependent manner, through direct or indirect downregulation of key EPS matrix components. Our analyses also implicate the stringent response, as activated by the nitrosative stress conditions tested, in regulation of the biofilm cycle. Recently, the stringent response mediated by the ppGpp synthases RelA and SpoT, were implicated in a nutrient-starvation model of biofilm dispersal described in *Pseudomonas putida* (88). The stringent response has been linked to nitrogen starvation in *E. coli* via $\sigma^{54}$-activated *relA* transcription (89), whereas our results describe upregulation of *relA* in response to nitrosative stress. Additionally, several genes regulated by the alternative sigma factor $\sigma^{54}$ such as the virulence-associated *bkdA1-bkdA2-bkdB-lpdV* operon (90) are significantly upregulated in our pairwise comparisons of both nitrate and nitrite treatment groups to the wild type. The *bkdA1-bkdA2-bkdB-lpdV* cluster encodes a keto acid dehydrogenase that has been identified in transcriptomic studies of planktonic *P. aeruginosa* compared to developing biofilms (91, 92). These differential expression patterns are not surprising considering $\sigma^{54}$ is responsible for nitrogen regulation and is responsive to ppGpp signaling in *E. coli* (85). In contrast to the classical nutrient starvation model of stringent response in antibiotic tolerant biofilms (93), we propose a similar outcome due to nitrosative stress in *B. pseudomallei*. Indeed, the responses to both nitrate and nitrite stress in conjunction

with biofilm inhibition, revealed coordinated expression of virulence-associated loci, repression

of nonessential growth and activation of antibiotic tolerance factors. However, it is worth taking

these transcriptional trends with a grain of salt, considering that expression of genes required

for physiological factors such as efflux pumps can be induced during generalized stress

responses (94). Despite the transcriptional activation of *oxa* β-lactamase, and its implications in

ceftazidime resistance, our antibiotic tolerance assay did not reveal any differences between

static growth conditions with or without nitrate-supplemented media (**Figure 4.14**).
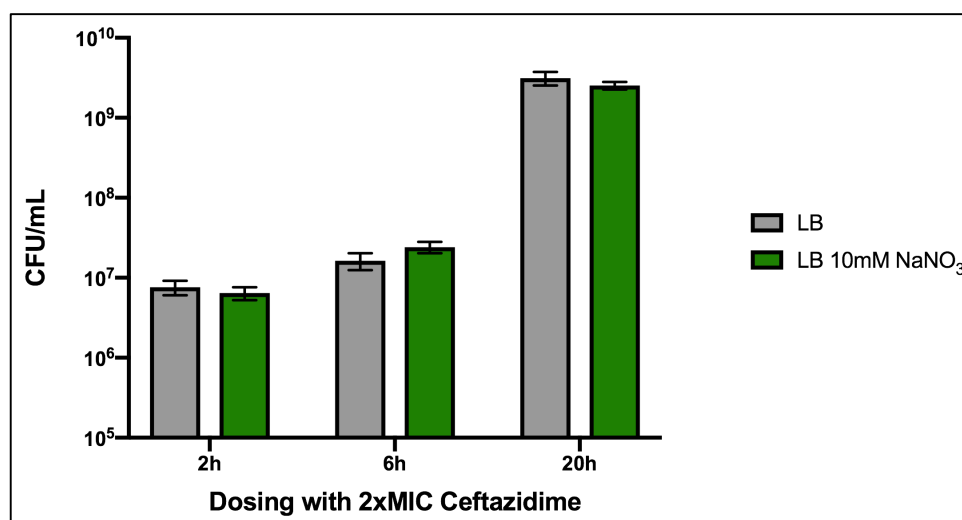


**Figure 4.14 Static biofilm cultures grown in nitrate-supplemented conditions do not confer added resistance to the cephalosporin ceftazidime under conditions tested.** Using the same time-points from the intracellular infection assays, we tested the antibiotic tolerance profiles of *B. pseudomallei* 1026b with or without 10 mM $NaNO_3$ supplemented in media. No differences where observed from this assay calculating CFU from cultures tested with twice the minimum inhibitory concentration of ceftazidime, a third-generation cephalosporin and frontline antibiotic for *B. pseudomallei* infection.

Nonetheless, the *in vitro* transcriptional response to nitrosative stress provides an

opportunity for beginning to understand the important physiological response in the context of

both environmental survival and *in vivo* infection scenarios. Facultative intracellular pathogens

must withstand several innate immune response molecules, such as reactive oxygen and

nitrogen species, sparking an interest in potential intrinsic genetic and enzymatic resistance

mechanisms in bacteria. Resistance to RNI has been shown to involve methionine and

homocysteine metabolism in *M. tuberculosis* and *Salmonella typhimurium* (23, 49, 95), which couples with our observation that *metE* is the most significantly upregulated locus in both nitrate-supplemented and nitrite-supplemented conditions. Further mutational analyses will be necessary to determine if transcripts identified in this study are implicated in response to RNI. To bridge this gap, we analyzed the fitness of Δ*narX* and Δ*narL* *B. pseudomallei* 1026b mutants in a model of eukaryotic cell infection, and observed a significant defect in intracellular replication efficiency in both mutants (**Figure 4.12**). Although susceptible to the bactericidal activity of IFN-γ-stimulated macrophages, with RNI having a stronger effect than ROI (22), *B. pseudomallei* can survive intracellularly in phagocytic cells (96). Our observation of replication-deficient *B. pseudomallei* lacking either the NarX histidine kinase or the NarL DNA-binding regulator suggests that nitrate metabolism is important for intracellular survival. The intracellular growth deficiency of Δ*narX/L B. pseudomallei* is best explained by lack of active NarG and subsequent nitrate reductase activity, which is important for *Mycobacterium tuberculosis* intracellular growth (46), although this connection remains to be characterized in *B. pseudomallei.* Intriguingly, respiration of nitrate to nitrite in *M. tuberculosis* leads to growth retardation and increase of antibiotic tolerance (41), which is similar to the trends we observed in *B. pseudomallei*.

The differing responses to nitrate and nitrite in our *B. pseudomallei* anaerobic growth model (**Fig. 2C**) raises the possibility of a disparity between exogenous nitrite and endogenously-produced nitrite via nitrate respiration, as seen in *M. tuberculosis* (41). Opposing this theory; however, our transcriptomic analyses of exogenous nitrate and nitrite revealed a strikingly similar genome-wide response. One possible explanation for this observation is that our global analysis is based on a transcriptional response from cells grown in oxic conditions, although oxygen limitation is a hallmark of biofilms that shift towards anaerobic metabolism during infections (97). Nonetheless, the responses of *in vitro* biofilms to nitrate and nitrite were

strikingly similar in our study (**Fig. 7A, 7B**). The transcriptional trends identified by the nitrate stress response is dependent on both components of the NarX-NarL system, as the differential expression patterns of both Δ*narX* and Δ*narL* in the nitrate condition were opposite to that of the wild type (**Fig. 9**).

Among the clearest examples of a similar response to both N-oxides is the regulation of secondary metabolism biosynthetic gene clusters (BGCs). Transcriptional activation of the complete bactobolin and malleilactone clusters as well as the cryptic cluster 16, coupled with the downregulation of the complete syrbactin biosynthesis cluster follow the same trends for either nitrate and nitrite, yet are dependent on a functioning NarX-NarL system (**Fig. 9**). In *B. thailandensis*, a global repressor of BGCs, MftR regulates both bactobolin and malleilactone production as well as *narX* and *narL*, and the T3SS regulator *bsaN*, suggesting that BGC regulation is inherently linked to host environment adaptation and ultimately virulence (98). In *B. pseudomallei* bactobolin and malleilactone are quorum sensing (QS)-controlled secondary metabolites, which may have implications for the intricate QS regulation of virulence in this organism (51). Our results further link these key QS-regulated factors to the stringent response as activated by nitrosative stress in *B. pseudomallei*. That the stringent response is linked to quorum sensing in *B. pseudomallei* is not surprising, considering the strong association between these two systems in *P. aeruginosa* (99, 100). In this context, we hypothesize that nitrosative stress activates QS-regulated metabolites that can aid *B. pseudomallei* in adapting to host environments.

Together, the results presented here provide a window into the complex signaling cascades that result in a nitrate-dependent model of biofilm inhibition in *B. pseudomallei* 1026b. Our analyses implicate the NarX-NarL two-component system in the regulation of a phenotype connected to biofilm inhibition, secondary metabolism, and the stringent response in relation to exogenous N-oxide stressors. Mutations in both partners of the NarX-NarL system revealed deficiencies during intracellular growth, which highlights the importance of the denitrification

pathway during host-pathogen interactions. That such a widespread and environmentally beneficial pathway is important for intracellular survival is intriguing and worth future characterization *in vivo* in stimulated macrophage and animal models of acute and chronic infection. Of special interest to host-pathogen interactions, is the differential expression of QS-regulated metabolites that are suspected virulence factors in *B. pseudomallei*. Genetic and metabolomic characterization of bactobolin, malleilactone, syrbactin and cluster 16 is required to better understand the role of these clusters in response to nitrate sensing and metabolism as mediated by the NarX-NarL system in *B. pseudomallei.* Furthermore, the attenuation of the Δ*narX* and Δ*narL B. pseudomallei* 1026b mutants in a cellular infection model should be characterized in stimulated phagocytes as well as non-phagocytic cells before determining if animal studies with these mutants would provide useful information for developing a live attenuated vaccine.

# References

1.	Gottschalk G. Bacterial Metabolism. Starr MP, editor. New York: Springer-Verlag; 1979.
2.	Rinaldo S, Giardina G, Mantoni F, Paone A, Cutruzzola F. Beyond nitrogen metabolism: nitric oxide, cyclic-di-GMP and bacterial biofilms. FEMS Microbiol Lett. 2018;365(6).
3.	Cheng AC, Currie BJ. Melioidosis: epidemiology, pathophysiology, and management. Clin Microbiol Rev. 2005;18(2):383-416.
4.	Kuris AM, Lafferty KD, Sokolow SH. Sapronosis: a distinctive type of infectious agent. Trends Parasitol. 2014;30(8):386-93.
5.	Mangalea MR, Plumley BA, Borlee BR. Nitrate Sensing and Metabolism Inhibit Biofilm Formation in the Opportunistic Pathogen *Burkholderia pseudomallei* by Reducing the Intracellular Concentration of c-di-GMP. Front Microbiol. 2017;8:1353.
6.	DeShazer D, Brett PJ, Carlyon R, Woods DE. Mutagenesis of *Burkholderia pseudomallei* with Tn5-OT182: isolation of motility mutants and molecular characterization of the flagellin structural gene. J Bacteriol. 1997;179(7):2116-25.
7.	Shapleigh JP. The Denitrifying Prokaryotes. Prokaryotes: A Handbook on the Biology of Bacteria, Vol 2, Third Edition. 2006:769-92.
8.	Walker MS, DeMoss JA. Phosphorylation and dephosphorylation catalyzed *in vitro* by purified components of the nitrate sensing system, NarX and NarL. J Biol Chem. 1993;268(12):8391-3.
9.	Stewart V. Biochemical Society Special Lecture. Nitrate- and nitrite-responsive sensors NarX and NarQ of proteobacteria. Biochem Soc Trans. 2003;31(Pt 1):1-10.
10.	Appleman JA, Stewart V. Mutational analysis of a conserved signal-transducing element: the HAMP linker of the *Escherichia coli* nitrate sensor NarX. J Bacteriol. 2003;185(1):89-97.
11.	Egan SM, Stewart V. Mutational analysis of nitrate regulatory gene *narL* in *Escherichia coli* K-12. J Bacteriol. 1991;173(14):4424-32.
12.	Williams SB, Stewart V. Nitrate- and nitrite-sensing protein NarX of *Escherichia coli* K-12: mutational analysis of the amino-terminal tail and first transmembrane segment. J Bacteriol. 1997;179(3):721-9.
13.	Lee AI, Delgado A, Gunsalus RP. Signal-dependent phosphorylation of the membrane-bound NarX two-component sensor-transmitter protein of *Escherichia coli*: nitrate elicits a superior anion ligand response compared to nitrite. J Bacteriol. 1999;181(17):5309-16.
14.	Goh EB, Bledsoe PJ, Chen LL, Gyaneshwar P, Stewart V, Igo MM. Hierarchical control of anaerobic gene expression in *Escherichia coli* K-12: the nitrate-responsive NarX-NarL regulatory system represses synthesis of the fumarate-responsive DcuS-DcuR regulatory system. J Bacteriol. 2005;187(14):4890-9.
15.	Hartig E, Schiek U, Vollack KU, Zumft WG. Nitrate and nitrite control of respiratory nitrate reduction in denitrifying *Pseudomonas stutzeri* by a two-component regulatory system homologous to NarXL of *Escherichia coli*. J Bacteriol. 1999;181(12):3658-65.
16.	Benkert B, Quack N, Schreiber K, Jaensch L, Jahn D, Schobert M. Nitrate-responsive NarX-NarL represses arginine-mediated induction of the *Pseudomonas aeruginosa* arginine fermentation *arcDABC* operon. Microbiology. 2008;154(Pt 10):3053-60.
17.	Martin-Mora D, Ortega A, Matilla MA, Martinez-Rodriguez S, Gavira JA, Krell T. The Molecular Mechanism of Nitrate Chemotaxis via Direct Ligand Binding to the PilJ Domain of McpN. MBio. 2019;10(1).
18.	Gupta A, Bedre R, Thapa SS, Sabrin A, Wang G, Dassanayake M, Grove A. Correction to Global Awakening of Cryptic Biosynthetic Gene Clusters in *Burkholderia thailandensis*. ACS Chem Biol. 2018;13(1):282.

19. Kaestli M, Schmid M, Mayo M, Rothballer M, Harrington G, Richardson L, Hill A, Hill J, Tuanyok A, Keim P, Hartmann A, Currie BJ. Out of the ground: aerial and exotic habitats of the melioidosis bacterium *Burkholderia pseudomallei* in grasses in Australia. Environ Microbiol. 2012;14(8):2058-70.

20. Jones-Carson J, Zweifel AE, Tapscott T, Austin C, Brown JM, Jones KL, Voskuil MI, Vazquez-Torres A. Nitric oxide from IFNγ-primed macrophages modulates the antimicrobial activity of beta-lactams against the intracellular pathogens *Burkholderia pseudomallei* and Nontyphoidal Salmonella. PLoS Negl Trop Dis. 2014;8(8):e3079.

21. Limmathurotsakul D, Golding N, Dance DA, Messina JP, Pigott DM, Moyes CL, Rolim DB, Bertherat E, Day NP, Peacock SJ, Hay SI. Predicted global distribution of *Burkholderia pseudomallei* and burden of melioidosis. Nat Microbiol. 2016;1:15008.

22. Miyagi K, Kawakami K, Saito A. Role of reactive nitrogen and oxygen intermediates in gamma interferon-stimulated murine macrophage bactericidal activity against *Burkholderia pseudomallei*. Infect Immun. 1997;65(10):4108-13.

23. Nathan C, Shiloh MU. Reactive oxygen and nitrogen intermediates in the relationship between mammalian hosts and microbial pathogens. Proc Natl Acad Sci U S A. 2000;97(16):8841-8.

24. Brett PJ, Deshazer D, Woods DE. Characterization of *Burkholderia pseudomallei* and *Burkholderia pseudomallei*-like strains. Epidemiol Infect. 1997;118(2):137-48.

25. Propst KL, Mima T, Choi KH, Dow SW, Schweizer HP. A *Burkholderia pseudomallei* Δ*purM* mutant is avirulent in immunocompetent and immunodeficient animals: candidate strain for exclusion from select-agent lists. Infect Immun. 2010;78(7):3136-43.

26. Heckman KL, Pease LR. Gene splicing and mutagenesis by PCR-driven overlap extension. Nat Protoc. 2007;2(4):924-32.

27. Lopez CM, Rholl DA, Trunck LA, Schweizer HP. Versatile dual-technology system for markerless allele replacement in *Burkholderia pseudomallei*. Appl Environ Microbiol. 2009;75(20):6496-503.

28. Rholl DA, Papp-Wallace KM, Tomaras AP, Vasil ML, Bonomo RA, Schweizer HP. Molecular Investigations of PenA-mediated beta-lactam Resistance in *Burkholderia pseudomallei*. Front Microbiol. 2011;2:139.

29. Plumley BA, Martin KH, Borlee GI, Marlenee NL, Burtnick MN, Brett PJ, AuCoin DP, Bowen RA, Schweizer HP, Borlee BR. Thermoregulation of biofilm formation in *Burkholderia pseudomallei* is disrupted by mutation of a putative diguanylate cyclase. J Bacteriol. 2017;199(5).

30. Mima T, Schweizer HP. The BpeAB-OprB efflux pump of *Burkholderia pseudomallei* 1026b does not play a role in quorum sensing, virulence factor production, or extrusion of aminoglycosides but is a broad-spectrum drug efflux system. Antimicrob Agents Chemother. 2010;54(8):3113-20.

31. Andrews S. FastQC: a quality control tool for high throughput sequence data http://www.bioinformatics.babraham.ac.uk/projects/fastqc2010.

32. Love MI, Huber W, Anders S. Moderated estimation of fold change and dispersion for RNA-seq data with DESeq2. Genome Biol. 2014;15(12):550.

33. Pfaffl MW. A new mathematical model for relative quantification in real-time RT-PCR. Nucleic Acids Res. 2001;29(9):e45.

34. Rabin RS, Stewart V. Dual response regulators (NarL and NarP) interact with dual sensors (NarX and NarQ) to control nitrate-regulated and nitrite-regulated gene-expression in *Escherichia coli* K-12. J Bacteriol. 1993;175(11):3259-68.

35. Darwin AJ, Stewart V. Expression of the NarX, NarL, NarP, and NarQ genes of *Escherichia coli* K-12 - regulation of the regulators. J Bacteriol. 1995;177(13):3865-9.

36.     Noriega CE, Lin HY, Chen LL, Williams SB, Stewart V. Asymmetric cross-regulation between the nitrate-responsive NarX-NarL and NarQ-NarP two-component regulatory systems from Escherichia coli K-12. Mol Microbiol. 2010;75(2):394-412.

37.     Cheung J, Le-Khac M, Hendrickson WA. Crystal structure of a histidine kinase sensor domain with similarity to periplasmic binding proteins. Proteins. 2009;77(1):235-41.

38.     Aravind L, Ponting CP. The cytoplasmic helical linker domain of receptor histidine kinase and methyl-accepting proteins is common to many prokaryotic signalling proteins. FEMS Microbiol Lett. 1999;176(1):111-6.

39.     Dunin-Horkawicz S, Lupas AN. Comprehensive analysis of HAMP domains: implications for transmembrane signal transduction. J Mol Biol. 2010;397(5):1156-74.

40.     James GA, Ge Zhao A, Usui M, Underwood RA, Nguyen H, Beyenal H, deLancey Pulcini E, Agostinho Hunt A, Bernstein HC, Fleckman P, Olerud J, Williamson KS, Franklin MJ, Stewart PS. Microsensor and transcriptomic signatures of oxygen depletion in biofilms associated with chronic wounds. Wound Repair Regen. 2016;24(2):373-83.

41.     Cunningham-Bussel A, Zhang T, Nathan CF. Nitrite produced by *Mycobacterium tuberculosis* in human macrophages in physiologic oxygen impacts bacterial ATP consumption and gene expression. Proc Natl Acad Sci U S A. 2013;110(45):E4256-65.

42.     Hamad MA, Austin CR, Stewart AL, Higgins M, Vazquez-Torres A, Voskuil MI. Adaptation and antibiotic tolerance of anaerobic *Burkholderia pseudomallei*. Antimicrob Agents Chemother. 2011;55(7):3313-23.

43.     Anders S, Pyl PT, Huber W. HTSeq--a Python framework to work with high-throughput sequencing data. Bioinformatics. 2015;31(2):166-9.

44.     Puccio S, Grillo G, Licciulli F, Severgnini M, Liuni S, Bicciato S, De Bellis G, Ferrari F, Peano C. WoPPER: Web server for Position Related data analysis of gene Expression in Prokaryotes. Nucleic Acids Res. 2017;45(W1):W109-W15.

45.     Andreae CA, Titball RW, Butler CS. Influence of the molybdenum cofactor biosynthesis on anaerobic respiration, biofilm formation and motility in *Burkholderia thailandensis*. Res Microbiol. 2014;165(1):41-9.

46.     Vazquez-Torres A, Baumler AJ. Nitrate, nitrite and nitric oxide reductases: from the last universal common ancestor to modern bacterial pathogens. Curr Opin Microbiol. 2016;29:1-8.

47.     Pejchal R, Ludwig ML. Cobalamin-independent methionine synthase (MetE): a face-to-face double barrel that evolved by gene duplication. PLoS Biol. 2005;3(2):e31.

48.     Mordukhova EA, Pan JG. Evolved cobalamin-independent methionine synthase (MetE) improves the acetate and thermal tolerance of *Escherichia coli*. Appl Environ Microbiol. 2013;79(24):7905-15.

49.     De Groote MA, Testerman T, Xu Y, Stauffer G, Fang FC. Homocysteine antagonism of nitric oxide-related cytostasis in *Salmonella typhimurium*. Science. 1996;272(5260):414-7.

50.     Biggins JB, Kang HS, Ternei MA, DeShazer D, Brady SF. The chemical arsenal of *Burkholderia pseudomallei* is essential for pathogenicity. J Am Chem Soc. 2014;136(26):9484-90.

51.     Majerczyk CD, Brittnacher MJ, Jacobs MA, Armour CD, Radey MC, Bunt R, Hayden HS, Bydalek R, Greenberg EP. Cross-species comparison of the *Burkholderia pseudomallei*, *Burkholderia thailandensis*, and *Burkholderia mallei* quorum-sensing regulons. J Bacteriol. 2014;196(22):3862-71.

52.     Lee SJ, Ko JH, Kang HY, Lee Y. Coupled expression of MhpE aldolase and MhpF dehydrogenase in *Escherichia coli*. Biochem Biophys Res Commun. 2006;346(3):1009-15.

53.     Suvorova IA, Ravcheev DA, Gelfand MS. Regulation and evolution of malonate and propionate catabolism in proteobacteria. J Bacteriol. 2012;194(12):3234-40.

54. Duong LT, Schwarz S, Gross H, Breitbach K, Hochgrafe F, Mostertz J, Eske-Pogodda K, Wagner GE, Steinmetz I, Kohler C. GvmR - A Novel LysR-Type Transcriptional regulator involved in virulence and primary and secondary metabolism of *Burkholderia pseudomallei*. Front Microbiol. 2018;9:935.

55. Schell MA, Ulrich RL, Ribot WJ, Brueggemann EE, Hines HB, Chen D, Lipscomb L, Kim HS, Mrazek J, Nierman WC, Deshazer D. Type VI secretion is a major virulence determinant in *Burkholderia mallei*. Mol Microbiol. 2007;64(6):1466-85.

56. Burtnick MN, Brett PJ, Harding SV, Ngugi SA, Ribot WJ, Chantratita N, Scorpio A, Milne TS, Dean RE, Fritz DL, Peacock SJ, Prior JL, Atkins TP, Deshazer D. The cluster 1 type VI secretion system is a major virulence determinant in *Burkholderia pseudomallei*. Infect Immun. 2011;79(4):1512-25.

57. Burtnick MN, Brett PJ. *Burkholderia mallei* and *Burkholderia pseudomallei* cluster 1 type VI secretion system gene expression is negatively regulated by iron and zinc. PLoS One. 2013;8(10):e76767.

58. Gutierrez MG, Pfeffer TL, Warawa JM. Type 3 secretion system cluster 3 is a critical virulence determinant for lung-specific melioidosis. PLoS Negl Trop Dis. 2015;9(1):e3441.

59. Stevens MP, Stevens JM, Jeng RL, Taylor LA, Wood MW, Hawes P, Monaghan P, Welch MD, Galyov EE. Identification of a bacterial factor required for actin-based motility of *Burkholderia pseudomallei*. Mol Microbiol. 2005;56(1):40-53.

60. Burtnick MN, Brett PJ, Nair V, Warawa JM, Woods DE, Gherardini FC. *Burkholderia pseudomallei* type III secretion system mutants exhibit delayed vacuolar escape phenotypes in RAW 264.7 murine macrophages. Infect Immun. 2008;76(7):2991-3000.

61. Moore RA, Reckseidler-Zenteno S, Kim H, Nierman W, Yu Y, Tuanyok A, Warawa J, DeShazer D, Woods DE. Contribution of gene loss to the pathogenic evolution of *Burkholderia pseudomallei* and *Burkholderia mallei*. Infect Immun. 2004;72(7):4172-87.

62. Reckseidler SL, DeShazer D, Sokol PA, Woods DE. Detection of bacterial virulence genes by subtractive hybridization: Identification of capsular polysaccharide of *Burkholderia pseudomallei* as a major virulence determinant. Infection and Immunity. 2001;69(1):34-44.

63. Mangalea MR, Borlee, G. I., Borlee, B. R. The Current Status of Extracellular Polymeric Substances Produced by *Burkholderia pseudomallei*. Current Tropical Medicine Reports. 2017;4(3):117-26.

64. Phokrai P, Karoonboonyanan W, Thanapattarapairoj N, Promkong C, Dulsuk A, Koosakulnirand S, Canovali S, Indrawattana N, Jutrakul Y, Wuthiekanun V, Limmathurotsakul D, Brett PJ, Burtnick MN, Lertmemongkolchai G, Chantratita N. A rapid immunochromatography test based on Hcp1 Is a potential point-of-care test for serological diagnosis of melioidosis. J Clin Microbiol. 2018;56(8).

65. Schweizer HP. Mechanisms of antibiotic resistance in *Burkholderia pseudomallei*: implications for treatment of melioidosis. Future Microbiol. 2012;7(12):1389-99.

66. Podnecky NL, Rhodes KA, Schweizer HP. Efflux pump-mediated drug resistance in *Burkholderia*. Front Microbiol. 2015;6:305.

67. Piddock LJ. Multidrug-resistance efflux pumps - not just for resistance. Nat Rev Microbiol. 2006;4(8):629-36.

68. Poole K. Efflux pumps as antimicrobial resistance mechanisms. Annals of Medicine. 2007;39(3):162-76.

69. Keith KE, Oyston PC, Crossett B, Fairweather NF, Titball RW, Walsh TR, Brown KA. Functional characterization of OXA-57, a class D beta-lactamase from *Burkholderia pseudomallei*. Antimicrob Agents Chemother. 2005;49(4):1639-41.

70. Niumsup P, Wuthiekanun V. Cloning of the class D beta-lactamase gene from *Burkholderia pseudomallei* and studies on its expression in ceftazidime-susceptible and -resistant strains. J Antimicrob Chemother. 2002;50(4):445-55.

71. Cummings JE, Slayden RA. Transient In Vivo Resistance Mechanisms of *Burkholderia pseudomallei* to ceftazidime and molecular markers for monitoring treatment response. PLoS Negl Trop Dis. 2017;11(1):e0005209.

72. Podnecky NL, Rhodes KA, Mima T, Drew HR, Chirakul S, Wuthiekanun V, Schupp JM, Sarovich DS, Currie BJ, Keim P, Schweizer HP. Mechanisms of resistance to folate pathway inhibitors in *Burkholderia pseudomallei*: deviation from the norm. MBio. 2017;8(5).

73. Rhodes KA, Schweizer HP. Antibiotic resistance in *Burkholderia* species. Drug Resist Updat. 2016;28:82-90.

74. Ferreira AS, Leitao JH, Silva IN, Pinheiro PF, Sousa SA, Ramos CG, Moreira LM. Distribution of cepacian biosynthesis genes among environmental and clinical *Burkholderia* strains and role of cepacian exopolysaccharide in resistance to stress conditions. Appl Environ Microbiol. 2010;76(2):441-50.

75. Borlee GI, Plumley BA, Martin KH, Somprasong N, Mangalea MR, Islam MN, Burtnick MN, Brett PJ, Steinmetz I, AuCoin DP, Belisle JT, Crick DC, Schweizer HP, Borlee BR. Genome-scale analysis of the genes that contribute to *Burkholderia pseudomallei* biofilm formation identifies a crucial exopolysaccharide biosynthesis gene cluster. PLoS Negl Trop Dis. 2017;11(6):e0005689.

76. Depoorter E, Bull MJ, Peeters C, Coenye T, Vandamme P, Mahenthiralingam E. Burkholderia: an update on taxonomy and biotechnological potential as antibiotic producers. Appl Microbiol Biotechnol. 2016;100(12):5215-29.

77. Duerkop BA, Varga J, Chandler JR, Peterson SB, Herman JP, Churchill ME, Parsek MR, Nierman WC, Greenberg EP. Quorum-sensing control of antibiotic synthesis in *Burkholderia thailandensis*. J Bacteriol. 2009;191(12):3909-18.

78. Seyedsayamdost MR, Chandler JR, Blodgett JA, Lima PS, Duerkop BA, Oinuma K, Greenberg EP, Clardy J. Quorum-sensing-regulated bactobolin production by *Burkholderia thailandensis* E264. Org Lett. 2010;12(4):716-9.

79. Biggins JB, Ternei MA, Brady SF. Malleilactone, a polyketide synthase-derived virulence factor encoded by the cryptic secondary metabolome of *Burkholderia pseudomallei* group pathogens. J Am Chem Soc. 2012;134(32):13192-5.

80. Mao D, Bushin LB, Moon K, Wu Y, Seyedsayamdost MR. Discovery of *scmR* as a global regulator of secondary metabolism and virulence in *Burkholderia thailandensis* E264. Proc Natl Acad Sci U S A. 2017;114(14):E2920-E8.

81. Potrykus K, Cashel M. (p)ppGpp: still magical? Annu Rev Microbiol. 2008;62:35-51.

82. de la Fuente-Nunez C, Reffuveille F, Haney EF, Straus SK, Hancock RE. Broad-spectrum anti-biofilm peptide that targets a cellular stress response. PLoS Pathog. 2014;10(5):e1004152.

83. Muller CM, Conejero L, Spink N, Wand ME, Bancroft GJ, Titball RW. Role of RelA and SpoT in *Burkholderia pseudomallei* virulence and immunity. Infect Immun. 2012;80(9):3247-55.

84. Honsa ES, Cooper VS, Mhaissen MN, Frank M, Shaker J, Iverson A, Rubnitz J, Hayden RT, Lee RE, Rock CO, Tuomanen EI, Wolf J, Rosch JW. RelA mutant *Enterococcus faecium* with multiantibiotic tolerance arising in an immunocompromised Host. MBio. 2017;8(1).

85. Magnusson LU, Farewell A, Nystrom T. ppGpp: a global regulator in *Escherichia coli*. Trends Microbiol. 2005;13(5):236-42.

86. Whiteley L, Meffert T, Haug M, Weidenmaier C, Hopf V, Bitschar K, Schittek B, Kohler C, Steinmetz I, West TE, Schwarz S. Entry, intracellular survival, and multinucleated-giant-

cell-forming activity of *Burkholderia pseudomallei* in human primary phagocytic and Nonphagocytic Cells. Infect Immun. 2017;85(10).

87.     Merrick MJ, Edwards RA. Nitrogen control in bacteria. Microbiol Rev. 1995;59(4):604-22.

88.     Diaz-Salazar C, Calero P, Espinosa-Portero R, Jimenez-Fernandez A, Wirebrand L, Velasco-Dominguez MG, Lopez-Sanchez A, Shingler V, Govantes F. The stringent response promotes biofilm dispersal in *Pseudomonas putida*. Sci Rep. 2017;7(1):18055.

89.     Brown DR, Barton G, Pan Z, Buck M, Wigneshweraraj S. Nitrogen stress response and stringent response are coupled in *Escherichia coli*. Nat Commun. 2014;5:4115.

90.     Zhu B, Ibrahim M, Cui Z, Xie G, Jin G, Kube M, Li B, Zhou X. Multi-omics analysis of niche specificity provides new insights into ecological adaptation in bacteria. ISME J. 2016;10(8):2072-5.

91.     Patell S, Gu M, Davenport P, Givskov M, Waite RD, Welch M. Comparative microarray analysis reveals that the core biofilm-associated transcriptome of *Pseudomonas aeruginosa* comprises relatively few genes. Environ Microbiol Rep. 2010;2(3):440-8.

92.     Waite RD, Paccanaro A, Papakonstantinopoulou A, Hurst JM, Saqi M, Littler E, Curtis MA. Clustering of *Pseudomonas aeruginosa* transcriptomes from planktonic cultures, developing and mature biofilms reveals distinct expression profiles. BMC Genomics. 2006;7:162.

93.     Nguyen D, Joshi-Datar A, Lepine F, Bauerle E, Olakanmi O, Beer K, McKay G, Siehnel R, Schafhauser J, Wang Y, Britigan BE, Singh PK. Active starvation responses mediate antibiotic tolerance in biofilms and nutrient-limited bacteria. Science. 2011;334(6058):982-6.

94.     Poole K. Bacterial multidrug efflux pumps serve other functions. ASM Microbe. 2008;3(4):179-85.

95.     Shiloh MU, Nathan CF. Reactive nitrogen intermediates and the pathogenesis of *Salmonella* and mycobacteria. Curr Opin Microbiol. 2000;3(1):35-42.

96.     Jones AL, Beveridge TJ, Woods DE. Intracellular survival of *Burkholderia pseudomallei*. Infect Immun. 1996;64(3):782-90.

97.     Wu Y, Klapper I, Stewart PS. Hypoxia arising from concerted oxygen consumption by neutrophils and microorganisms in biofilms. Pathog Dis. 2018;76(4).

98.     Gupta A, Bedre R, Thapa SS, Sabrin A, Wang G, Dassanayake M, Grove A. Global awakening of cryptic biosynthetic gene clusters in *Burkholderia thailandensis*. ACS Chem Biol. 2017;12(12):3012-21.

99.     Schafhauser J, Lepine F, McKay G, Ahlgren HG, Khakimova M, Nguyen D. The stringent response modulates 4-hydroxy-2-alkylquinoline biosynthesis and quorum-sensing hierarchy in *Pseudomonas aeruginosa*. J Bacteriol. 2014;196(9):1641-50.

100.    van Delden C, Comte R, Bally AM. Stringent response activates quorum sensing and modulates cell density-dependent gene expression in *Pseudomonas aeruginosa*. J Bacteriol. 2001;183(18):5376-84.

# CHAPTER 5: Concluding Remarks

*Burkholderia pseudomallei* is an environmental bacterium and sapronotic disease agent that is becoming increasingly recognized as a global health threat throughout the tropics worldwide. Melioidosis, the complex infectious disease caused by *B. pseudomallei* has long been overshadowed by more well-known tropical diseases despite causing an estimated 89,000 deaths from 165,000 human cases each year (1, 2). As such, there is a critical need to better understand the factors that define risks of exposure to and infection with *B. pseudomallei.* Previous studies have provided a framework for the ecological and genetic determinants of environmental survival (3, 4), biofilm formation (5, 6), anaerobic metabolism and denitrification (7, 8) in *B. pseudomallei*; however, a defined link between nitrate metabolism, biofilm formation, and pathogenic factors has not been established. The work presented in this dissertation aimed to characterize the response of *B. pseudomallei* to the exogenous N-oxides, nitrate and nitrite, with relation to biofilm dynamics. As is commonly the case for scientific exploration, the results described in these studies have exposed more questions than they resolved. Linking together biofilm dynamics and the nitrate-dependent biofilm-inhibitory stress response was a seemingly daunting task due to the convergence of physiological, genetic, and biochemical mechanisms. Through the course of these studies, we described genetic and molecular mechanisms for biofilm inhibition that are linked to key metabolic processes in *B. pseudomallei*. The versatility of *B. pseudomallei* in the environment in relation to the epidemiology of melioidosis (**Chapter 1**) is compounded by its equally complex biofilm forming capabilities (**Chapter 2**). The global regulatory responses identified herein (**Chapter 4**) and the initial genetic characterization of a mechanism for denitrification and nitrate sensing in this organism (**Chapter 3**) will hopefully further clarify the denitrification and biofilm response in *B. pseudomallei*. Future studies are

necessary to explore the bioenergetics of nitrate respiration and further characterize nitrate sensing and metabolism as it relates to host-pathogen interactions *in vivo*.

Denitrification and anaerobic metabolism are common bacterial mechanisms that have a profound impact on the natural world, facilitating nitrogen (N) nutrient cycling through the environment (9). The process of denitrification in bacteria is dependent on the presence of dedicated denitrification genes that are variably encoded among sequenced bacteria in soil and aquatic environments (10). Anthropogenic manipulation of ecosystems by supplementing large amounts of N-based fertilizers leads to nutrient imbalance and shifts in bacterial community structure (11). Specifically, N fertilizer can influence organic matter biomass thereby promoting Proteobacteria propagation alongside nitrifying bacteria in eutrophic ecosystems (11). In bacteria capable of denitrification such as *B. pseudomallei* (10), the enzymatic process is induced by the presence of exogenous nitrate ($NO_3^-$) and nitrite ($NO_2^-$) and oxygen depletion (12). The impetus for the studies described here came from a culmination of reports on the association of N-based anthropogenic manipulation of environments where *B. pseudomallei* is endemic. Observations of N-rich fertilizer leading to *B. pseudomallei* occurrence in domestic gardens (13), anthrosol soil (2), and livestock and animal housing (14), and a general association with elevated nitrate and total nitrogen (14, 15) led to the hypotheses explored in this dissertation. Additionally, global trends in infectious disease follow a familiar pattern as described by the late Dr. Stanley Falkow: "the problems we've had in infectious disease medicine… are traced to the opportunities that changes in human behavior have presented [potentially pathogenic] organisms (16)."

In **Chapter 3** we identified a mechanism for nitrate-dependent biofilm inhibition in a clinical isolate, *B. pseudomallei* 1026b. After initially characterizing $NO_3^-$ and $NO_2^-$ dose-dependent biofilm inhibition phenotypes that are not confounded by sodium chloride (NaCl) or any bactericidal effects of exogenous N-oxides, *in silico* analysis of predicted denitrification gene loci yielded putative targets for intervention. Using a two-allele sequence-defined

transposon mutant library, we identified genes that are resistant to biofilm inhibition in the presence of exogenous $NO_3^-$. We determined that five genes predicted to regulate nitrate sensing and metabolism (*narX, narL, narG-1, narH-1,* and *narK-1*) contribute to pellicle biofilm inhibition in the presence of exogenous nitrate in *B. pseudomallei* 1026b. Interestingly, a concurrent transcriptional profiling study of a "high biofilm-producing" *B. pseudomallei* isolate revealed that the same five genes are significantly up-regulated during biofilm growth (17). These observations suggest that denitrification enzyme pathways are important for mediating the intrinsic oxygen limitation of biofilms via anaerobic respiration in *B. pseudomallei*. Using qualitative and quantitative assays, we further corroborated the link between nitrate metabolism and biofilm dynamics, as well as proposed a mechanism of action. By modifying and developing a method for quantifying the intracellular concentration of the second messenger cyclic di-GMP, we showed a significant reduction in this key biofilm-regulating molecule in response to nitrate. Using LC-MS/MS, we showed intracellular c-di-GMP was reduced by 38% after 24h after static incubation with exogenous $NO_3^-$, which is lead to questions surrounding the role of c-di-GMP metabolic enzymes in this response.

The role of c-di-GMP regulation of *B. pseudomallei* biofilm dynamics has remained mysterious, especially regarding how *B. pseudomallei* responds to environmental stressors to regulate such an important aspect of its physiology. Given the limited scope of the genetic regulation of c-di-GMP in this arena, we chose to evaluate the expression of previously described diguanylate cyclases and phosphodiesterases (c-di-GMP metabolic enzymes) known to be involved in *B. pseudomallei* biofilm dynamics (18, 19). Our analysis of the transcriptional activity of *cdpA*, the only well-characterized phosphodiesterase, revealed its up-regulation in response to nitrate. Although, mutational analysis also revealed that *cdpA* is not required for nitrate- or nitrite-dependent biofilm inhibition in the conditions tested. Thus, a remaining "black box" in characterizing the connection between N-oxide biofilm inhibition and biofilm dynamics is the activity of other c-di-GMP enzymes and their regulatory signaling cascades in this

phenotype. Given that there are 23 loci predicted to modulate c-di-GMP in *B. pseudomallei*, which presumably orchestrate a complex temporal response to external stimuli (19), future research is needed in determining these global metabolic cascades in response to exogenous N-oxides.

In **Chapter 4**, we aimed to characterize the global transcriptional response to nitrate and nitrite in *B. pseudomallei*, and in doing so characterize the c-di-GMP and N-oxide signaling cascades that correspond to the biofilm inhibition phenotype. We created separate in-frame deletions of both modules of the predicted *narX-narL* two-component system to evaluate this sensory system in relation to biofilm dynamics. Separate deletions of these components allowed us to evaluate any differences between mutant signal and receiver domain-containing proteins in the global regulation kinetics of N-oxides, which have been shown to activate duplicate sensing systems in other organisms (20, 21). Considering previous *in silico* analyses comparing the predicted nitrate sensing and metabolism gene loci across both *B. pseudomallei* 1026b chromosomes (**Figure 3.2**), metabolism loci are duplicated while the *narX-narL* system is not. Thus, separate deletions are thought to mitigate any potential cross-talk between hypothetical nitrate- or nitrite- responsive sensors or regulators that were not identified previously in this organism. By replicating the nitrate- and nitrite-dependent biofilm inhibition phenotype using Δ*narX* and Δ*narL* mutants, a surprising and notable difference was observed in a disparate effect on this system dependent on the N-oxide donor tested. In response to sodium nitrite, Δ*narX* and Δ*narL* mutants behave like the wild type, suggesting that the *narX-narL* system responds to nitrate but not nitrite under the conditions tested here.

A comprehensive comparison of wild-type *B. pseudomallei* 1026b to Δ*narX* and Δ*narL* mutants in conditions of LB media, with or without 10 mM $NaNO_3$ or 10 mM $NaNO_2$ added, allowed for pair-wise analyses of transcriptional activity in response to these signals. Using Illumina NextSeq technology, differential expression analysis was possible due to the sufficient coverage of single-read sequences across all cDNA libraries included in the experiment. While it

is not surprising that treatment with $NaNO_3$ and $NaNO_2$ produced divergent differentially regulated datasets when compared to LB, both treatments elicit a similar transcriptomic response in wild-type *B. pseudomallei* 1026b. 590 transcripts (9.7% of coding sequences) were differentially expressed in the nitrate treatment group compared to 508 (8.4% of coding sequences) in the nitrite treatment. Among these transcripts passing our thresholds for level of expression and false discovery rate, several clusters of adjacent gene loci were identified by our analysis: biofilm-associated polysaccharides, general metabolism and respiration, antibiotic-resistance, virulence-associated, and secondary metabolite biosynthesis clusters. Interestingly, several loci associated with the stringent response were found to be differentially regulated, leading to interesting hypotheses connecting the nitrosative stress response to antibiotic tolerance. The down-regulation of translation initiation factors and ribosomal structural components, in addition to regulation of *relA* in a biofilm-inhibition background lends further credence to the stringent response activation in response to both nitrate and nitrite. While RelA and SpoT have recently been characterized in *B. pseudomallei* (22), future studies could further characterize the ppGpp response to exogenous N-oxide, using mutational assays and quantification of intracellular metabolites as described in our studies.

Similarly, our discovery of a connection between the nitrosative stress and stringent responses to QS-regulated secondary metabolites warrants further proteomic and metabolomics analyses. Transcriptome studies do not necessarily correlate to functional product biosynthesis, so it would be worthwhile to characterize bactobolin, malleilactone, and syrbactin in relation to nitrate and nitrite sensing *in vitro* as well as *in vivo*. Characterizing a connection between the nitrosative stress response and any pathogenicity-associated byproducts hinges on functional descriptions that link proteomics to transcriptionally-regulated gene clusters. Recently, a connection was established between the stationary phase sigma factor RpoS and QS-regulated extracellular products, whereby the alternative sigma factor exhibits hierarchical control over target biosynthetic clusters (23). During the course of our work,

170

another study described the role of the nitrogen-regulated sigma factor RpoN in the control of QS-regulated clusters as well as the important pathogenicity determinant, the type VI secretion system, in *P. aeruginosa* (24). Given that RpoN is important for exploiting exogenous nitrates, urea, and amino acids for nitrogen utilization (25), it is a worthwhile venture to explore the role of RpoN in our model of *B. pseudomallei* biofilm dynamics in response to nitrate and nitrite. It is our hope that future studies can elucidate the regulation and function of the biosynthetic clusters we have identified in our transcriptomic analyses in the context of environmental transmission of *B. pseudomallei* and *in vivo* during host-pathogen interactions.

Lastly, an important area to focus future work is the distinction between respiratory nitrate and nitrite reductases and possible intervention strategies for exploiting bacterial bioenergetics during *in vivo* infection models using *B. pseudomallei*. In our analyses, we observed a disparity between nitrate and nitrite sensing in the *narX-narL* system that presumably does not interact as strongly with nitrite. However, similar transcriptomic responses were observed, suggesting that a similar system responds to exogenous nitrite to exert parallel global changes to the *B. pseudomallei* transcriptome. Though our analyses did not detect up-regulation of the predicted nitrite reductases in the conditions tested, the roles of nitrite reductases during nitrosative stress should be explored and compared to the high expression of the dissimilatory nitrate reductase in our study. An additional role of the *B. psedudomallei* nitrate reductase may be to generate a proton motive force that supports the persistence of slow-growing hypoxic cells (26). Similarly, nitrite reduction to ammonium has been shown to be essential for both *in vitro* and *in vivo* survival in macrophages for *M. tuberculosis* (27). In this context of bioenergetics, further characterization of the intracellular kinetics of NarX and NarL are necessary. It is possible that the reduced intracellular survival we observed in Δ*narX* and Δ*narL* mutant *B. pseudomallei* 1026b is a result of a disruption of the proton motive force redox-loop, thus this area should be further explored to identify potential intervention strategies for *B. pseudomallei* infections.

# References

1.  Dance DA, Limmathurotsakul D. Global Burden and Challenges of Melioidosis. Trop Med Infect Dis. 2018;3(1).
2.  Limmathurotsakul D, Golding N, Dance DA, Messina JP, Pigott DM, Moyes CL, Rolim DB, Bertherat E, Day NP, Peacock SJ, Hay SI. Predicted global distribution of *Burkholderia pseudomallei* and burden of melioidosis. Nat Microbiol. 2016;1:15008.
3.  Inglis TJ, Sagripanti JL. Environmental factors that affect the survival and persistence of *Burkholderia pseudomallei*. Applied and environmental microbiology. 2006;72(11):6865-75.
4.  Dance DA. Ecology of *Burkholderia pseudomallei* and the interactions between environmental *Burkholderia* spp. and human-animal hosts. Acta Trop. 2000;74(2-3):159-68.
5.  Ramli NS, Eng Guan C, Nathan S, Vadivelu J. The effect of environmental conditions on biofilm formation of *Burkholderia pseudomallei* clinical isolates. PloS one. 2012;7(9):e44104.
6.  Sawasdidoln C, Taweechaisupapong S, Sermswan RW, Tattawasart U, Tungpradabkul S, Wongratanacheewin S. Growing Burkholderia pseudomallei in biofilm stimulating conditions significantly induces antimicrobial resistance. PloS one. 2010;5(2):e9196.
7.  Wongwanich S, Chotanachan P, Kondo E, Kanai K. Multifactorial pathogenic mechanisms of *Burkholderia pseudomallei* as suggested from comparison with *Burkholderia cepacia*. Southeast Asian J Trop Med Public Health. 1996;27(1):111-8.
8.  Philippot L. Tracking nitrate reducers and denitrifiers in the environment. Biochem Soc Trans. 2005;33(Pt 1):200-4.
9.  Payne WJ. Denitrification. New York, NY: John Wiley and Sons, Inc.; 1981.
10. Shapleigh JP. The Denitrifying Prokaryotes. Prokaryotes: A Handbook on the Biology of Bacteria, Vol 2, Third Edition. 2006:769-92.
11. Eo J, Park KC. Long-term effects of imbalanced fertilization on the composition and diversity of soil bacterial community. Agr Ecosyst Environ. 2016;231:176-82.
12. Hayatsu M, Tago K, Saito M. Various players in the nitrogen cycle: Diversity and functions of the microorganisms involved in nitrification and denitrification. Soil Sci Plant Nutr. 2008;54(1):33-45.
13. Kaestli M, Harrington G, Mayo M, Chatfield MD, Harrington I, Hill A, Munksgaard N, Gibb K, Currie BJ. What drives the occurrence of the melioidosis bacterium *Burkholderia pseudomallei* in domestic gardens? PLoS Negl Trop Dis. 2015;9(3):e0003635.
14. Palasatien S, Lertsirivorakul R, Royros P, Wongratanacheewin S, Sermswan RW. Soil physicochemical properties related to the presence of *Burkholderia pseudomallei*. Trans R Soc Trop Med Hyg. 2008;102 Suppl 1:S5-9.
15. Hantrakun V, Rongkard P, Oyuchua M, Amornchai P, Lim C, Wuthiekanun V, Day NP, Peacock SJ, Limmathurotsakul D. Soil Nutrient Depletion Is Associated with the Presence of *Burkholderia pseudomallei*. Applied and environmental microbiology. 2016;82(24):7086-92.
16. Falkow S. 21st Century Microbe Hunter. In: Buckley MR, editor. Meet the Scientist: American Society for Microbiology; 2008.
17. Chin CY, Hara Y, Ghazali AK, Yap SJ, Kong C, Wong YC, Rozali N, Koh SF, Hoh CC, Puthucheary SD, Nathan S. Global transcriptional analysis of *Burkholderia pseudomallei* high and low biofilm producers reveals insights into biofilm production and virulence. BMC Genomics. 2015;16:471.

18. Lee HS, Gu F, Ching SM, Lam Y, Chua KL. CdpA is a *Burkholderia pseudomallei* cyclic di-GMP phosphodiesterase involved in autoaggregation, flagellum synthesis, motility, biofilm formation, cell invasion, and cytotoxicity. Infect Immun. 2010;78(5):1832-40.
19. Plumley BA, Martin KH, Borlee GI, Marlenee NL, Burtnick MN, Brett PJ, AuCoin DP, Bowen RA, Schweizer HP, Borlee BR. Thermoregulation of Biofilm Formation in *Burkholderia pseudomallei* Is Disrupted by Mutation of a Putative Diguanylate Cyclase. Journal of bacteriology. 2017;199(5).
20. Capra EJ, Perchuk BS, Skerker JM, Laub MT. Adaptive mutations that prevent crosstalk enable the expansion of paralogous signaling protein families. Cell. 2012;150(1):222-32.
21. Noriega CE, Lin HY, Chen LL, Williams SB, Stewart V. Asymmetric cross-regulation between the nitrate-responsive NarX-NarL and NarQ-NarP two-component regulatory systems from *Escherichia coli* K-12. Molecular microbiology. 2010;75(2):394-412.
22. Muller CM, Conejero L, Spink N, Wand ME, Bancroft GJ, Titball RW. Role of RelA and SpoT in *Burkholderia pseudomallei* virulence and immunity. Infect Immun. 2012;80(9):3247-55.
23. Wongtrakoongate P, Tumapa S, Tungpradabkul S. Regulation of a quorum sensing system by stationary phase sigma factor RpoS and their co-regulation of target genes in *Burkholderia pseudomallei*. Microbiol Immunol. 2012;56(5):281-94.
24. Shao X, Zhang X, Zhang Y, Zhu M, Yang P, Yuan J, Xie Y, Zhou T, Wang W, Chen S, Liang H, Deng X. RpoN-Dependent Direct Regulation of Quorum Sensing and the Type VI Secretion System in *Pseudomonas aeruginosa* PAO1. Journal of bacteriology. 2018;200(16).
25. Kohler T, Harayama S, Ramos JL, Timmis KN. Involvement of *Pseudomonas putida* RpoN sigma factor in regulation of various metabolic functions. Journal of bacteriology. 1989;171(8):4326-33.
26. Cook GM, Greening C, Hards K, Berney M. Energetics of Pathogenic Bacteria and Opportunities for Drug Development. Adv Microb Physiol. 2014;65:1-62.
27. Akhtar S, Khan A, Sohaskey CD, Jagannath C, Sarkar D. Nitrite reductase NirBD is induced and plays an important role during in vitro dormancy of *Mycobacterium tuberculosis*. Journal of bacteriology. 2013;195(20):4592-9.

**APPENDIX 1: Development of cyclic di-GMP extraction and detection methods from animal tissues as a biomarker for biofilm-associated infections**

This Appendix describes the development of a novel method for extracting the bacterial second messenger cyclic diguanylate (c-di-GMP) from animal tissues. The work presented in this appendix and published research article[7] represent the first documentation for utilizing c-di-GMP as a biomarker of a bacterial-associated biofilm infection in animal tissues. Using a model of *Pseudomonas aeruginosa* endometritis in mares, we demonstrated that c-di-GMP can be detected *in vivo* in intra-luminal fluid and from biopsied tissue samples. The results obtained using the extraction and quantitation methods described herein indicate the potential for c-di-GMP as a diagnostic marker for bacterial biofilm-associated infections.

**A1.1 Cyclic di-GMP and *in vivo* bacterial pathogenesis**

Cyclic di-GMP is a cytoplasmic nucleotide molecule that conveys extracellular signals from the cell surface of most bacteria into an intracellular signal regulating cellular physiology, biochemistry, and ultimately bacterial pathogenesis (1). C-di-GMP is considered a "second messenger molecule" because it relays the extracellular cues or the "first messengers" to specific molecules inside the bacterial cell (1). Given that c-di-GMP is a nearly universal messenger in bacteria that facilitates the transition from planktonic to sessile bacteria in a biofilm state (1, 2), this molecule has the potential to serve as a biomarker for *in vivo* biofilms. C-di-GMP has been shown to control virulence properties associated with adhesion to eukaryotic epithelial tissue in the enteric pathogens *Salmonella enterica* serovar Typhimurim (3) and *Escherichia coli* O157:H7 (4). Additionally, *Pseudomonas aeruginosa* biofilms implanted in mice

---

[7] This work is presented in: Ferris, R.A., McCue, P., Borlee, G.I., Glapa, K., Martin, K.H., **Mangalea, M.R.**, Hennet, M., Wolfe, L., Broeckling, C.X., and Borlee, B.R. 2017. Model of Chronic Equine Endometritis Involving a *Pseudomonas aeruginosa* Biofilm. Infection and Immunity, 85 (12) e00332-17; DOI: 10.1128/IAI.00332-17

have been shown to be dispersed *in vivo* by reducing the concentration of c-di-GMP via induction of a c-di-GMP-reducing enzyme (5). While these experiments are extremely valuable for describing the role of c-di-GMP during *in vivo* biofilm infections, they do not provide methods for quantifying this important indicator of bacterial biofilm production. The techniques for intracellular quantification of c-di-GMP from an *in vivo* biofilm-associated infection are described here. These methods can be potentially further developed into a diagnostic biomarker for identifying biofilm-associated infections.

### A1.2 Development of a cyclic di-GMP tissue extraction method

Nucleotide extraction methods using perchloric acid were adapted from Irie and Parsek (6). Tissue samples with adherent biofilm material and bacterial extracellular non-adherent material were collected each in quadruplicate from randomly selected locations in the mare uterus.  Biological samples were kept warm (37°C) during collection and transport between the Veterinary Teaching Hospital and the Research Innovation Center. Wet weight of each sample was recorded prior to the extraction procedure for normalization. Samples were suspended in 900 $\mu$L fresh chilled extraction buffer (80% LC-MS grade water/20% acetonitrile) containing an internal control of chemically synthesized 2-Chloroadenosine-5'-O-monophosphate (2-Cl-5'-AMP, Axxora) at 100 nM. 70% vol/vol perchloric acid was added to a final concentration of 0.6 M and each sample was vortexed for 5 seconds followed by 30-minute incubation on ice. Samples were spun at 16,000 X g for 10 minutes at 4°C. Supernatant was transferred to a larger 15 mL conical tube before the addition of 219 $\mu$L 2.5 M $KHCO_3$ for acid neutralization. Neutralized samples were spun at 4000 X g for 10 minutes at 4°C before supernatant was removed and transferred to new 1.7 mL tubes. Samples were spun at 16,000 X g for 10 minutes at 4°C to remove remaining perchlorate salt precipitates. A calibration curve using known standards of chemically synthesized c-di-GMP in a 3-fold dilution series was generated in fresh

chilled extraction buffer (80% LC-MS grade water/20% acetonitrile) containing 100 nM 2-Cl-5'-AMP.

### A1.3 Development of LC-MS/MS methods for detection of cyclic-di-GMP

The following section (A1.3) and c-di-GMP detection protocol was written and developed by my collaborator Dr. Lisa Wolfe at the CSU Proteomics and Metabolomics Facility (PMF) for presentation in the Ferris et al. (7) publication referenced on the first page. Here are her methods:

LC-MS/MS was performed on a Waters Acquity M-Class UPLC coupled to a Waters Xevo TQ-S triple quadrupole mass spectrometer. Chromatographic separations were carried out on a Waters Atlantis dC18 stationary phase column (300 µm x 150 mm, 3.0-µm) column. Mobile phases were 99.9% acetonitrile, 0.1% formic acid (B) and water with 0.1% formic acid (A). The analytical gradient was as follows: time = 0 min, 5% B; time = 6.0 min, 97% B; time = 7 min, 97% B; time 8 min, 5% B; time 13 min, 5% B. The flow rate was 11.5 µL/min and injection volume was 1.0 µL. Samples were held at 4 °C in the autosampler, and the column was operated at 30 °C.  The MS was operated in selected reaction monitoring (SRM) mode, where a parent ion is selected by the first quadrupole, fragmented in the collision cell, then a fragment ion selected for by the third quadrupole. Transition ion mass-to-charge ratios (*m/z*) were the following for cyclic di-GMP: 691.1 > 540.1, 691.1 > 248.1, and 691.1 > 152.1. Transition ions for the internal standard (2-chloro-AMP) were set at 382.0 > 170.1. SMR transitions for target compounds, as well as collision energies and retention times, are described in **Table A1.1**. Product ions, collision energies, and cone voltages were optimized for each analyte by direct injection of individual synthetic standards. Inter-channel delay was set to 3 ms. The MS was operated in positive ionization mode with the capillary voltage set to 3.6 kV. Source temperature was 120 °C and desolvation temperature 350 °C. Desolvation gas flow was 1000 liters/hr, cone gas flow was 150 liters/hr, and collision gas flow was 0.2 ml/min. Nebulizer pressure (nitrogen)

was set to 7 Bar. Argon was used as the collision gas.  A calibration curve was generated using

authentic standards for each compound and their corresponding stable isotope labeled internal

standards in 100% methanol solution.

**Table A1.1 SRM transitions for target compounds.** Transition ion mass-to-charge (*m/z*)
ratios for c-di-GMP and the internal standard 2-cl-AMP, as well as explicit collision energies and
retention times.

| Ion Name | Precursor *m/z* | Product *m/z* | Explicit Collision Energy | Explicit Retention Time |
|---|---|---|---|---|
| cyclic-di-GMP | 691.11 | 540.1 | 42 | 2.1 |
| cyclic-di-GMP | 691.11 | 248.1 | 42 | 2.1 |
| cyclic-di-GMP | 691.11 | 152.1 | 42 | 2.1 |
| 2-chloro-AMP | 382 | 170.09 | 22 | 2.2 |

All raw data files were imported into the Skyline open source software package (8). Each

target analyte was visually inspected for retention time and peak area integration. Peak areas

were extracted for target compounds detected in biological samples and normalized to the peak

area of the appropriate internal standard in each sample. Normalized peak areas were exported

to Excel and absolute quantitation was obtained by using the linear regression equation

generated for each compound from the calibration curve.  Limits of detection (LOD) and limits of

quantification (LOQ) were calculated as 3 times or 10 times the standard deviation of the blank

divided by the slope of the calibration curve respectively (9). The limit of detection (LOD) was

calculated to be 0.64 pM and the limit of quantification (LOQ) was 2.14 pM (**Table A1.2**).

**Table A1.2 Limit of Detection (LOD) and Limit of Quantification (LOQ) for cyclic di-GMP.**
LOD and LOQ were calculated based on the standard deviation of the blank and the slope of
the calibration curve in the same matrix used for experimental extractions. Corrected values
represent the LOD and LOQ divided by the mass of c-di-GMP (690.1) multiplied by 1000 for pM.

| LOD/LOQ | | CORRECTED |
|---|---|---|
| STD DEV BLANK | 0.21582268 | |
| SLOPE | 0.002 | |
| LOD (NG/ML) | 0.443 | 0.64 |
| LOQ (NG/ML) | 1.478 | 2.14 |

## A1.4 *P. aeruginosa* equine endometriosis model of biofilm infection

A previously established model of equine endometriosis developed (10) in the lab of Dr. Ryan Ferris at the CSU Equine Reproduction Laboratories (ERL) was used to investigate bacterial biofilm-associated infection in an animal model. Healthy mares (n = 6) with no signs of current infections were inoculated with a mixture of three *lux*-labeled *P. aeruginosa* clinical isolates (PA004, PA035, and PA069) (11). After establishment of infection, the mares were sacrificed and uteruses were collected. Intra-luminal fluid was collected via wash and pipetting, while tissue samples were collected via biopsy. Four samples were collected at random for each intra-luminal fluid or tissue sample from each horse. Additionally, four control samples were collected by standard uterine biopsy for two uninfected control mares at the ERL.

Biological samples were maintained at consistent temperature and c-di-GMP was extracted directly following biopsy, as mentioned above. The c-di-GMP metabolite was extracted as above, and quantified via normalization to the internal standard 2-Cl-5'-AMP, as calculated by Dr. Lisa Wolfe under the supervision of Dr. Corey Broeckling at the CSU Proteomics and Metabolomics Facility (PMF). A standard curve using chemically synthesized c-di-GMP was used to normalize peak areas for experimental samples and absolute quantification was determined using the linear regression equation generated from the standards (**Figure A1.1**).
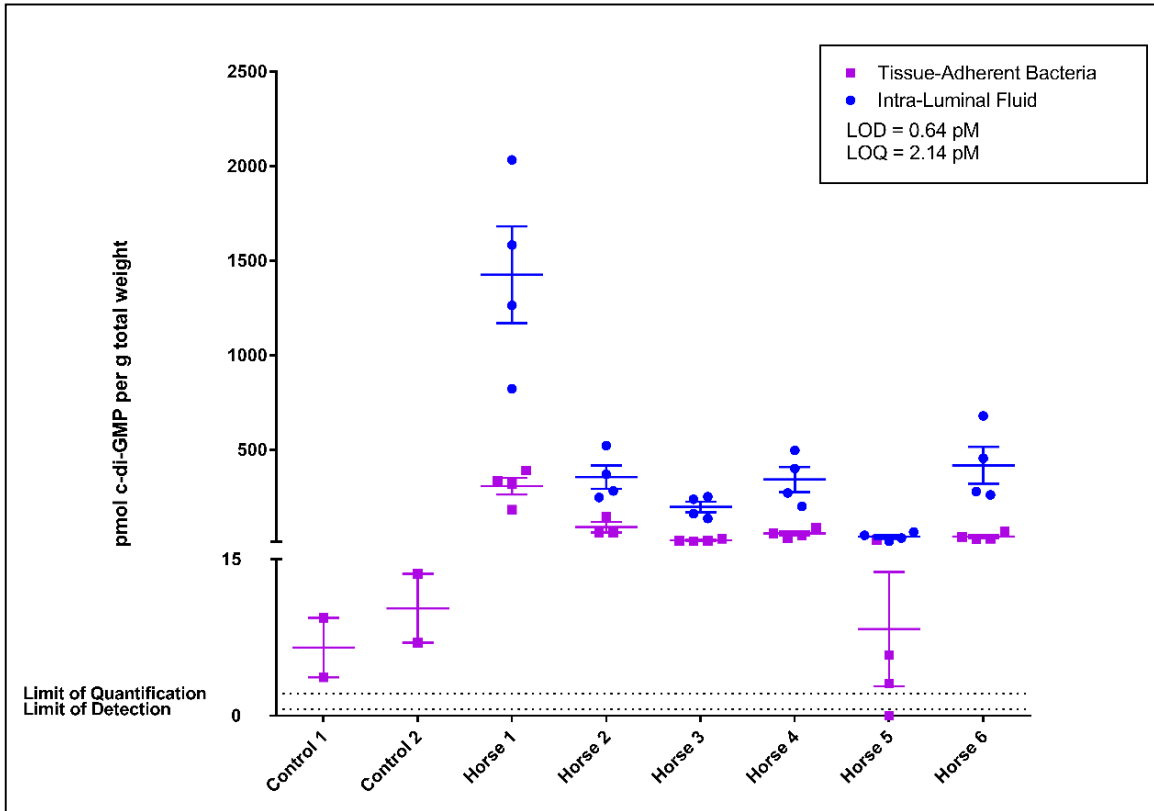
**Figure A1.1 LC-MS/MS quantitative analysis of the bacterial secondary messenger molecule, cyclic di-GMP, from uterine infections to detect *P. aeruginosa* biofilms.** Elevated cyclic di-GMP levels were detected in most tissue-adherent bacterial samples, except for those from samples obtained from horse 5, which were not elevated compared to those of control samples. Four samples of intraluminal fluid and tissue-adherent bacteria were collected at random locations from each infected uterus (n = 6). Four control samples were collected by uterine biopsy procedure from two uninfected mares. Amounts are represented as picomoles of cyclic di-GMP per gram of sample. The calculated limit of detection (LOD) is 0.64 pmol, and the calculated limit of quantification (LOQ) is 2.14 pmol. Experimental samples range from 3.1 pmol/g to 2,033 pmol/g cyclic di-GMP. Samples from which no cyclic di-GMP was detected are represented under the LOD line.

For each experimental horse in this study, c-di-GMP was measured successfully from the intra-luminal fluid in all four biological samples, while tissue-adherent bacteria samples did not produce significant levels of c-di-GMP from Horse 5 (**Figure A1.1**) For intra-luminal fluid samples, the average concentration of c-di-GMP detected was 463.65 pM, with a standard error of +/- 102.69 pM. The absolute quantification values for intra-luminal fluid (ILF) samples and the calculations for pmol/g based on sample weight are presented in **Table A1.3**. Horse 1 had the

highest observed c-di-GMP concentration, with the average of the four samples 1A – 1D being

1435.89 pM with a standard error of +/- 255.60 pM. The lowest c-di-GMP values were observed

for Horse 5, with the average of the four samples 5A – 5D being 40.66 pM +/- 10.51 pM.

Relative differences in absolute quantification of c-di-GMP exist across all samples despite

consistent sample weights (206.8 mg average for all samples).

**Table A1.3 Cyclic di-GMP absolute quantification values for intra-luminal fluid normalized to the sample weight.** Four biological samples of intra-luminal fluid were collected for each horse 1 – 6, indicated by letters A – D. Concentrations of c-di-GMP were standardized to 900 $\mu$L of extraction buffer used to suspend samples and normalized per gram of sample weight. Final concentrations are presented in the far-right column as pmol/g or pM.

| | c-di-GMP | | | weight | | |
| SAMPLE | ng/mL | ng/0.9 mL | pmol | mg | g | pmol/g |
|---|---|---|---|---|---|---|
| ILF 1A | 196.874 | 218.7 | 316.981 | 200.2 | 0.2002 | 1583.3239 |
| ILF 1B | 166.277 | 184.8 | 267.717 | 211.8 | 0.2118 | 1264.0102 |
| ILF 1C | 139.247 | 154.7 | 224.197 | 272.5 | 0.2725 | 822.7415 |
| ILF 1D | 296.801 | 329.8 | 477.871 | 235.0 | 0.2350 | 2033.4941 |
| ILF 2A | 37.090 | 41.2 | 59.718 | 240.9 | 0.2409 | 247.8948 |
| ILF 2B | 73.398 | 81.6 | 118.176 | 418.6 | 0.4186 | 282.3123 |
| ILF 2C | 57.827 | 64.3 | 93.106 | 178.2 | 0.1782 | 522.4829 |
| ILF 2D | 68.994 | 76.7 | 111.085 | 299.9 | 0.2999 | 370.4068 |
| ILF 3A | 12.238 | 13.6 | 19.704 | 143.3 | 0.1433 | 137.4995 |
| ILF 3B | 33.361 | 37.1 | 53.713 | 225.3 | 0.2253 | 238.4082 |
| ILF 3C | 28.012 | 31.1 | 45.101 | 178.6 | 0.1786 | 252.5233 |
| ILF 3D | 20.039 | 22.3 | 32.264 | 198.5 | 0.1985 | 162.5367 |
| ILF 4A | 63.425 | 70.5 | 102.118 | 205.2 | 0.2052 | 497.6532 |
| ILF 4B | 52.616 | 58.5 | 84.715 | 211.1 | 0.2111 | 401.3022 |
| ILF 4C | 24.652 | 27.4 | 39.692 | 145.8 | 0.1458 | 272.2327 |
| ILF 4D | 26.637 | 29.6 | 42.887 | 214.0 | 0.2140 | 200.4083 |
| ILF 5A | 4.206 | 4.7 | 6.773 | 103.3 | 0.1033 | 65.5627 |
| ILF 5B | 4.273 | 4.7 | 6.879 | 143.7 | 0.1437 | 47.8735 |
| ILF 5C | 1.313 | 1.5 | 2.113 | 129.5 | 0.1295 | 16.3200 |
| ILF 5D | 2.607 | 2.9 | 4.198 | 127.6 | 0.1276 | 32.8985 |
| ILF 6A | 26.834 | 29.8 | 43.205 | 154.8 | 0.1548 | 279.1012 |
| ILF 6B | 128.460 | 142.7 | 206.830 | 304.2 | 0.3042 | 679.9153 |
| ILF 6C | 65.911 | 73.2 | 106.121 | 233.3 | 0.2333 | 454.8695 |
| ILF 6D | 30.612 | 34.0 | 49.287 | 188.2 | 0.1882 | 261.8871 |

For tissue-adherent bacterial samples, the average concentration of c-di-GMP detected

was 87.12 pM with a standard error of 23.61 pM, which is considerably lower than intra-luminal

fluid samples. The absolute quantification values for tissue-adherent bacterial (TBA) samples

and the calculations for pmol/g based on sample weight are presented in **Table A1.4**. An

explanation for the lower observed c-di-GMP values in tissue-adherent bacterial samples is that these samples had a greater amount of host tissue, of which sample weight was used as a normalization method between samples.

**Table A1.4 Cyclic di-GMP absolute quantification values for tissue-adhered bacteria normalized to the sample weight.** Four biological samples of intra-luminal fluid were collected for each horse 1 – 6, indicated by letters A – D. Concentrations of c-di-GMP were standardized to 900 µL of extraction buffer used to suspend samples and normalized per gram of sample weight. Final concentrations are presented in the far-right column as pmol/g or pM. Rows are colored red for samples TBA indicate no c-di-GMP detected (TBA 2D) or improbable levels of c-di-GMP (TBA 5C) based on internal standard normalization. Rows in red indicate samples below limit of detection.

| SAMPLE | c-di-GMP ng/mL | ng/0.9 mL | pmol | weight mg | g | pmol/g |
|---|---|---|---|---|---|---|
| TBA 1A | 54.741 | 60.8 | 88.1 | 261.5 | 0.2615 | 337.0428952 |
| TBA 1B | 52.151 | 57.9 | 84.0 | 459.1 | 0.4591 | 182.8947748 |
| TBA 1C | 107.137 | 119.0 | 172.5 | 442.1 | 0.4421 | 390.1778671 |
| TBA 1D | 113.882 | 126.5 | 183.4 | 571.8 | 0.5718 | 320.6674397 |
| TBA 2A | 28.948 | 32.2 | 46.6 | 317.7 | 0.3177 | 146.7064359 |
| TBA 2B | 11.916 | 13.2 | 19.2 | 300 | 0.3 | 63.95075919 |
| TBA 2C | 9.414 | 10.5 | 15.2 | 246.2 | 0.2462 | 61.56742681 |
| TBA 2D | N/A | N/A | N/A | 482.8 | 0.4828 | N/A |
| TBA 3A | 2.694 | 3.0 | 4.3 | 224.4 | 0.2244 | 19.32636678 |
| TBA 3B | 2.734 | 3.0 | 4.4 | 242 | 0.242 | 18.18960228 |
| TBA 3C | 1.639 | 1.8 | 2.6 | 163.5 | 0.1635 | 16.13557612 |
| TBA 3D | 2.886 | 3.2 | 4.6 | 153.1 | 0.1531 | 30.35019852 |
| TBA 4A | 13.442 | 14.9 | 21.6 | 245.1 | 0.2451 | 88.30024474 |
| TBA 4B | 10.222 | 11.4 | 16.5 | 281.8 | 0.2818 | 58.40513557 |
| TBA 4C | 3.782 | 4.2 | 6.1 | 186.5 | 0.1865 | 32.65065603 |
| TBA 4D | 7.202 | 8.0 | 11.6 | 237.1 | 0.2371 | 48.90562052 |
| TBA 5A | 2.204 | 2.4 | 3.5 | 146.0 | 0.146 | 24.30317688 |
| TBA 5B | 0.450 | 0.5 | 0.7 | 233.8 | 0.2338 | 3.096365649 |
| TBA 5C | N/A | N/A | N/A | 157.3 | 0.1573 | N/A |
| TBA 5D | 0.626 | 0.7 | 1.0 | 173.3 | 0.1733 | 5.815662064 |
| TBA 6A | 3.176 | 3.5 | 5.1 | 168.3 | 0.1683 | 30.38034696 |
| TBA 6B | 3.469 | 3.9 | 5.6 | 204.2 | 0.2042 | 27.35220764 |
| TBA 6C | 12.397 | 13.8 | 20.0 | 295.8 | 0.2958 | 67.47883232 |
| TBA 6D | 7.705 | 8.6 | 12.4 | 311.3 | 0.3113 | 39.85331876 |

Control samples (CTR) were collected via biopsy from healthy mares that were not inoculated with *P. aeruginosa* and were free of infection (**Table A1.5**). C-di-GMP was detected at low levels, with an average concentration of 8.5 +/- 2.1 pM across four samples from two horses. These very low concentrations of c-di-GMP, when compared to ILF or TBA samples,

indicates either bacterial contamination from the vagina during sample collection or the

presence of subclinical bacterial infection.

**Table A1.5 Cyclic di-GMP absolute quantification values for control horse biopsies normalized to sample weight.** Two biological samples (A – B) were collected from two healthy mares (1 – 2) at the ERL.

| SAMPLE | c-di-GMP | | | weight | | |
| | ng/mL | ng/0.9 mL | pmol | mg | g | pmol/g |
| --- | --- | --- | --- | --- | --- | --- |
| CTR 1A | 0.791 | 0.8786 | 1.2731 | 135.5000 | 0.1355 | 9.4 |
| CTR 1B | 0.347 | 0.3861 | 0.5595 | 149.4000 | 0.1494 | 3.7 |
| CTR 2A | 0.630 | 0.7004 | 1.0150 | 144.3000 | 0.1443 | 7.0 |
| CTR 2B | 0.759 | 0.8433 | 1.2220 | 89.8000 | 0.0898 | 13.6 |

# References

1. Tamayo R, Pratt JT, Camilli A. Roles of cyclic diguanylate in the regulation of bacterial pathogenesis. Annual review of microbiology. 2007;61:131-48.
2. Hengge R. Principles of c-di-GMP signalling in bacteria. Nature reviews Microbiology. 2009;7(4):263-73.
3. Lamprokostopoulou A, Monteiro C, Rhen M, Romling U. Cyclic di-GMP signalling controls virulence properties of *Salmonella enterica serovar Typhimurium* at the mucosal lining. Environ Microbiol. 2010;12(1):40-53.
4. Hu J, Wang B, Fang X, Means WJ, McCormick RJ, Gomelsky M, Zhu MJ. c-di-GMP signaling regulates *E. coli* O157:H7 adhesion to colonic epithelium. Vet Microbiol. 2013;164(3-4):344-51.
5. Christensen LD, van Gennip M, Rybtke MT, Wu H, Chiang WC, Alhede M, Hoiby N, Nielsen TE, Givskov M, Tolker-Nielsen T. Clearance of *Pseudomonas aeruginosa* foreign-body biofilm infections through reduction of the cyclic Di-GMP level in the bacteria. Infect Immun. 2013;81(8):2705-13.
6. Irie Y, Parsek MR. LC/MS/MS-based quantitative assay for the secondary messenger molecule, c-di-GMP. Methods Mol Biol. 2014;1149:271-9.
7. Ferris RA, McCue PM, Borlee GI, Glapa KE, Martin KH, Mangalea MR, Hennet ML, Wolfe LM, Broeckling CD, Borlee BR. Model of Chronic Equine Endometritis Involving a *Pseudomonas aeruginosa* Biofilm. Infect Immun. 2017;85(12).
8. MacLean B, Tomazela DM, Shulman N, Chambers M, Finney GL, Frewen B, Kern R, Tabb DL, Liebler DC, MacCoss MJ. Skyline: an open source document editor for creating and analyzing targeted proteomics experiments. Bioinformatics. 2010;26(7):966-8.
9. Broccardo CJ, Schauer KL, Kohrt WM, Schwartz RS, Murphy JP, Prenni JE. Multiplexed analysis of steroid hormones in human serum using novel microflow tile technology and LC-MS/MS. J Chromatogr B Analyt Technol Biomed Life Sci. 2013;934:16-21.
10. Hinrichs K, Spensley MS, Mcdonough PL. Evaluation of Progesterone Treatment to Create a Model for Equine Endometritis. Equine Vet J. 1992;24(6):457-61.
11. Ferris RA, McCue PM, Borlee GI, Loncar KD, Hennet ML, Borlee BR. In Vitro Efficacy of Nonantibiotic Treatments on Biofilm Disruption of Gram-Negative Pathogens and an In Vivo Model of Infectious Endometritis Utilizing Isolates from the Equine Uterus. J Clin Microbiol. 2016;54(3):631-9.

**APPENDIX 2: Isolation of *Pandoraea pnomenusa sp.* from TerraForma 2.0 ecosystem box**

This appendix describes the discovery, isolation, and identification of an unexpected bacterial contaminant, *Pandoraea pnomenusa*, from the first experiment in the TerraForma 2.0 ecosystem. The overall goal of the experiment was to establish a *Burkholderia thailandensis* – *Oryza sativa* colonization model using the newly constructed TerraForma Box and to test bacterial dispersal in a controlled microcosm. Nitrate dosing was chosen as a treatment based on previous observations regarding nitrate's inhibitory effect of *B. pseudomallei* biofilms. A flooding treatment, independent of nitrate supplementation, was included to simulate real-world rice paddy scenarios. *B. thailandensis* was used as a non-infectious model organism and as a proxy for *B. pseudomallei*, which is a select agent and thus requires biosafety level 3 (BSL-3) approvals. The model rice cultivar Kitaake (*Oryza sativa L.* ssp*. japonica*) was used for the *in planta* model undergoing experimental treatments after *B. thailandensis* colonization. *Pandoraea pnomenusa* (identity confirmed by MALDI-TOF) was initially recovered from Kitaake plant roots in both the control and experimental soil plots in the TerraForma box and was also isolated from freshly germinated Kitaake seedlings prior to planting in soil. The complete genome of this newly-isolated *P. pnomenusa* was determined via *de novo* assembly at Pacific Biosciences. The complete genome sequence will be submitted to Microbiology Resource Announcements and deposited to GenBank.

**A2.1 *Burkholderia thailandensis* and materials for TerraForma 2.0 ecosystem**

*Burkholderia thailandensis* E264 was used in place of *B. pseudomallei* because it is exempt from select agent regulations and significantly less infectious (1, 2). *B. thailandensis* E264 was genetically engineered to constitutively bioluminesce via the integration of the *luxABCDE* operon into its chromosome (3). *B. thailandensis* E264 mini-Tn*7*-P1::-*lux* and a promoter-less negative control were visualized side-by-side in an IVIS Spectrum In Vivo

Imaging System (PerkinElmer) measuring luminescence counts after 24 hours of growth at

37°C on NAP-A agar plates (**Figure A2.1**). NAP-A medium is a modified Ashdown Agar

developed by the Dow Lab at CSU (4) containing a final composition of the following

ingredients: 4% glycerol, 5 mg/L crystal violet, 50 mg/L neutral red, 4 mg/L gentamicin, 4 mg/L

norfloxacin,10 mg/L ampicillin, and 3000 Units/L polymixin B in Trypsin-Soy agar (TSA). The

NAP-A medium contains four separate classes of antibiotics: aminoglycoside (gentamicin),
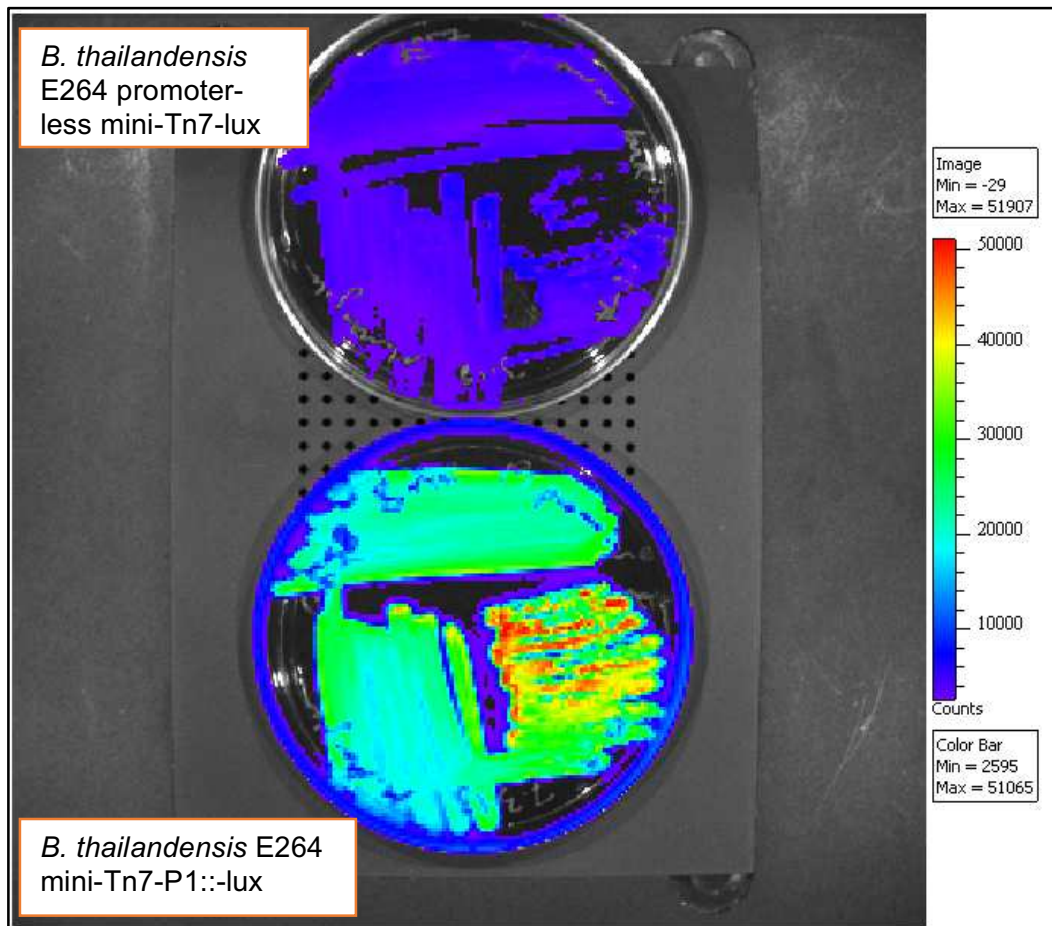


**Figure A2.1 Proof of concept visualization of *B. thailandensis* E264 mini-Tn7-P1::-*lux*
grown on NAP-A agar plates and imaged via IVIS luminescence.**

fluoroquinolone (norfloxin), beta-lactam (ampicillin), polymixin family (polymixin B); and was also

modified with the addition of a eukaryotic protein synthesis inhibitor (cycloheximide) to inhibit

fungal contamination from soil samples. The NAP-A medium was originally developed for the

detection of *B. pseudomallei* from gastro-intestinal tissues and feces from mice colonization

experiments (4), thus it was expected that only *Burkholderia* spp. would be capable of growth on this medium.

The TerraForma 2.0 ecosystem box (**Figure A2.2**) was built by senior undergraduate engineering students at CSU as part of their final thesis project. The box is sealed with rubber gaskets at every port of entry, maintains negative pressure, and has cross-current ventilation with air turnover every three minutes. The temperature and humidity of the box were maintained with engineered iridescent heaters and spray misting. The box allowed for four planting trays with soil atop a water reservoir for root hydration. Each of the planting trays contained 25 Kitaake plants, with soil mix up to 1 inch from top of the tray, and water levels were maintained up to the base of the planting tray.

Soil for experimental planting trays was a 50:50 mix of ProMix potting soil (Premier Tech) and Greens Grade porous ceramic (Profile). ProMix contains 65-85% Canadian sphagnum peat moss, perlite, vermiculite, dolomitic and calcitic limestone, and wetting agent. Kitaake were planted after germinatio, and root soak with *B. thailandensis* E264 as indicated, five by five and equidistant in the trays (**Figure A2.3**). In total, 100 Kitaake seedlings were used for the duration of this experiment.
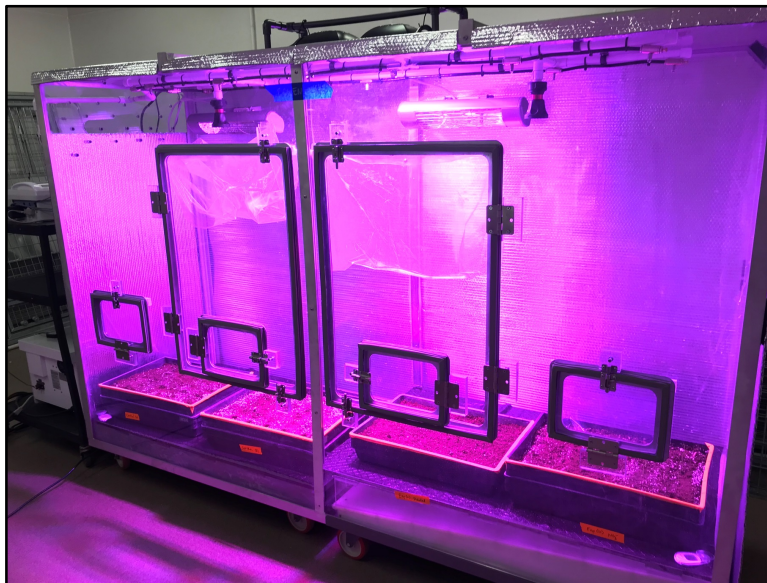


**Figure A2.2 TerraForma 2.0 ecosystem box.** Setup with the experimental planting trays used.
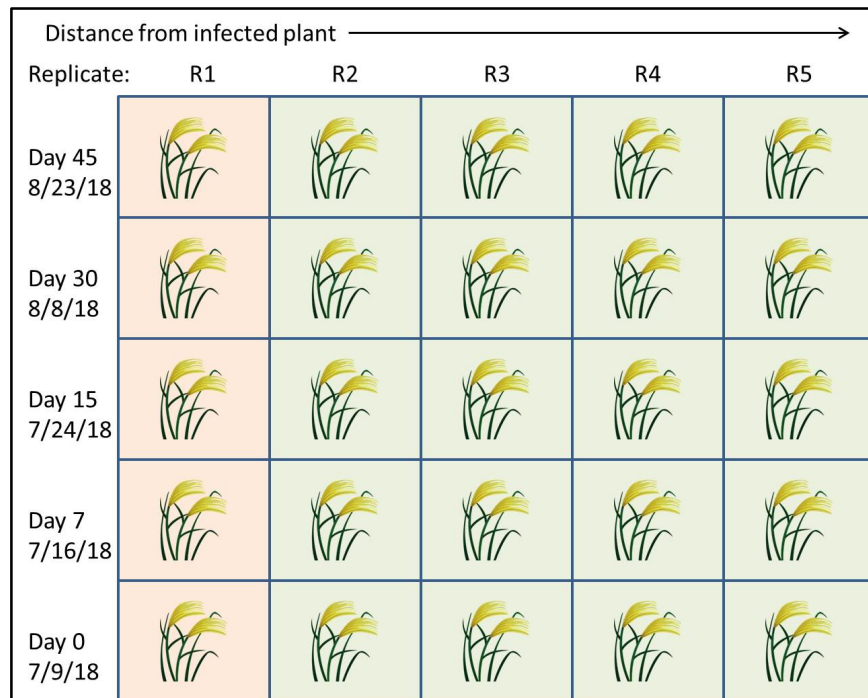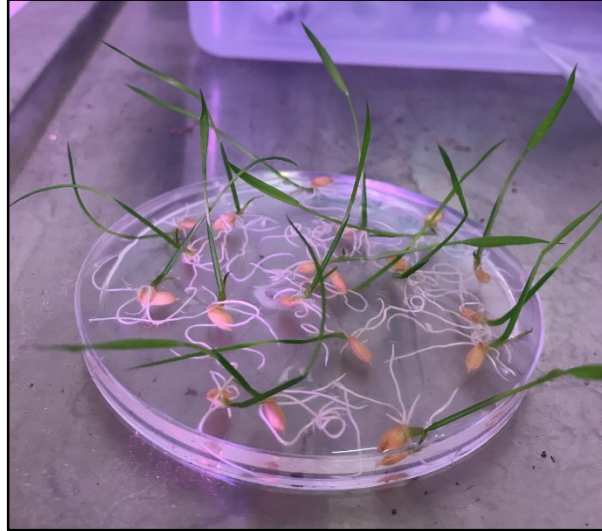
**Figure A2.3 Kitaake (*Oryza sativa L.* ssp*. japonica* tray setup.** 25 Kitaake rice plants were planted in five rows (R1 – R5), and collected as sets of five as perpendicular rows based on the labeled time-course (day post infection = 0, 7, 15, 30, 45). R1 (red) indicates infected plants for experimental treatment groups and R2 – R5 (green) indicate uninfected plants.

### A2.2 Experimental design for Kitaake rice plant colonization with *B. thailandensis*

The design for this experiment was formulated to answer two basic research questions:

1. Can we establish *Burkholderia* biofilm communities on rice plant seedlings using rice as the *in planta* model in the TerraForma 2.0 ecosystem box?

2. Does nitrate dosing of plant-associated *Burkholderia* biofilms *in situ* enhance colonization of plant body from roots and/or dispersal to neighboring plants?
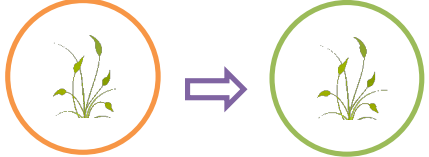
To answer the first question, we inoculated Kitaake seedlings with *lux*-labeled *B. thailandensis* using root-soaking methods described by Kaestli et al. (5) and Mattos et al. (6). First, Kitaake seedlings were germinated on wet sterile Whatman paper inside a petri dish. Next, seedlings were colonized with 1.7 x $10^9$ CFU/mL *B. thailandensis* for 1 hour by soaking the root system and seed in a petri dish (**Figure A2.4**). Root-soaked seedlings were then hand planted in row R1 of the treatment group planting trays as shown in in **Figure A2.3**. Treatment

**Figure A2.4 Root-soaking method for colonization of Kitaake seedlings (*Oryza sativa L. ssp*. *japonica*).** Germinated seedlings soaking in *B. thailandensis* culture for 1 h at room temperature.

of the experimental planting trays included dosing with 10 mM sodium nitrate every 2-3 days for all plants in one cohort and a flooding treatment for another, resulting in two experimental planting trays. The control planting trays included one tray with no bacterial root-soaked plants and no treatment, as well as another with *B. thailandensis* root-soaked plants in row R1 but with no treatment, resulting in two control trays. These groups and treatment conditions are represented in **Table A2.1**.

**Table A2.1 Experimental design for *Burkholderia thailandensis* E264 *(B. thai)* colonization experiments in the TerraForma 2.0 ecosystem box.** Orange circles represent established *B. thailandensis* plant-associated colonization and green circles represent plants that are initially free of any intentional bacterial contamination. Each row represents a planting tray in the box.

| Treatment | *in planta* colonization |
|-----------|--------------------------|
| **(A)** Control<br><br>No bacteria<br>No treatment |  |
| **(B)** Control<br><br>*B. thailandensis* E264<br>mini-Tn7-P1::-lux<br>No treatment |  |
| **(C)** Experimental<br><br>*B. thailandensis* E264<br>mini-Tn7-P1::-lux<br>10mM NaNO$_3$ added |  |
| **(D)** Experimental<br><br>*B. thailandensis* E264<br>mini-Tn7-P1::-lux<br>Flooded |  |

The primary goal of the first research question was to determine the feasibility of such a microcosm experiment starting in Biosafety Level 2 conditions using *B. thailandensis* before potential up-scaling to Biosafety Level 3 plus Select Agent regulations concerning *B. pseudomallei*. Additional goals were to develop a quantitative or semi-quantitative method to measure plant-associated bacterial loads at experimental end points, and to determine if there is an effect on plant growth after inoculation with *B. thailandensis*.

To answer the second research question, experimental treatments were applied to the plant cohorts illustrated in the bottom two rows of **Table A2.1**; nitrate dosing or flooding. The

first of these treatments, nitrate dosing, is derived from my observations in Chapter 3 suggesting that nitrate sensing and metabolism inhibit biofilm formation in *B. pseudomallei*. My hypothesis for the nitrate dosing experimental treatment was that *B. thailandensis* would not form localized biofilms in the rhizosphere of the Kitaake plants in nitrate-rich conditions, and therefore be more likely to colonize neighboring plants. In support of this hypothesis, Dalsing and Allen (7) have shown that nitrate metabolism enhances plant virulence and host root attachment by *Ralstonia solanacearum*, although nitrate assimilation decreases the amount of total extracellular polysaccharides (exopolysaccharides). The opposite physiology to a biofilm-dwelling sessile bacterium rich in exopolysaccharide production are planktonic free-swimming bacteria which are more likely to produce eukaryotic virulence factors (8). Interestingly, bacterial biofilms in the rhizosphere offer fundamental advantages to plant life, including metal and nutrient sequestrations, adhesion of plant roots to abiotic surfaces, overall soil structure, and nitrification of rice roots in rice paddies (9). Rice paddies are often flooded, producing anoxic conditions below the soil-water interface where species that are capable of nitrogen fixation and ammonia oxidation (i.e. *Nitrosomas*) form root-associated biofilms.

Flooded soils are heterogeneous throughout the soil column with the formation of oxic sites during soil aeration and anoxic zones where alternative terminal electron acceptors, such as nitrate, are utilized (10). Despite this dichotomy that leads to simultaneous nitrification and denitrification in oxic and anoxic microsites, respectively, nitrate can still accumulate in soils due to the slower denitrification process (10). To differentiate between conditions of nitrate metabolism and anoxic flooding, I separated these variables across the two treatment groups (**Table A2.1**), although realistically, these variables are co-occurring in rice paddy ecosystems.

### A2.3 Measurement of physiochemical parameters in TerraForma 2.0 box

To measure basic soil physiochemical properties, we used waterproof pH/temperature Testers (pHep®4 HI98127, Hanna Instruments). Testers were calibrated and used by

submerging approximately one inch into the soil until pH and temperature readings stabilized.

Two identical testers were used, and readings were taken in triplicate at random throughout

each planting tray (**Figure A2.5**). The air temperature was intentionally lowered on the

TerraForma box command panel after 35 days to test responsiveness of the soil temperature

(**Figure A2.6**). These results indicate that soil pH reached equilibrium around pH = 7 after

roughly 10 days and the soil temperature was noticeably lower for tray D, which was on the far-

right side of the box.
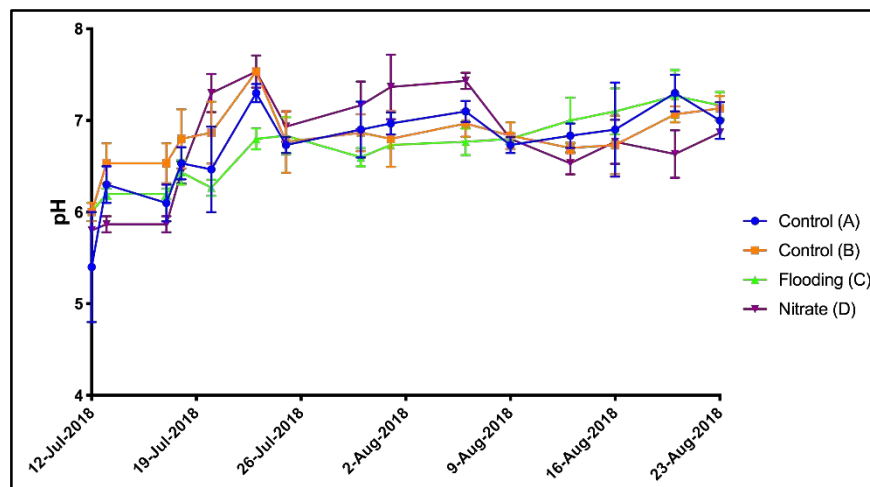


**Figure A2.5 Soil pH measurements throughout the course of the study.**
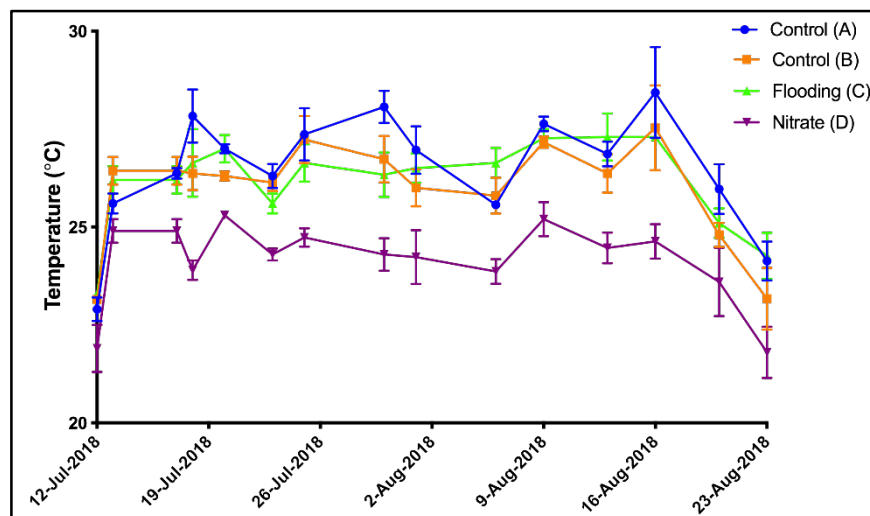


**Figure A2.6 Soil temperature measurements throughout the course of the study.**

191

## A2.4 Results from *B. thailandensis* colonization experiment

Five plants from each of the four planting trays (A – D) were collected at each time-point as indicated in **Figure A2.3** (d.p.i. = 0, 7, 15, 30, 45). Loose soil was gently brushed from the roots, but any root-adhered soil was transferred with the plant in a zip-lock bag. We visualized whole plants and attached root systems in the IVIS Spectrum, although these images were inconclusive for detecting luminescent bacteria due to the basal autofluorescence of plants (11). The roots were then rinsed with sterile 1X PBS, and the rinsed off soil and PBS was retained in the bag. Roots systems were removed from the leaves and transferred to 15 mL conical tubes, and suspended in 5 mL sterile 1X PBS. Root suspensions were placed in a bath sonicator (Branson) at 40 kHz for three 5-minute rounds with 5-second rounds of vortexing and incubation at room temperature for 5 minutes between each sonication. 100 $\mu$L of fluid from post-sonication root suspensions was removed and serially diluted in 10-fold dilutions, and 100 $\mu$L of the $10^{-2}$ dilutions were plated from each plant on NAP-A agar plates and incubated overnight at 37°C. Plates were visualized to calculate CFU/mL (**Figures A2.7 – A2.10**).
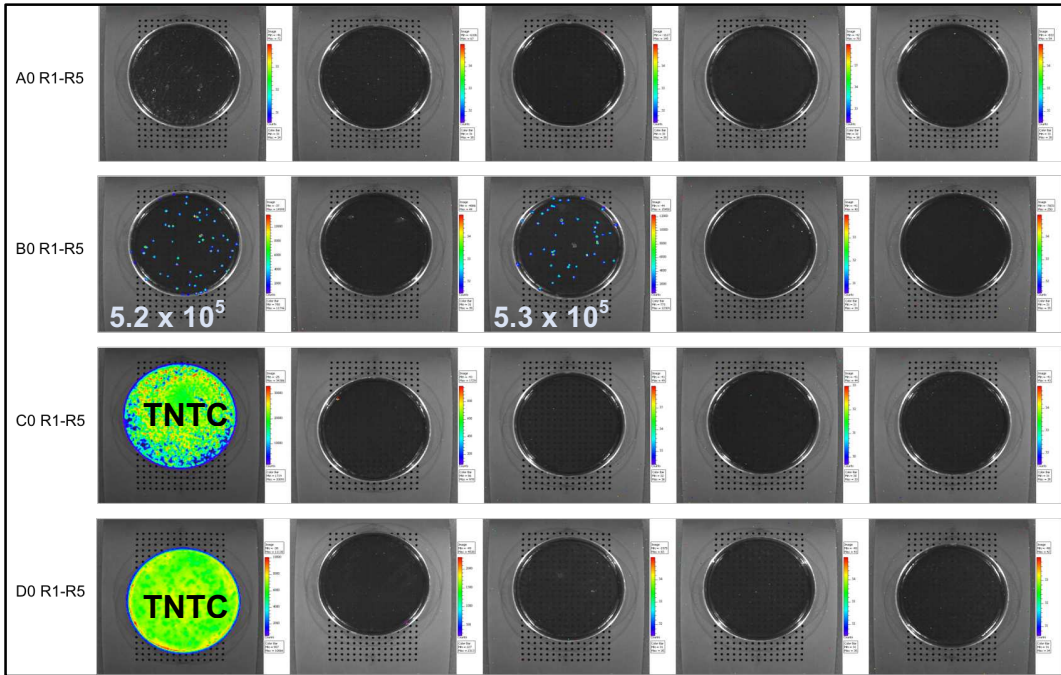
**Figure A2.7 Day 0 post root-soak infection.** Kitaake seedlings were mock-planted and removed after 1hr root soak. Values represent CFU/mL. TNTC = Too numerous to count.
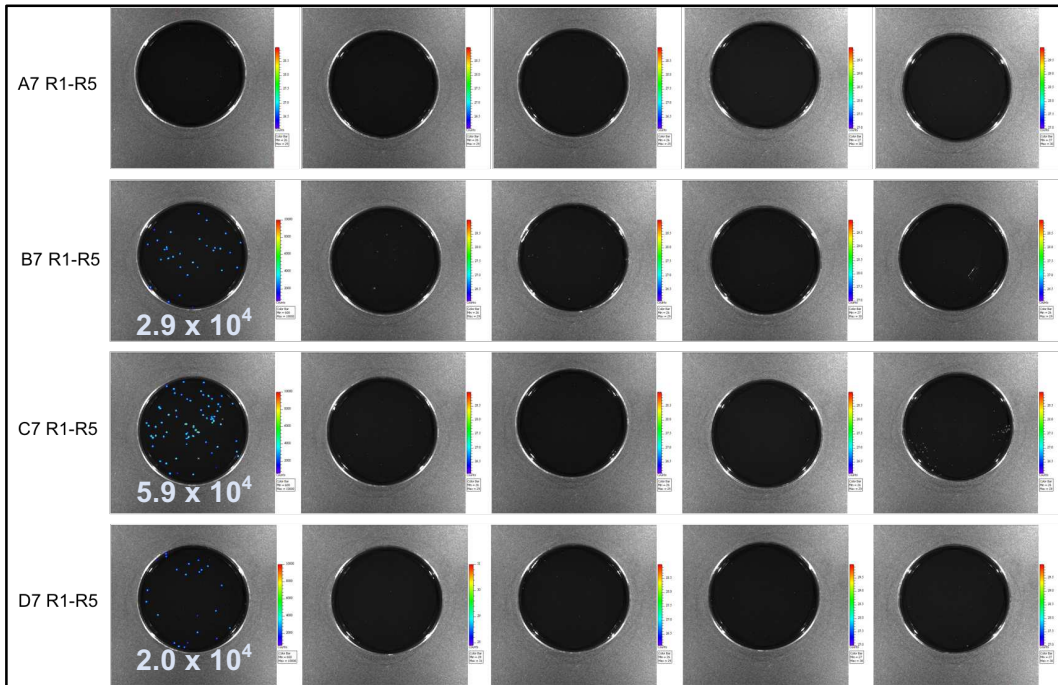


**Figure A2.8 Day 7 post root-soak infection.** Plants harvested after 7 days in soil. Values represent CFU/mL of resuspension buffer (1X PBS) for root sonication after uprooting from soil.
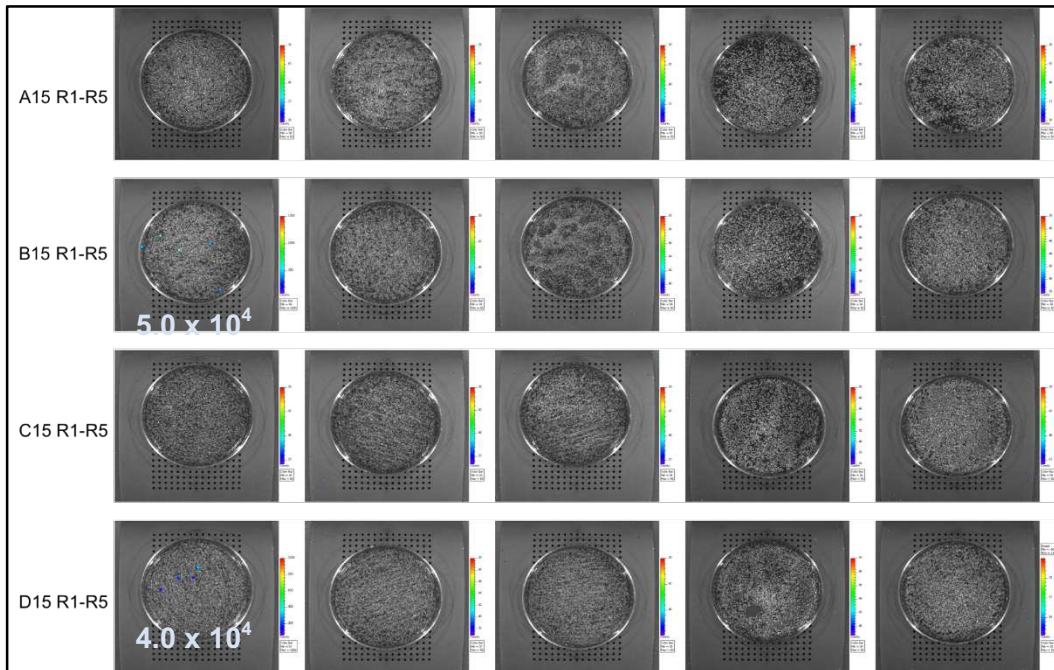
**Figure A2.9 Day 15 post root-soak infection.** Plants harvested after 15 days in soil. Values represent CFU/mL of resuspension buffer (PBS) for root sonication after uprooting from soil.
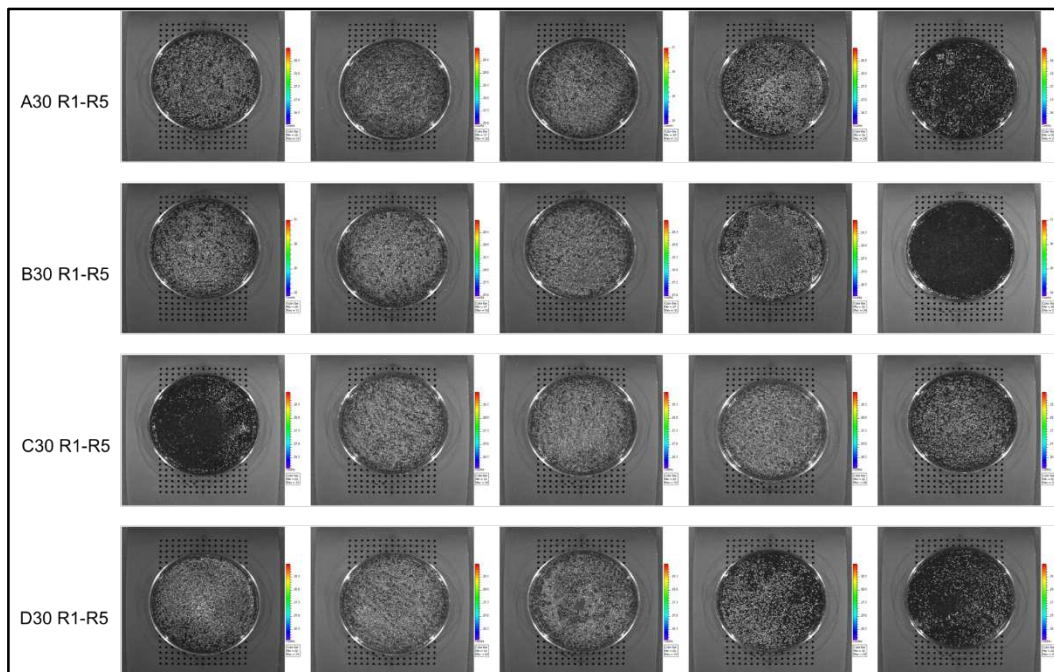


**Figure A2.10 Day 30 post root-soak infection.** Plants harvested after 30 days in soil. No more *lux*-labeled *B. thailandensis* is visible from any plant roots in any treatment or control group.

Luminescent *B. thailandensis* was recovered from roots at Day 0, Day 7, and Day 15 post infection. No luminescence was visible in the IVIS Spectrum from Day 30 (**Figure A2.10**) and Day 45 samples (data not shown). The initial bacterial inoculum for the root soak colonization was 1.7 x 10$^9$ CFU/mL, a relatively high calculation considering the target dosage was 2 x 10$^7$ CFU/mL *B. thailandensis*. Surprisingly, bacterial counts recovered from samples at Days 0, 7, and 15 were several orders of magnitude lower, ranging from 2 x 10$^4$ CFU/mL to 5.3 x 10$^5$ CFU/mL, although two samples were too many too count (**Figure A2.7**). All the observed luminescent bacteria throughout the course of the experiment was recovered from roots that were initially inoculated, R1 rows in planting trays B – D, except for the plant in R3 in planting tray B on Day 0 (**Figure A2.7**), suggesting possible contamination during the plant extraction process. Interestingly and coinciding with the loss of *lux*-labeled *B. thailandensis*, an unknown contaminating bacterium was recovered from roots at Day 15 and Day 30 (**Figures A2.9 and A2.10).** Every root system that was analyzed via sonication and plating on NAP-A medium generated a bacterial lawn from each of the four planting trays. All Day 45 NAP-A agar plates grew complete bacterial lawns that did not luminesce, indicating consistent contamination from Day 15 onward, and thus were not photographed.

## A2.5 Isolation of *Pandoraea pnomenusa*

The unidentified contaminating bacterium was isolated from multiple plates (A30-R5, B30-R1, B30-R5), struck for isolation on fresh NAP-A agar plates, and banked at -80°C in 50% glycerol. To determine whether these bacteria were native to the soil used in the TerraForma box experiments, we sampled germinating Kitaake seedlings that were not planted following the same procedure as the experimental plants. Surprisingly, colonies showing similar morphology to the contaminant were recovered from Kitaake seedlings that had no contact with the soil. To classify the unknown bacterium, we grew fresh colonies overnight on NAP-A medium at 37°C

and sampled colonies directly from the agar plates for MALDI Biotyper (Bruker) analysis. Colonies were patched onto the grid for the matrix-assisted laser desorption/ionization (MALDI) mass spectrometer along with 70% formic acid and α-cyano-4 -hydroxycinnamic acid (HCAA) matrix. Bacterial test standard (Bruker), which is *Escherichia coli* spiked with high molecular weight proteins, was used as a positive control. Four samples of the unknown bacteria, representing four separate agar plates, were analyzed in duplicate. Each sample assayed on the MALDI Biotyper was classified as *Pandoraea pnomenusa* or *Pandoraea* spp., with classification score values ranging from 2.0 – 2.2. Mass spectrometry data is compared to reference peaks, with score values between 0.00 – 3.00, and a value of greater or equal to 2.00 considered very high probability for test organism identification at the species level (12). The bacterial test standard was matched to *E. coli* with a classification score value of 2.308.

## A2.6 *Pandoraea pnomenusa* genome sequence analysis

The genus *Pandoraea* was characterized in 2000 by Coyne et al. (13) and was proposed to contain five species: *P. apista, P. pulmonicola, P. pnomenusa, P. sputorum,* and *P. norimbergensis* (formerly *Burkholderia norimbergensis*). These strains were isolated from the sputa of cystic fibrosis (CF) patients across North America (Canada and USA), South America (Brazil), and Europe (Denmark) (13) and therefore represent novel CF pathogens worldwide. The genus' name refers to Pandora's box, the origin of all disease, in Greek mythology (13). Phylogenetic analysis via 16S rDNA sequences shows close hierarchical clustering of the *Pandoraea* genus, which is intermediate to the *Burkholderia* and *Ralstonia* genera (**Figure A2.11**). Subsequent clinical investigations revealed that *Pandoraea pnomenusa* is capable of severe and fatal infections in patients with chronic lung disease, not unlike *Burkholderia spp.* (14-17). More recently, a novel respiratory pathogen has been described in the genus, *Pandoraea fibrosis* (18). To date, only 39 publications exist in the US National Library of Medicine (PubMed) with the search term "Pandoraea pnomenusa".
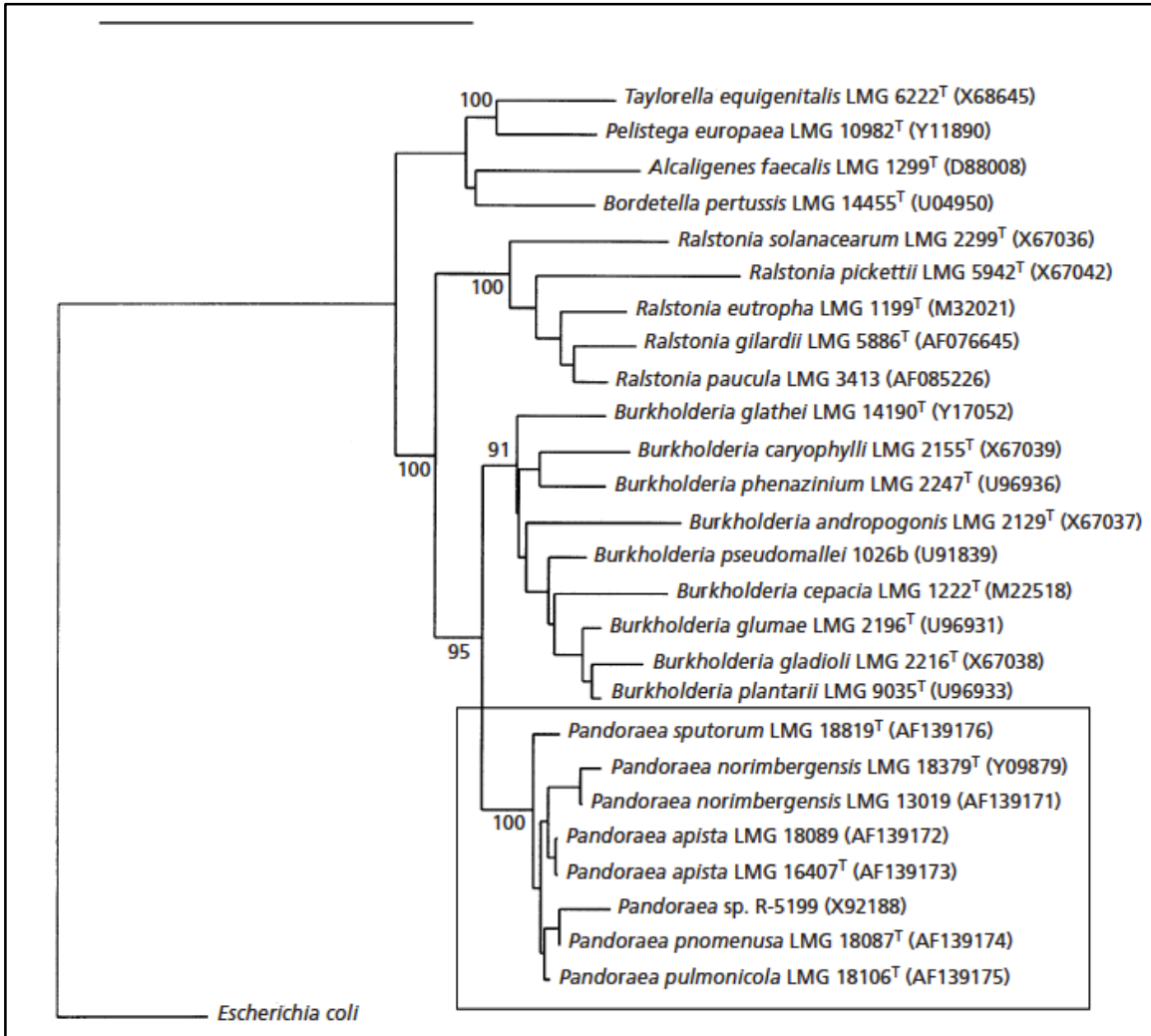
**Figure A2.11 Taken from Coyne et al., 2000 (13). Phylogenetic relationships of the genus *Pandoraea* (boxed) to other betaproteobacteria based on 16S rDNA sequences.** Relative phylogenetic distances are calculated to human, plant, and animal pathogens, including *B. pseudomallei* 1026b. *E. coli* represents the outgroup. Scale bar represents 10% similarity.

For *de novo* genome sequencing on the PacBio platform, the following protocol was used to extract genomic DNA from the *Pandoraea pnomenusa*. Fresh overnight colonies were resuspended directly from an LB agar plate into 200 μL 1X PBS and 200 μL 1% SDS plus 100 μL Proteinase K (Sigma) and incubated at 37°C for 30 min. Next, 100 μL of 0.5M NaCl was added before another incubation at 65°C for 30 min to lyse cells. After lysis, 200 μL of a fresh solution of 25:24:1 phenol: chloroform: isoamyl alcohol was added, followed by vigorous vortexing, and a centrifugation at 14,000 rpm for 12 min at 4°C. Next, the aqueous layer was

removed and transferred to a new tube with a cut pipette tip to avoid shearing. 800 μL of 25:24:1 phenol: chloroform: isoamyl alcohol was added before another vortex and spin at 14,000 rpm for 12 min at 4°C. The aqueous solution was then removed and transferred to a new tube, again with a cut tip to avoid shearing, before the addition of 800 μL 95% ethanol, mixing, and spinning at 14,000 rpm for 12 min at 4°C. The supernatant was decanted before adding 300 μL 80% ethanol and spinning at 14,000 rpm for 15 min at 4°C. The remaining pellet was resuspended in 100 μL 10mM Tris-HCL before treatment with 0.1 mg/mL RNase A (Sigma) and incubated at 37°C for 30 min. Genomic DNA was stored at -20°C until transport to sequencing facility.

Extracted genomic DNA was sent to Pacific Biosciences for single molecule real-time (SMRT) sequencing for *de novo* assembly of the *Pandoraea pnomenusa* genome and assembly into a single contig. The assembled contig is 5,499,432 bases that encodes a predicted 5106 genes from one DNA scaffold and no plasmids with 64.8% GC-rich content. Rapid Annotations using Subsystems Technology (RAST) (19) server analysis revealed that 30% of the predicted coding sequences coincided with 353 subsystems in the metabolic reconstruction of the genome (**Figure A2.12**). Interestingly, in the "Virulence, Disease, and Defense" Subsystem, *Pandoraea pnomenusa* contains 41 genetic features associated with "resistance to antibiotics and toxic compounds", including 5 multidrug resistance efflux pumps and 1 beta-lactamase. These comprehensive mechanisms for antibiotic resistance partially explain why we could isolate this bacterium on the NAP-A medium agar. The sequenced genome of this isolate confirms the characterization of the MALDI Biotyper. Analysis via RAST denotes the following taxonomy: Bacteria; Proteobacteria; Betaproteobacteria; Burkholderiales; Burkholderiacaea; Pandoraea; Pandoraea pnomenusa.

Lastly, whole genome sequence comparisons were performed using MAUVE (**Figure A2.13**) and EasyFig (**Figure A2.14**). By aligning whole genome sequences in this manner, a

broad picture of genome evolution can be illustrated, characterizing orthologous regions and potential duplications, losses, inversions, and horizontal transfer. MAUVE uses Locally Collinear Blocks (LCBs), conserved orthologous segments that did not undergo genome rearrangement to visualize genome alignments (20). Based on my analysis, *Pandoraea pnomenusa* DSM16536 and *Pandoraea pnomenusa* TF 2018 share two LCBs showing a region of sequence inversion at the ends of each chromosome (**Figure A2.13**). This genome analysis was further verified using blastn homology in the EasyFig pipeline, set with minimum blastn thresholds of 60% identity and E-value of 1E10-3 (**Figure A2.14**). According to this analysis, it is evident that the two sequences are extremely similar, with largescale genome inversions comprising two LCBs that correspond directly to the MAUVE analysis.
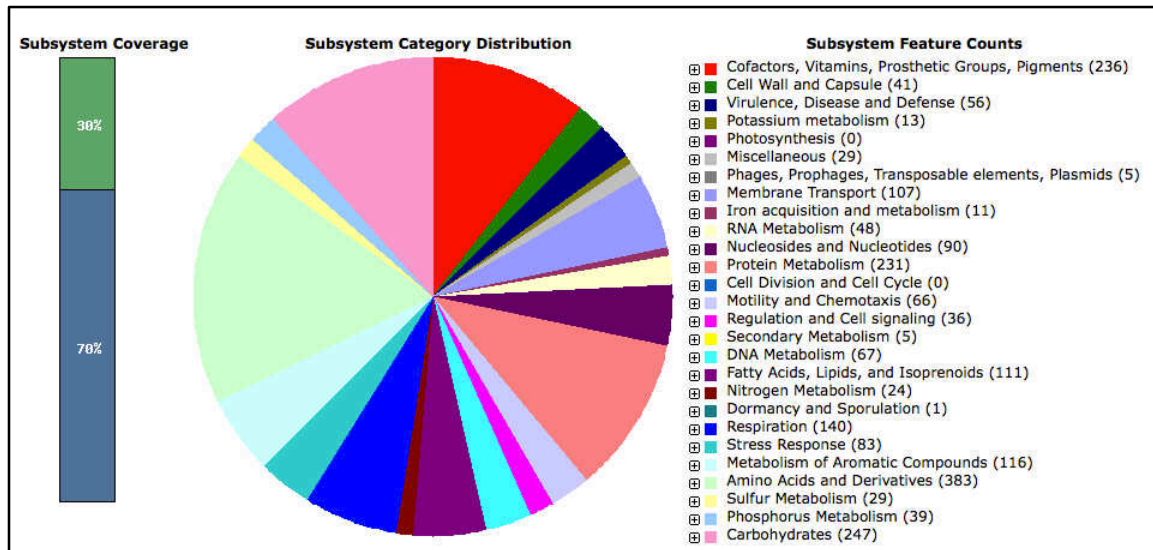


**Figure A2.12 RAST Server Subsystem Coverage and Category Distribution for *Pandoraea pnomenusa***
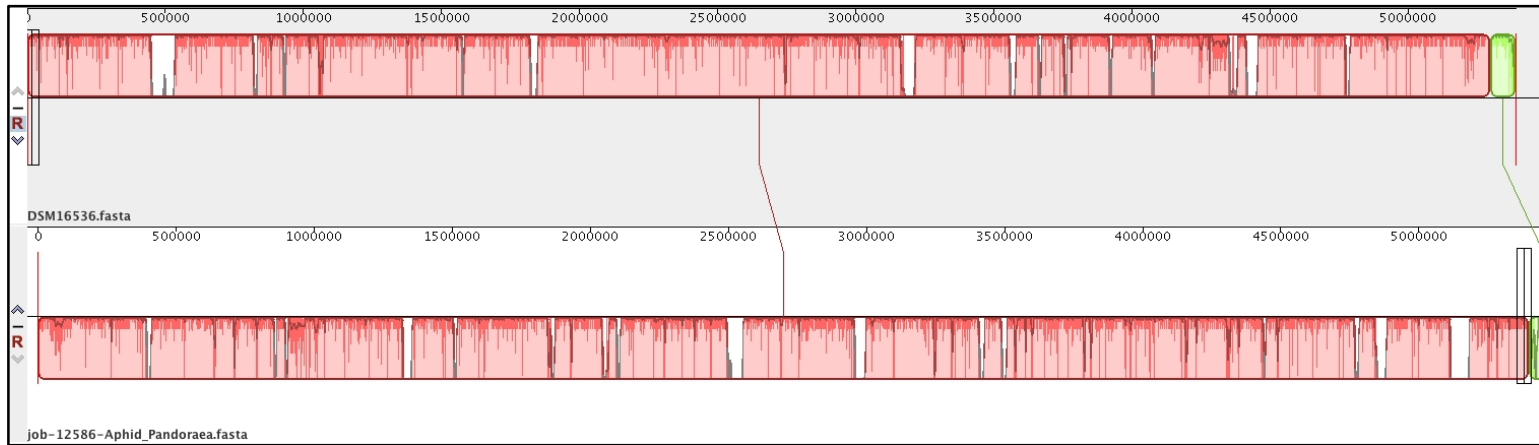
**Figure A2.13 MAUVE genome alignment of *Pandoraea pnomenusa* DSM16536 and *Pandoraea pnomenusa* TF 2018**
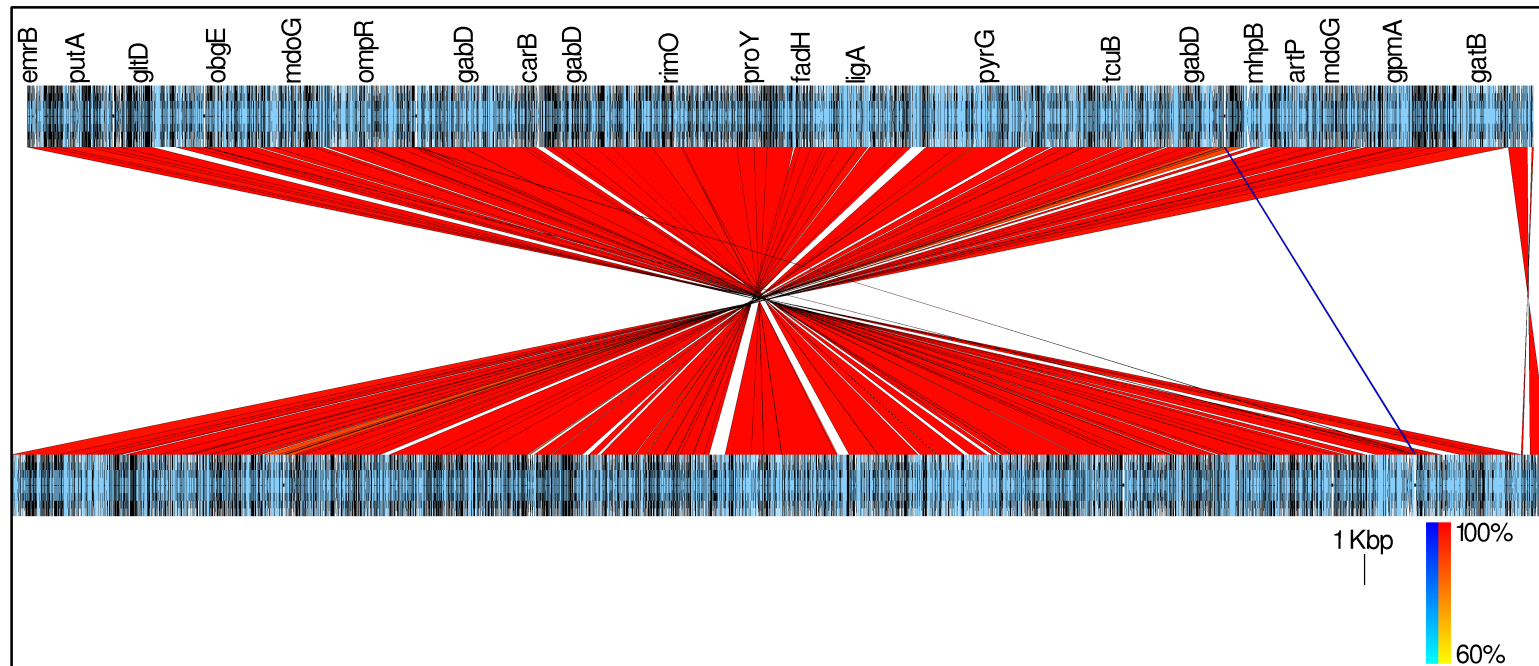


**Figure A2.14 Whole genome blast comparison of *Pandoraea pnomenusa* DSM16536 and *Pandoraea pnomenusa* TF 2018**

# References

1.  Haraga A, West TE, Brittnacher MJ, Skerrett SJ, Miller SI. *Burkholderia thailandensis* as a model system for the study of the virulence-associated type III secretion system of *Burkholderia pseudomallei*. Infect Immun. 2008;76(11):5402-11.
2.  Brett PJ, Deshazer D, Woods DE. Characterization of *Burkholderia pseudomallei* and *Burkholderia pseudomallei*-like strains. Epidemiol Infect. 1997;118(2):137-48.
3.  Choi KH, Gaynor JB, White KG, Lopez C, Bosio CM, Karkhoff-Schweizer RR, Schweizer HP. A Tn7-based broad-range bacterial cloning and expression system. Nat Methods. 2005;2(6):443-8.
4.  Goodyear A, Strange L, Rholl DA, Silisouk J, Dance DA, Schweizer HP, Dow S. An improved selective culture medium enhances the isolation of *Burkholderia pseudomallei* from contaminated specimens. Am J Trop Med Hyg. 2013;89(5):973-82.
5.  Kaestli M, Schmid M, Mayo M, Rothballer M, Harrington G, Richardson L, Hill A, Hill J, Tuanyok A, Keim P, Hartmann A, Currie BJ. Out of the ground: aerial and exotic habitats of the melioidosis bacterium *Burkholderia pseudomallei* in grasses in Australia. Environ Microbiol. 2012;14(8):2058-70.
6.  Mattos KA, Padua VL, Romeiro A, Hallack LF, Neves BC, Ulisses TM, Barros CF, Todeschini AR, Previato JO, Mendonca-Previato L. Endophytic colonization of rice (*Oryza sativa* L.) by the diazotrophic bacterium *Burkholderia kururiensis* and its ability to enhance plant growth. An Acad Bras Cienc. 2008;80(3):477-93.
7.  Dalsing BL, Allen C. Nitrate assimilation contributes to *Ralstonia solanacearum* root attachment, stem colonization, and virulence. J Bacteriol. 2014;196(5):949-60.
8.  Chen Y, Lv M, Liao L, Gu Y, Liang Z, Shi Z, Liu S, Zhou J, Zhang L. Genetic Modulation of c-di-GMP Turnover Affects Multiple Virulence Traits and Bacterial Virulence in Rice Pathogen *Dickeya zeae*. PLoS One. 2016;11(11):e0165979.
9.  Morris CE, Monier JM. The ecological significance of biofilm formation by plant-associated bacteria. Annu Rev Phytopathol. 2003;41:429-53.
10. Fritzsche A, Pagels B, Totsche KU. The composition of mobile matter in a floodplain topsoil: A comparative study with soil columns and field lysimeters. Journal of Plant Nutrition and Soil Science. 2016;179(1):18-28.
11. Garcia-Plazaola JI, Fernandez-Marin B, Duke SO, Hernandez A, Lopez-Arbeloa F, Becerril JM. Autofluorescence: Biological functions and technical applications. Plant Sci. 2015;236:136-45.
12. Bruker. MALDI Biotyper CA System - Clinical Application for Identification of Microorganisms. In: Bruker, editor. https://wwwbrukercom/fileadmin/user_upload/8-PDF-Docs/Separations_MassSpectrometry/Literature/Brochures/MALDI-biotyper-CA-Brochure_08-2014_ebookpdf: Bruker Daltronics Inc.; 2014.
13. Coenye T, Falsen E, Hoste B, Ohlen M, Goris J, Govan JR, Gillis M, Vandamme P. Description of *Pandoraea* gen. nov. with *Pandoraea apista* sp. nov., *Pandoraea pulmonicola* sp. nov., *Pandoraea pnomenusa* sp. nov., *Pandoraea sputorum* sp. nov. and *Pandoraea norimbergensis* comb. nov. Int J Syst Evol Microbiol. 2000;50 Pt 2:887-99.
14. Ambrose M, Malley RC, Warren SJ, Beggs SA, Swallow OF, McEwan B, Stock D, Roddam LF. *Pandoraea pnomenusa* Isolated from an Australian Patient with Cystic Fibrosis. Front Microbiol. 2016;7:692.
15. Ee R, Ambrose M, Lazenby J, Williams P, Chan KG, Roddam L. Genome Sequences of Two *Pandoraea pnomenusa* Isolates Recovered 11 Months Apart from a Cystic Fibrosis Patient. Genome Announc. 2015;3(1).

16. Lim YL, Ee R, Yong D, Yu CY, Ang GY, Tee KK, Yin WF, Chan KG. Complete Genome Sequence Analysis of *Pandoraea pnomenusa* Type Strain DSM 16536(T) Isolated from a Cystic Fibrosis Patient. Front Microbiol. 2016;7:109.

17. Stryjewski ME, LiPuma JJ, Messier RH, Jr., Reller LB, Alexander BD. Sepsis, multiple organ failure, and death due to *Pandoraea pnomenusa* infection after lung transplantation. J Clin Microbiol. 2003;41(5):2255-7.

18. See-Too WS, Ambrose M, Malley R, Ee R, Mulcahy E, Manche E, Lazenby J, McEwan B, Pagnon J, Chen JW, Chan KG, Turnbull L, Whitchurch CB, Roddam LF. *Pandoraea fibrosis* sp. nov., a novel *Pandoraea* species isolated from clinical respiratory samples. Int J Syst Evol Microbiol. 2019.

19. Aziz RK, Bartels D, Best AA, DeJongh M, Disz T, Edwards RA, Formsma K, Gerdes S, Glass EM, Kubal M, Meyer F, Olsen GJ, Olson R, Osterman AL, Overbeek RA, McNeil LK, Paarmann D, Paczian T, Parrello B, Pusch GD, Reich C, Stevens R, Vassieva O, Vonstein V, Wilke A, Zagnitko O. The RAST Server: rapid annotations using subsystems technology. BMC Genomics. 2008;9:75.

20. Darling AC, Mau B, Blattner FR, Perna NT. Mauve: multiple alignment of conserved genomic sequence with rearrangements. Genome Res. 2004;14(7):1394-403.

**APPENDIX 3: Bioinformatics toolkit for comparative analyses and illustration of *Burkholderia spp.* polysaccharide clusters[8]**

This appendix describes the application of various computational biology resources used for the analysis, illustration, and comparison of several polysaccharide gene clusters across relevant *Burkholderia* species. Several of the figures and methods presented in this appendix have been contributions to published research articles or articles in preparation for publication. The overall goals of this work were to develop methods for visualizing relatively large gene sets across species in the *Burkholderia pseudomallei* cluster (BPC), and to provide a framework for comparing homologous polysaccharide clusters that have remained ambiguous in the *Burkholderia* literature. The results and methods presented here will hopefully be an aid for researchers by contributing a clearer genomic understanding of the many clinically relevant polysaccharides produced by *Burkholderia*.

**A3.1 Identification of capsular polysaccharide clusters in *B. pseudomallei* 1026b**

Bacterial polysaccharides are defined and categorized as capsules (CPS), extracellular polysaccharides (exopolysaccharides), lipopolysaccharides (LPS); and copolymers such as teichoic acids (TA) and peptidoglycans (1). These polysaccharides are ubiquitous across a broad range of bacterial species in varying abundance, whether Gram-negative, Gram-positive, or Gram-variable. The omnipresence of polysaccharide production in bacteria can be explained by the essential physical functions provided by these sugars. In general, bacterial polysaccharides provide protection from environmental stressors and predators, mediate

---

[8] This work is presented in: Borlee, G.I., Plumley, B.A., Martin, K.H., Somprasong, N., **Mangalea, M.R.**, Islam, N.M., Burtnick, M.N., Brett, P.J., Steinmetz, I., AuCoin, D.P., Belisle, J.T., Crick, D., Schweizer, H.P., and Borlee, B.R. 2017. Genome-scale analysis of the genes that contribute to *Burkholderia pseudomallei* biofilm formation identifies a crucial exopolysaccharide biosynthesis gene cluster. *PLoS Neglected Tropical Diseases*, 11 (6): e0005689

bacteria-bacteria interactions, and are primary antigens at the host-pathogen interface. Bacterial polysaccharides are also key components of the extracellular polymeric substance (EPS) matrix that makes up bacterial biofilms, structures relevant to bacterial survival in both environmental and clinical settings.

Burkholderia pseudomallei produces four known polysaccharide clusters defined as CPS (2), of which CPSI has been defined as a primary antigen and potential vaccine candidate (3-5). Most, if not all, previous work describing B. pseudomallei CPS coding regions have been in the strain B. pseudomallei K96243. Because our lab works with the clinical isolate B. pseudomallei 1026b, I characterized CPSI – CPSIV clusters in this closely related species (**Tables A3.1 – A3.4**). The four clusters described in these tables were identified in a 2012 book chapter (2) and were based on sequence analysis of the whole-genome complete sequence of B. pseudomallei strain K96243 (6). Homologous genes in Bp1026b were identified by blastn (NCBI) comparing K96243 gene nucleotide sequences against the Bp1026b reference genome on the Burkholderia Genome Data Base (7). Capsule cluster CPSI, which has been shown to be a major virulence factor (8), spans loci BPSL2786-2810/Bp1026b_0499-0524 on chromosome 1. CPSI encodes glycosyltransferases, transporters, sugar and lipid biosynthesis genes, along with genes of unknown function and the pseudogene BPSL2806a (9). Gene annotations and putative functions for CPS I were cross-referenced with the Burkholderia Genome Data Base for gene names and product descriptions (7). Capsule cluster CPSII spans loci BPSS0417-0429/Bp1026b_II0468-0480 on chromosome 2. Capsule cluster CPSIII, which has been shown to not be a virulence determinant but possibly important for environmental resilience (10), spans loci BPSS1825-1835/Bp1026b1956-1966 on chromosome 2. CPSIII encodes genes for galactose, glucose, mannose, and xylose synthesis (10). Capsule cluster CPSIV spans loci BPSL2769-2785/Bp1026b_I0543-0525 on chromosome 1. Interestingly, Bp1026b has two additional hypothetical genes annotated in capsule cluster CPSIV, Bp1026b_I0527 and Bp1026b_I0528. CPSII, III, and IV gene names were proposed by Reckseidler-Zenteno (2)

**Table A3.1 Homologous gene loci for the CPSI biosynthesis cluster between *Bp* 1026b and *Bp* K96243, including names and putative functions for each gene.**

| *B. pseudomallei* 1026b locus | Gene Name | *B. pseudomallei* K96243 locus | Putative Function |
|---|---|---|---|
| BP1026B_I0499 | *manC* | BPSL2810 | Sugar biosynthesis; mannose-1-phosphate guanylyltransferase/ mannose-6-phosphate isomerase |
| BP1026B_I0500 | *wcbA* | BPSL2809 | Transporter; capsular polysaccharide biosynthesis/export periplasmic protein |
| BP1026B_I0501 | *wcbB* | BPSL2808 | Glycosyltransferase; capsular polysaccharide biosynthesis/export periplasmic protein |
| BP1026B_I0502 | *wcbC* | BPSL2807 | Transporter; capsular polysaccharide biosynthesis/export periplasmic protein |
| N/A | *manB* | BPSL2806a | Pseudogene; capsular polysaccharide export/inner membrane |
| BP1026B_I0503 | *wcbD* | BPSL2806 | Transporter; capsular polysaccharide export system inner membrane protein |
| BP1026B_I0504 | *wzm2* | BPSL2805 | Transporter; ABC-2 type transport system integral membrane protein |
| BP1026B_I0505 | *wzt2* | BPSL2804 | Transporter; polysaccharide ABC transporter, ATP-binding protein |
| BP1026B_I0506 | *wcbE* | BPSL2803 | Glycosyltransferase; group 1 family protein |
| BP1026B_I0507 | *wcbF* | BPSL2802 | CPS biosynthesis protein |
| BP1026B_I0508 | *wcbG* | BPSL2801 | CPS biosynthesis protein |
| BP1026B_I0510 | *wcbH* | BPSL2800 | Glycosyltransferase; group 1 family protein |
| BP1026B_I0511 | *wcbI* | BPSL2799 | CPS biosynthesis protein |
| BP1026B_I0512 | *wcbJ* | BPSL2798 | capsular polysaccharide biosynthesis protein, NAD-dependent epimerase |
| BP1026B_I0513 | *wcbK* | BPSL2797 | Sugar biosynthesis; GDP-mannose 4,6-dehydratase |
| BP1026B_I0514 | *wcbL* | BPSL2796 | Sugar biosynthesis; D,D-heptose 7-phosphate kinase |
| BP1026B_I0515 | *gmhA* | BPSL2795 | Sugar biosynthesis; Sedoheptulose-7-phosphate isomerase |
| BP1026B_I0516 | *wcbM* | BPSL2794 | Sugar biosynthesis, D-glycero-D-manno-heptose 1-phosphateguanosyltransferase |
| BP1026B_I0517 | *wcbN* | BPSL2793 | Sugar biosynthesis, D-glycero-D-manno-heptose 1,7-bisphosphatephosphatase |
| BP1026B_I0518 | *wcbO* | BPSL2792 | capsular polysaccharide export protein |
| BP1026B_I0519 | *wcbP* | BPSL2791 | Lipid biosynthesis; short chain dehydrogenase/reductase family oxidoreductase |
| BP1026B_I0520 | *wcbQ* | BPSL2790 | Lipid biosynthesis; CPS biosynthesis |
| BP1026B_I0521 | *wcbR* | BPSL2789 | Lipid biosynthesis; CPS biosynthesis fatty acid synthase |
| BP1026B_I0522 | *wcbS* | BPSL2788 | Lipid biosynthesis; UDP-3-O-[3-hydroxymyristoyl] N-acetylglucosamine deacetylase |
| BP1026B_I0523 | *wcbT* | BPSL2787 | Lipid biosynthesis; class-I aminotransferase |
| BP1026B_I0524 | N/A | BPSL2786 | Acetyltransferase |

**Table A3.2 Homologous gene loci for the CPSII biosynthesis cluster.**

| *B. pseudomallei* 1026b locus | Gene Name | *B. pseudomallei* K96243 locus | Putative Function |
|---|---|---|---|
| BP1026B_II0468 | *kpsD* | BPSS0417 | Capsule polysaccharide export system periplasmic protein |
| BP1026B_II0469 | *kpsE* | BPSS0418 | Transport-related membrane protein |
| BP1026B_II0470 | *rfbF* | BPSS0419 | Glucose-1-phosphate cytidylyltransferase |
| BP1026B_II0471 | *rfbG* | BPSS0420 | CDP-glucose 4,6-dehydratase |
| BP1026B_II0472 | *rfbH* | BPSS0421 | CDP-6deoxy-D-xylo-4-hexulose-3-dehydrase |
| BP1026B_II0473 | *rfbE* | BPSS0422 | Perosamine synthetase/aminotransferase |
| BP1026B_II0474 | *hyp* | BPSS0423 | Hypothetical |
| BP1026B_II0475 | *wbaR* | BPSS0424 | Glycosyl transferase |
| BP1026B_II0476 | *rfaQ* | BPSS0425 | ADP-heptose-- lipooligosaccharideheptosyltransferase II |
| BP1026B_II0477 | *waaQ* | BPSS0426 | ADP-heptose--LPS heptosyltransferase II (O-antigen related) |
| BP1026B_II0478 | *wbbJ* | BPSS0427 | Galactoside O-acetyltransferase |
| BP1026B_II0479 | *wbcC* | BPSS0428 | Glycosl/rhamnosyl transferase (O-antigen related) |
| BP1026B_II0480 | *hyp* | BPSS0429 | Hypothetical |

**Table A3.3 Homologous gene loci for the CPSIII biosynthesis cluster.** This cluster is also homologous to the *bce*-I cluster in BCC species (See **Chapter 2**).

| *B. pseudomallei* 1026b locus | Gene Name | *B. pseudomallei* K96243 locus | Putative Function |
|---|---|---|---|
| BP1026B_II1956 | *hepB* | BPSS1825 | Glycosyltransferase |
| BP1026B_II1957 | *wbpY* | BPSS1826 | Glycosyltransferase |
| BP1026B_II1958 | *pgi* | BPSS1827 | Glucose-6-phosphate isomerase |
| BP1026B_II1959 | *wbtD* | BPSS1828 | Glycosyltransferase group 1 protein |
| BP1026B_II1960 | *bceG* | BPSS1829 | Glycosyltransferase |
| BP1026B_II1961 | *bceF/wzc* | BPSS1830 | Capsule export; exopolysaccharide biosynthesis-like tyrosine-protein kinase |
| BP1026B_II1962 | *bceE/wza* | BPSS1831 | Capsule export; exopolysaccharide biosynthesis related polysaccharide lipoprotein |
| BP1026B_II1963 | *bceD/wzb* | BPSS1832 | Transport; exopolysaccharide biosynthesis-like low molecular weight protein-tyrosine-phosphatase |
| BP1026B_II1964 | *udg2* | BPSS1833 | UDP-glucose 6-dehydrogenase 2 |
| BP1026B_II1965 | *wcaJ* | BPSS1834 | Sugar transferase; lipopolysaccharide biosynthesis-like protein |
| BP1026B_II1966 | *manC* | BPSS1835 | Mannose-1-phosphate guanyltransferase |

**Table A3.4 Homologous gene loci for the CPSIV biosynthesis cluster.**

| *B. pseudomallei* 1026b locus | Gene Name | *B. pseudomallei* K96243 locus | Putative Function |
|---|---|---|---|
| BP1026B_I0543 | *epsT* | BPSL2769 | UTP-glucose-1-phosphate uridylyltransferase |
| BP1026B_I0542 | *kpsF* | BPSL2770 | LPS biosynthesis; arabinose-5-phosphate isomerase; capsule expression protein |
| BP1026B_I0540 | *kdsC* | BPSL2771 | LPS biosynthesis; haloacid dehalogenase-like hydrolase |
| BP1026B_I0541 | *kdsA* | BPSL2772 | LPS biosynthesis; 2-dehydro-3-deoxyphosphooctonate aldolase |
| BP1026B_I0538 | *cpsl* | BPSL2773 | Glycosyltransferase |
| BP1026B_I0539 | *wbpH* | BPSL2774 | Hypothetical |
| BP1026B_I0537 | *wcaB/cysE* | BPSL2775 | Colanic acid biosynthesis acetyltransferase |
| BP1026B_I0536 | *kpsS* | BPSL2776 | CPS biosynthesis/export protein (hypothetical) |
| BP1026B_I0535 | *wbpF* | BPSL2777 | O-antigen translocase |
| BP1026B_I0534 | *espB* | BPSL2778 | Tyrosine-protein kinase involved in EPS biosynthesis |
| BP1026B_I0533 | *wzb* | BPSL2779 | Protein-tyrosine-phosphatase |
| BP1026B_I0532 | *wza* | BPSL2780 | CPS export outer membrane protein |
| BP1026B_I0531 | *wcaJ* | BPSL2781 | Transmembrane sugar transferase |
| BP1026B_I0530 | *araC* | BPSL2782 | AraC family transcriptional regulator |
| BP1026B_I0529 | *ligA* | BPSL2783 | NAD-dependent DNA ligase |
| BP1026B_I0526 | *hyp* | BPSL2784 | Hypothetical |
| BP1026B_I0525 | *hyp* | BPSL2785 | Hypothetical |
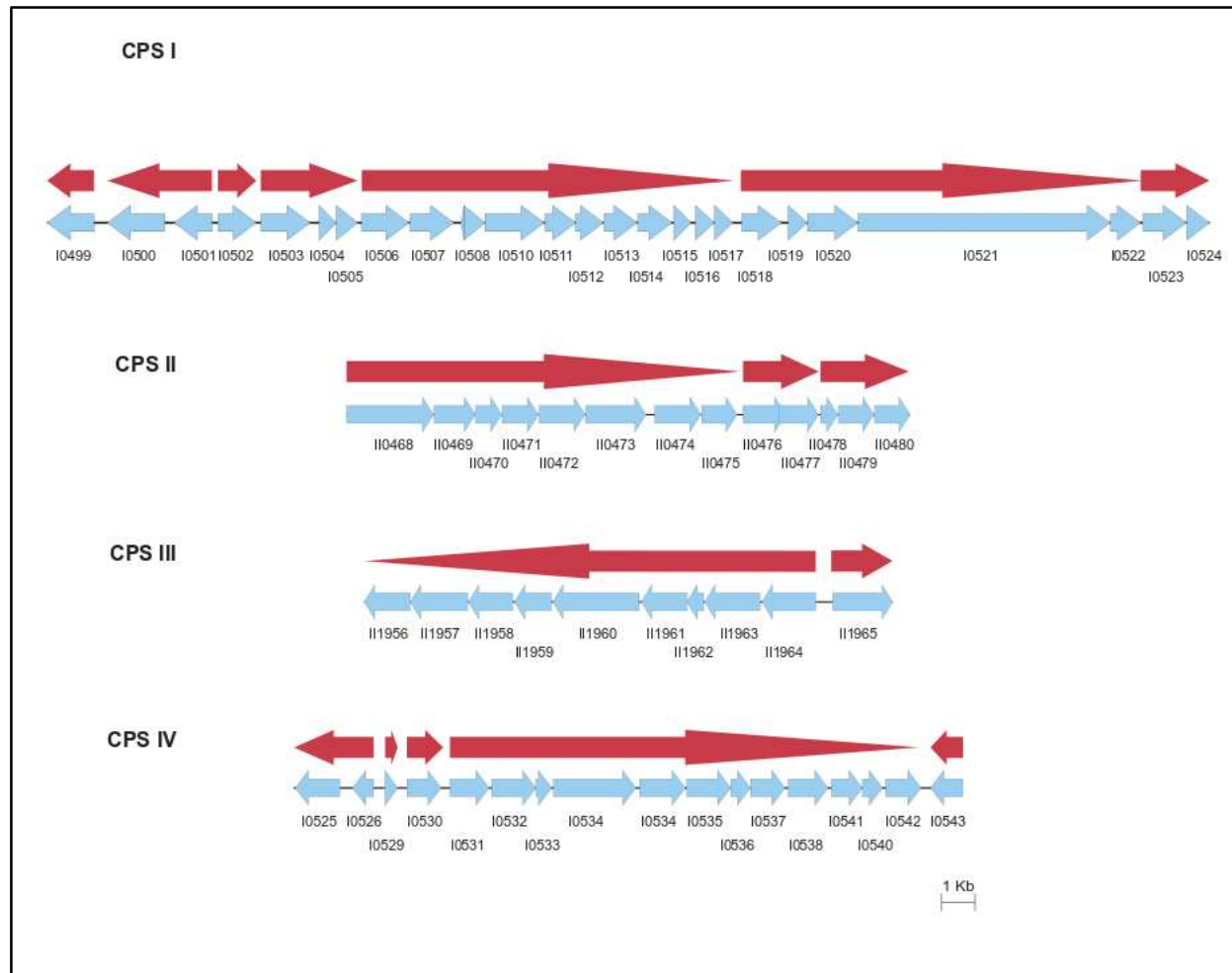
**Figure A3.1 Genomic orientation of capsule biosynthesis clusters CPSI – CPSIV in *B. pseudomallei* 1026b.** Coding sequences are depicted by blue arrows per positive or negative strand orientation and sizes of genes and intergenic regions are to scale. Putative operons are depicted by red arrows representing size and orientation as predicted by the DOOR 2.0 algorithm.

based on ORF homology in *B. pseudomallei* and putative gene functions were cross-referenced with the Burkholderia Genome Data Base (7).

To further categorize clusters CPSI – CPSIV, I conducted additional bioinformatics analyses to establish the number and orientation of gene operons, which were determined with the DOOR 2.0 operon analysis algorithm (11). Based on DOOR 2.0 analysis, I determined that seven co-regulated gene operons exist within CPSI, three in CPSII, two in CPSIII, and five in CPSIV (**Figure A3.1**). These results indicate that the predicted capsule biosynthetic clusters contain several polycistronic mRNA units, transcribed in opposing directions, thus suggesting intricate transcriptional regulation and possible variability in production of a final CPS product. However, the apparent complexity of the predicted capsular polysaccharide biosynthetic clusters becomes more tangled with the characterization of exopolysaccharide biosynthesis.

## A3.2 Characterization of the *B. pseudomallei* biofilm exopolysaccharide gene cluster *becA-R*

In addition to the surface-associated polysaccharides characterized in *B. pseudomallei*, namely the primary antigen CPSI (9), the acidic polysaccharide (12), and the predicted capsule CPSII – CPSIV, our lab identified a novel exopolysaccharide biosynthetic cluster (13). Based on a screen of transposon insertion mutants, we identified a 28 Kb cluster of 18 gene loci and 3 pseudogene remnants spanning Bp1026b_l2907 – Bp1026b_l2927. The exopolysaccharide cluster has been previously annotated for the genetic loci BCAM1330 – 1341 on chromosome II of *B. cenocepacia* J2315 and experimentally validated as a major structural component of biofilms (14). Bioinformatics analysis comparing the putative exopolysaccharide gene clusters of *B. pseudomallei* 1026b and *B. cenocepacia* J2315 revealed high sequence conservation amid genetic rearrangement among the closely related opportunistic pathogens. We examined genetic sequence similarity from species likely sharing an ancestral sequence origin to confirm the location of the major exopolysaccharide in *B. pseudomallei* 1026b. Local pairwise

alignments of genomic sequences using blastn showed high sequence homology among a region on chromosome I of *B. pseudomallei* 1026b and the cluster on chromosome II of *B. cenocepacia* J2315 (**Table A3.5**). Of the 18 predicted coding sequences, 14 are directly homologous to the exopolysaccharide cluster in *B. cenocepacia* J2315, spanning BCAM1334 – 1350. The DNA sequences from 14 coding regions are 75.8% identical altogether at the nucleotide level and represent gene cluster homologues between the two *Burkholderia* species. Among species in the *Burkholderia pseudomallei* complex (BPC), sequence similarities are much higher, representing a high level of genomic conservation.

Nearly identical gene clusters were identified in the sequenced genomes of *B. mallei* ATCC 23344 and *B. thailandensis* E264 spanning the loci BMA0027-BMA0048 and BTH_I0520-BTH_I0537, respectively (**Table A3.6**). Genetic alignments for *B. pseudomallei* and *B. mallei* revealed greater than 99% sequence identity at the nucleotide level or almost full conservation of this cluster. Alignments for *B. pseudomallei* and *B. thailandensis* identified an average sequence identity of 93.2% among the 18 loci, indicating a similarly high level of conservation. The gene locus predicted to encode for the mannose-1-phosphate guanylyltransferase, *manC* (Bp1026b_I2925, *becP*), shares 99.8% identity with BMA0029 in *B. mallei* and 94.1% identity with BTH_I0522 in *B. thailandensis*. These observations indicate a high degree of genetic conservation for this EPS cluster among closely related species despite differences in human and animal pathogenicity and environmental niche adaptation.


**A3.3 Visualization and comparison of the *becA-R* biosynthetic cluster using EasyFig**

I used a combination of bioinformatics tools and open-access genomic databases to compare the putative exopolysaccharide gene clusters from the sequenced genomes of *B. pseudomallei* 1026b (taxid: 884204) and *B. cenocepacia* J2315 (taxid: 216591). Regions of

**Table A3.5 Similarity among predicted biofilm-associated *bec* exopolysaccharide coding sequences.**

| *Burkholderia pseudomallei* 1026b | *Burkholderia cenocepacia* J2315 | Nucleotide Percent Identity | AA Percent Identity | Max Score | Total Score | Query Cover | E-value |
|---|---|---|---|---|---|---|---|
| I2907 | N/A | N/A | N/A | N/A | N/A | N/A | N/A |
| I2908 | N/A | N/A | N/A | N/A | N/A | N/A | N/A |
| I2909 | BCAM1350 | 76.44 | 54.80 | 699 | 699 | 57% | 0.0 |
| I2910 | BCAM1349 | 74.87 | 62.20 | 471 | 514 | 78% | 5e-137 |
| I2914 | BCAM1348 | 72.14 | 62.16 | 425 | 446 | 87% | 7e-123 |
| I2915 | BCAM1347 | 81.12 | 78.31 | 221 | 221 | 99% | 1e-62 |
| I2916 | BCAM1346 | 76.22 | 67.00 | 839 | 1054 | 92% | 0.0 |
| I2917 | BCAM1344 | 77.49 | 65.29 | 764 | 859 | 82% | 0.0 |
| I2918 | BCAM1345 | 84.25 | 81.31 | 1047 | 1140 | 95% | 0.0 |
| I2919 | BCAM1343 | 73.82 | 59.93 | 1342 | 2270 | 93% | 0.0 |
| I2920 | BCAM1334 | 66.16 | 52.08 | 179 | 651 | 66% | 3e-48 |
| I2921 | BCAM1342 | 81.02 | 78.05 | 1252 | 1549 | 99% | 0.0 |
| I2922 | N/A | N/A | N/A | N/A | N/A | N/A | N/A |
| I2923 | N/A | N/A | N/A | N/A | N/A | N/A | N/A |
| I2924 | BCAM1341 | 72.32 | 58.95 | 284 | 284 | 71% | 9e-81 |
| I2925 | BCAM1340 | 82.33 | 74.90 | 1483 | 1644 | 91% | 0.0 |
| I2926 | BCAM1335 | 69.83 | 60.00 | 417 | 594 | 92% | 2e-120 |
| I2927 | BCAM1336 | 72.74 | 67.15 | 731 | 802 | 94% | 0.0 |

**Table A3.6 Similarity among predicted biofilm-associated *bec* exopolysaccharide coding sequences.**

| *Burkholderia mallei* ATCC 23344 | Nucleotide Percent Identity | AA Percent Identity | *Burkholderia pseudomallei* 1026b | Nucleotide Percent Identity | AA Percent Identity | *Burkholderia thailandensis* E264 |
|---|---|---|---|---|---|---|
| BMA0048 | 99.45 | 99.45 | I2907 | 92.33 | 93.41 | BTH_I0537 |
| BMA0047 | 99.84 | 99.53 | I2908 | 94.26 | 96.97 | BTH_I0536 |
| BMA0046 | 99.85 | 99.56 | I2909 | 94.01 | 93.11 | BTH_I0535 |
| BMA0045 | 99.75 | 100.00 | I2910 | 93.70 | 98.51 | BTH_I0534 |
| BMA0044 | 99.75 | 100.00 | I2914 | 94.21 | 96.21 | BTH_I0533 |
| BMA0043 | 99.60 | 98.80 | I2915 | 95.63 | 96.39 | BTH_I0532 |
| BMA0042 | 99.75 | 99.75 | I2916 | 94.85 | 96.81 | BTH_I0531 |
| BMA0041 | 99.90 | 100.00 | I2918 | 93.79 | 95.33 | BTH_I0530 |
| BMA0040 | 99.82 | 100.00 | I2917 | 94.21 | 94.48 | BTH_I0529 |
| BMA0039 | 99.88 | 100.00 | I2919 | 91.67 | 91.42 | BTH_I0528 |
| BMA0038 | 99.80 | 99.39 | I2920 | 89.16 | 86.88 | BTH_I0527 |
| BMA0037 | 99.92 | 99.77 | I2921 | 95.20 | 97.07 | BTH_I0526 |
| BMA0033 | 99.57 | 99.57 | I2922 | 85.46 | 76.70 | BTH_I0525 |
| BMA0032 | 99.92 | 100.00 | I2923 | 93.16 | 93.46 | BTH_I0524 |
| BMA0030 | 99.69 | 99.54 | I2924 | 93.43 | 89.42 | BTH_I0523 |
| BMA0029 | 99.81 | 99.43 | I2925 | 94.10 | 93.02 | BTH_I0522 |
| BMA0028 | 99.67 | 99.50 | I2926 | 94.49 | 93.72 | BTH_I0521 |
| BMA0027 | 99.76 | 99.53 | I2927 | 94.72 | 96.45 | BTH_I0520 |

homology were initially identified using blastn (NCBI) under standard conditions and the

Burkholderia Orthologous Groups classification system from the Burkholderia Genome

Database (http://www.burkholderia.com, (7)). Genome sequences for *B. pseudomallei* 1026b

chromosome I (accession number: NC_017831.1) and *B. cenocepacia* J2315 chromosome II

(accession number: NC_011001.1) were downloaded from the GenBank sequence database

(NCBI, NIH) and regions of interest were extracted using Geneious version 7.1.7

(http://www.geneious.com, (15)). Trimmed GenBank files were assembled with Easyfig version

2.2.3 (16) and Python programming language version 2.7 (http://www.python.org). Homology

and inversions among gene loci were calculated using blastn with a minimum identity cutoff of

60%. Individual percent identities for each locus were calculated using Multiple Sequence

Comparison by Log-Expectation (MUSCLE) tool provided by the European Bioinformatics

Institute (EMBL-EBI), which creates percent identity matrices using Clustal 2.1 (17).

   I confirmed conditions for sequence comparisons using the BLAST+ command line

application from the BLAST FTP site: ftp://ftp.ncbi.nlm.nih.gov/blast/executables/blast+/. The

ncbi-blast-2.6.0+ package was used to validate blasn parameters for EasyFig comparisons and

illustrations. For sequence comparisons included in **Figure A3.2**, a nucleotide database of the

fasta extraction from *B. cenocepacia* J2315 was assembled and queried with the fasta

nucleotide extraction from *B. pseudomallei* 1026b. I used the 'blastn' –task option for a

traditional BLASTN requiring an exact match of 11, which is "better suited for interspecies

comparisons with a shorter word-size" according to the BLAST Command Line Applications

User Manual (NCBI). Output was specified in tabular format to visualize % identity, alignment

length, mismatches, gap opens, queries and subjects starts/ends, E-value, and bit score.  For

14 of the total 18 CDS nucleotide queries from *B. pseudomallei* 1026b, the E-values range from

0.00 to 3.96E-04 and nucleotide % identities range from 67.03 – 82.9%, with a minimum

alignment length of 464bp. Thus, a nucleotide identity cut-off of 67% would produce similar

results to the ones initially reported. A false-positive alignment was reported for a 42bp length of
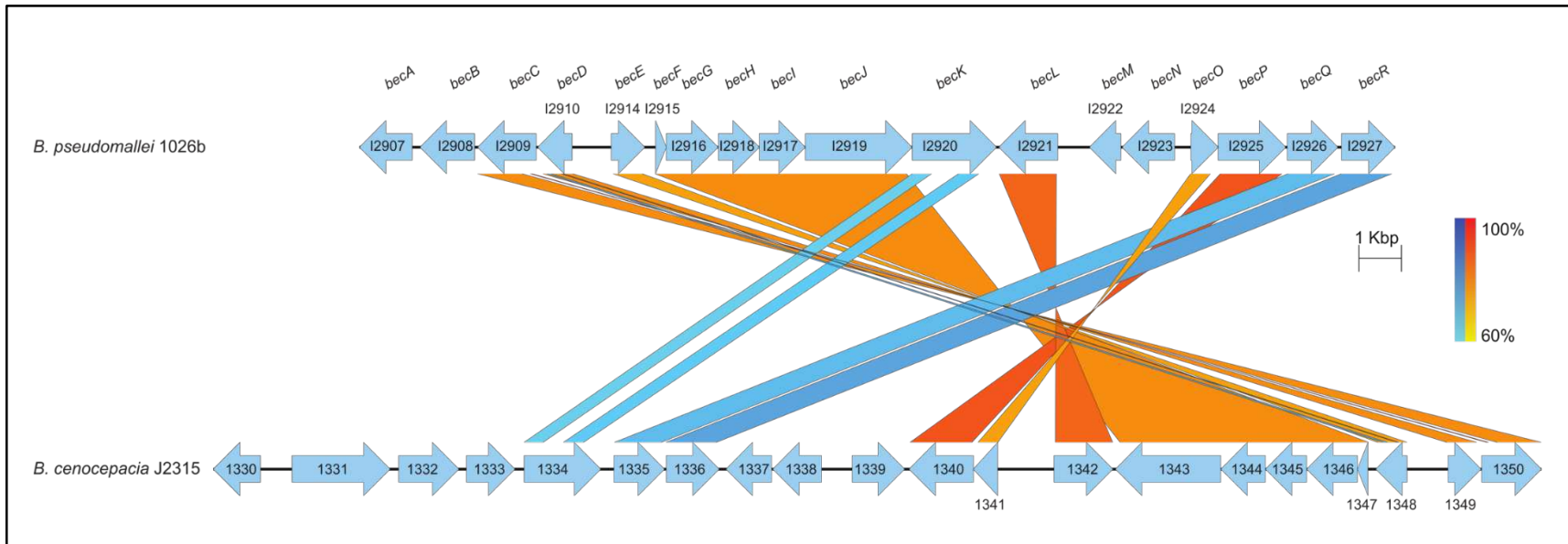
**Figure A3.2 Biofilm-associated exopolysaccharide gene cluster from *B. pseudomallei* and comparative analysis with *B. cenocepacia.*** Adapted from Borlee et al. (13). The putative exopolysaccharide gene clusters from the sequenced genomes of *Burkholderia pseudomallei* 1026b (top) and *Burkholderia cenocepacia* J2315 (bottom). A total of 18 loci spanning Bp1026b_I2907 – Bp1026b_I2927 on chromosome I of *B. pseudomallei* 1026b, not including a cluster of 3 pseudogenes, are aligned with 21 loci spanning BCAM1330 – BCAM1350 on chromosome II of *B. cenocepacia* J2315. Coding sequences are depicted by arrows per positive or negative strand orientation and sizes of genes and intergenic regions are to scale. The results of blastn annotations with minimum identity of 60% are aligned to regions of similarity. Red bars depict sequence inversions and blue bars depict direct homology in a color density gradient.

Bp1026b_I2907 (for which we do not report an available homolog in *B. cenocepacia* J2315) with an e-value of 1E-03. The remainder of non-homologous alignments (negatives) had e-values ranging from 4E-03 – 7.8. We generated a frequency distribution of log (e-value) and observed most non-homologous alignments were at or above log(e-value) = -3. Thus, we feel confident in our ability to predict inter-species homologs with using an E-value cut-off of 1E-03.

Thus, with these considerations for homology identification in mind, I generated a genomic comparison between our putative exopolysaccharide cluster in *B. pseudomallei* 1026b to the previously described cluster in *B. cenocepacia* J2315. This comparison revealed high sequence conservation amid genetic rearrangement among the closely related opportunistic pathogens. The exopolysaccharide cluster has been previously annotated for the genetic loci BCAM1330 – BCAM1341 on chromosome II of *B. cenocepacia* J2315 and experimentally validated as a major structural component of biofilms (14). Interestingly, most of the homologous coding regions have flipped directional arrangements while maintaining high sequence identity; the red color gradient represent percent identity of inverted blastn hits, while the blue color gradient represents direct blastn hit identities (**Figure A3.2**). To calculate and visualize sequence homology, we used a threshold E-value of 0.001 and minimum identity value of 0.60 for blast hits drawn. Except for Bp1026b_I2920, which has additional unique sequence in the middle of the gene interrupting alignment (data not shown), the coding regions of the *B. pseudomallei* 1026b cluster fully or almost fully align to homologues in *B. cenocepacia* J2315 and percent identities range from 66 – 84% at the nucleotide level. A notable locus, Bp1026b_I2925, predicted to encode for mannose-1-phosphate guanylyltransferase *manC*, the enzyme required to catalyze the formation of nucleotide sugar GDP-mannose, shares 82.3% identity with BCAM1340. Additionally, Bp1026b_I2910, shares 74.9% identity with BCAM1349, the proposed transcriptional regulator of the exopolysaccharide gene cluster in *B. cenocepacia* J2315 (14).

These results indicate functional conservation of the exopolysaccharide cluster; however, our bioinformatics analysis revealed some crucial differences. Four loci in the 1026b predicted EPS cluster showed no homology to the J2315 cluster. The loci Bp1026b_I2907, I2908, I2922, and I2923, are predicted to encode a glycosyltransferase protein, a polysaccharide export periplasmic protein, a PAP2 superfamily protein, and a glycoside hydrolase family protein, respectively. Bp1026b_I2907 shares similarity to two predicted glycosyltransferases in the *B. cenocepacia* J2315 EPS cluster, BCAM1337 and BCAM1338 with 60.15% and 62.56% respective nucleotide identities. Likewise, Bp1026b_I2908 shares 61.89% nucleotide identity to BCAM1330, which is predicted to encode a putative polysaccharide export protein. However, the sequence correlations of Bp1026b_I2907 and Bp1026b_I2908 to *B. cenocepacia* J2315 do not pass our E-value threshold of 1e-3, representing a 0.001 chance of random sequence alignment, indicating that these correlations are not biologically significant or homologous. Bp1026b_I2922 and Bp1026b_I2923 also do not show significant sequence correlations to the *B. cenocepacia* J2315 genome; however, the flanking coding sequences of Bp1026b_I2921 and Bp1026b_I2924 appear homologous to BCAM1341 and BCAM32, respectively, amid directional inversions (**Figure A3.2**). Interestingly, Bp1026b_I2921 and Bp1026b_I2924 are flanked by large noncoding intergenic regions totaling 1176bp, which co-localizes to an intergenic region spanning 1319bp in *B. cenocepacia* J2315. One explanation for this disparity involves the acquisition of the two coding sequences by *B. pseudomallei* 1026b for a species-specific fitness advantage.

In contrast to the disparities with *B. cenocepacia* J2315 sequence alignment, the *becA-R* cluster from *B. pseudomallei* 1026b aligns almost perfectly with putative homologs in both *B. mallei* ATCC 23344 and *B. thailandensis* E264 (**Figure A3.3**). The homology between these species within the *Burkholderia pseudomallei* cluster (BPC) again highlights the functional conservation of the *becA-R* cluster and its potential importance in biofilm formation both in host-adapted organisms (*B. mallei*) and environmental saprophytes (*B. thailandensis)*.
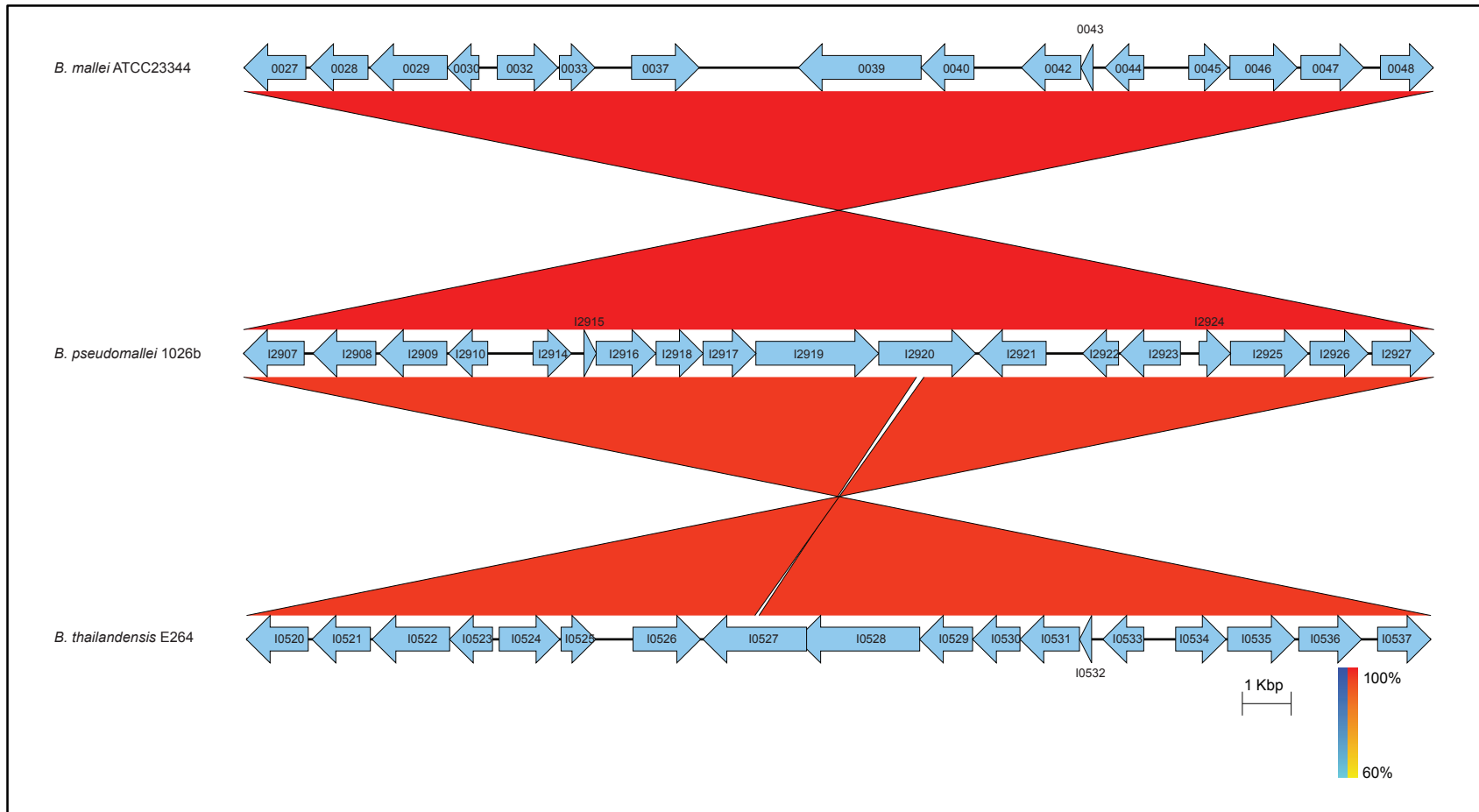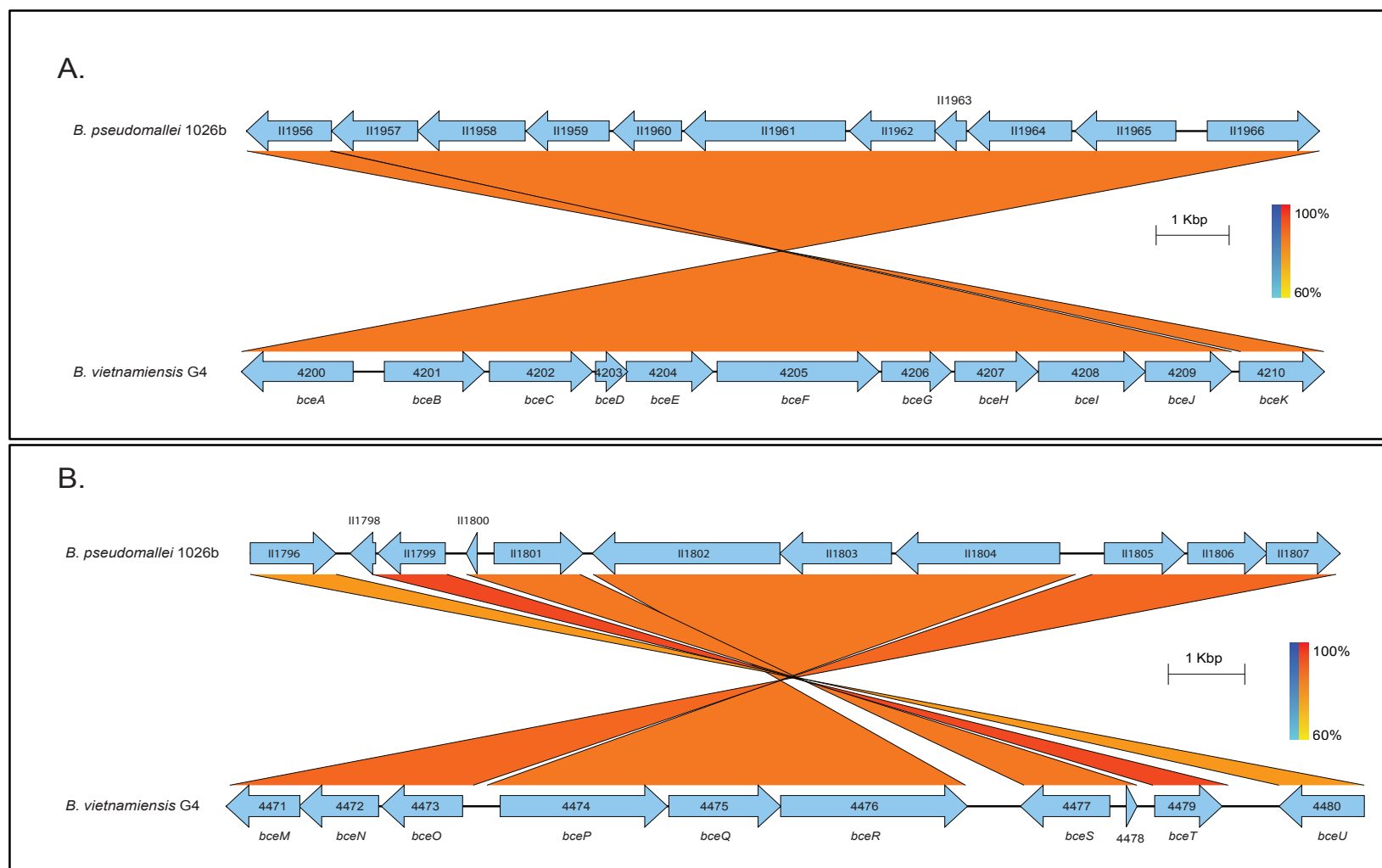
**Figure A3.3 Comparative analysis of *becA-R* biofilm gene cluster from *B. mallei* ATCC 23344, *B. pseudomallei* 1026b, and *B. thailandensis* E264.** Adapted from Borlee et al. (13). The *becA-R* gene cluster from the sequenced genomes of *B. mallei* ATCC 23344 (top), *B. pseudomallei* 1026b (middle), and *B. thailandensis* E264 (bottom). Genes from *becA-R* of *B. pseudomallei* 1026b, Bp1026b_I2907 – Bp1026b_I2927 (*becA-R*) are aligned with BMA0027 – BMA0048 from *B. mallei* ATCC 23344 and *B. thailandensis* E264 BTH_I0520 – BTH_0537. Coding sequences are depicted by arrows per positive or negative strand orientation and sizes of genes and intergenic regions are to scale. The results of blastn annotations with minimum identity of 60% and threshold E-value of 1E-3 are aligned to regions of similarity. Red bars depict sequence inversions and blue bars depict direct homology in a color density gradient.

218

**A3.4 Identification and visualization of a link between the CPSIII and *bce-I* gene clusters**


While analyzing the transposon insertion mutants identified as deficient in biofilm formation in the Borlee et al., study (13), a hit in Bp1026b_II1959 sparked a bioinformatics analysis in the CPSIII gene cluster (Bp1026b_II1956 – Bp1026b_II1966). CPSIII has been described in *B. pseudomallei* as a capsular polysaccharide that does not contribute to virulence, but is induced in water (10). The 11-gene cluster was characterized to produce a purified capsule composed of mostly galactose and glucose, with mannose, xylose, and rhamnose residues (10). Interestingly, the *wza* gene (Bp1026b_II1962, Table A3.3) was found to have some homology to *amsK* from *Bacillus cereus* (10)*;* a gene that in part drives production of amylovoran, an exopolysaccharide derived from *Erwinia amylovora* biofilms (18).

My bioinformatics analysis revealed that the CPSIII cluster from *B. pseudomallei* 1026b is homologous to the *bce-I* cluster (Table A3.7) contributing to the production of cepacian in *B. vietnamiensis* G4, a member of the *Burkholderia cepacia* complex (BCC) (19). Cepacian has been shown to be important for virulence in the BCC by inhibiting parts of the host innate immune response, and for the development of mature biofilms (19). Importantly, the cepacian biosynthesis genes are arranged in two adjacent clusters, *bce-I* and *bce-II*, which are split by several kilobases of insertion sequence related to phage-encoding proteins (19). According to the homology based on blastn (NCBI) and sequences from the Burkholderia Genome Database (7), *B. pseudomallei* 1026b shares 76 – 88% nucleotide identity to the *bce-I* and *bce-II gene* clusters identified in *B. vietnamiensis* G4 (Table A3.7). These homologous regions were then arranged via EasyFig for comparative visualization analysis (Figure A3.4). Interestingly, although these gene clusters are present in their entirety in both *B. cenocepacia* J2315 (BCC) and *B. thailandensis* E264 (BPC)*,* the host-adapted *B. mallei* ATCC 23344 lacks the *bce-I*/CPSIII cluster while maintaining *bce-II* completely. This indicates that *bce-I* may not be required for host survival, but environmental biofilm formation.

**Table A3.7 Similarity among *bce-I* (*bceA – bceK*) and *bce-II* (*bceM – bceU*) coding sequences.** Adapted from Borlee et al. (13).

| B. pseudomallei 1026b | B. vietnamiensis G4 | Nucleotide Percent Identity | B. cenocepacia J2315 | Nucleotide Percent Identity | B. thailandensis E264 | Nucleotide Percent Identity | B. mallei ATCC 23344 | Nucleotide Percent Identity |
|---|---|---|---|---|---|---|---|---|
| *bce-I* | | | | | | | | |
| II1966 | Bcep1808_4200 | 81.91 | BCAM0854 | 78.68 | BTH_II0542 | 93.53 | N/A | N/A |
| II1965 | Bcep1808_4201 | 85.38 | BCAM0856 | 84.55 | BTH_II0543 | 94.14 | N/A | N/A |
| II1964 | Bcep1808_4202 | 86.16 | BCAM0855 | 86.33 | BTH_II0544 | 93.60 | N/A | N/A |
| II1963 | Bcep1808_4203 | 83.64 | BCAM0857 | 81.36 | BTH_II0545 | 93.13 | N/A | N/A |
| II1962 | Bcep1808_4204 | 81.06 | BCAM0858 | 80.66 | BTH_II0546 | 94.13 | N/A | N/A |
| II1961 | Bcep1808_4205 | 83.18 | BCAM0859 | 82.33 | BTH_II0547 | 95.72 | N/A | N/A |
| II1960 | Bcep1808_4206 | 82.43 | BCAM0860 | 72.95 | BTH_II0548 | 93.14 | N/A | N/A |
| II1959 | Bcep1808_4207 | 78.41 | BCAM0861 | 75.07 | BTH_II0549 | 93.60 | N/A | N/A |
| II1958 | Bcep1808_4208 | 83.10 | BCAM0862 | 79.35 | BTH_II0550 | 95.05 | N/A | N/A |
| II1957 | Bcep1808_4209 | 83.43 | BCAM0863 | 82.59 | BTH_II0551 | 92.92 | N/A | N/A |
| II1956 | Bcep1808_4210 | 80.63 | BCAM0864 | 74.83 | BTH_II0552 | 94.52 | N/A | N/A |
| *bce-II* | | | | | | | | |
| II1807 | Bcep1808_4471 | 78.38 | BCAM1003 | 76.84 | BTH_II0689 | 93.29 | BMA1710 | 99.58 |
| II1806 | Bcep1808_4472 | 87.72 | BCAM1004 | 82.11 | BTH_II0690 | 94.73 | BMA1709 | 99.71 |
| II1805 | Bcep1808_4473 | 84.11 | BCAM1005 | 84.43 | BTH_II0691 | 93.30 | BMA1708 | 99.72 |
| II1804 | Bcep1808_4474 | 82.46 | BCAM1006 | 81.16 | BTH_II0693 | 94.07 | BMA1707 | 99.60 |
| II1803 | Bcep1808_4475 | 87.22 | BCAM1007 | 87.59 | BTH_II0694 | 96.06 | BMA1706 | 99.86 |
| II1802 | Bcep1808_4476 | 83.15 | BCAM1008 | 81.53 | BTH_II0695 | 95.33 | BMA1705 | 99.84 |
| II1801 | Bcep1808_4477 | 83.82 | BCAM1009 | 80.05 | BTH_II0697 | 90.28 | BMA1704 | 99.83 |
| II1799 | Bcep1808_4479 | 90.25 | BCAM1010 | 91.53 | BTH_II0699 | 97.40 | BMA1702 | 100.00 |
| II1796 | Bcep1808_4480 | 76.05 | BCAM1011 | 77.49 | BTH_II0700 | 91.67 | BMA1701 | 98.05 |

**Figure A3.4 Comparative analysis of *bce-I* and *bce-II* gene clusters from *B. pseudomallei* and *B. vietnamiensis* G4.** Adapted from Borlee et al. (13). The cepacian biosynthesis (*bce-I* and *bce-II*) gene clusters from the sequenced genomes of *B. pseudomallei* 1026b (top) and *B. vietnamiensis* G4 (bottom). (A) Genes for *bce-I* of *B. pseudomallei* 1026b, Bp1026b_II1966 – Bp1026b_II1965 are aligned with Bcep1808_4200 – Bcep1808_4210 from *B. vietnamiensis* G4. (B) Genes for *bce-II* of *B. pseudomallei* 1026b, Bp1026b_II1796 – Bp1026b_II1807 are aligned with Bcep1808_4471 – Bcep1808_4480 from *B. vietnamiensis* G4. Coding sequences are depicted by arrows per positive or negative strand orientation and sizes of genes and intergenic regions are to scale.

## A3.5 Genomic visualization of CPSI – CPSIV capsular polysaccharide synthesis clusters

To characterize the capsular polysaccharide clusters (CPSI – CPSIV) identified in *B. pseudomallei* 1026b, I employed the same technique of genomic extraction and comparative visualization described above.  As described in **section A3.4** and **Chapter 2** of this dissertation, there is a clear overlap among gene clusters annotated as CPSIII in *B. pseudomallei* (10) and the cepacian biosynthesis genes characterized in the Bcc organisms (19, 20). The following figures provide visual aids for the comparative analyses regarding the two gene clusters *bce-I* and *bce-II* involved in the biosynthesis of cepacian, which is considered a Bcc polysaccharide. *B. pseudomallei* 1026b encodes complete *bce-I* (**Figure A3.5**) and *bce-II* (**Figure A3.6**), sharing high homology with *B. thailandensis* E264 in the Bpc as well as *B. cenocepacia* J2315 in the Bcc. Importantly, however, *B. cenocepacia* J2315 does not encode a functional cepacian expolysaccharide due to a mutation in *bceB*, a glycosyltransferase that is essential for the addition of glucose to the lipid carrier (19). Cepacian is a clinically important molecule because it can modulate the innate immune response in humans by inhibiting neutrophil chemotaxis and quenching the effects of reactive oxygen species (21). Thus, the fact that bacteria in the Bpc may be capable of cepacian production is relevant to the clinical profile of *B. pseudomallei.*

One of the most important antigens in *B. pseudomallei*, the primary capsular polysaccharide (CPSI) has been shown to be both immunogenic and protective (9). My comparative analysis shows large genomic regions of CPSI are missing from organisms in both the Bpc and the Bcc, although homologous flanking regions are present in both (**Figure A3.7**). Interestingly, some environmental strains of *B. thailandensis* encode a *B. pseudomallei*-like capsular polysaccharide (BTCV), which induces antibodies against *B. pseudomallei* and partial protection from melioidosis in mouse models of infection (22). Much less is known about CPSII (**Figure A3.8**) and CPSIV (**Figure A3.9**), yet it is evident from these comparative analyses that these clusters are not present in *B. cenocepacia* J2315, while highly conserved in the Bpc.
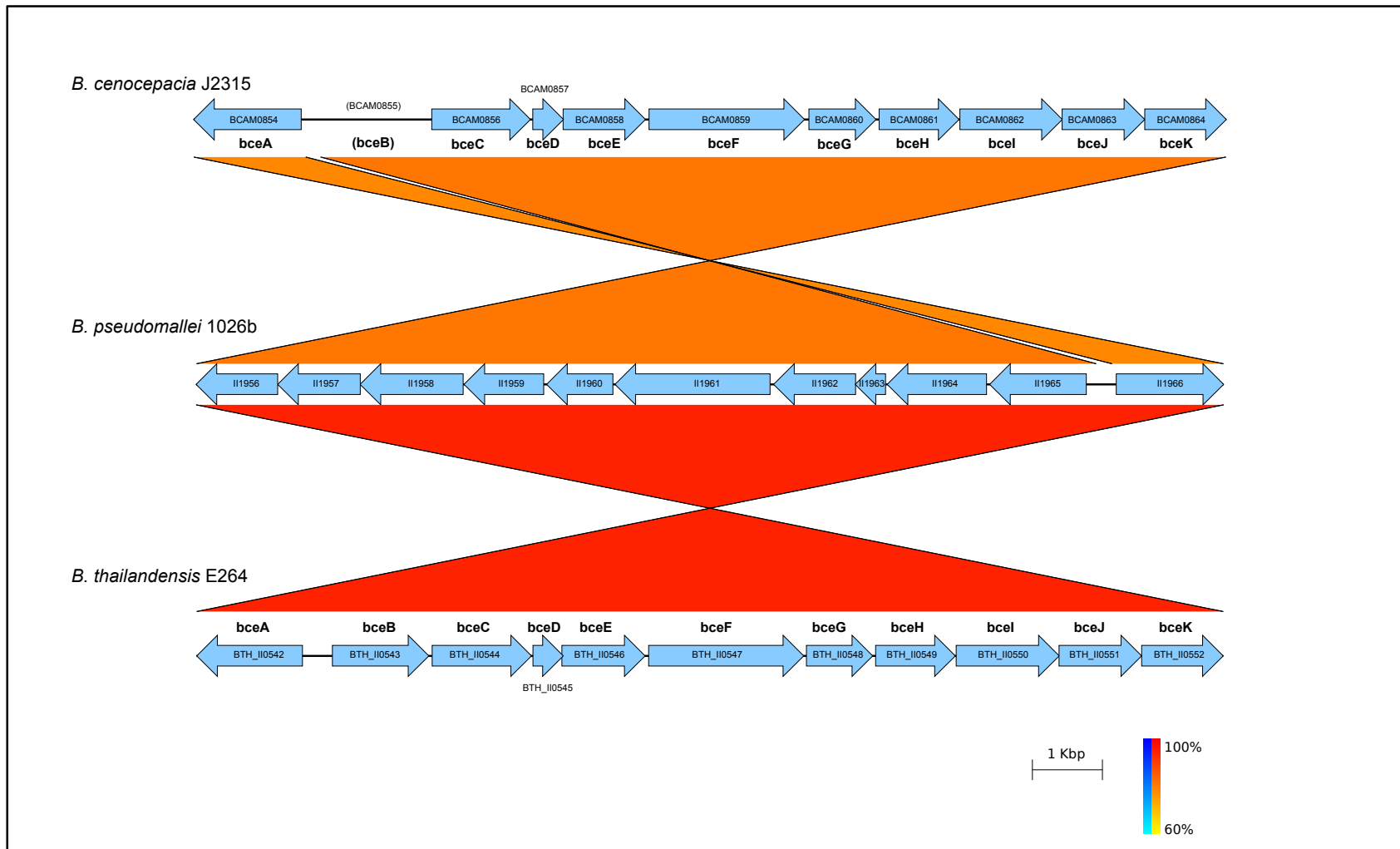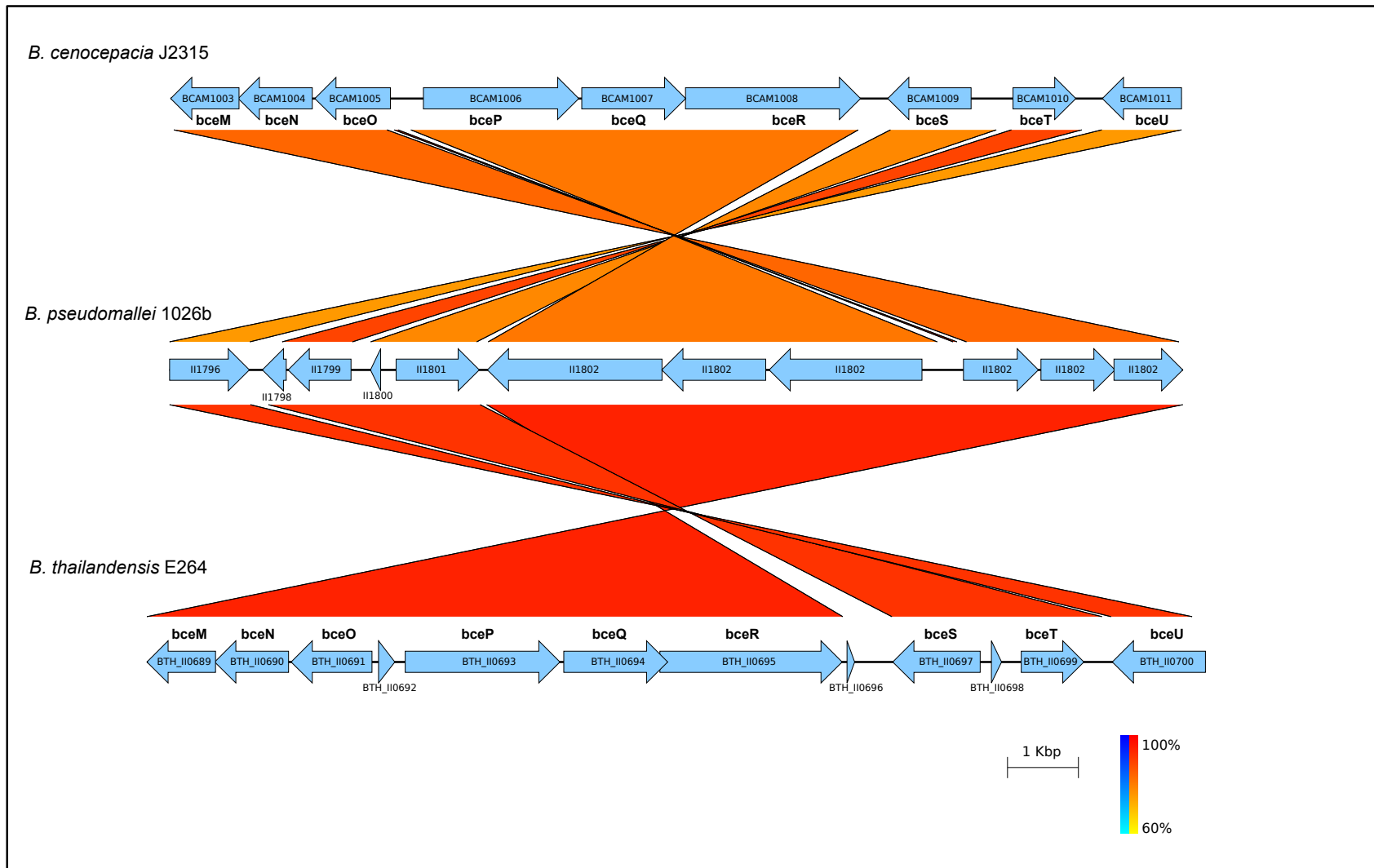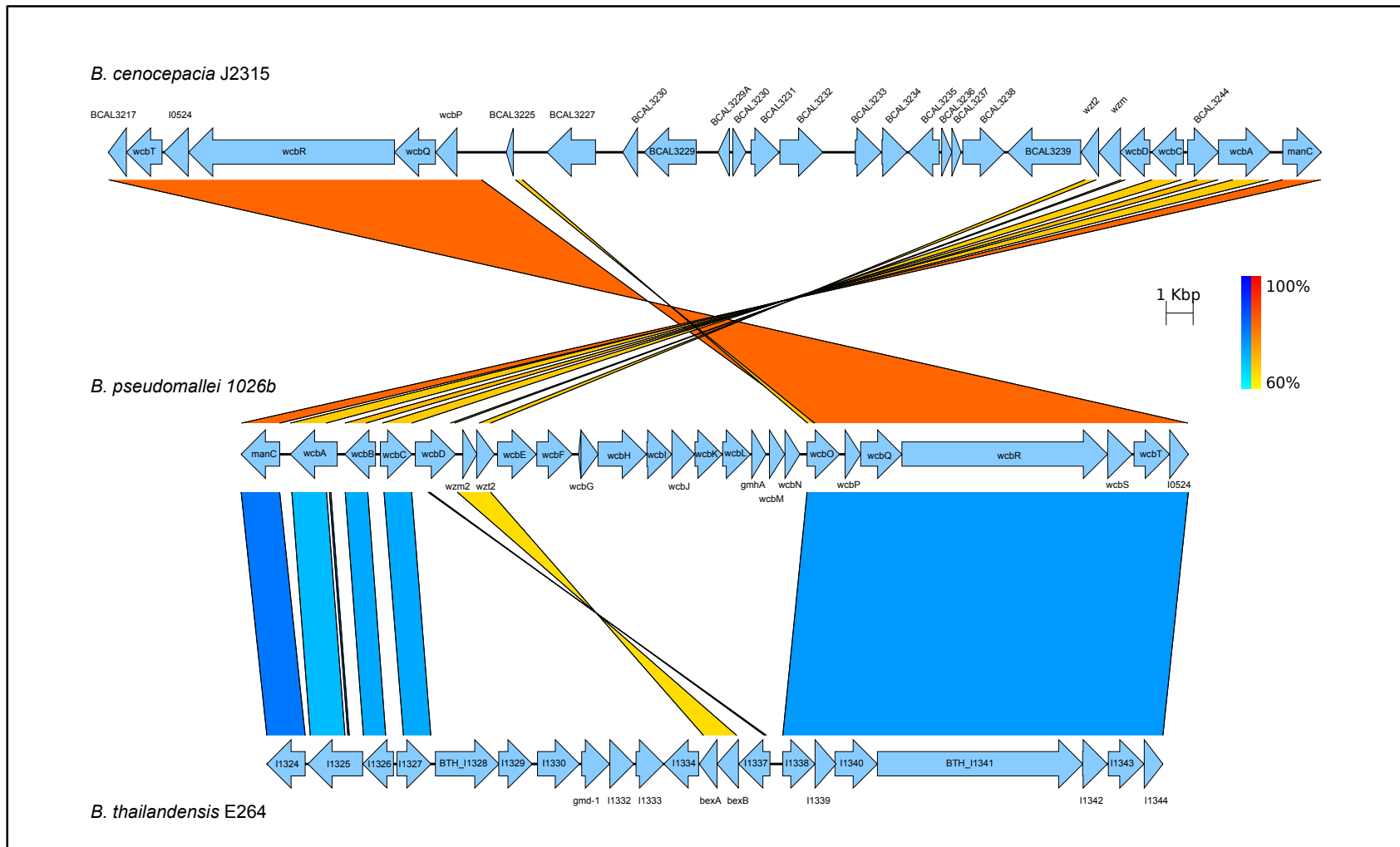
**Figure A3.5 Comparative analysis of the *bce-I*/CPSIII cluster in *B. pseudomallei* 1026b, *B. thailandensis* E264, and *B. cenocepacia* J2315.** *B. pseudomallei 1026b* shares strong homology with *B. thailandensis* E264 for CPSIII (*bce-I* Cepacian cluster), amid complete sequence inversion. Although less robust, a high level of homology amid sequence inversion exists for this cluster in *B. cenocepacia* J2315. However, the *bce-I* biosynthetic cluster in *B. cenocepacia* J2315 does not produce a functional expoloysaccharide due to a mutation in the *bceB* homolog.
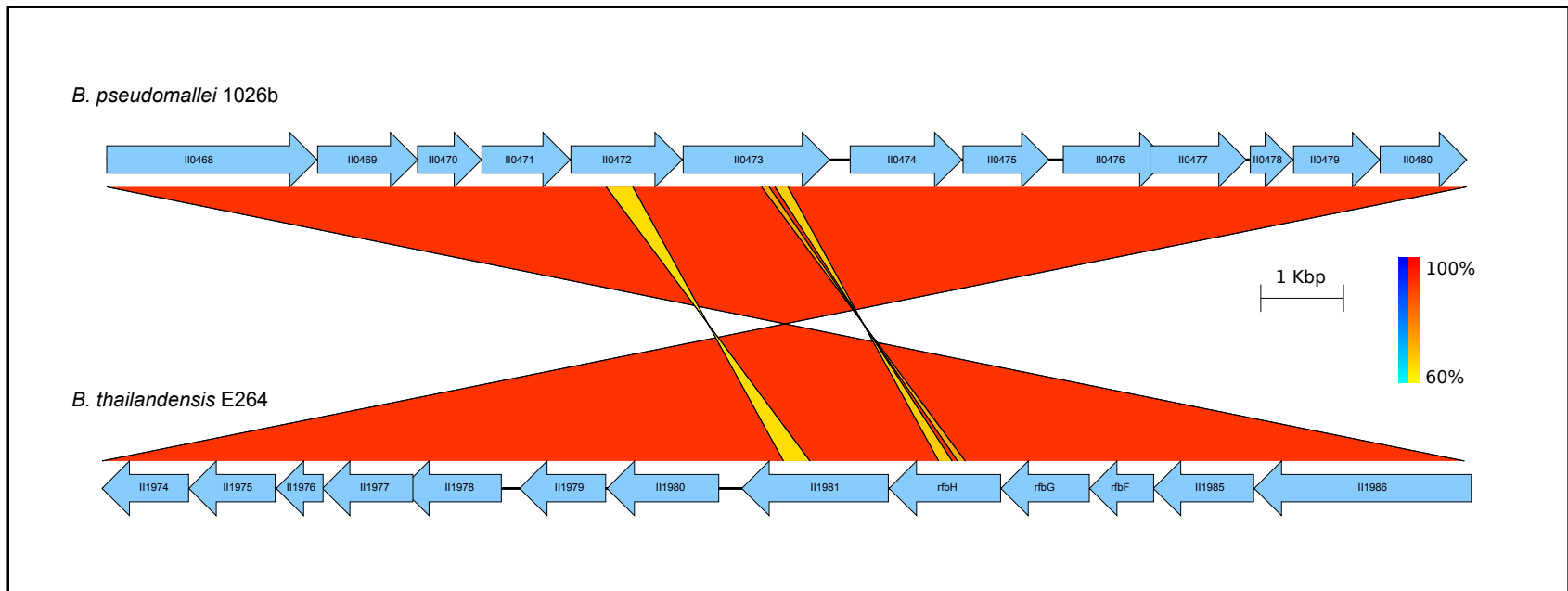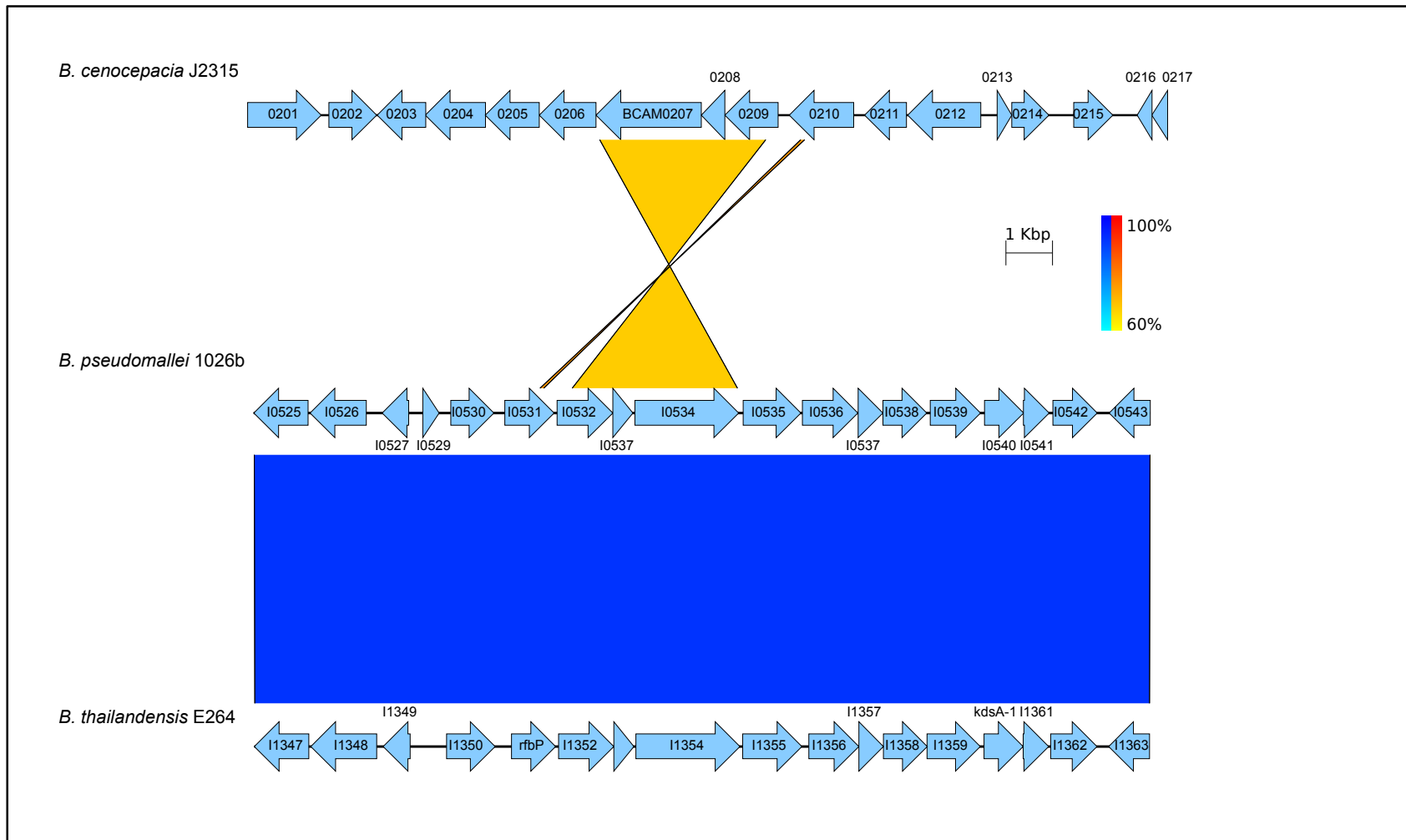
**Figure A3.6 Comparative analysis of the *bce-II* cluster in *B. pseudomallei* 1026b, *B. thailandensis* E264, and *B. cenocepacia* J2315.** The *bce-II* cluster is highly conserved between these three species, similarly to *bce-I* homology, except all genes are present.

**Figure A3.7 Comparative analysis of the CPSI cluster in *B. pseudomallei* 1026b, *B. thailandensis* E264, and *B. cenocepacia* J2315.** A primary antigenic component of *B. pseudomallei*, CPSI is not equally encoded among Bcc and Bpc bacteria, although regions of homology exist among these three strains. Interestingly, *B. thailandensis* E264 is considered a non-pathogenic saprophyte with similar ecology and physiology to *B. pseudomallei* 1026b. Perhaps the lack of a complete CPSI contributes to the avirulence of *B. thailandensis.*

**Figure A3.8 Comparative analysis of the CPSII cluster in *B. pseudomallei* 1026b and *B. thailandensis* E264.** Our analysis did not predict a homologous gene cluster for CPSII in *B. cenocepacia* J2315.

**Figure A3.9 Comparative analysis of the CPSIV cluster in *B. pseudomallei* 1026b, *B. thailandensis* E264, and *B. cenocepacia* J2315.** *B. pseudomallei* 1026b and *B. thailandensis* E264 share high homology along the entirety of this cluster region, while *B. cenocepacia* J2315 is only predicted to encode two of the genes from CPSIV, indicating an evolutionary divergence in CPSIV among the Bpc and the Bcc.

# References

1.      Kamerling JP, Gerwig, G. J. 2.01 - Strategies for the Structural Analysis of Carbohydrates. Comprehensive Glycoscience. 2007:1-68.
2.      Reckseidler-Zenteno SL. Capsular Polysaccharides Produced by the Bacterial Pathogen *Burkholderia pseudomallei*. Complex World of Polysaccharides. 2012:127-52.
3.      Marchetti R, Dillon MJ, Burtnick MN, Hubbard MA, Kenfack MT, Bleriot Y, Gauthier C, Brett PJ, AuCoin DP, Lanzetta R, Silipo A, Molinaro A. *Burkholderia pseudomallei* Capsular Polysaccharide Recognition by a Monoclonal Antibody Reveals Key Details toward a Biodefense Vaccine and Diagnostics against Melioidosis. ACS Chem Biol. 2015;10(10):2295-302.
4.      Nualnoi T, Kirosingh A, Pandit SG, Thorkildson P, Brett PJ, Burtnick MN, AuCoin DP. In vivo Distribution and Clearance of Purified Capsular Polysaccharide from *Burkholderia pseudomallei* in a Murine Model. PLoS Negl Trop Dis. 2016;10(12):e0005217.
5.      Scott AE, Burtnick MN, Stokes MG, Whelan AO, Williamson ED, Atkins TP, Prior JL, Brett PJ. *Burkholderia pseudomallei* capsular polysaccharide conjugates provide protection against acute melioidosis. Infect Immun. 2014;82(8):3206-13.
6.      Holden MTG, Titball RW, Peacock SJ, Cerdeno-Tarraga AM, Atkins T, Crossman LC, Pitt T, Churcher C, Mungall K, Bentley SD, Sebaihia M, Thomson NR, Bason N, Beacham IR, Brooks K, Brown KA, Brown NF, Challis GL, Cherevach I, Chillingworth T, Cronin A, Crossett B, Davis P, DeShazer D, Feltwell T, Fraser A, Hance Z, Hauser H, Holroyd S, Jagels K, Keith KE, Maddison M, Moule S, Price C, Quail MA, Rabbinowitsch E, Rutherford K, Sanders M, Simmonds M, Songsivilai S, Stevens K, Tumapa S, Vesaratchavest M, Whitehead S, Yeats C, Barrell BG, Oyston PCF, Parkhill J. Genornic plasticity of the causative agent of melioidosis, *Burkholderia pseudomallei*. Proceedings of the National Academy of Sciences of the United States of America. 2004;101(39):14240-5.
7.      Winsor GL, Khaira B, Van Rossum T, Lo R, Whiteside MD, Brinkman FSL. The Burkholderia Genome Database: facilitating flexible queries and comparative analyses. Bioinformatics. 2008;24(23):2803-4.
8.      Reckseidler SL, DeShazer D, Sokol PA, Woods DE. Detection of bacterial virulence genes by subtractive hybridization: Identification of capsular polysaccharide of *Burkholderia pseudomallei* as a major virulence determinant. Infection and Immunity. 2001;69(1):34-44.
9.      Cuccui J, Milne TS, Harmer N, George AJ, Harding SV, Dean RE, Scott AE, Sarkar-Tyson M, Wren BW, Titball RW, Prior JL. Characterization of the *Burkholderia pseudomallei* K96243 Capsular Polysaccharide I Coding Region. Infection and Immunity. 2012;80(3):1209-21.
10.     Reckseidler-Zenteno SL, Viteri DF, Moore R, Wong E, Tuanyok A, Woods DE. Characterization of the type III capsular polysaccharide produced by *Burkholderia pseudomallei*. Journal of medical microbiology. 2010;59(12):1403-14.
11.     Mao X, Ma Q, Zhou C, Chen X, Zhang H, Yang J, Mao F, Lai W, Xu Y. DOOR 2.0: presenting operons and their functions through dynamic and integrated views. Nucleic Acids Res. 2014;42(Database issue):D654-9.
12.     Nimtz M, Wray V, Domke T, Brenneke B, Haussler S, Steinmetz I. Structure of an acidic exopolysaccharide of *Burkholderia pseudomallei*. Eur J Biochem. 1997;250(2):608-16.
13.     Borlee GI, Plumley BA, Martin KH, Somprasong N, Mangalea MR, Islam MN, Burtnick MN, Brett PJ, Steinmetz I, AuCoin DP, Belisle JT, Crick DC, Schweizer HP, Borlee BR. Genome-scale analysis of the genes that contribute to *Burkholderia pseudomallei* biofilm

formation identifies a crucial exopolysaccharide biosynthesis gene cluster. PLoS Negl Trop Dis. 2017;11(6):e0005689.

14.     Fazli M, McCarthy Y, Givskov M, Ryan RP, Tolker-Nielsen T. The exopolysaccharide gene cluster Bcam1330-Bcam1341 is involved in *Burkholderia cenocepacia* biofilm formation, and its expression is regulated by c-di-GMP and Bcam1349. Microbiologyopen. 2013;2(1):105-22.

15.     Kearse M, Moir R, Wilson A, Stones-Havas S, Cheung M, Sturrock S, Buxton S, Cooper A, Markowitz S, Duran C, Thierer T, Ashton B, Meintjes P, Drummond A. Geneious Basic: an integrated and extendable desktop software platform for the organization and analysis of sequence data. Bioinformatics. 2012;28(12):1647-9.

16.     Sullivan MJ, Petty NK, Beatson SA. Easyfig: a genome comparison visualizer. Bioinformatics. 2011;27(7):1009-10.

17.     Edgar RC. MUSCLE: multiple sequence alignment with high accuracy and high throughput. Nucleic Acids Res. 2004;32(5):1792-7.

18.     Koczan JM, McGrath MJ, Zhao Y, Sundin GW. Contribution of *Erwinia amylovora* exopolysaccharides amylovoran and levan to biofilm formation: implications in pathogenicity. Phytopathology. 2009;99(11):1237-44.

19.     Ferreira AS, Leitao JH, Silva IN, Pinheiro PF, Sousa SA, Ramos CG, Moreira LM. Distribution of cepacian biosynthesis genes among environmental and clinical *Burkholderia* strains and role of cepacian exopolysaccharide in resistance to stress conditions. Applied and environmental microbiology. 2010;76(2):441-50.

20.     Moreira LM, Videira PA, Sousa SA, Leitao JH, Cunha MV, Sa-Correia I. Identification and physical organization of the gene cluster involved in the biosynthesis of *Burkholderia cepacia* complex exopolysaccharide. Biochem Biophys Res Commun. 2003;312(2):323-33.

21.     Bylund J, Burgess LA, Cescutti P, Ernst RK, Speert DP. Exopolysaccharides from *Burkholderia cenocepacia* inhibit neutrophil chemotaxis and scavenge reactive oxygen species. The Journal of biological chemistry. 2006;281(5):2526-32.

22.     Hantrakun V, Thaipadungpanit J, Rongkard P, Srilohasin P, Amornchai P, Langla S, Mukaka M, Chantratita N, Wuthiekanun V, Dance DAB, Day NPJ, Peacock SJ, Limmathurotsakul D. Presence of *B. thailandensis* and *B. thailandensis* expressing *B. pseudomallei*-like capsular polysaccharide in Thailand, and their associations with serological response to *B. pseudomallei*. PLoS Negl Trop Dis. 2018;12(1):e0006193.
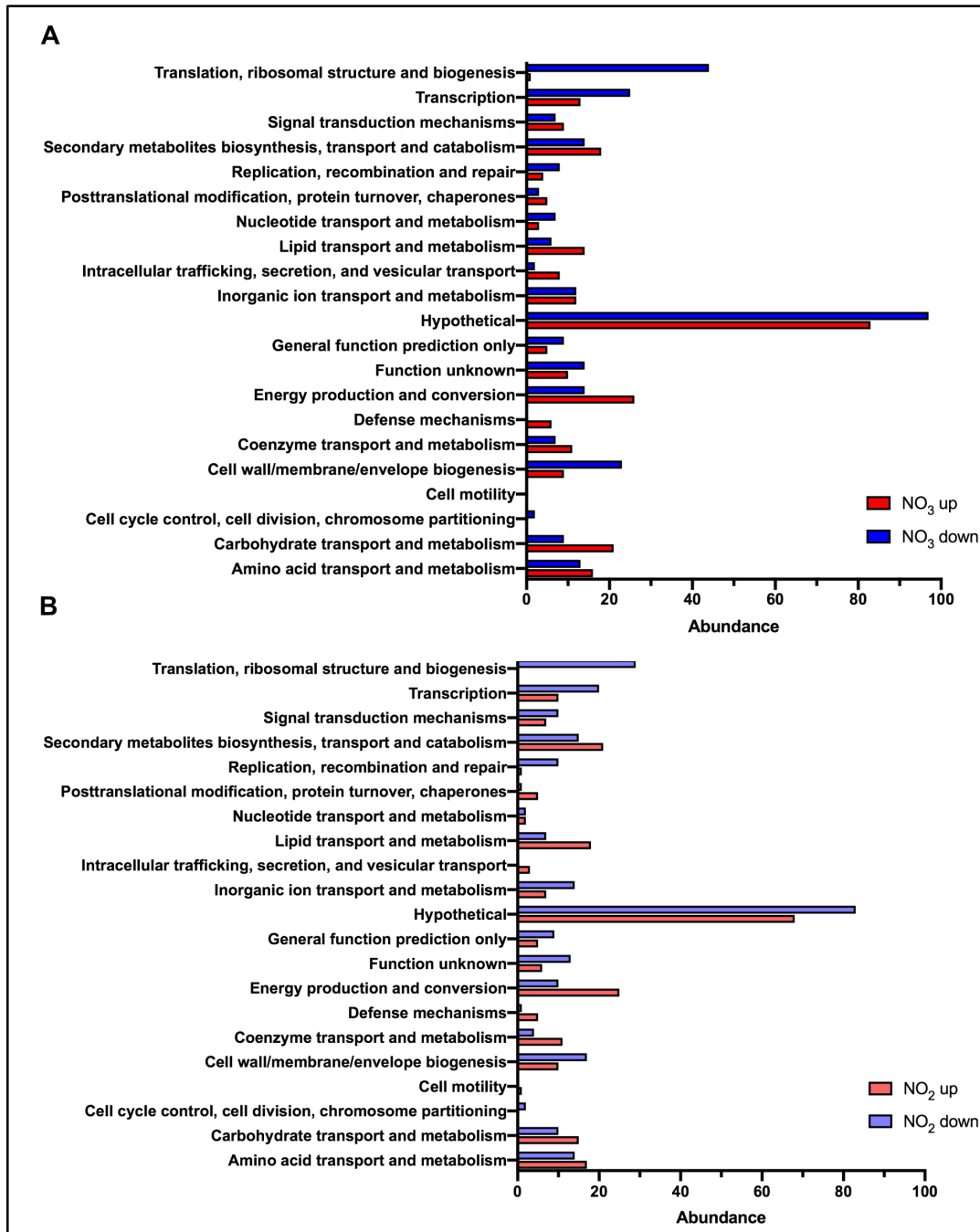
**Figure A4.1 Functional characterization of transcriptionally active and differentially regulated genes reveals defects in translation, ribosomal structure and biogenesis.** Cluster of orthologous groups comparisons of up- and down-regulated loci from both nitrate-supplemented (top) and nitrite-supplemented (bottom) treatment conditions.
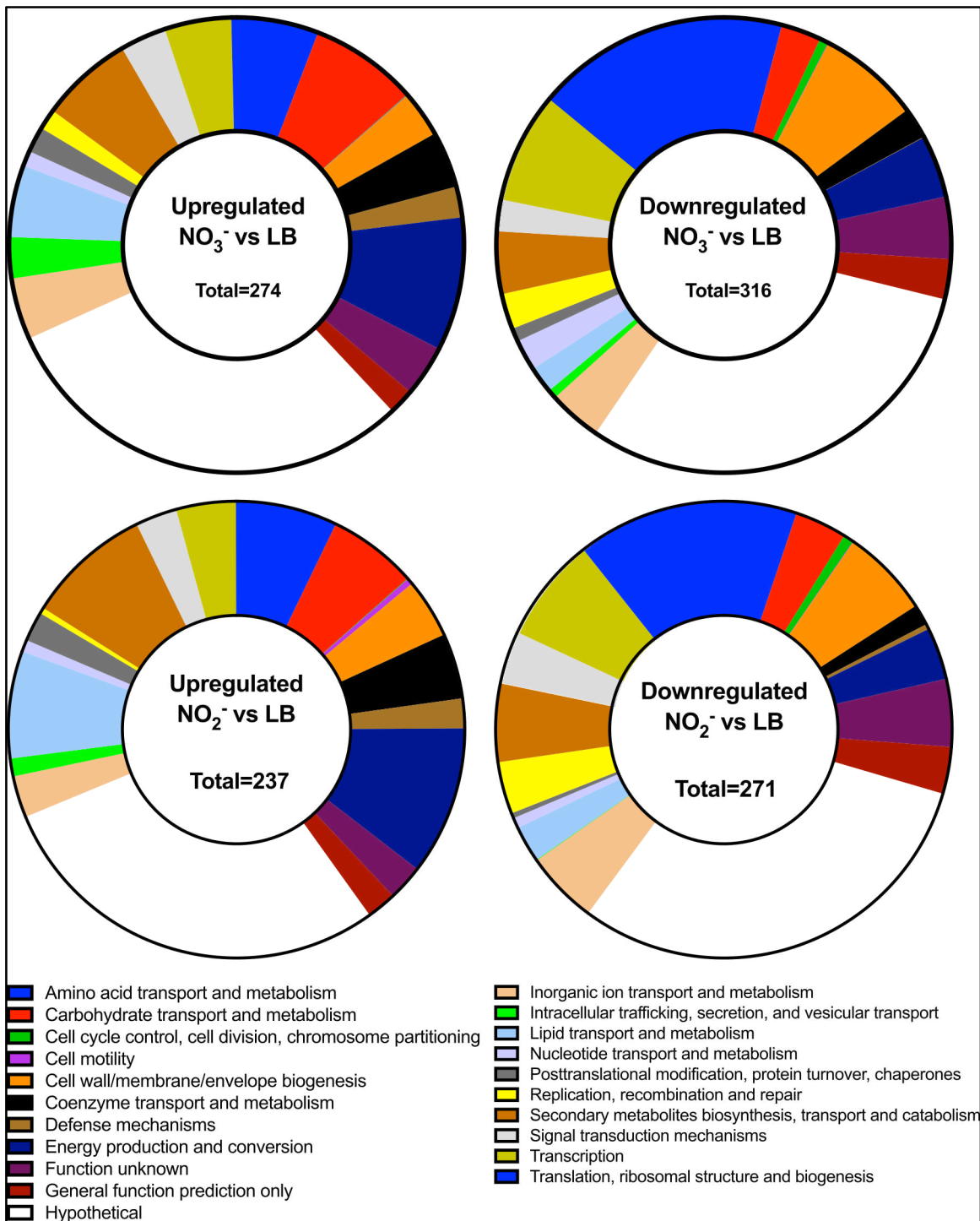
**Figure A4.2 Cluster of orthologous groups assigned to the significant differentially regulated transcripts identified in this study responding to either nitrate nor nitrite stress.** Functional characterization of the differentially expressed genes in response to nitrate-supplemented and nitrite-supplemented treatment.
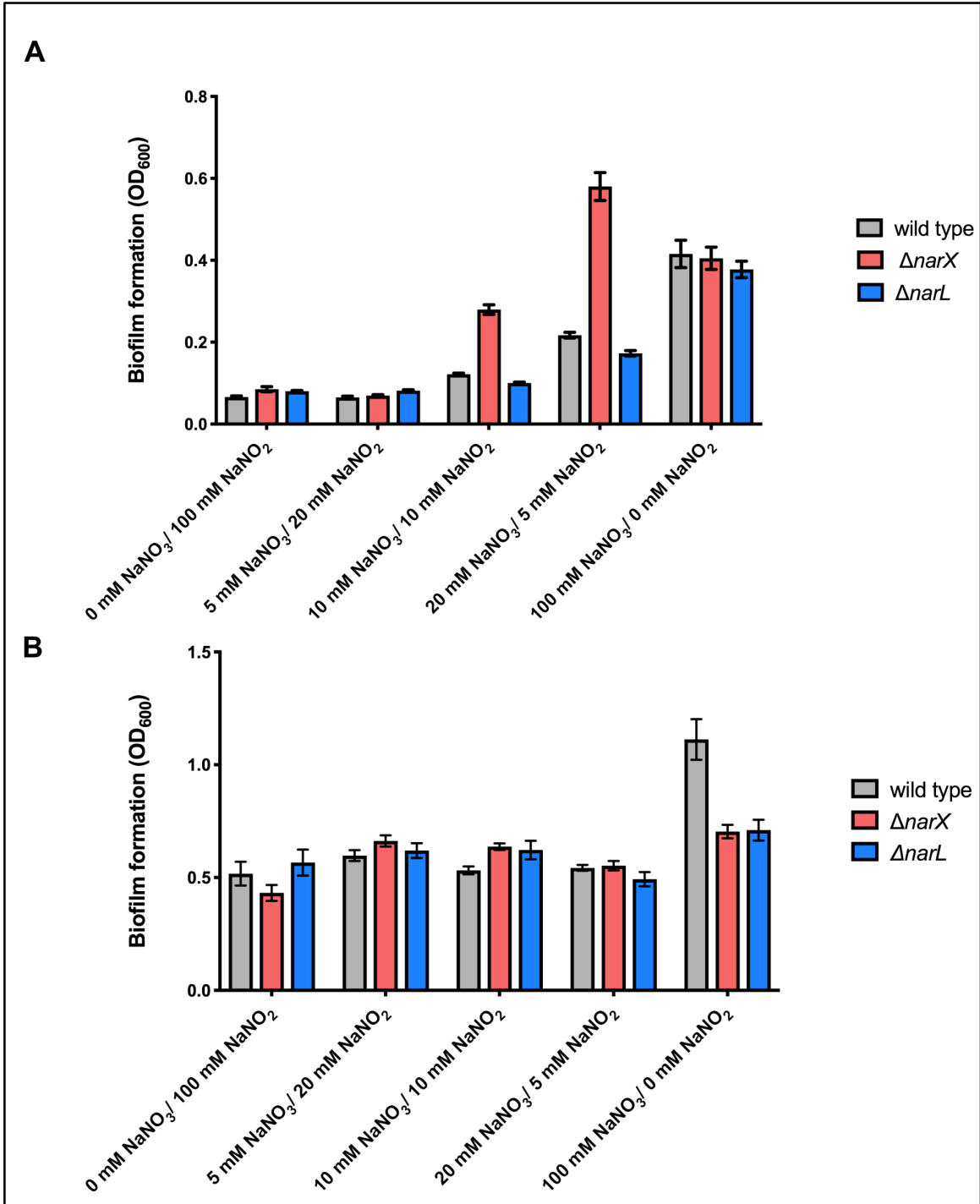
**Figure A4.3 Anaerobic biofilm formation in the presence of competing N-oxide donors.** Anaerobic static growth cultures were supplemented with both sodium nitrate and sodium nitrite, in a crisscross concentration gradient and grown for 48h (A) and 168h (B) before measuring biofilm adherence. The increased growth kinetics seen for the $\Delta narX$ mutant at 48h in lower concentrations of $NaNO_2$ and higher concentrations of $NaNO_3$ were normalized after continued growth for 168h, where only extreme levels of $NaNO_3$ provided the wild type with a growth advantage.
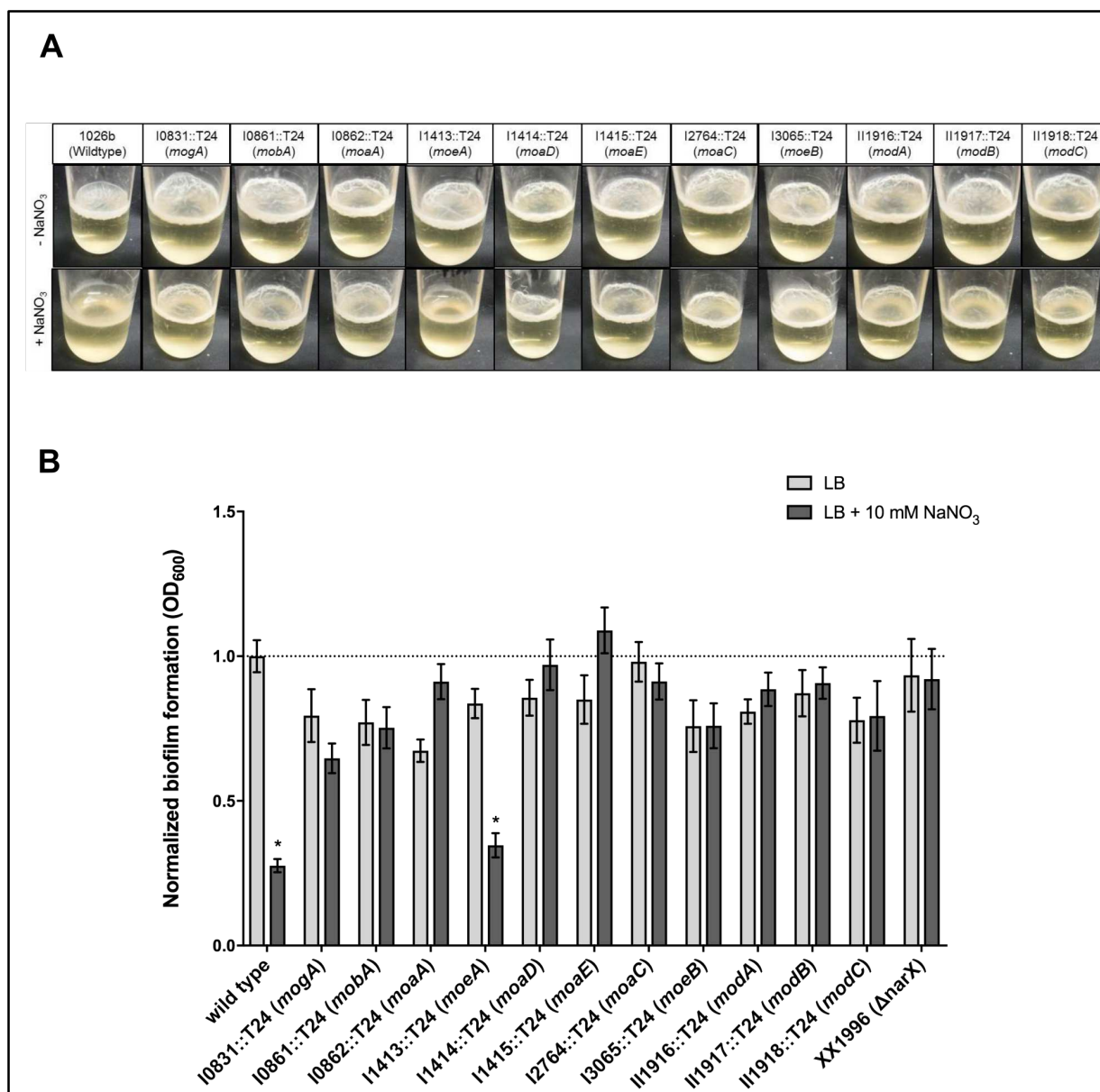
**Figure A4.4 Qualitative and quantitative evaluation of relative biofilm formation in the presence and absence of sodium nitrate.** Insertional transposon mutants in loci identified to be important in the molybdopterin biosynthetic pathway, which is essential for biosynthesis of the co-factor for a functioning NarG-1 in *B. pseudomallei*, were evaluated for pellicle formation. (A) Wild-type *B. pseudomallei* 1026b forms a distinct pellicle biofilm when grown statically in liquid culture; however, it is unable to form a pellicle biofilm in the presence of 10 mM NaNO$_3$. Transposon insertion mutants into all molybdopterin biosynthesis loci except I1413 (*moeA*) were resistant to biofilm inhibition, suggesting that this biosynthetic pathway is important for the nitrate-dependent biofilm inhibition phenotype in a similar fashion as *narG-1*. (B) Quantitive evaluation of the same transposon insertion mutants analyzed in the pellicle assay, using the Δ*narX* mutant as a positive control for resistance in the nitrate-dependent biofilm inhibition model.